A novel method to fabricate open-cell silicon nitride foams with a high and controlled level of porosity

Ali Alem

A Thesis

In the Department

of

Mechanical and Industrial Engineering

Presented in Partial Fulfillment of the Requirements

For the Degree of Doctor of Philosophy at

Concordia University

Montreal, Quebec, Canada

June 2014

CONCORDIA UNIVERSITY
SCHOOL OF GRADUATE STUDIES

This is to certify that the thesis prepared

By: Ali Alem

Entitled: A novel method to fabricate open-cell silicon nitride foams with
                a high and controlled level of porosity

and submitted in partial fulfillment of the requirements for the degree of

Doctor of Philosophy   (Mechanical Engineering)

complies with the regulations of the University and meets the accepted standards with respect to originality and quality.

Signed by the final examining committee:

_____Chair
Dr. R. Raut

_____External Examiner
Dr. K. Plucknett

_____External to Program
Dr. M. Nokken

_____Examiner
Dr. M. Medraj

_____Examiner
Dr. R. Wuthrich

_____Thesis Co-Supervisor
Dr. M.D. Pugh

_____Thesis Co-Supervisor
Dr. R.A.L. Drew

Approved by: _____
            Dr. A. Dolatabadi, Graduate Program Director

June 19, 2014   _____
                       Dr. C. Trueman, Interim Dean
                       Faculty of Engineering and Computer Science

ABSTRACT

A novel method to fabricate open-cell silicon nitride foams with a high and controlled level of porosity

Ali Alem, Ph.D.
Concordia University, 2014

There is a significant lack of study on silicon nitride (Si_3N_4) foams. This is due to the fabrication issues and difficulties of working with silicon nitride powder. In this study a new fabrication procedure has been designed to fabricate highly porous and homogeneous silicon nitride foams with open-cell structures and controlled porosity levels. The combination of three methods including the sacrificial template method, gel-casting, and reaction bonding techniques resulted in the fabrication of reaction bonded silicon nitride (RBSN) foams. The fabrication procedure was studied and optimized in terms of suspension preparation and rheology, gel-casting parameters, and also reaction bonding conditions. The results revealed that pH 8.5 and the presence of 1.5 wt% DS001 would lead to the highest suspension stability. Therefore, the least sediment height and the highest zeta potential would be obtained. Si-PMMA suspensions showed a near Newtonian behavior at pH 8.5 and for 60 wt% solid. The gel-casting parameters including the monomer content, the ratio of monomer to cross-linker, the gelation time, and the sample warpage were also studied. Based on the result the optimum monomer to cross-linker weight ratio was selected to be 15:1. After nitridation, the foams have a precisely controlled level of porosity, which can be controlled between 41 vol% to 87

vol%. The pore interconnectivity was examined both before and after nitriding and showed complete interconnectedness in the foam porosity.

The parameters influencing the mechanical strength of the RBSN foams were also investigated. These considerations include the foam porosity, homogeneity, gel-casting parameters, and nitriding conditions. Depending on the foam porosity, the strength can vary between 1 MPa and 18 MPa. It was also observed that for high Si/PMMA ratios, a monomer content of more than 25 wt% in the premix solution is required. Otherwise, the foam strength drops significantly due to inhomogeneities formed in the cast body. In terms of the effect of nitriding conditions on the foam strength, maximum strength was obtained under N_2-H_2 atmospheres rather than N_2. Extensive investigation on the nitridation process also revealed that the high porosity level of the foam and consequently its large surface area significantly affect the nitriding mechanisms and microstructures compared to conventional RBSN ceramics. It was observed that α- and β-Si_3N_4 form based on specific reactions and each phase has distinct morphologies depending on the nitriding reactions.

The effect of iron disilicide ($FeSi_2$) on the properties and microstructure of the fabricated RBSN foams was studied in the next step of the investigation. It was observed that the addition of 1 wt% of $FeSi_2$ significantly increases the foam strength regardless of the nitriding condition. After the addition of $FeSi_2$, a maximum strength of 3.41 MPa was achieved under a N_2 atmosphere at 1390°C with a foam of 71 vol% porosity. $FeSi_2$ also affects the α/β phase ratio considerably. It was observed that a considerable increase in the α-Si_3N_4 content occurs up to 1 wt% $FeSi_2$ while the β-Si_3N_4 content starts to increase thereafter. The XRD and microstructural analysis showed that α-Si_3N_4 is present in the

form of both matte and whiskers while β-Si_3N_4 forms as whiskers and large faceted angular grains.

The influence of α- and β-Si_3N_4 seeds has also been investigated. It was observed that both α- and β-seeds improve the foam strength by 30% and 85%, respectively. The optimum contents of the α- and β-seeds correspond to the maximum foam strength which was observed for 5 wt% α-Si_3N_4 and 10 wt% β-Si_3N_4 seeds. The vapor phase reactions were also enhanced by the addition of β-seeds resulting in a significant increase in the β-whisker content of the microstructure.

Sintered reaction bonded silicon nitride (SRBSN) foams were also fabricated via sintering of RBSN foams in the presence of MgO as a sintering aid. The effect of different amounts of MgO on the foam microstructure and porosity was also studied both before and after sintering. The addition of MgO resulted in significant changes to the microstructure of the RBSN and SRBSN foams. MgO stopped whisker-forming reactions during nitriding; therefore, foams with clean porosity and without the presence of whiskers were produced. The SRBSN foams can have a maximum of 85 vol% porosity and the foam microstructure contained only β-Si_3N_4 grains embedded in an amorphous intergranular phase.

Dedicated to

My Mom Azam and My Dad Hasan

Acknowledgement

First and foremost I would like to express my special appreciation to my supervisors Dr. Martin D. Pugh and Dr. Robin A.L. Drew for their advice, guidance, and continuous support. During four years of working under their supervision, their endless positive and encouraging attitude was priceless.

I would like to also thank the administrative staff of the department including Leslie Hosein, Sophie Mérineau, Maureen Thuringer, and Arlene Zimmerman. I am also particularly grateful to Henry Szczawinski and Robert Oliver for their technical assistance.

My special thanks to my family and also my spouse, Maryam Aramesh, for their continuous and unconditional support.

I also wish to thank my amazing friends Ehsan Rezabeigi and Sina Chaeichian for their friendship, encouragement, and support during all these years.

Contributions of Authors

The thesis contains journal articles, which have been published already. These articles have been presented in the unaltered and original format. The thesis also includes manuscripts that are under the review process for publication. The list of articles has been provided below.

Chapter 3: Ali Alem, Martin D. Pugh, Robin A.L. Drew, "Open-cell reaction bonded silicon nitride foams: Fabrication and characterization", Journal of the European Ceramic Society 34 (2014) 599–609.

Chapter 4: Ali Alem, Robin A.L. Drew, Martin D. Pugh, "The influence of the nitriding parameters on the microstructure and strength of the open-cell reaction bonded silicon nitride foams fabricated via wet processing", Journal of Materials Science 49 (2014) 4780–4789.

Chapter 5: Ali Alem, Martin D. Pugh, Robin A.L. Drew, "Reaction bonded silicon nitride foams; the influence of iron disilicide on the foam microstructure and mechanical strength", Journal of the American Ceramic Society, under review.

Chapter 6: Ali Alem, Robin A.L. Drew, Martin D. Pugh, "The influence of α- and β-Si_3N_4 seeds on the properties of the reaction bonded silicon nitride foams", Journal of Ceramics International, accepted, June 2014, DOI: 10.1016/j.ceramint.2014.06.019.

Chapter 7: Ali Alem, Robin A.L. Drew, Martin D. Pugh, "Sintered reaction bonded silicon nitride foams with a high level of interconnected porosity", To be submitted.

Appendix: Ali Alem and Martin D. Pugh, "The Influence of Chromium Oxide on the Sintering Behavior of Silicon Nitride", International Journal of Applied Ceramic Technology 10 [S1] E258–E266 (2013).

All the journal articles presented in this thesis have been reviewed by my supervisors, Dr. Martin D. Pugh and Robin A.L. Drew, prior to submission.

Table of Contents

List of Figures

List of Tables

Abbreviations

AM	Acrylamide
APS	Ammonium persulfate
BET	Brunauer - Emmett - Teller
DPF	Diesel particulate filters
DSC	Differential scanning calorimetry
FAC	Fly ash cenosphere
GPSRBSN	Gas-pressure sintered reaction bonded silicon nitride
IEP	Isoelectric point
LDPE	Low-density polyethylene
MBAM	N,N´-methylenbisacrylamide
PAM	Polyacrylamide
PMMA	Poly(methyl methacrylate)
PS	Polystyrene
PVA	Polyvinyl alcohol
PVB	Polyvinyl butyral
PVC	Poly(vinyl chloride)
RBSN	Reaction bonded silicon nitride
SEM	Scanning electron microscopy
SRBSN	Sintered reaction bonded silicon nitride
TEM	Transmission electron microscopy
TEMED	N,N,N´,N´-tetramethylethylenediamine

TBA	Tertiary-butyl alcohol
TGA	Thermogravimetric analysis
XRD	X-ray diffraction
VLS	Vapor-liquid-solid
YSZ	Yttria-stabilized zirconia

Chapter 1

1.1. Introduction

Man uses dense solids such as steel and concrete to make load-bearing structures but nature does the same with cellular materials such as wood, bone, and coral. Cellular solids have been recently found to be very interesting since the porosity in their structure introduces unique features and properties including permeability, low density, high thermal shock resistance, and controlled heat transfer [1, 2]. These materials with tailored porosity exhibit special functionalities which cannot be found in their dense counterparts. Among all the three general classes of materials including polymers, ceramics and metals, ceramic materials can withstand harsh in-service conditions. Traditionally, it was customary to try to make ceramic materials as dense as possible to reduce the possibility of sudden failure and fracture of this brittle group of materials. But recently, many technological applications have been found in which porous ceramics must be utilized. On one hand, ceramic foams show remarkable characteristics including high temperature resistance, tailored electrical properties, high wear resistance, and high corrosion resistance due to their ceramic nature and on the other hand, due to their porous nature, they have the advantages of low thermal mass, low thermal conductivity, low density, high surface area, low dielectric constant, high specific strength, and controlled permeability [3].

Based on the outstanding combination of properties, ceramic foams can be utilized in many high-tech applications and harsh environments. Cellular ceramics are utilized as molten metal filters to remove inclusions and trapped gas bubbles from the melt. For

aluminium alloys, Al_2O_3 foams can be used up to 1350°C. SiC foams can be utilized up to 1500°C which makes it suitable for cast iron and nonferrous alloys. For steel alloys with higher melting points, ZrO_2 foams can be used up to 1700°C [1]. Diesel particulate filters (DPF) are now mandatorily installed in vehicle exhausts. These filters remove soot emissions formed due to combustion. Different ceramic foams can be used for DPF such as cordierite, SiC, Si_3N_4, aluminium titanate, or mullite foams [1]. Ceramic foams can also be used for catalytic reaction supports such as in ammonia oxidation, steam reforming, photocatalytic decomposition of volatile organic compounds of water, and methane reforming [1]. Other applications of ceramic foams include hot gas filters, thermal protection, refractory materials and kiln furniture, heat exchangers, high temperature sound attenuation modules, porous medium burners, membranes for separation processes, porous scaffolds and biomedical implants, bioreactors, lightweight structural ceramics, and fabrication of polymer and metal matrix composites [3 - 6]. Depending on the properties of different ceramic materials and the feasibility of their processing, several ceramic foams including alumina, zirconia, mullite, cordierite, silicon carbide, and silica have been produced commercially [7]. However, there are some other ceramic foams such as silicon nitride which need further investigation.

1.2. Objectives

Producing silicon nitride foams based on a straightforward and inexpensive process is the main objective of the current investigation. In order to open up new and advanced applications for the fabricated ceramic foam, an open-cell foam which possesses a high level of porosity and also pore interconnectivity must be fabricated. To achieve that, there are two possibilities for the general trend of the fabrication procedure. Either silicon

nitride powder must be employed followed by sintering; this process requires dealing with major fabrication issues and costly products. The second alternative is to use silicon powder followed by the reaction bonding process. This study was focused on developing and designing a new way to produce tailored silicon nitride foams based on gel-casting and reaction bonding of silicon compacts. In order to accomplish this goal, several major areas must be studied and understood. Here is the step-by-step classification of the methodology to define the objectives of the current investigation.

❖ The foaming technique has the most significant influence on the foam microstructure. The first step is to find the most suitable technique, which is capable of producing homogeneous silicon foams which are then converted to silicon nitride foams via reaction bonding.

❖ Modify and design the selected fabrication procedure in a way that it can satisfy the required foam properties including the structural homogeneity, pore interconnectivity, and a high but controlled level of porosity. This step includes the selection of the sacrificial phases and their size and properties. A selection between wet and dry processing techniques must be performed based on the characteristics of each process. Defining all the steps of the fabrication procedure from the starting point up to the reaction bonding step.

❖ Silicon nitridation must be understood perfectly in order to obtain Si_3N_4 foams with the desired properties based on the reaction bonding process. Understanding the nitriding reactions and the related mechanisms have always been very challenging. A deep study on nitridation of porous silicon compacts is another objective of this study.

3

❖ Iron compounds are the most common impurities in silicon powder and consequently in reaction bonded silicon nitride ceramics. In order to have a more realistic understanding of the nitriding phenomenon and to modify the foam microstructures and consequently its properties, the influence of iron compounds on the RBSN foam properties must be investigated.

❖ The modification of the foam microstructure must be performed based on other available tools such as silicon nitride seeding. Seeding affects both the nitridation process and also the properties of the fabricated RBSN foam including the porosity level and its interconnectivity. Therefore, α- and β-silicon nitride phases can be utilized to study the structure and properties of the seeded RBSN foam.

❖ The combination of a high strength and a high porosity level has been always challenging to obtain. It is advantageous to add an extra sintering step to the process to fabricate sintered reaction bonded silicon nitride foams, which may show different microstructures and properties than RBSN foams. Therefore, fabrication of SRBSN foams in the presence of magnesium oxide as a sintering additive is another objective of this study.

1.3. Thesis organization

This thesis contains 9 chapters. Chapter 1 provides a brief introduction and the objectives of the investigation. In the second chapter, a comprehensive literature review has been presented regarding silicon nitride ceramics and their structures, foam fabrication techniques, consolidation techniques, and the silicon nitride foams fabricated. Chapter 3 presents the foam fabrication procedure designed and developed in this study to produce reaction bonded silicon nitride (RBSN) foams. This chapter includes the optimization of

the fabrication process including the Si-PMMA suspensions, gel-casting, and polymer pyrolysis. The chapter also presents the characterization of the RBSN foams in terms of porosity, interconnectivity, and microstructure. Chapter 4 focuses on the nitridation of the fabricated RBSN foams and the influence of the nitriding parameters on the foam properties such as strength. Different nitriding atmospheres and a range of temperatures have been utilized to study the nitriding reactions and the nitriding mechanisms in depth. The influence of the iron disilicide addition on the RBSN foam properties will be studied in chapter 5. This chapter investigates the influence of iron disilicide on silicon nitridation, foam strength, and microstructure. In chapter 6 the seeding of RBSN foams as a technique to modify the foam microstructure and its properties will be discussed. The study focuses on how seeding can influence the nitriding reactions, the foam microstructure, and its mechanical strength. Chapter 7 explains the fabrication of sintered reaction bonded silicon nitride (SRBSN) foams with the addition of MgO. The influence of both MgO addition and the sintering procedure on the foam properties including porosity, density, and microstructure will be provided in this chapter. In chapter 8, a general conclusion about the whole study, its contributions, and also several suggestions for potential future work will be presented. Finally, chapter 9 as the thesis appendix provides some extra information. It includes the details of the experimental procedure, foam infiltration, initial topic of the investigation, etc.

Chapter 2

Literature review

2.1. Silicon nitride structure

2.1.1. Introduction

Strong engineering ceramics are those materials that can tolerate a high stress per unit strain which means a high modulus of elasticity. Since lightweight materials are also of significant importance, materials with a high ratio of elastic modulus to specific gravity are also more interesting. Ceramics with covalent atomic bonds can fulfill the high strength to weight ratio requirement. Among all the three different types of primary bonding, covalent bonds can offer a high elastic modulus due to a high binding energy and on the other hand; they can also offer low densities due to the bond directionality which results in low coordination numbers [8]. There are several ceramic materials including AlN, Al_2O_3, BeO, carbon whiskers, SiC, and Si_3N_4 which show a high specific modulus. Among these materials, AlN hydrolyses very easily, Al_2O_3 has poor thermal shock resistance, beryllia has toxicity issues, and carbon has oxidation problems. However, of all these materials, silicon nitride has high strength, good wear resistance, high chemical and thermal stability, low friction coefficient, high thermal shock resistance, and good oxidation resistance. All these properties make this ceramic material a great candidate for engineering applications. However, Si_3N_4 ceramics mainly suffer from a major fabrication issue. Due to a high degree of covalency, Si_3N_4 has a very small self-diffusivity and sinterability [8].

6

2.1.2. Si_3N_4 polymorphs and structures

Silicon nitride has two polymorphs, α and β, which both have hexagonal structures. The structure of β-Si_3N_4 is the phenacite type structure, $BeSiO_4$, in which oxygen atoms have been replaced by nitrogen and silicon atoms has replaced the beryllium atoms. It results in SiN_4 tetrahedra which are connected by sharing nitrogen atoms at the corners of the tetrahedra. The dimensions of the SiN_4 tetrahedron are very similar to that of the SiO_4 tetrahedron. Therefore, each nitrogen atom is shared between three tetrahedra. The final structure is composed of puckered rings of alternating Si and N atoms in a layered structure. In the β-Si_3N_4 structure, only one layer of SiN_4 tetrahedra exists; therefore, a stacking sequence of ABAB is obtained. This stacking creates long continuous channels in the c direction of the β-Si_3N_4 structure [9, 10]. The structure is shown in Figure 2-1-a. From the figure it can be seen that the β-Si_3N_4 structure shows channels parallel to the c-axis. These channels have a diameter of about 0.5 nm which results in a high nitrogen diffusion coefficient ($D_{Nβ}= 5.8 \times 10^6$ $cm^{-2}.S^{-1}$) [10].

The α-Si_3N_4 structure has two layers of SiN_4 tetrahedra; therefore, it has the stacking sequence of ABCDABCD. The CD layer has the same atomic arrangement as AB but it has been rotated by 180° along the c axis. Therefore, the channels in the β-Si_3N_4 structure change into two large interstitial positions in the α-Si_3N_4 structure which result in a decreased nitrogen diffusion coefficient ($D_{Nα}= 1.2 \times 10^{-12}$ $cm^{-2}.S^{-1}$) compared to β-Si_3N_4. It is assumed that α-Si_3N_4 is an oxynitride in which oxygen replaces nitrogen while nitrogen vacancies do exist to maintain charge neutrality [11]. The lattice parameter of α phase is also dependent on the oxygen content dissolved in its structure. This is considered as another reason for the presence of oxygen as an impurity in the structure of

α-Si$_3$N$_4$. As the oxygen content of the structure increases, the a-parameter of the unit cell decreases to 0.775 nm and the c-parameter increases to 0.5625 nm [8, 10]. α-Si$_3$N$_4$ is the stable modification at room temperature but it is metastable at high sintering temperatures and irreversibly transforms to β-Si$_3$N$_4$ [8, 10].
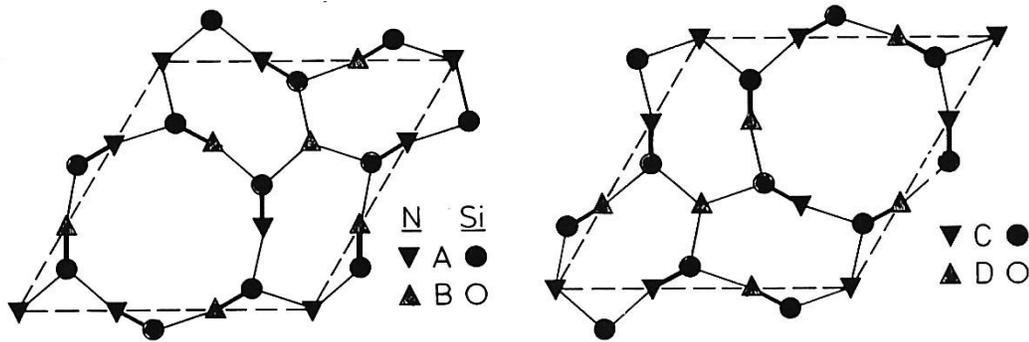
Figure 2-1. a) AB layers in the β-Si$_3$N$_4$ structure with the stacking of ABAB, b) CD layers in the α-Si$_3$N$_4$ structure with the stacking of ABCDABCD [12].

2.1.3. β-Si$_3$N$_4$ and α-Si$_3$N$_4$ solid solutions; β-SiAlON and α-SiAlON

Aluminium can be dissolved extensively in β-Si$_3$N$_4$. Al ions can replace Si ions which results in the replacement of N ions by O ions to maintain charge neutrality. This replacement results in an extended solid solution called β-SiAlON with the Si$_{6-z}$Al$_z$O$_z$N$_{8-z}$ chemical formula. In this formula z is the number of Si and N ions replaced by Al and O, respectively. Z reaches a maximum between 4 and 5 at about 2000 K and decreases with decreasing temperature [10].

As was mentioned before, the longitudinal channels in the β structure are closed and isolated in the α structure. Those interstitial positions in the α-Si$_3$N$_4$ structure can be partially filled with cations with the ionic radius of about 0.1 nm resulting in the stabilization of this metastable structure. These cations may include Li$^+$, Mg^{2+}, Ca^{2+}, and Y^{3+} and also lanthanides with the atomic number higher than 60. It must be mentioned

8

that charge neutrality must be maintained in the structure. Therefore, Si^{4+} and N^{3-} must be replaced by Al^{3+} and O^{2-}, respectively [10]. This results in α-SiAlON with the chemical formula of $M_xSi_{12-(m+n)}Al_{(m+n)}O_nN_{16-n}$ where x is the amount of the stabilizing cation with the valence v^+, and n is the amount of N^{3-} ions replaced by O^{2-} ions. To maintain charge neutrality, the amount of Al^{3+} cations which replace for Si^{4+} cations must be $x \cdot v^+ + n$ in which $x \cdot v^+$ is shown by m [10].

2.1.4. Sintering and densification of Si_3N_4 as fabrication issues

There is a high degree of covalency in Si-N atomic bonds which results in intrinsically high strength and hardness of this ceramic. On the other hand, this strong covalent bond is a major disadvantage in sintering and densification of Si_3N_4 in a way that sintering of Si_3N_4 compacts is considered as a major fabrication issue. Self-diffusivity in Si_3N_4 is also quite low and densification starts at extremely high temperatures (>1850°C) when decomposition of Si_3N_4 has already started [12]. Therefore, the only possible alternative to densify Si_3N_4 compacts is to use sintering additives. These additives including Y_2O_3, Al_2O_3, and MgO form a liquid phase which accelerates densification through particle rearrangement and solution-precipitation mechanisms. The surface silica layer on Si_3N_4 particles forms an M-Si-O-N (M = Mg, Al, Y, etc.) oxynitride liquid phase via reaction with the nitride itself and the oxide additives (M_xO_y) such as Al_2O_3, MgO, and Y_2O_3 [13]. It must be mentioned that, although these additives promote densification, they typically form an amorphous secondary intergranular phase upon cooling which deteriorates the high temperature properties of the compact including the creep resistance. There are several ways to reduce or avoid the deterioration of the mechanical properties at high temperatures which all are dependent on the used sintering aid system. These methods

include using less sintering additive, crystallization of the amorphous intergranular phase by performing post sintering heat treatments, and designing the additive system in a way that it dissolves in the Si_3N_4 grains after sintering. The crystallization of the intergranular glassy phase through post sintering heat treatment reduces the detrimental effect of the secondary phases and improves the mechanical properties of the ceramic body [13, 14].

The densification of Si_3N_4 ceramics in the presence of sintering additives is explained based on the Kingery liquid phase sintering model. This model explains the densification process in three steps. The first step is the particle rearrangement which occurs after the formation of the liquid phase. The amount and the viscosity of the liquid phase determine the rate and magnitude of shrinkage. This step is also considered as the induction time of α to β phase transformation which is explained below. The second step of densification is solution-diffusion-precipitation. The shrinkage in this step is determined by Equation 2-1 where t is time and n is 3 if solution into, or precipitaion from, the liquid is the rate determining step as is the case when MgO is the additive and n is 5 if diffusion through the liquid is rate determining which is the case for Y_2O_3 as the additive. The α to β phase transformation starts during this step. The last step in densification is coalescence in which closed porosity is eliminated and depending on the liquid phase chemistry, the elongated β-Si_3N_4 grains grow furthur [12].

$$\Delta V/V_0 \approx t^{1/n} \hspace{3cm} (2\text{-}1)$$

Even in the presence of sintering additives which promote liquid phase sintering, the densification of Si_3N_4 is still problematic. At temperatures above 1700°C, decomposition of Si_3N_4 is competitive with densification and results in significant weight losses. The decomposition of Si_3N_4 occurs via Reactions 2-2 to 2-4. In order to overcome this issue,

powder beds which are composed of Si_3N_4 and BN can be used. The powder bed increases the local vapor pressure around the compact which in turn reduces the volatilization rate of Si_3N_4. The addition of SiO_2 to the powder bed was obserevd to be helpful in increasing the SiO partial pressure and suppressing weight loss via Reaction 2-4. Utilizing the gas pressure sintering (GPS) technique through increasing the N_2 pressure to higher levels of up to 10 MPa can also reduce the weight loss and improve the densification rate [12, 15].

$$Si_3N_4 \text{ (s)} \rightarrow 3Si \text{ (l)} + 2N_2 \qquad\qquad (2\text{-}2)$$

$$Si_3N_4 \text{ (s)} + 1.5\ O_2 \rightarrow 3SiO \text{ (g)} + 2N_2 \qquad\qquad (2\text{-}3)$$

$$Si_3N_4 \text{ (s)} + 3\ SiO_2 \text{ (s,l)} \rightarrow 6\ SiO \text{ (g)} + 2N_2 \qquad\qquad (2\text{-}4)$$

Upon increasing the temperature, irreversible α to β phase transformation can occur. α-Si_3N_4 which is less stable at higher temperatures transforms to β-Si_3N_4 through the solution-precipitation mechanism. While α-Si_3N_4 phase dissolves in the liquid phase due to its lower stability and more solubility, precipitation of the more stable and less soluble β-Si_3N_4 with a rod-like morphology occurs. This results in an interlocked microstructure in which the liquid phase forms an intergranular glassy phase upon cooling [8]. The phase transformation is shown in Reaction 2-5.

$$\alpha\text{-}Si_3N_4 + SiO_2 + M_xO_y \rightarrow \beta\text{-}Si_3N_4 + \text{M-Si-O-N phase} \qquad\qquad (2\text{-}5)$$

The rates of phase transformation and densification phenomena can be controlled during sintering through designing the chemical composition and consequently the viscosity of the liquid phase. There can be three cases based on the relationship between the densification and the phase transformation rates. All these three situations are shown in Figure 2-2. The first situation is when the densification rate is faster than the phase

11

transformation. It means that almost full densification occurs before phase transformation is complete [16, 17]. This is the case when compacts containing additives which produce low viscosity liquids are hot pressed. Sintering additives of 10 wt% Al_2O_3 or 1 wt% Y_2O_3 and 6 wt% Al_2O_3 can lead to this situation. The second case is when the densification and the phase transformation rates are almost the same. This can happen in the presence of viscous liquid phases [16, 17]. Therefore, a wide grain size distribution may be obtained. An example can be a sintering additive sytem which contains 5 wt% Y_2O_3 and 2 wt% Al_2O_3. The last case is when there is a very limited amount of the liquid phase present during sintering. Under this condition, the densification is impeded while the α to β phase transformation can proceed. This small amount of liquid can be easily saturated with nitrides, therefore, β-Si_3N_4 can precipitate faster from the melt which results in faster transformation. On the other hand, the small amount of liquid phase is not enough for densification [16]. It must be mentioned that designing the sintering aid system in sintering of Si_3N_4 is of great importance and has a significant influence on densification, phase transformation, and the end point application. The sintering additive system must significantly enhance the sinterability while resulting in a minimum amount of refractory intergranular phase.
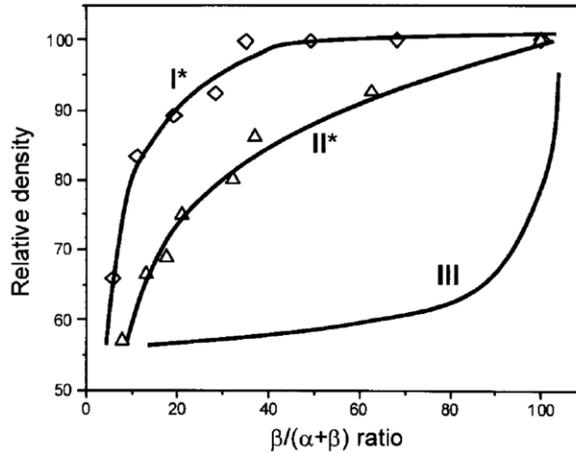
Figure 2-2. The relationship between densification and phase transformation rates showing three different cases; ◊ is the system containing 1 wt% Y_2O_3 and 6 wt% Al_2O_3, Δ is the system containing 5 wt% Y_2O_3 and 2 wt% Al_2O_3, and III is the system when densification is much slower than phase transformation [16].

2.2. Reaction bonded silicon nitride (RBSN) ceramics

Silicon nitride bodies are typically fabricated by pressureless sintering, pressure sintering, hot pressing, or hot isostatic pressing of silicon nitride powder. The high cost of Si_3N_4 powder is always a major issue which limits extensive applications of Si_3N_4. There are also some other major problems in working with Si_3N_4 powder. As was mentioned before, fabrication of Si_3N_4 bodies has always been difficult due to the high degree of covalency of the Si-N atomic bond. A large amount of sintering additives (up to 10 wt%) will be required to get sufficient liquid phases during sintering and consequently accelerate the diffusion rates and sintering kinetics. These additives form large amounts of glassy phases at grain boundaries and they are detrimental to high temperature properties of the sample since they cause subcritical crack growth and grain sliding at high temperatures [18]. Large linear shrinkage (15-20%) of the Si_3N_4 bodies after sintering is also problematic since it makes time consuming and costly post-sintering

13

machining steps an essential part of the fabrication process to get the required sample dimensions [19]. There is also inconsistency in wet-processing of Si_3N_4 suspensions. Due to the variety of particle shapes and production methods, dispersion of Si_3N_4 particles in a medium can be quite different from batch to batch. Therefore, continuous modification of the processing parameters is necessary, resulting in a difficult production process [20]. Si_3N_4 suspensions also show high shear thickening behavior which is absolutely undesirable in wet processing of ceramics [21]. An alternative to overcome all these fabrication issues is the reaction bonding process.

The reaction bonding process is an interesting alternative to direct sintering of Si_3N_4. Reaction bonded silicon nitride (RBSN) was also the first Si_3N_4 ceramic invented and produced in the 1950s [10]. RBSN offers incredible advantages over sintered Si_3N_4 including an easy and economical fabrication procedure, low thermal expansion coefficient and consequently high resistance to thermally induced failures, good mechanical properties maintained at high temperatures, and high corrosion resistance [11]. In RBSN ceramics where inexpensive Si powder replaces costly Si_3N_4 powder, silicon compacts can be fabricated by various techniques such as slip casting, uniaxial or isostatic pressing, injection molding, gel-casting, or extrusion, followed by nitriding under N_2-containing atmospheres at temperatures in the range of 1200 to 1450°C [11, 19].

Another remarkable feature of the RBSN ceramics is the negligible size changes (~0.1%) during nitriding of RBSN bodies which make it possible to produce near-net shape specimens without any expensive post sintering machining processes. It must be mentioned that 22% volume expansion occurs during Si to Si_3N_4 conversion. Since the

expansion takes place in the specimen porosity, there will be no marked dimensional changes after nitriding. Expansion in the spaces between the particles decreases gas diffusion through the pores. This reduction in gas permeability makes it more difficult to get full conversion from Si to Si_3N_4 in conventional RBSN bodies after a reasonable nitriding time. Complete densification cannot be achieved through a reaction bonding process and ~20 vol% fine porosity will remain in the final specimen in which 80 vol% of the pores are less than 0.1 μm [11, 19]. The remaining porosity can be considered as a drawback of the reaction bonding technique in the fabrication of fully dense Si_3N_4 bodies with densities very close to the theoretical values. On the other hand, one can take advantage of the remaining porosity in the fabrication of RBSN foams.

2.2.1. Nitriding reactions in RBSN ceramics

During nitridation, different reactions occur at the same time including nitridation of Si, sintering of Si, oxidation by oxide impurities in the atmosphere, and evaporation of the surface SiO_2 layer on Si particles [10]. All these reactions affect the nitridation rate, microstructure, and properties of the RBSN ceramics. Generally, the nitridation of silicon compacts includes two steps; the movement of nitrogen into the pore channels of the compact and the chemical reaction between nitrogen and silicon resulting in Si_3N_4 formation. In the early stages, the reaction is based on the nucleation and growth of Si_3N_4. However, the Si_3N_4 product slowly covers the Si particles and separates the reactants. After the formation of a Si_3N_4 layer and without melting of Si, there can be two rate determining phenomena. The nitriding reaction goes forward if new open spaces are created. Therefore, the rate of porosity formation can be the rate controlling step. On the other hand, nitrogen diffusion through the Si_3N_4 layer can be the rate determining step if

15

the space is already available. The nitrogen diffusion in Si_3N_4 is a very slow process which is much slower than the chemical reactions [22].

Both α- and β-Si_3N_4 polymorphs can form during nitriding of Si compacts but typically, α-Si_3N_4 is dominating. Theoretically, Reactions 2-6 to 2-8 reveal the possible nitridation reactions in which Si in all physical states can react with N_2 to form Si_3N_4 [11]. In Reaction 2-9, Si_3N_4 forms due to the reaction between silicon oxide vapor and N_2. The major source of SiO(g) in this reaction is the reduction of SiO_2 by either Si (Reaction 2-10) or H_2 (Reaction 2-11) in the presence of H_2 containing atmospheres [19].

$$3 \text{ Si (s)} + 2 \text{ N}_2 \leftrightarrow \text{Si}_3\text{N}_4 \text{ (s)} \qquad\qquad (2\text{-}6)$$

$$3 \text{ Si (l)} + 2 \text{ N}_2 \leftrightarrow \text{Si}_3\text{N}_4 \text{ (s)} \qquad\qquad (2\text{-}7)$$

$$3 \text{ Si (g)} + 2 \text{ N}_2 \leftrightarrow \text{Si}_3\text{N}_4 \text{ (s)} \qquad\qquad (2\text{-}8)$$

$$3 \text{ SiO (g)} + 2 \text{ N}_2 \leftrightarrow \text{Si}_3\text{N}_4 \text{ (s)} + 3/2 \text{ O}_2 \qquad\qquad (2\text{-}9)$$

$$\text{SiO}_2 + \text{Si (s)} \leftrightarrow 2 \text{ SiO (g)} \qquad\qquad (2\text{-}10)$$

$$\text{SiO}_2 + \text{H}_2 \leftrightarrow \text{H}_2\text{O (g)} + 2 \text{ SiO (g)} \qquad\qquad (2\text{-}11)$$

The microstructure of a RBSN ceramic may contain both α- and β-Si_3N_4 polymorphs, unreacted Si, impurity phases, and porosity [23]. There are different mechanisms proposed for the formation of α- and β-Si_3N_4 phases. These mechanisms may be dominating under certain nitriding conditions. It must be mentioned that there are some major disagreements in the literature between researchers in terms of nitriding reactions and the possible nitriding mechanisms.

α-Si_3N_4 may form in two different morphologies known as α-whisker and α-matte. It is well known that in the CVD process of Si in the N_2 atmosphere, Si_3N_4 grows in the form of α-Si_3N_4 [11]. Moulson [11, 24] believes that vapor phase reactions are responsible

only for α-Si$_3$N$_4$ formation and not β-Si$_3$N$_4$. These reactions include Reactions 2-8 and 2-9 [11, 19, 23]. On the other hand, Jennings [22, 25] has concluded that α-Si$_3$N$_4$ forms only based on the reactions between gaseous Si and molecular nitrogen.

In the case of α-Si$_3$N$_4$ whiskers, gaseous silicon reacts in the vapor phase and redeposits as fine needles of α-Si$_3$N$_4$ [10]. In the case of α-matte which forms as fine grains, nitrogen will be adsorbed chemically on the Si surface resulting in Si$_3$N$_4$ nuclei formation at the beginning of the reaction. Si will be transported to the reaction site by evaporation-condensation and/or surface diffusion mechanisms to continue the nitriding reactions. When a dense layer of Si$_3$N$_4$ forms, silicon diffuses through the Si$_3$N$_4$ layer to react with nitrogen, leaving vacancies in the unreacted Si. These vacancies combine to form new pores. The nitrogen which has diffused through the Si$_3$N$_4$ layer can then react with either Si or SiO in these pores to form more Si$_3$N$_4$. The reaction results in volume expansion which fills the porosity via forming Si$_3$N$_4$. As soon as a silicon nitride layer forms, the reaction will be controlled either by N$_2$ diffusion through the Si$_3$N$_4$ layer or by the rate of porosity formation based on silicon volatilization or vacancy condensation mechanisms [22, 23, 26]. The explained model is shown in Figure 2-3.
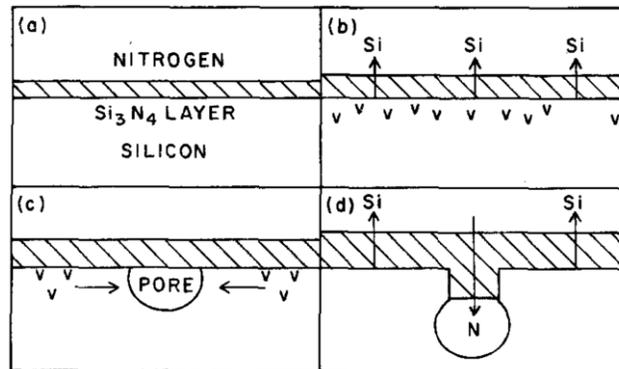
Figure 2-3. α- Si$_3$N$_4$ matte formation mechanism; a) Si$_3$N$_4$ layer formation, b) Vacancy formation due to Si vaporization or diffusion, c) pore formation based on vacancy condensation, d) nitride growth [27].

It is also believed that in the presence of impurities which result in the formation of liquid phases during nitriding, α-Si_3N_4 whiskers may also form based on the vapor-liquid-solid (VLS) mechanism [23, 27]. In the VLS mechanism, Si is transported to the whisker origin in the vapor form and condenses. Nitrogen cannot react with liquid silicon and the reaction occurs at the solid-liquid interface resulting in Si_3N_4 formation and whisker growth [27]. Figure 2-4 shows a schematic of the VLS mechanism.
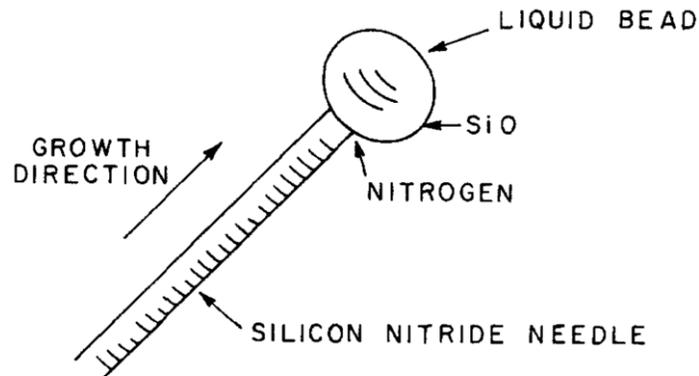
Figure 2-4. Schematic of the VLS mechanism [27].

It must be mentioned that, generally, Si_3N_4 formation mechanisms are all dependent on Si evaporation. Any factor that decreases the evaporation rate results in the reduced nitridation rate. These factors include the surface SiO_2 layer and the Si_3N_4 product layer which forms on the surface. Due to the Si_3N_4 layer, the nitriding reaction cannot be completed isothermally at low temperatures since extensive nucleation of Si_3N_4 in the compact reduces the evaporation rate of Si [10].

β-Si_3N_4 phase has also different morphologies. It can form as equiaxed grains and rod-like phases [23, 28]. It also forms at higher nitriding temperatures compared to α-Si_3N_4 [22]. Regarding β-Si_3N_4 formation, Moulson has concluded that this phase forms in the presence of a liquid phase based on the VLS mechanism and to a minor extent it may form due to a reaction between solid silicon and N_2 (Reactions 2-6 and 2-7) [11, 24, 29].

He has also mentioned that the reaction between solid Si and N_2 results in a coherent dense layer of β-Si_3N_4 [11]. On the other hand, Jennings has disagreed with the mechanism proposed by Moulson and concluded that the presence of a liquid phase is not necessary for β-Si_3N_4 formation although it enhances the formation of this phase. He has also concluded that the solid-state reaction will not also occur during β-Si_3N_4 formation; however, atomic nitrogen and solid-state diffusion mechanisms are dominant [18, 19]. He has stated that the reaction between gaseous Si and atomic nitrogen results in β-Si_3N_4 formation [22, 25]. Jennings also concluded that since during nitriding, 22% volume expansion occurs while the specimen dimensions do not change, the reaction continues only if some new spaces are created in the compact. These new open spaces are created via Si transportation out of the particles in a form of liquid or vapor Si. Therefore, the reaction does not take place in a solid state [22]. In Jennings' model, after the formation of initial β-Si_3N_4, the β-Si_3N_4 forming reactions can continue via nitrogen diffusion through the hexagonal channels in the β-Si_3N_4 structure, as shown in Figure 2-5. The diffused nitrogen reacts with Si at the Si-Si_3N_4 interface. Since nitrogen diffusion rate in these hexagonal channels of the structure is high, the reaction at the Si-Si_3N_4 interface is the rate-determining step for the nitriding reactions [23]. If other options are not available, this is the only possible route for β-Si_3N_4 formation. The channels also favor the epitaxial growth of β-Si_3N_4 in this direction due to high nitrogen diffusion rate. The second possible way can be the diffusion of nitrogen through molten Si if liquid silicon exists in the system. This reaction path has a much lower activation energy resulting in the fastest rate. Therefore, in this way large β-Si_3N_4 crystals can form when a liquid phase exists [22]. Jennings suggested that although both solid state diffusion and melting

19

of Si or FeSi$_x$ compounds are promoted by increasing the nitriding temperature, it must be kept in mind that the presence of a liquid phase only decreases the activation energy of the nitriding reactions and is not mandatory for β-Si$_3$N$_4$ formation [18, 22]. Therefore, he concludes that both α- and β-Si$_3$N$_4$ can form from the gas phase reactions occurring on a solid surface depending on the presence of molecular and atomic nitrogen, respectively [22].
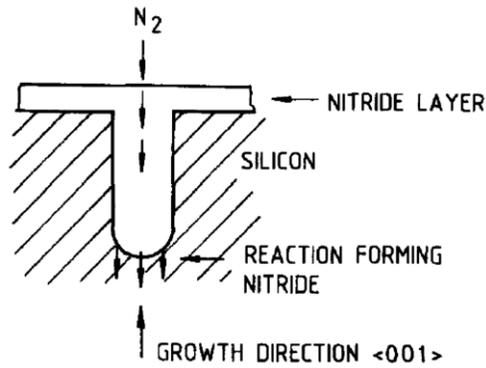
Figure 2-5. β-Si$_3$N$_4$ growth into a Si grain by nitrogen diffusion through the hexagonal channels; reaction occurs at the Si-Si$_3$N$_4$ interface at the bottom of the channel [23].

Finally, depending on how soon the under-lying silicon is sealed off from nitrogen, the nitriding reactions may stop and there may be some residual Si in the dense compact.

2.2.2. Parameters affecting the nitriding mechanisms

There are various parameters affecting the dominating nitriding mechanism. These parameters can be generally classified into firstly, impurities and secondly, process parameters including the fabrication method, nitridation temperature and pressure, the heating profile, nitriding atmosphere, Si particles size and shape, nitriding time, heating rate etc. [19, 23]. These variables can have an influence on both silicon (melting point,

diffusivity, etc.) and nitrogen reactivity [22]. The influence of some of these parameters will be explained here.

The finer the silicon particle size is, the more reaction area is available for Si and N_2 and also for Si vaporization [19]. Therefore, nitridation will be faster and less unreacted Si will remain at the end. This results in a significant decrease in the required nitriding temperature and time [23]. Finer Si powder also results in a higher α/β ratio due to accelerated Si vaporization causing Reaction 2-8 and 2-9 to move forward faster. A higher content of surface oxide in the form of SiO_2 on the Si particles may result in the formation of more SiO vapor based on Reaction 2-10. More SiO vapor causes a higher α/β ratio based on Reaction 2-9. Another influence of Si particle size is that finer α- and/or β-Si_3N_4 grains are produced from finer Si powder [23]. Finer Si powder also results in smaller porosity in the silicon green compact. Therefore, α-Si_3N_4 needles which grow in the porosity of the compact are impeded resulting in finer α-Si_3N_4. Regarding the β-Si_3N_4 formation mechanism, each Si_3N_4 grain forms from a Si grain; therefore, finer Si grains results in finer β-Si_3N_4 grains as well [23].

Metal impurities will influence the nitriding reactions significantly through the formation of molten metal silicides. These impurities may also dissociate N_2 to produce atomic nitrogen. Fe, which is the most common impurity in commercial RBSN ceramics, has several influences on the nitriding reactions. A small amount of Fe (~50 ppm) may cause a three-fold increase in the nitriding reaction rate [29]. Fe will help remove the native SiO_2 layer on silicon particles by increasing the oxygen ion mobility in the silica layer or providing nucleation sites for the devitrification phenomenon [11, 19]. It also accelerates β-Si_3N_4 growth in the presence of molten $FeSi_x$ and/or atomic nitrogen. It may also

promote α-Si$_3$N$_4$ formation (Reaction 2-9) through devitrification of the amorphous surface SiO$_2$ which leads to SiO vapor formation at the Si/SiO$_2$ interface [11, 29]. It also accelerates the nitriding reactions based on the melt movement (FeSi$_2$ melting point is 1207°C) in the compact and an increase in the reaction surface area [11]. Figure 2-6 shows the three effects of Fe impurity on the nitriding process. Generally, Fe significantly enhances the total rate of silicon conversion and basically, it is mentioned that Fe impurity promotes β-Si$_3$N$_4$ formation. The reasons why β-Si$_3$N$_4$ formation is enhanced are firstly, the formation of molten FeSi$_x$ as a rapid diffusion path and secondly, the dissociation of molecular nitrogen to atomic nitrogen [19, 22]. It can also be seen from Figure 2-6 that melting of Fe can leave pores in the conventional RBSN microstructure. These pores have a detrimental effect on the mechanical strength of the conventional RBSN ceramic.
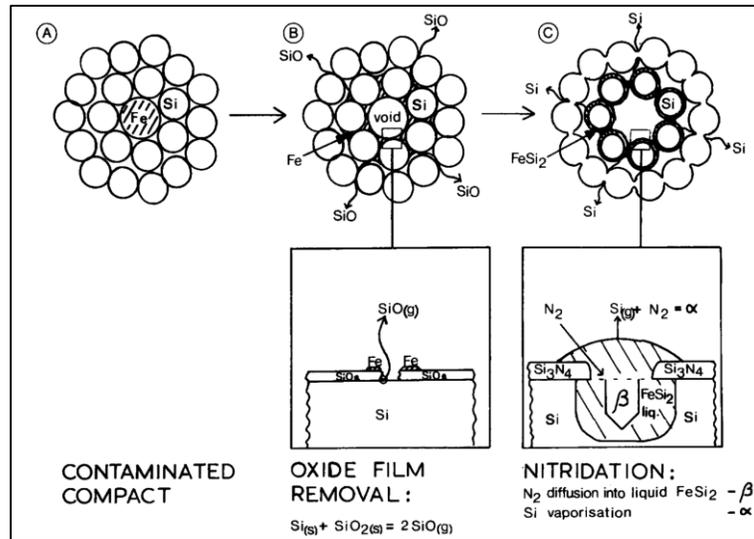
Figure 2-6. The effects of Fe impurity on the nitriding processes; b) removal of SiO$_2$ forming SiO and consequently α-Si$_3$N$_4$, c) formation of both α-Si$_3$N$_4$ and β-Si$_3$N$_4$ can be accelerated from molten FeSi$_x$ [29].

Other metallic impurities such as Al or Ca may have the same effect as iron. They can form low-melting eutectics which enhances the reaction rate [23]. Cation impurities such as Mn, Fe, Co, or Ni can also accelerate the reaction rate significantly [11].

The composition of the nitriding gas has also a significant influence on the nitriding reactions and the final microstructure. Water vapor, hydrogen, argon, helium, and oxygen in the nitriding atmosphere affect the reaction kinetics. A small amount of oxygen does not affect the nitriding reactions but it increases the α/β phase ratio due to SiO formation [22, 27]. It is also believed that oxygen, even in small amounts, removes atomic nitrogen which is responsible for β-Si_3N_4 formation based on the Jennings' model; therefore, it again increases the α/β ratio in the final RBSN by reducing the β content [22]. On the other hand, a high oxygen partial pressure may lead to Si oxidation and consequently, formation of surface SiO_2 which will stop N_2 penetration toward the unreacted Si. Therefore, nitriding reactions are hindered [23]. Water vapor can react with silicon and produce SiO vapor shown in Reaction 2-12. If Reaction 2-13 is slow compared to Reaction 2-12, water may increase the reaction rate [22]. On the other hand, hydrogen in the nitriding atmosphere will enhance the nitriding reactions significantly. It reduces the oxygen partial pressure and devitrifies the native oxide layer on Si particles resulting in an increases in the SiO(g) vapor pressure. Therefore, the SiO/N_2 reaction proceeds faster than Si vapor/N_2 and β-Si_3N_4-forming reactions which leads to a high α/β ratio [11]. In the presence of H_2, a finely textured and defect-free microstructure results in improved mechanical properties of the specimen [19, 23]. Inert gasses such as helium may only provide the system with more uniform heat transfer and they do not interfere with nitriding reactions [23]. It has been mentioned that the presence of some inert gases such

as argon, krypton, and helium in the nitriding gas can also accelerate the dissociation of molecular nitrogen to atomic nitrogen. The atomic nitrogen is required for the β-Si_3N_4 formation based on the Jennings' nitridation model [22].

$$Si\ (s) + H_2O \leftrightarrow SiO\ (g) + H_2 \qquad\qquad (2\text{-}12)$$

$$H_2O \leftrightarrow 2\ H_2 + O_2 \qquad\qquad (2\text{-}13)$$

The nitrogen pressure of the nitriding gas also affects the RBSN microstructure. At high N_2 pressures, a large number of Si_3N_4 nuclei form on Si surfaces. The consequence will be a homogenous fine microstructure. A large number of nuclei can also quickly seal the underlying silicon and stop the reaction from moving forward [22]. On the other hand, reducing the nitrogen partial pressure, significantly decreases the nitriding rate. A decreased number of Si_3N_4 nuclei in this case results in a coarser microstructure [23]. Nitrogen flow also affects the phase ratio and microstructure of RBSN ceramics. In a stagnant atmosphere a higher ratio of α/β is obtained since the nitrogen flow in a flowing atmosphere removes SiO vapor from the reaction zone resulting in less α phase formation [27].

In conclusion, among all the mentioned parameters and impurities, high nitriding temperatures, helium, argon, krypton, and Fe will increase β/α ratio but lower reaction temperatures, higher surface area, and the presence of H_2O, O_2, and H_2 will increase α-Si_3N_4 formation [22].

Table 2-1 summarizes many parameters that influence the microstructure of RBSN ceramics.

Table 2-1. The influence of the nitriding parameters on the nitridation process, microstructure, and properties of RBSN ceramics [10, 22]

Nitriding parameter	Influence on the α/β ratio
Low nitriding temperature <1350°C	High α/β ratio, fine microstructure, low nitriding rate
Medium nitriding temperature 1350°C-1412°C	Coarser microstructure, pore size increases
High nitriding temperature >1412°C	Higher β content, coarse structure, low strength and K_{Ic}
Large Si particle size	Slow nitridation, low strength
Fine Si particle size	High conversion rate, high α/β ratio, higher strength and K_{Ic}
High green density > 65-70%	Difficult to reach complete nitridation, lower strength in the case of inhomogeneous nitridation
No SiO_2 surface layer	Fast nitridation, high α content
Thin SiO_2 surface layer	High α content, finer microstructure, high strength and K_{Ic}
Thick SiO_2 surface layer	Slow nitridation, low strength and K_{Ic}
Iron (fine, dispersed, low content) low temperature	Accelerated nitridation, high strength, high β content
Iron (inhomogeneous)	Higher β content, faster nitridation, defect formation due to silicide formation, reduced strength
Hydrogen or ammonia	More homogeneous nitriding, high α/β ratio, fine microstructure, high strength and K_{Ic}
Flowing N_2	Coarse microstructure, pore formation due to SiO removal, low strength and K_{Ic}

Since many parameters influence the final microstructure and properties of a RBSN ceramic, the fabrication procedure must be designed carefully and precisely to get tailored properties. To get a high strength RBSN ceramic, high α/β ratio, homogeneous narrow pore size distribution, and fine nitrided grains are required [18]. Regarding the

first parameter, it is believed that high β contents are accompanied by the presence of large amounts of liquid phase during nitridation. Penetration and redistribution of the liquid phase in the compact result in large voids and defects which decrease the sample strength (Figure 2-6-C) [11].

2.2.3. RBSN microstructure and mechanical properties

Characteristic features of RBSN ceramics include porosity, α- and β-Si_3N_4 grains, and residual Si. The strength of the sample is significantly affected by the amount, distribution, and size of these phases. Any unreacted Si or melting of Si or silicides which may result in large voids are considered as structural defects and significantly influence the strength. These defects can exist in various sizes which depend on the structure of the green body. Fracture toughness of the RBSN is also dependent on the nitriding conditions and the resulting microstructures. A well-designed nitriding process results in RBSN ceramics with fine porosity and good mechanical properties [10].

RBSN ceramics show constant strength up to 1200-1400°C under inert atmospheres since there is no intergranular glassy phase in these materials. They also show excellent thermal shock and creep resistance. It must be kept in mind that thermal shock resistance, hardness, and elastic modulus are properties which depend on the microstructure; therefore, they are lower in RBSN ceramics than dense, sintered Si_3N_4 [10]. The oxidation in air is different. At temperatures higher than 1100°C, SiO_2 formation closes the fine porosity network of the RBSN ceramic and an increase in the strength can be seen. This strength enhancement is due to surface crack healing and the creation of compression due to different thermal expansion coefficients of RBSN and SiO_2. In the case of fine porosity, oxidation stops as soon as the surface porosity is sealed. On the

other hand, if the porosity is large or the oxidation temperature is low (< 1100°C), internal oxidation also occurs since pore closure is delayed [10].

2.3. Foams

2.3.1. Classification of foams based on the structure

The level of interconnectedness is a very important foam property and it is absolutely dependent on the foam structure. Depending on the pore interconnectivity, cellular structures are classified into open-cell and closed-cell. They can have cells surrounded by walls. In this case individual cells are isolated by the cell walls which make the structure closed-cell. On the other hand, cellular structures may have only cell edges called struts with no cell walls. Since only the struts are solid, the foam has an open-cell structure. It must be mentioned that although cell walls isolate the adjacent pores, in some structures there are some voids in the solid cell walls called cell windows. These windows connect the adjacent cells and make the structure of the foam open. Therefore, ceramic foams may have closed, open or partially open pores. Open-cell structures have interconnected porosity and they have various applications where permeability and fluid transport are important [7].

2.3.2. Foam fabrication techniques

The foam properties can be designed and customized for any specific application based on the composition and the microstructural features of the foam including the pore size, pore size distribution, total porosity, pore morphology, and the degree of pore interconnectivity [3]. On the other hand, all these structural features are dependent on the processing method. The foam fabrication technique must be selected and designed in a

way that it is capable of providing the required foam properties including pore structure, permeability, strength, sample size and shape, chemical composition, cost, etc. [30].

There are various techniques by which cellular ceramics can be fabricated. Since there is a rising demand for ceramic foams which can be used in novel and future applications, the number of new fabrication techniques capable of producing foams with tailored properties is growing.

The most straight forward fabrication method to produce ceramic foams is partial sintering of powder compacts to obtain partial densification and consequently leaving residual porosity in the body. This partial sintering process can be performed by adjusting the sintering conditions including the sintering temperature, sintering time, and the amount of sintering aids. Solid state reactions during sintering which result in pore formation may also be used to produce ceramic foams. This technique typically results in low porosity levels (<60 vol%) and closed structures [3, 4].

There are other flexible foam fabrication techniques by which the foam structure and properties can be designed and controlled. They include the replication technique, the sacrificial template method, and the direct foaming process [6]. These techniques are utilized to produce macroporous foams (pore size > 50 nm) with tailored pore size, pore morphology, and pore distribution [3]. In the following sections, the three above-mentioned techniques and the freeze drying method will be explained.

2.3.2.1. Replication technique

The replica technique which was invented in 1963 by Schwartzwalder [31] is based on the impregnation of a flexible cellular structure (usually a polymeric sponge) with a suspension containing ceramic particles followed by pyrolysis of the organic material and

a subsequent high temperature sintering process. Figure 2-7 shows the schematic of the replica technique. The replicated macroporous foam will acquire the same pore morphology and pore size as the initial porous template. The replica technique has become the most common technique in industry to produce ceramic foams for molten metal filtration due to its simplicity and flexibility. It is basically used to produce open-cell foams with different pore sizes and chemical compositions [4]. Suspension preparation is an important step in this technique. Rheological properties of the slurries, including viscosity, are very important and must be controlled precisely. On one hand, the suspension must be fluid enough so the excess slurry can be removed from the template and on the other hand, it should be viscous enough to stick to the template and provide a coating with a sufficient thickness on the struts of the template. After impregnation of a highly porous sponge, the excess suspension will be removed by passing the sponge through rollers or by using centrifugal force [3, 32]. The excess slurry inside the template must be removed since it results in closed-pore inhomogeneous structures which consequently affects the foam permeability and strength [30, 32]. Figure 2-8 shows how poor suspension characteristics result in closed cells in a replicated foam. It is reported that he suspension must have a high solid content of the order of 50-70 wt% and it must show some shear-thinning behavior. Obviously, the suspension maximum solid content may vary depending on the density of the dispersed particles. Thixotropic and thickening agents such as clays, colloidal silica, and carboxymethyl cellulose with dispersants can help obtain good rheological properties and consequently appropriate coatings [3]. Binders, plasticizers, and other rheological agents are also added to the suspension to improve the green strength and also prevent cracking of the ceramic

coating during drying and pyrolysis [3, 30]. Typical binders are colloidal aluminum orthophosphate, potassium and sodium silicates, colloidal silica, and magnesium orthoborate [3]. It must be mentioned that the porous template in this technique can also be coated by electrodeposition or physical vapor deposition (CVD) methods [1].
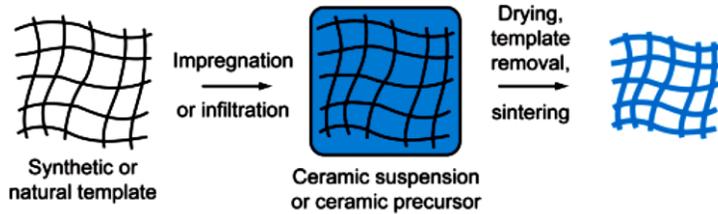
Figure 2-7. The schematic of the replica technique [3]
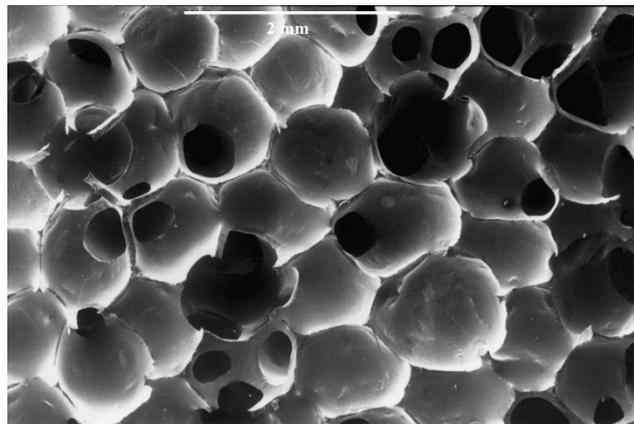
Figure 2-8. Closed cells in a replicated SiC foam containing 20 wt% TiC particles [33].

After drying of the ceramic-coated template, the polymer burn-out step must be performed. This is a critical step which must be controlled carefully. Based on the chemical composition of the polymeric template, the burn-out temperature can be selected in the range of 300 to 800°C [3]. Slow heating rates are typically used in order to avoid cracking of the coating due to rapid decomposition of the template and pressure build-up in the template struts. Sintering is the final step to densify the ceramic coating

which is performed under different atmospheres and at different temperatures based on the material.

Pyrolysis of the polymeric template leads to hollow ceramic struts which are characteristics of the replica technique. The hollow struts, which can be considered as the main disadvantage of the replication technique, will significantly affect the final mechanical properties of the foam including its strength. Due to gas evolution and different thermal expansion coefficients of the ceramic coating and the template, high internal stresses and consequently crack formation during pyrolysis cannot be prevented completely [4, 30, 34]. These cracks will obviously degrade the mechanical properties of the foam. Many attempts have been made to improve the strength of the replicated foams by improving the wettability of the suspension on the polymeric template, recoating the ceramic struts, and the addition of fibers (1-5 wt%) [3, 35] but the combination of cracks, hollow struts, triangular shapes of the voids, and high porosity result in very low strengths of the order of 0.5 to 2 MPa [30, 32]. Figure 2-9-a reveals an Al_2O_3 ceramic foam fabricated by using a polyurethane sponge template. A hollow ceramic strut of the foam fabricated via replication is also shown in Figure 2-9-b.
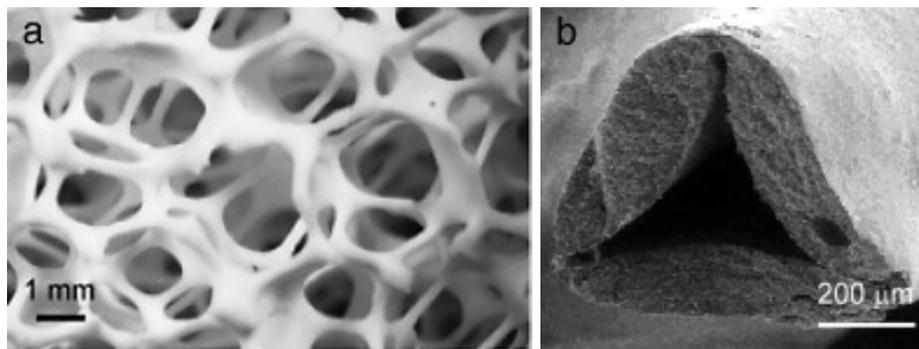
Figure 2-9. a) SEM image of an Al_2O_3 ceramic foam fabricated via replication, b) a hollow strut in a reticulated foam [3].

31

Many attempts have been made to improve the mechanical properties of the reticulated foam and fill the hollow struts. Repeating the impregnation of the template and the drying step increases the thickness of the foam struts resulting in higher strengths but lower permeability. Impregnation of the coated template can also be done after sintering of the previous layer using a suspension with a lower viscosity [1, 30]. To fill the hollow struts, infiltration with molten Si or glass can be performed. High wettability and low viscosity of the melts are very important in order to get desirable results. Immersion of the sintered foam in suspensions containing colloidal silica, alumina or other refractories results in improved strengths since these very fine particles can fill the voids and microcracks which exist in the microstructure [30].

Both synthetic and natural templates can be utilized for the replica technique. The most common templates are polyurethane sponges but other synthetic polymeric sponges can be used such as polyvinyl chloride, polystyrene, cellulose, and latex [30, 32]. The advantage of natural templates is their unique pore shape and morphology and their complex structures which typically cannot be found in synthetic templates. On the other hand, the main issues with the natural templates are low reproducibility and poor consistency of the foams and also unavoidable impurities which remain in the foam [32]. Important natural templates include calcium carbonate skeleton of algae or coral and wood. Corals are basically used to produce macroporous scaffolds for bone replacement and tissue engineering. Coral cellular structures can be directly converted into hydroxyapatite scaffolds by performing hydrothermal treatments at high temperatures and pressures [36]. The coral structure can also be used to produce hydroxyapatite scaffolds with improved mechanical properties via the sol-gel technique [3]. The cellular

structure of wood can also be utilized to produce ceramic foams. A carbon preform can be produced from wood through performing high temperature heat treatments under inert atmospheres. The preform can then be infiltrated with gases or liquids at high temperatures or with metal alkoxides followed by the sol-gel process to produce cellular ceramics [3]. Preceramic polymers, ceramic suspensions, or salt solutions may also be used to infiltrate the carbon preform. The replication of the carbon preform produces oxide, carbide, phosphate, and zeolite-containing cellular ceramics. It must be kept in mind that the wood replica technique is a time consuming and consequently, costly process. It also results in low strengths especially at high levels of porosity due to defects and flaws which form due to oxidation of residual carbon. Figure 2-10 shows different ways of transforming wood to a macroporous ceramic foam.
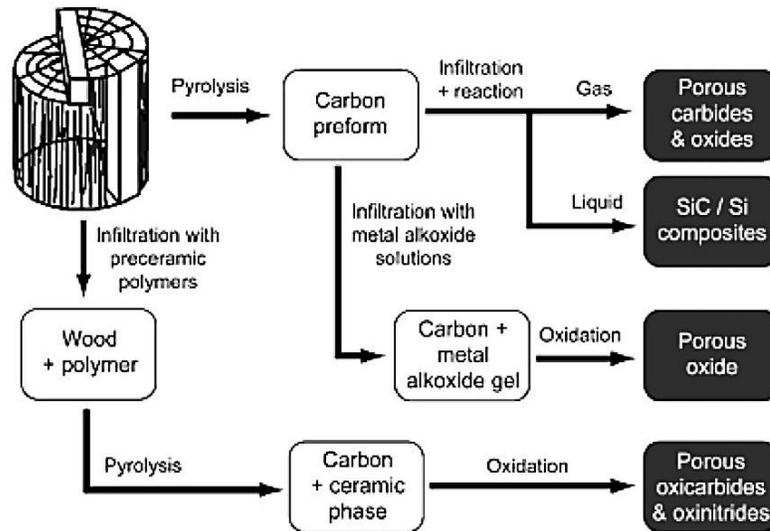
Figure 2-10. The schematic of the transformation of wood to macroporous cellular ceramics [3].

There are some other ways to produce carbon preforms. Organic polymer foams including phenolic resin or polyurethane foams can also be utilized to produce carbon foams through a high temperature heat treatment. Foaming petroleum pitch with

porogenic agents or coal pitch in the presence of volatile materials can lead to carbon preforms after a high temperature treatment at 2400-2600°C [30]. Graphite preforms can also be produced from mesophase pitch followed by a treatment at temperatures higher than 2800°C [37].

Generally, a ceramic suspension containing water, ceramic particles, and other additives can be replaced by preceramic polymers. In this case, the preceramic polymer is formed, then cross-linked and/or gelled to keep the desired shape. The last step is a high temperature pyrolysis step which converts the polymer to a ceramic material. Several ceramic foams such as ZrO_2, Al_2O_3, SiO_2, SiC, SiOC, mullite, and cordierite have been fabricated from polymeric precursors among which the most common compounds are SiC and SiOC [4]. The most common preceramic precursors for silicon-based ceramics are Si-based polymers including polycarbosilanes, polysiloxanes, polysilanes, and polysilazenes [4]. The backbone of these materials has Si atoms which will be converted to ceramic materials through a controlled high temperature heat treatment [4, 5, 7, 38, 39]. After cross-linking at a low temperature, pyrolysis of these polymers is performed between 900 and 1300°C in an inert atmosphere such as N_2 during which C-H covalent bonds will break and gaseous compounds such as H_2, CH_4, and other volatile compounds will be released. The use of preceramic polymers in the replication technique has some advantages [35]. On one hand, crack formation in the struts can be avoided if preceramic polymers are used. The reason is that they show higher wetting on the polymeric template and they also partially melt during pyrolysis both of which can avoid crack formation [4, 35]. On the other hand, the expansion and gas evolution during heating may cause large

stresses and consequently macrocracks in the foam struts [4]. Figure 2-11 shows a SiC-Si_3N_4 foam fabricated by the replication of a preceramic polymer.
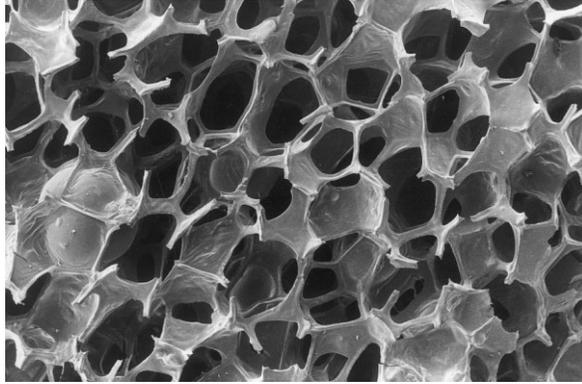
Figure 2-11. SiC-Si_3N_4 reticulated foam sintered at 1100°C [38].

As was mentioned before, the replica technique is quite flexible. Another variation of this technique is the conversion of the polymeric sponge to a vitreous carbon skeleton during pyrolysis. The carbon template can then be infiltrated with reactive gaseous species, typically by the CVD method, resulting in macroporous ceramic foams composed of a carbon core and an external layer of between 10 to 1000 μm. Based on the gas composition, foam with different compositions including oxides, carbides, borides, nitrides, and silicides can be produced [3, 30].

The replica technique is simple and it can be utilized to fabricate macroporous foams from any ceramic material which can form a slurry; therefore, it's very flexible in terms of the chemical composition of the final product. The foams fabricated by this technique basically have open-cell structures since the produced foam is a replication of the original template which must be fully accessible and interconnected to provide complete impregnation of the ceramic suspension or preceramic polymer. Various ceramic foams with different chemical compositions such as Al_2O_3, ZrO_2, ZrC, ZrN, SiC, Si_3N_4, SiO_2, TiO_2, TiN, TiC, TiB_2, MgO, Cr_2O_3, hydroxyapatite, mullite and several ceramic

35

composites have been fabricated by the replication technique [3]. A wide range of pore sizes, pore morphology, and porosity is achievable via this method. Foams fabricated by this technique have a very well-defined pore morphology with highly interconnected structures and their total open porosity may vary from 40 vol% to 95 vol% [1, 3, 32]. This technique provides us with an accurate control on the pore size, pore morphology, and pore size distribution since the fabricated foam is a replication of the initial template. The possible pore size range is from 200 μm to 3 mm. As can be seen the minimum pore size is approximately 200 μm which can be considered as another limitation of this technique. Coating of the template is problematic for pore sizes less than 200 μm since complete impregnation of the template may not occur [1, 3, 4].

2.3.2.2. Direct foaming

Direct foaming, is a foam fabrication process in which gas bubbles are the pore forming agents. In this technique, gas bubbles are incorporated into a ceramic slurry or a ceramic precursor followed by the consolidation, drying, and sintering processes. Figure 2-12 shows the schematic of the direct foaming technique.
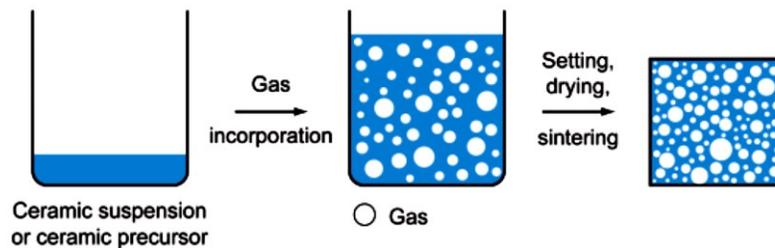
Figure 2-12. The schematic of the direct foaming technique [3]

Bubbles can be created either chemically via chemical reactions (such as cross-linking of a silicone resin resulting in water formation or oxidation of C or SiC causing CO_2 creation) or physically by a temperature rise (in the case of volatile liquids like freon and

pentane or solids which decompose upon heating like $CaCO_3$), pressure drop, use of blowing agents, gas injection, or mechanical frothing [1, 3, 4, 30, 32]. In this technique, the total porosity and the pore size are dependent on the amount of incorporated gas and the size of the gas bubbles at the setting time, respectively [3]. Due to drainage, coalescence, and Ostwald ripening phenomena, wet foams are not stable thermodynamically and the bubble size increases continuously. These are the main destabilization mechanisms which may even result in foam collapse within a few seconds after air incorporation into the suspension. In drainage, a physical separation occurs between the light bubbles and the heavier liquid due to gravity. Therefore, gas bubbles will float and form a very dense and highly packed foam on the top of the suspension while the liquid will be mainly at the bottom. In this case, due to a high accumulation of the bubbles, thin films are formed between the adjacent cells. This results in the formation of plateau borders at the intersection of three neighboring thin films [3]. The rate of drainage is dependent on the density and viscosity of the liquid [1]. In coalescence which is the second destabilization phenomenon, the thin film collapse may occur due to van der Waals attractive forces between the bubbles. The attractive forces push the bubbles toward each other resulting in very thin and weak cell walls which finally collapse [1]. Surfactants or solid particles with tailored surface chemistry can be utilized to stop coalescence. Ostwald ripening or disproportionation is the most challenging destabilization process in foams which happens due to different Laplace pressure between bubbles with different sizes. The pressure (ΔP) is dependent on the gas-liquid interface curvature and is equal to $2\gamma/R$ where γ is the gas-liquid surface energy and R is the gas bubble radius. Due to different Laplace pressures in different bubbles, there is

continuous gas diffusion from the smaller bubbles to the larger ones which causes the larger bubbles to grow at the cost of the smaller ones [3]. All these three phenomena may cause foam collapse in a few seconds after foaming. Therefore, the most problematic step in the direct foaming technique is to control the destabilization processes and obtain pore sizes within the desired range [1, 3, 4, 32]. The stability of the bubbles is dependent on many factors in the gas-liquid system including temperature, pressure, viscosity, surface tension, gas solubility, and stabilizing agents which can be surfactants or solid particles [1]. It should be mentioned that in this technique, the selection of the suspension additives may be critical since they may affect the foam stability and result in bubble destabilization or foam collapse. Figure 2-13 reveals two macroporous ceramic foams produced via the direct foaming technique.
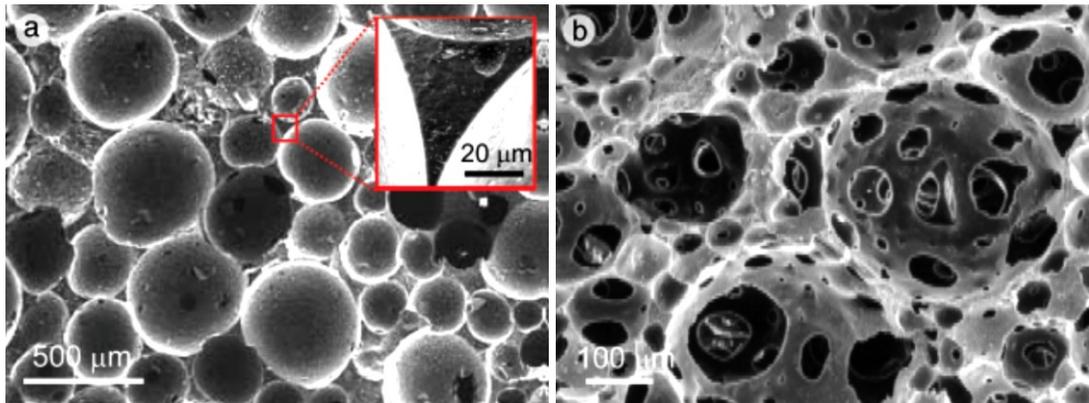
Figure 2-13. Macroporous ceramic foams fabricated by the direct foaming technique; a) a closed-cell foam produced from preceramic polymers and polyurethane precursors, b) an open-cell foam fabricated by in situ polymerization of monomers [3].

The stabilization processes can be performed by surfactants or solid particles with tailored surface chemistry [3]. Surfactants can be nonionic (PEG-8 octyl phenyl ether or poly(dimethylsiloxane) copolymer), anionic (sodium dodecyl sulfate), cationic (benzethonium chloride) and proteins (albumin) [3]. Surface active agents will be

38

adsorbed at the bubble surface and decrease the liquid-gas interfacial surface tension which results in delayed coalescence and disproportionation processes. Surfactants will stabilize air bubbles but due to their low adsorption energy at the gas-liquid interface, stabilization will not last very long. In the case of long-chain surfactants, bubbles will collapse after a few minutes but in the presence of proteins, foam breakdown may occur after a few hours [3, 30].

In the case of particle stabilized foams, due to long-term stability which can be achieved, finer pore sizes can be obtained [3]. The particle adsorption at the air-water interface is achieved through the adsorption of short-chain amphiphilic molecules (usually carboxylic acids) on the surface which increases hydrophobicity of the particles. These amphiphiles will be adsorbed on the particles surfaces by their polar sides and then leave their short hydrophobic tail in contact with water. There is a critical amphiphile concentration at which the surface tension of the suspension decreases sharply and the bubbles become stabilized [1, 3, 40]. Some of these amphiphiles include valeric acid for α-Al_2O_3, propyl gallate for ZrO_2, and hexyl amine for SiO_2 [3]. Figure 2-14 compares foams stabilized by surfactants and particles. It can be seen that in the foams stabilized by particles, bubble coalescence and disproportionation can be impeded for several days. The irreversible adsorption of colloidal particles at the gas-liquid interface is the reason why particle stabilized foams are much more stable that those stabilized by surfactant. In the case of surfactant stabilized foams, the continuous adsorption - desorption phenomena of the surfactant molecule results in faster destabilization and foam collapse [3].
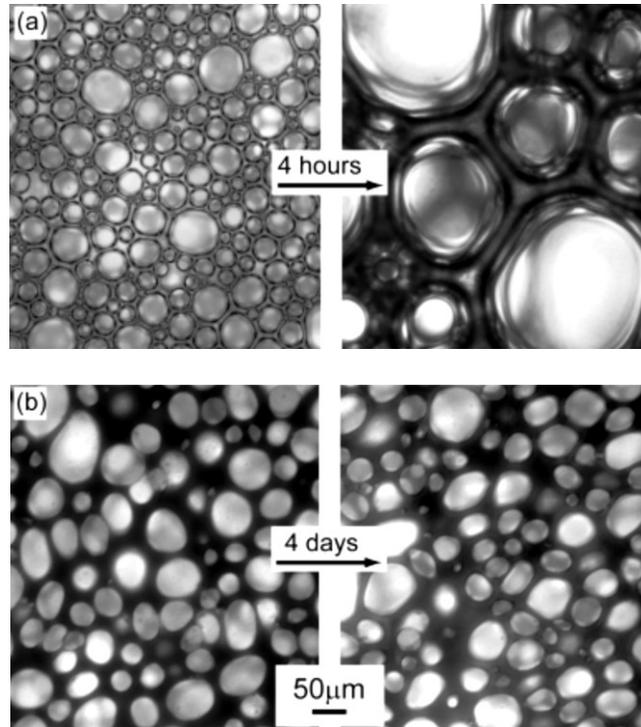
Figure 2-14. Comparison between foams stabilized by a) surfactants and b) particles [3]

Since direct foaming is based on creating gas bubbles in a liquid medium, consolidation of the system is typically required. Setting time in direct foaming is very critical since foam destabilization is highly probable right after bubble incorporation. The final foam cell size is mainly dependent on the setting time and the rate of the destabilization phenomena. Therefore, it is very challenging in direct foaming to obtain small pore sizes and a narrow pore size distribution in the foam. Small pore sizes of the order of 50 μm can only be obtained if the surfactant is highly effective and the setting time is very short. Some of the common consolidation techniques are condensation of thermosets [38], solidification of thermoplastics [41], sol-gel setting [42], gel-casting [43 - 46], temperature induced setting of polysaccharides [47, 48], and temperature or pH induced setting of proteins [47, 49].

The combination of direct foaming and sol-gel was also successful in fabricating foams. Colloidal silica or alkoxides can be used as the precursor to prepare silica foams while Freon or air incorporation was used for foaming [50 - 52].

Direct foaming could also be modified based on the concept of the replication technique in a way that hollow struts are avoided in the fabricated foam. In this case, the foam template is formed based on in situ polymerization reactions of polyurethane precursors such as polyols and isocyanates. The ceramic particles are dispersed in organic solutions containing the polyurethane precursors. The suspension is then foamed in the presence of surfactants and sets due to thermosetting reactions between the precursors. On one hand, the polyurethane precursors play the role of a blowing agent and on the other hand; they set the foam structure after polymerization. In this technique foaming occurs due to both physical and chemical blowing phenomena which are evaporation of the solvent due to the exothermic polymerization reaction and CO_2 formation due to the reaction between the chemicals, respectively [3]. It must be mentioned that polymerization of the polyurethane preforms and its burn-out process are not environmentally friendly since toxic NO_x gases will be produced [53].

Like the replica technique, preceramic polymers can also be used in direct foaming. In some studies macroporous ceramic foams including SiC, SiOC, and SiNC were also produced by direct co-foaming of preceramic polymers through in situ polymerization of the polyurethane precursors [2, 5, 6, 54, 55]. Polyurethane in this case has both the role of a blowing aid and also the structural template. A SiOC foam produced by this method is shown in Figure 2-15. The choice of the polyurethane precursors and the types and amounts of the solvents and surfactants will affect the final foam architecture,

interconnectivity, and flexibility since flexible, semi-rigid, and rigid polyurethane precursors can be used [56]. Ceramic foams with the compositions mentioned above can also be consolidated without the use of polyurethane precursors. In these cases, consolidation is based on silicone-based polymers which have thermosetting properties and the foaming part is done by using physical blowing agents [7] or applying a pressure drop technique [57]. It must be mentioned that these polymeric materials shrink significantly during conversion to ceramic materials. They also produce large amounts of gaseous by-products with extensive weight losses [7].
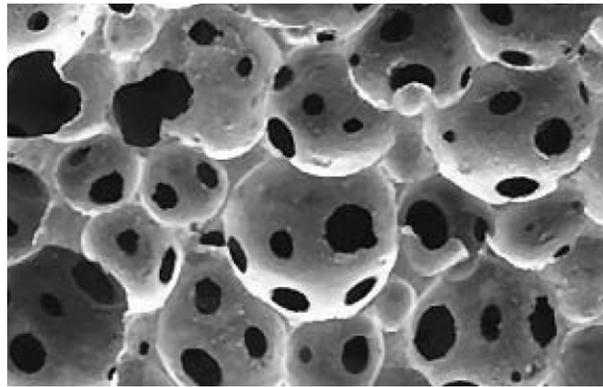
Figure 2-15. A SiOC foams produced by direct foaming of a preceramic polymer [7].

Glass foams can also be produced based on direct foaming. Glass powder is mixed with a foaming agent including hydroxides, carbonates, sulfates, carbides or carbon powder. Bubble formation occurs at higher temperatures when the glass becomes a viscous liquid. The created bubbles are trapped in the viscous melt resulting in a closed-cell foam [30]. The direct foaming technique in which bubble stabilization is done by surfactants, is capable of producing foams with pore sizes in the range of 35 μm to 1.2 mm and porosity from 40 vol% to 97 vol%. In the case of particle stabilized foams, pore sizes from 10 to 300 μm and porosity of the order of 40 vol% to 93 vol% can be obtained [3]. As can be seen in Figure 2-13, the production of both closed-cell and open-cell structures are

possible. The degree of interconnectivity can be designed by controlling the foam stability, air content, solid concentration, and setting time [1, 30, 32]. Closed cells are formed when no film rupture occurs during the consolidation step but open-cell foams will be produced if partial film rupture happens due to partial destabilization processes. Therefore, in order to get an interconnected structure, there must be a precise balance between the destabilization and stabilization phenomena. It must be mentioned that maintaining that accurate balance and controlling film rupture are critical and problematic in open-cell foam [1, 32]. Generally speaking, the direct foaming method may lead to graded and anisotropic structures since the rate of bubble expansion is different in the axial and lateral directions in the suspension. This inhomogeneity can be controlled and minimized by precisely designing the fabricating procedure. There are problems in both producing a narrow pore size distribution and also large cells in the foam due to bubble instability [1, 4, 30]. Another disadvantage of foams fabricated by direct foaming can be extremely thin cell walls at high porosity levels (> 90 vol%), which results in poor mechanical properties [3].

2.3.2.3. Sacrificial template

In the sacrificial template method, sacrificial pore-forming agents will be distributed in a continuous matrix of ceramic particles or ceramic precursors. After fabricating a biphasic body composed of both components, the sacrificial phase will be extracted to create a porous foam. Figure 2-16 reveals the schematic of the sacrificial template technique. In contrast to the replica technique, this method ends up in a negative replica of the original sacrificial template. Figure 2-17 reveals two foams fabricated using the sacrificial template technique.
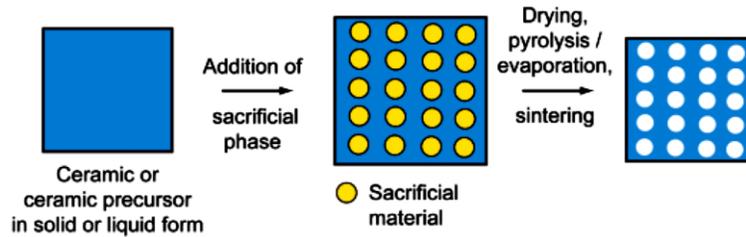
Figure 2-16. The schematic the sacrificial template technique [3].
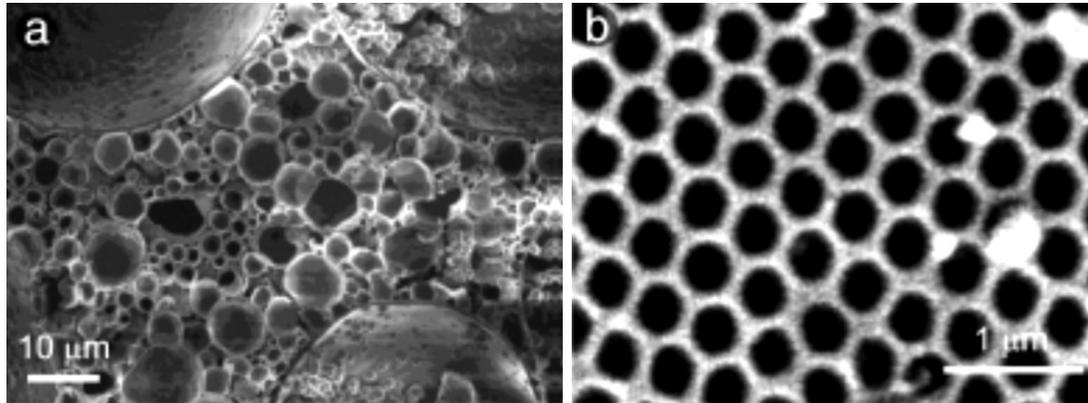
Figure 2-17. Macroporous ceramic foams fabricated via the sacrificial template method; a) TiO_2 foam

fabricated by emulsion templating, b) SiO_2 foam produced by using polystyrene beads [3].

There are various techniques with which the initial two-phase body can be fabricated from the sacrificial phase and ceramic particles. These techniques include all the traditional ceramic processing techniques such as pressing, making a suspension of the components followed by casting, and impregnation of the previously formed sacrificial preform with a preceramic polymer or a ceramic slurry [3, 32]. In all these processes, consolidation of the two-phase body must be performed in a way that the structure does not collapse during the sacrificial phase extraction. In the case of suspensions, setting agents and binders can be used for consolidation. Metal alkoxides and hydroxides as the precursor can also be set through sol-gel processes. If preceramic polymers are used as a ceramic precursor, cross-linking of the polymer molecules in a curing process performed at a temperature lower than the burn-out temperature consolidates the body [3].

44

Various sacrificial pore formers can be employed and based on the type of the pore former, different extraction processes are performed. The pore formers can be generally classified into synthetic and natural organics, liquids, salts, metals, and ceramics. Some common organic pore formers are polymer beads (PVC, PS, PVB, PMMA, LDPE), nylon, sucrose, starch, graphite, carbon black, wax, cellulose, gelatine, dextrin, saw dust, almond crust, etc. [1, 3, 30, 32]. The pyrolysis step is very critical in this technique since the gaseous by-products of the pyrolysis reactions and the difference in the thermal expansion coefficients of the components may cause cracks within the porous body [3, 30, 32]. Generally, synthetic and natural organic materials can be pyrolized between 200 to 600°C. Other sacrificial materials including salts (NaCl [58], $BaSO_4$, and K_2SO_4 [59]), ceramics (ZnO, SiO_2), and metals (nickel) can be extracted by chemical dissolution such as washing by water or chemical leaching [3, 32]. The consolidation step must be done in a way that a continuous ceramic phase forms prior to leaching. The chemical leaching process must also be designed in a way that the pore-forming agent is removed but the ceramic matrix stays unaffected. There are some other pore forming agents such as water, oils, and materials that can be easily sublimated such as naphthalene. This group of materials does not accelerate the slow extraction process but on the other hand, they may create less gaseous products and residual stresses during extraction [3, 32]. A combination of these sacrificial phases can also be used such as NaCl and a soluble polymer such as PVA both of which can be chemically leached by water [60].

In another class of the sacrificial template technique, aqueous or non-aqueous emulsions can be used to make ceramic foams. Oil in water can be an example in which the oil-water interface can be stabilized by surface modified particles. The utilization of a third

phase such as water in non-aqueous systems or air in aqueous emulsions can help obtain a desired pore size distribution [3].

Expandable polymeric microbeads can also be used to produce ceramic foams through the sacrificial template technique. The microspheres are dispersed in ceramic suspensions which are cast in a mold. Temperature-induced expansion and setting phenomena occur concurrently. Upon temperature increase, the polymer shell of the beads softens above the glass transition temperature of the thermoplastic component of the copolymer. The combination of shell softening and an increase in the internal pressure of the microsphere can result in expansion of more than 40 times if the temperature is high enough. After expansion of the beads, ceramic particles are trapped in the empty spaces between the expanded beads resulting in the formation of a macroporous ceramic foam [61].

Like the other two foam fabrication methods, preceramic polymers can be used with the sacrificial template technique. In terms of consolidation and forming a two-phase body, preceramic polymers can be shaped by uniaxial pressing or conventional plastic forming techniques such as extrusion, injection molding, resin transfer molding, and melt spinning with low processing costs [7, 62]. The first step after fabricating the two-phase body is the burn-out of the sacrificial phase followed by a high temperature pyrolysis step under an inert atmosphere to convert the preceramic polymer to a ceramic material [62]. Typically, a cross-linking step is performed before burn-out to strengthen the body and avoid sample collapse [4]. Figure 2-18 shows SiOC foams fabricated by the sacrificial template technique using expandable and PMMA beads.
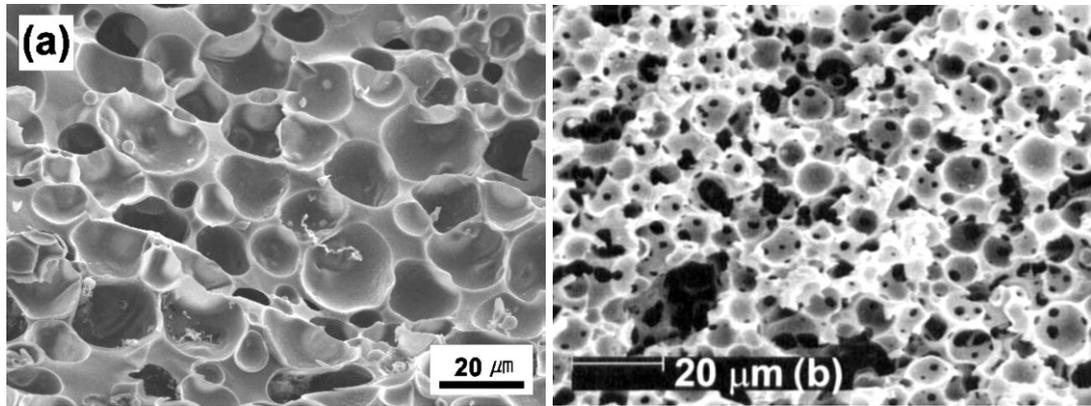
Figure 2-18. SiOC foams fabricated by the sacrificial template technique using a preceramic polymer and; (a) 9-15 μm expandable microbeads [63], (b) 5-100 μm PMMA beads [62].

The sacrificial template technique is very flexible in terms of the chemical composition of the foam that can be produced. Al_2O_3, YSZ, SiC, Si_3N_4, SiO_2, TiO_2, zeolite, cordierite, hydroxyapatite, glasses, mullite and other ceramic composites can be produced by this method. The main advantage of the sacrificial technique is its capability for tailoring properties. Pore size, pore morphology, pore size distribution, total porosity, and pore interconnectivity can be precisely controlled based on the use of an appropriate sacrificial pore former [1]. It must be mentioned that foams with very narrow and even monomodal pore size distribution can be produced by this technique in comparison to other methods which may result in a wide range of pore size [32]. This technique is also capable of producing graded structures through templates composed of layers of sacrificial phases of different sizes [32]. Depending on the volume fraction of the sacrificial agent and its nature, both open and closed cells are possible [1, 30]. Cellular ceramics with long anisotropic pores can also be produced. This technique is capable of producing foams with a wide range of porosity from 20 vol% to 90 vol% and a broad range of pore sizes from 1 μm to 700 μm [3]. Compressive strength of the ceramic foams fabricated by the sacrificial template can be in the range of 10 to 300 MPa [4]. Another important feature

47

of this technique is that the extraction of the pore former does not introduce flaws in the ceramic struts in contrast to the replica technique. Therefore, foams with much higher strengths can be produced by this method compared to the replicated foams.

2.3.2.3.1. Freeze drying (freeze casting)

Freeze drying can also be utilized to produce ceramic foams [64, 65]. This method can be classified as a sacrificial template technique since a sacrificial phase, which can be a frozen material with a low sublimation temperature, will be extracted from the system to produce porosity in the structure. High porosity and interconnectivity can be obtained by this technique and the final microstructure depends on the slurry concentration, freezing rate, and sintering conditions [66]. It is clear that the pore morphology is a duplicate of the dendritic frozen vehicle and is typically in the form of channels, shown in Figure 2-19. It must be mentioned that by controlling the solidification phenomenon and the temperature gradient, aligned pore channels can be produced in the sample [40]. The major disadvantage of the freeze casting technique is the difficulty of controlling the pore size, pore size distribution, and pore shape. The green body after sublimation has also a low strength which makes the body very fragile and difficult to handle [40].
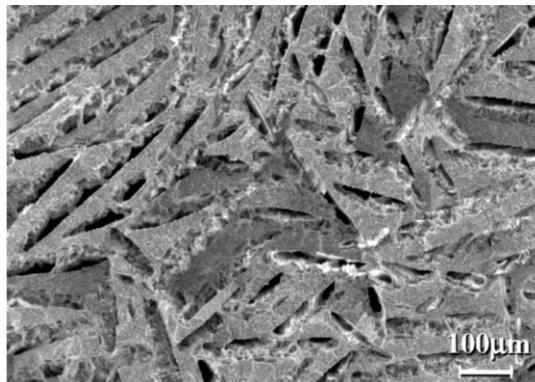
Figure 2-19. Microstructure of an Al_2O_3 foam produced by freeze casting; the cross-section perpendicular to the freezing direction [64].

48

Two common materials for freeze drying are water and camphene ($C_{10}H_{16}$, T_m=44-48°C). The reason that water is replaced with camphene is the very low processing temperature of -40°C required for freeze casting of aqueous suspensions [67]. In an investigation, hydroxyapatite foams have been produced by freeze drying of suspensions containing hydroxyapatite particles (10-20 vol%), camphene as the freezing vehicle, dispersant, and binder. The suspensions were prepared at 60°C. Solidification of the slurry occurred in less than 30 min at 20°C followed by sublimation and sintering [65]. The microstructure of the fabricated foam is shown in Figure 2-20.
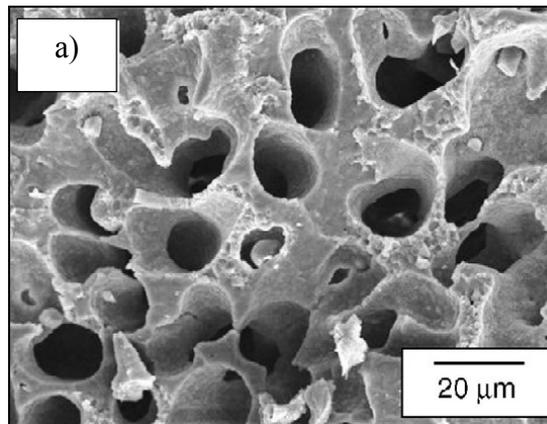
Figure 2-20. Microstructure of a porous hydroxyapatite foam produced by freeze casting; the cross-section parallel to the freezing direction [65].

In a study, freeze casting was combined with the gel-casting and the replication techniques to make hydroxyapatite foams [68]. Tertiary-butyl alcohol (TBA) with a melting point of 25.3°C was used as the freezing component. Polyurethane foams were dipped in a warm suspension. Then, directional solidification occurred on a stainless steel plate at <0°C followed by heating at 80°C for polymerization of the monomer. Sublimation, polymer pyrolysis, and sintering were the last steps to make the

hydroxyapatite foam with a wide range of pore size from less than 2 μm to more than 200 μm [60].

2.3.2.4. A comparison between the main foam fabrication techniques

Figure 2-21 reveals the range of porosity and pore size that can be obtained by the three main foam fabrication techniques including the replica, sacrificial template, and direct foaming. The graph shows that direct foaming technique based on surfactants may provide the highest level of porosity while the sacrificial template technique has the highest flexibility in terms of average pore size.
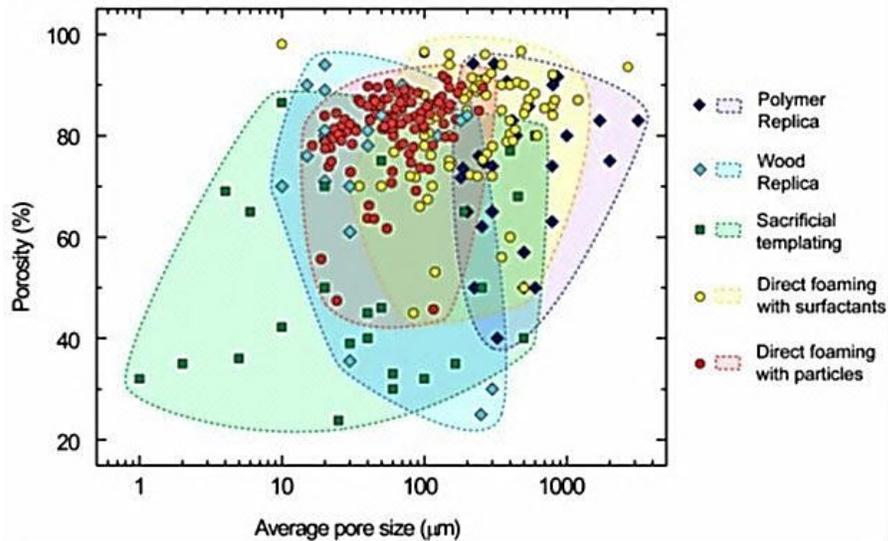
Figure 2-21. Porosity and average pore size obtained by the main foam fabrication techniques including replica, sacrificial template, and direct foaming [3].

Figure 2-22 shows a comparison between the three main foam fabrication techniques in terms of compressive strength of the foam. As was mentioned before, the replica technique leads to foams with very poor mechanical properties. Both the sacrificial template method and the direct foaming technique, based on surfactants, provide much higher strengths. But the critical issue of the surfactant stabilized foams is the short

lifetime of the bubbles which limits the pore size and pore size distribution of the produced foams.
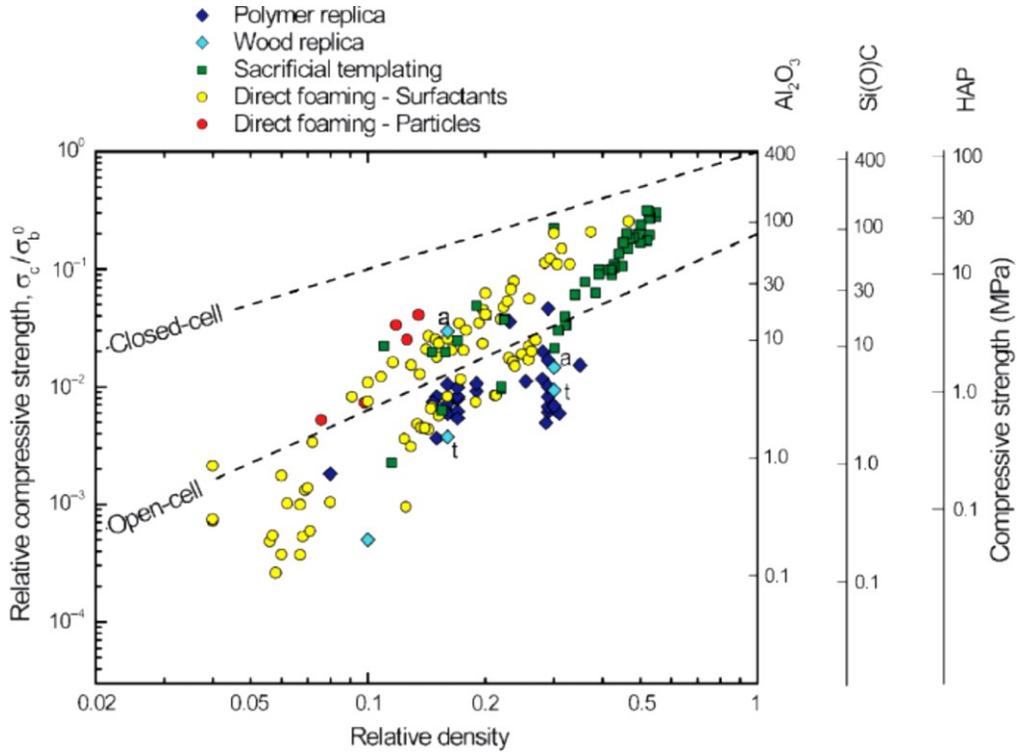
Figure 2-22. A comparison between the replication, sacrificial template, and direct foaming techniques in terms of compressive strength of the foam [3].

As was mentioned before, replicated foams suffer from hollow struts which result in poor mechanical properties. In terms of pore structure including the pore size, pore morphology, and pore size distribution, the sacrificial technique is much more powerful than the direct foaming technique in which the stabilization of the bubbles is the major challenge. Thus, sacrificial template technique was utilized as the foam fabrication technique in this study.

2.4. Gel-casting as a consolidation technique

Generally, consolidation is an unavoidable step in the fabrication of either dense or porous ceramic bodies. All the ceramic foams which have been produced from ceramic suspensions or preceramic polymers must go through a consolidation step to make solid monoliths before the completion of the fabrication procedure. On the other hand, one of the most challenging steps in ceramic processing is the fabrication of complex-shaped ceramics with a high reliability and low cost. In most high-tech applications, the component must fulfill specific and complicated geometrical requirements. In order to produce the final complex shape with exact dimensions, a costly routine procedure is sintering a simple-shaped green body which is followed by machining to meet the geometrical requirements. An alternative to avoid or reduce the machining of the ceramic body is to design and utilize a consolidation technique which is capable of producing complex shapes. Recently, consolidation techniques which offer near-net shape forming advantages are of particular interest due to the high costs of the post sintering machining processes. The possible consolidation method is dependent on the processing technique which can be generally classified into dry- and wet-processing routes. In comparison, wet-processing methods such as colloidal processing have many advantages such as a lower production cost, higher homogeneity and reliability and less flaws and defects in the final products [40]. There are various colloidal forming techniques such as slip casting, tape casting, direct coagulation, injection molding, and gel-casting which are able to consolidate ceramic slurries into a solid green body.

Gel-casting is a near-net shape, in-situ consolidation technique capable of producing high-quality advanced ceramic components with complicated shapes. Gel-casting was

first developed by Omatete and Janney in the 1960s [40]. The process is based on polymerization of monomers in a ceramic suspension resulting in a three dimensional macromolecular network which immobilizes the ceramic particles together to create the desired shape [40]. It offers many advantages including high homogeneity compared to dry processing techniques, short processing times in comparison to slip casting, no flaw creation during polymer pyrolysis compared to injection molding, high green strength even sufficient for machining, low cost machining, and capability of producing complex shapes [40]. Gel-casting can also be combined with different foam fabrication techniques including replica, direct foaming, and sacrificial template to consolidate the body. In this process, gel-formers such as a monomer and a cross-linker are dissolved in a solvent such as water to get a premix solution. In the next step, a suspension with a high solid content and low viscosity will be obtained by the addition of ceramic particles and other required additives. This suspension is finally set by free radical polymerization of the monomers resulting in a three dimensional network of a polymer which immobilizes the dispersed particles to form the desired shape. Polymerization may be accelerated and facilitated in the presence of an initiator and a catalyst. Regarding the organic monomers used in gel-casting, the main monomer is typically monofunctional which has a single double bond and is capable of forming a homopolymer with a linear structure. In contrast, the cross-linker has at least two double bonds to form a gel with a cross-linked or network structure [69]. After setting, drying is the next step followed by binder removal and high temperature sintering. It must be mentioned that the gel-cast sample can be machined in its dried state to even more complex shapes since the sample is strong enough to support stresses imposed during handling and machining. This results in low-cost and easy

machining if required. This technique has many other remarkable advantages including a short processing time, the possibility of using both aqueous and nonaqueous solvents, high wet and dry strengths, the option of using different mold materials, machinability, and the capability of producing large samples [70, 71]. Table 2-2 shows a comparison between the three most common processing techniques including slip casting, gel-casting, and injection molding.

Table 2-2. A comparison between slip casting, gel-casting, and injection molding [69, 70].

Parameter	Slip casting	Gel-casting	Injection molding
Setting time	1-10 h	5-60 min	1-2 min
Green strength	Low	Very high	High
Mold material	Plaster	Very flexible (metal, ceramic, polymer)	Metal
Binder removal	2-3 h	2-3 h	Up to 7 days
Specimen size	> 1m	>1 m	Diameter must be ≤ 3 cm
Distortion during drying or binder removal	Minimal	Minimal	Can be severe

Internal stresses in gel-cast bodies can be created due to non-uniform shrinkage during forming (temperature or initiator gradients) or drying (moisture or temperature gradient) [40]. In gel-casting the water content of the suspension is not removed by the mold like in slip casting and it is trapped in the sample. Removing the whole water content of the sample must be performed in a controlled manner which makes the drying step one of the most critical steps in gel-casting. If not carefully designed, it may cause large internal stresses and consequently warpage and cracking of the component. Another parameter which can cause cracks and distortion in the gel-cast sample is the amount of drying

54

shrinkage which is significantly dependent on the suspension solid content. The suspension solid content must be above 50 vol% in gel-casting to avoid a large drying shrinkage. After drying, the sample contains ~3 wt% polymer compared to ~30 wt% binder in injection molding [72].

The most common gel-formers are monofunctional acrylamide as the monomer and difunctional N,N′-methylenbisacrylamide as the cross-linker. There are also some alternative gel formers shown in Table 2-3. There are some factors which must be taken into consideration when selecting a monomer – cross-linker system. Some monomers are highly ionic which adversely influence the particle dispersion in the suspension. Some other monomers only form a gel at very high concentrations (>40 wt%) which make the processing difficult and expensive [70]. The gel strength is also very important. It shows the efficiency of the monomers. It also significantly affects the possibility of performing machining steps before sintering. The gelling precursors should also be able to provide fast gelation especially in the case of direct foaming where foam collapse is the major issue. They must not significantly increase the suspension viscosity when trying to produce homogeneous foams with uniform and strong struts.

Table 2-3. Common monomers, cross-linkers and initiators in gel-casting [44, 70].

Monomer	Cross-linker	Initiator
Ammonium acrylate	Poly(ethylene glycol) diacrylate	Ammonium persulfate
N-hydroxymethylacrylamide	Poly(ethylene glycol) dimethacrylate	Azobis [2- (2-imidazolin-2yl) propane]
Methacrylic acid	Trialyl amine	Azobis (2-amidinopropane)
Methacrylamide		
Dimethyl aminoethyl methacrylate		
Methoxy poly(ethylene glycol) monomethacrylate		
N-vinyl pyrrollidone		

It must be mentioned that some of these monomers such as acrylamide are toxic [3]. There are some other natural and less harmful polymerizable gelling agents such as gelatine [49, 73], ovalbumin [47, 53], bovine serum albumin [46], sucrose [74, 75], agar [76], agarose [77], carrageenans [78], methylcellulose [48, 79], ammonium alginate [80], starch [81], and proteins [82] which can replace for toxic monomers. These setting agents are less efficient compared to monomers and setting occurs after a temperature change or a pH change. The setting process in these systems will be more problematic if increasing the temperature or changing pH is not possible. As an example, heating to higher temperatures before casting may cause unwanted evaporation of the solvent or other components. Another major limitation of these environmental-friendly gelling agents is the slow rate of gelation which makes the situation more critical especially in direct

foaming processes where small pores less than 200 μm with a narrow pore size distribution are desired.

Gel-casting has been used for consolidation of many dense and porous oxide and non-oxide ceramics including Al_2O_3 [43, 44, 83 - 86], SiC [87, 88], hydroxyapatite [89, 90, 91], Si_3N_4 [20, 92, 93] etc. To the best of the author's knowledge, this method has also been utilized only for dense silicon bodies [94 - 98].

2.5. Silicon nitride foams

2.5.1. Sintered Si_3N_4 foams

Si_3N_4 foams have recently received great attention due to their remarkable properties and potential. They offer high strength, high stiffness, good toughness, high temperature resistance, high corrosion resistance, good wear resistance as a Si_3N_4 ceramic and they show permeability, special thermal properties, and low densities as a foam [99]. Although several ceramic foams have been produced commercially, Si_3N_4 foams are still under investigation.

As was mentioned previously, the simplest method to produce porous Si_3N_4 foams is partial sintering of a ceramic compact by adjusting the sintering conditions. The foams produced by partial sintering are not permeable since they have very fine pores with closed structures. In an investigation, Ohji et al produced porous Si_3N_4 bodies with low porosity of the order of 14 vol% and 24 vol% by tape casting and hot pressing, respectively [100]. In the tape casting method, β-Si_3N_4 powder was mixed with 5 wt% Y_2O_3 and 2 wt% Al_2O_3 followed by sintering at 1850°C under 1 MPa N_2 pressure. For the hot pressed sample, α-Si_3N_4 powder was mixed with 5 wt% Y_2O_3 followed by

sintering at 1850°C under the pressure of 30 MPa for 180 min. Figure 2-23 reveals a typical microstructure of a Si_3N_4 foam which has been produced by partial sintering of a tape cast body.
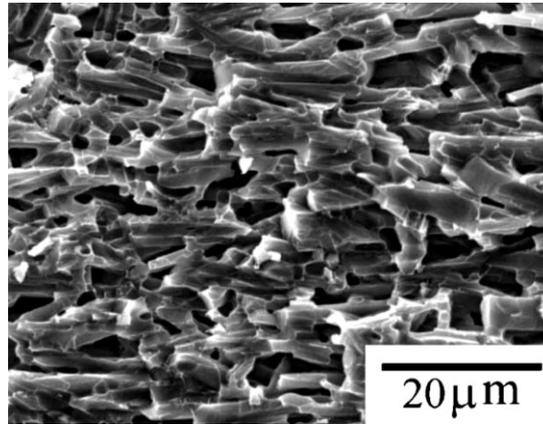
Figure 2-23. Micrograph of a polished and plasma-etched porous Si_3N_4 fabricated by partial sintering [100].

The most common technique that has been used to fabricate silicon nitride foams is the replication technique. As was mentioned before, replication is the easiest way to fabricate a ceramic foam and the produced foams suffer from very poor mechanical properties. In an investigation a β-Si_3N_4 suspension has been produced in the presence of a sintering additive, binder, thickening agent, and antifoaming agent and was used to impregnate polyurethane sponges [101]. In another work, SiC-Si_3N_4 composite foams have been fabricated by the same technique from preceramic polymers [38]. In this work Si_3N_4 particles were added to a polysilane precursor solution. A polyurethane sponge was coated by the solution followed by high temperature pyrolysis and sintering. It was observed that increasing the Si_3N_4 content causes cracks and voids due to inhomogeneous distribution of the particles.

Ye et al have fabricated porous silicon nitride ceramics by freeze casting of an aqueous Si_3N_4 slurry containing 2 wt% Al_2O_3 and 6 wt% Y_2O_3 as sintering additives [66].

Unidirectional solidification was done in liquid nitrogen followed by freeze drying and sintering at 1850°C under 0.1 MPa N_2 pressure for 1.5 h. The produced foam has a maximum porosity of 64 vol%. In another study, Fukasawa et al produced Si_3N_4 foams based on freeze casting of Si_3N_4 suspensions with 7 wt% of sintering aids including Al_2O_3 and Y_2O_3 [102]. Sintering was performed between 1700 to 1850°C for 2 h under N_2 pressures of 0.8 MPa. The maximum porosity reported by the authors was 69.6 vol%. Figure 2-24 shows a porous Si_3N_4 foam produced by freeze drying.
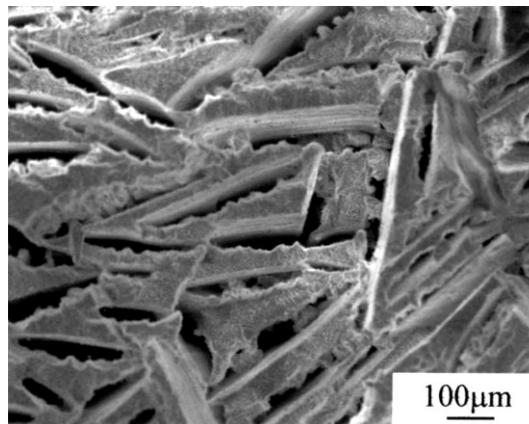
Figure 2-24. Micrograph of porous Si_3N_4 produced by freeze drying [102].

Sacrificial pore formers have also been used with Si_3N_4 powder to produce porous sintered Si_3N_4 foams. In an investigation, a ceramic suspension containing Si_3N_4, 6 wt% Y_2O_3, 2 wt% Al_2O_3, and corn starch was prepared. After drying, starch removal and sintering were performed [103]. The maximum porosity obtained in this investigation was 35 vol%. In another study Yang et al produced porous sintered Si_3N_4 bodies with rod-shaped pore structures [99]. In this study a ceramic slurry containing α-Si_3N_4, 5 wt% Y_2O_3, 2 wt% Al_2O_3, and organic whiskers composed of phenol-formaldehyde resin was slip cast followed by polymer burn-out at 800 °C and firing at 1850°C for 4 hours under a

N$_2$ pressure of 0.63 MPa. For 60 vol% whisker in the suspension the maximum porosity obtained was 42 vol%. Figure 2-25 reveals the microstructure of the fabricated foam.
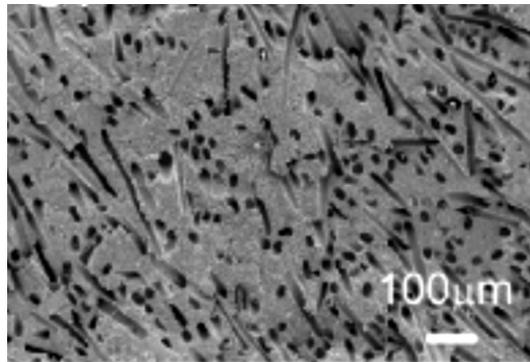
Figure 2-25. Microstructure of a porous Si$_3$N$_4$ foam produced by using 300 μm long organic whiskers as s sacrificial phase [99].

In another study, Jia et al used fly ash cenosphere (FAC, aluminosilicate-based hollow glass spheres) as the pore forming agent to omit the polymer burn-out step [104]. Aqueous suspensions of Si$_3$N$_4$, FAC, deflocculant, and agarose as a gelling agent were cast at 60°C followed by cooling to 1°C to consolidate the body. A closed-cell silicon nitride/silicon oxynitride foam composed of α- , β-Si$_3$N$_4$ and Al$_6$Si$_2$O$_{13}$ phases was produced. The foam maximum porosity was 67 vol%. Figure 2-26 shows the foam microstructure.
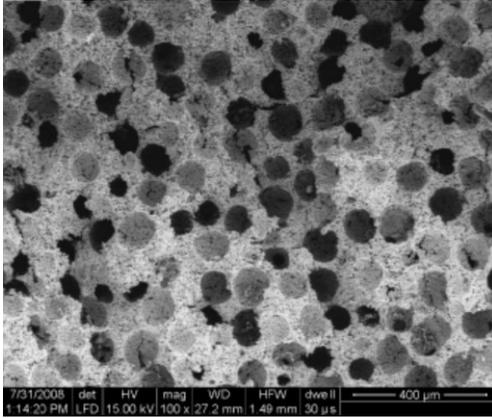
Figure 2-26. Microstructure of a closed-cell silicon nitride/silicon oxynitride foam fabricated via fly ash

cenospheres sintered at 1700°C [104].

The direct foaming technique has also been used to produce sintered Si_3N_4 foams with a closed-cell structure. Yang et al fabricated a Si_3N_4 foam based on foaming and casting a Si_3N_4 suspension with 10 wt% sintering additives (Al_2O_3 and Y_2O_3) containing long-chain surfactants or short-chain amphiphiles [105]. Sintering was performed at 1750°C for 1.5 h. Figure 2-27 reveals the microstructure of the produced Si_3N_4 foam. The wide pore size distribution which is a characteristic of the direct foaming technique is obvious in the figure.
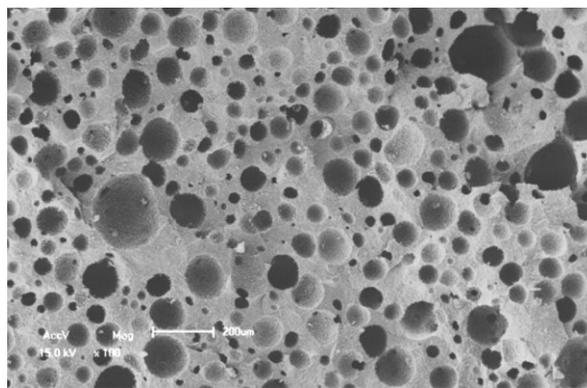
Figure 2-27. A porous Si_3N_4 foam produced via direct foaming of a particle-stabilized Si_3N_4 suspension

[105].

Wang et al produced Si_3N_4 foams merely by using gel-casting as both the consolidation technique and the pore forming part without using any other pore forming agent [106]. Al_2O_3 (1 wt%) and Y_2O_3 (2 wt%) were used as sintering aids and sintering was performed at 1730°C. A maximum of 63 vol% porosity was obtained. Figure 2-28 shows the microstructure of the foam which contains elongated β-Si_3N_4 grains.
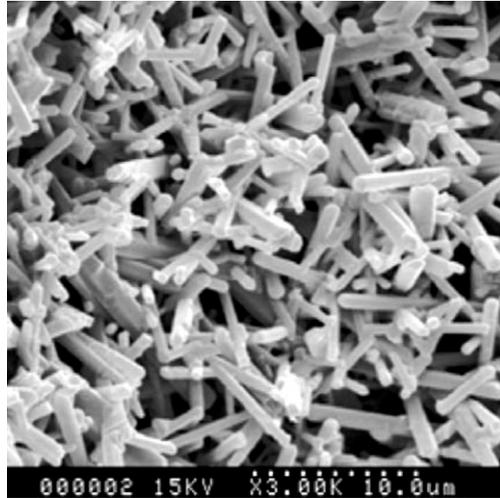
Figure 2-28. Microstructure of a Si_3N_4 foam fabricated based on gel-casting [106].

2.5.2. RBSN foams

Up to here, the starting material for all the silicon nitride foams was Si_3N_4 particles which make the high temperature sintering step unavoidable. Working with Si_3N_4 powder also causes some other major issues including large linear shrinkage and poor rheological properties which all result in the high cost of the final product. To the best of the author's knowledge, there are only a very limited number of investigations related to the reaction bonded silicon nitride foams in which the starting material is silicon powder.

Zhang et al. fabricated an RBSN foam with a close-cell structure [107]. In this study, silicon powder and sacrificial materials, including KCl or urea, were pressed uniaxially under 100 MPa pressure. In the case of urea as the pore forming agent, volatilization was

performed at 200°C but in specimens containing KCl, the pore former was extracted by soaking in water for 24 h. Reaction bonding was performed under a N_2 flow at temperatures between 1150 to 1450°C. The maximum porosity values obtained by urea and KCl extraction were 65 vol% and 57 vol%, respectively. The problem that requires further investigation in this study is the oxidation of the Si compact during soaking in water to extract KCl. The microstructure of the fabricated RBSN is shown in Figure 2-29.
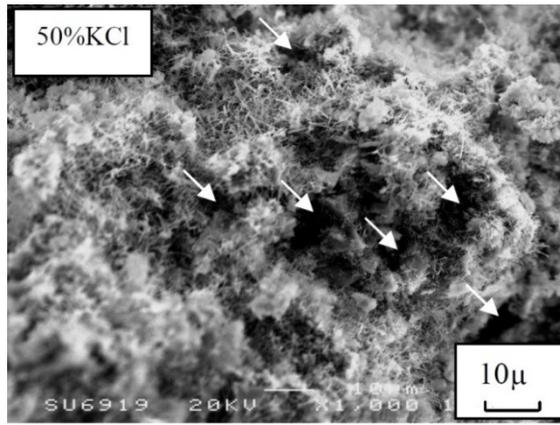
Figure 2-29. Fracture surface of an RBSN foam; 50% KCl was used as the pore forming agent [107].

In another study, Xu et al followed almost the same procedure with benzoic acid as a pore forming agent [108]. Uniaxial pressing of the powder mixture was performed at 40 MPa. After volatilization of the pore former at 200°C, nitriding was performed at 1380°C for 28 h under the flowing N_2-5%H_2 atmosphere. The maximum porosity which could be achieved was 60 vol%.

Lee et al also fabricated a gas-pressure sintered reaction bonded silicon nitride (GPSRBSN) foam in the presence of 6 wt% Y_2O_3 and 2 wt% MgO as sintering additives [109]. In this study Si powder, sintering additives, and PMMA beads were pressed uniaxially. Polymer burn-out at 600°C was followed by reaction bonding at 1350° for 8 h under a flowing N_2-10%H_2 gas mixture to make RBSN foams. The foams were then gas

pressure sintered at different temperatures from 1550 to 1850°C for 6 h under 5 MPa N_2 pressure while embedded in a Si_3N_4-BN powder bed. The maximum porosity in the RBSN foam was 54 vol% while the maximum porosity of the sintered foam was 48 vol% [109]. Figure 2-30 shows the microstructural images of the fabricated GPSRBSN foams.
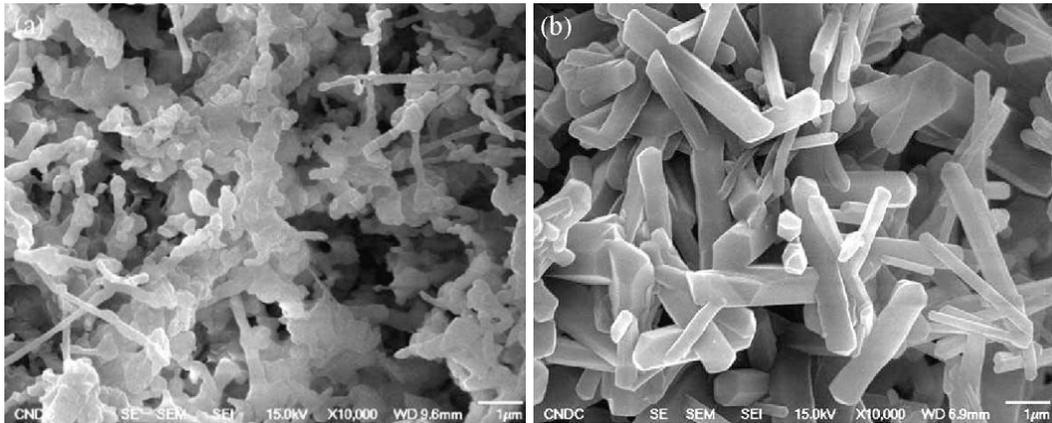
Figure 2-30. Microstructure of GPSRBSN foams; sintered at 1550°C for a) 3 h and b) 9 h [109].

GPSRBSN foams have been also produced by Park et al [110, 111]. A mixture of Si powder, 2.3 wt% of sintering additives including Y_2O_3 and Al_2O_3, PMMA as a pore former, and Si_3N_4 powder was uniaxially pressed and then cold isostatically pressed at 200 MPa. Nitridation was performed at 1350°C under the flowing N_2-5%H_2 atmosphere. Sintering was also done at temperatures between 1700°C to 1900°C for up to 10 h under a N_2 pressure of 0.1 or 0.9 MPa. The maximum reported porosity of the foam in these two studies was 60 vol%.

Park et al also fabricated SRBSN porous bodies based on granulation of Si [112 - 114]. Si and the sintering aids including Y_2O_3, Al_2O_3, and $CaCO_3$ were spray dried followed by Ar sintering at 1200 or 1350°C for 10 min to strengthen the granules. Granules were then uniaxially pressed under 3.7 MPa pressure to make green bodies. Nitriding under N_2-5%H_2 gas mixture at 1450°C was followed by sintering at temperatures between 1700 to

1900°C for 2 h. The N_2 pressure during sintering was 0.1 MPa up to 1800°C and it was 0.9 MPa for sintering at 1900°C. The maximum porosity of 60 vol% was reported for samples sintered at 1700°C. The fracture surface of the porous SRBSN is shown in Figure 2-31.
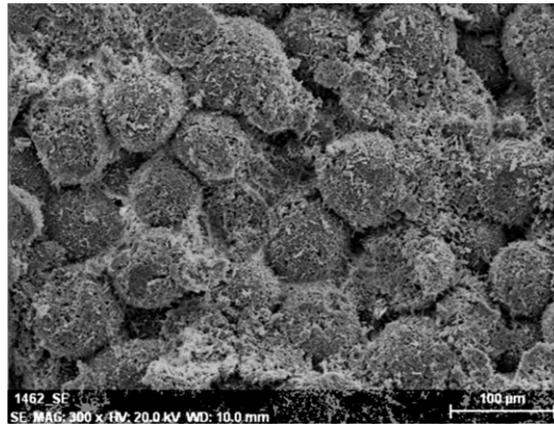
Figure 2-31. Fracture surface of a porous SRBSN body; sintering temperature is 1800°C [112].

Xu et al also worked on RBSN foams [115]. In their investigation, Si powder, benzoic acid balls as a pore forming agent, 5 wt% Y_2O_3 and 5 wt% Al_2O_3 were pressed uniaxially at 40 MPa. After volatilization of the sacrificial phase, presintering in vacuum at 1250°C was followed by nitriding at 1350° for 20 h under a flowing N_2-5%H_2 gas mixture and 0.1 MPa pressure. The reported porosity was 53 vol% and the microstructure of the foam is completely inhomogeneous, showing nun-uniform distribution of the pores. It has been reported in this investigation that the porous samples produced after extraction of the pore former and presintered for 2 h at 1250°C before nitriding, show a flexural strength of 50 MPa. This is definitely impossible to achieve since after extracting the sacrificial phase, the foam is quite fragile and has a very low strength. On the other hand, Ar sintering cannot increase the sample strength that much. Figure 2-32 shows the fracture

65

surface of the porous RBSN sample containing 10 wt% sintering additives and without presintering in vacuum.
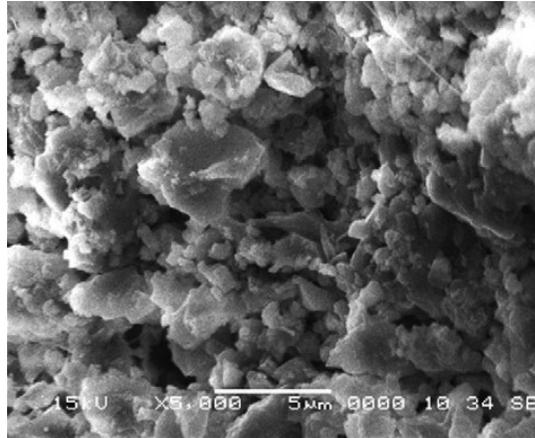
Figure 2-32. Fracture surface of a porous RBSN body containing 5 wt% Y_2O_3 and 5 wt% Al_2O_3 [115].

It must be mentioned that in all these investigations, the RBSN foams have been fabricated via dry pressing which causes inhomogeneity in the final foam structure. All the foams also suffer from low levels of porosity and they lack pore interconnectivity.

2.6. Summary

To make a Si_3N_4 foam, a foam fabrication technique must be selected. As discussed above, the sacrificial template technique results in a higher foam strength and also provides precise control over pore size, pore size distribution, and pore morphology compared to direct foaming and replication techniques.

In order to produce Si_3N_4 foams and simultaneously avoid the issues associated with Si_3N_4 powder, reaction bonding is considered as an alternative. In this technique, inexpensive Si powder reacts with N_2 resulting in Si_3N_4 formation. Among many advantages of reaction bonding, the good rheological properties of Si suspensions

compared to Si_3N_4 suspensions would be an asset and provide the possibility of wet processing of Si_3N_4 foams rather than dry pressing.

A consolidation technique is also required to make a solid monolith from a Si suspension. Among the discussed techniques, gel-casting is capable of producing homogeneous bodies with complex shapes in a very short time. Therefore, a new fabrication procedure will be designed based on a combination of sacrificial template technique, gel-casting, and reaction bonding to make open-cell Si_3N_4 foams with a high level of controlled porosity.

Chapter 3

Open-cell reaction bonded silicon nitride foams; fabrication and characterization

Ali Alem, Martin D. Pugh, Robin A.L. Drew

Mechanical and Industrial Engineering Department, Concordia University, 1455 De Maisonneuve Blvd. W., Montreal, Quebec, Canada H3G 1M8

Abstract

In this study, a newly designed fabrication procedure was utilized to produce silicon nitride foams. The main goal of the present study was to obtain Si_3N_4 foams with high levels of porosity and pore interconnectivity via an economical fabrication procedure including sacrificial template technique, gel-casting and reaction bonding processes. The fabrication procedure was studied and optimized in terms of suspension preparation and rheology, gel-casting parameters, and reaction bonding conditions. The produced foams have a precisely controlled level of porosity which can be varied up to 87 vol%. BET analysis showed that the surface area of the foam is of the order of 2.01 m^2/gr. The pore interconnectivity of the foam was investigated via polyester resin infiltration. Based on XRD and SEM analysis, the dominant nitriding reactions are the gas-phase reactions which lead to α-Si_3N_4 in the form of whiskers.

Keywords: Silicon nitride; Reaction bonding; Foam; Gel-casting; Pore interconnectivity

3.1. Introduction

Traditionally, ceramic materials have been made as dense as possible to reduce the possibility of sudden failure and fracture of this brittle group of materials. Recently, cellular ceramics have been found to be very interesting due to their unique and remarkable characteristics [1, 4]. Although these materials exhibit special features and functionalities, they are not being used to their full potential. Designing new ways to fabricate homogenous ceramic foams with tailored properties including pore structure,

68

pore size, and pore interconnectivity will make them suitable for many new and high-tech applications such as bioimplants, diesel particulate filters (DPF), separation membranes, and for the fabrication of interpenetrating composites [3 - 6]. There are two properties in the foam structure which have not received sufficient attention. The first one is pore interconnectivity which is necessary in all the above mentioned applications where fluid transport is necessary. The second property is the porosity level of the foam which affects many foam characteristics such as surface area and permeability.

Among all the ceramic materials, Si_3N_4 has outstanding properties and potential including high strength and toughness, high temperature resistance, high thermo-chemical corrosion resistance, good wear resistance, and good thermal shock resistance which make this ceramic material a great candidate for many engineering applications [99]. Several methods have been used to fabricate Si_3N_4 foams including partial sintering of a Si_3N_4 compact [100], impregnation of polyurethane sponge [38, 101], freeze drying [66, 102], sacrificial template technique [99, 104], and direct foaming method [105] but all the produced foams suffer from low levels of porosity and also lack pore interconnectivity. There are also some other fabrication issues and difficulties in working with silicon nitride powders including the high cost of the starting material, the high sintering temperatures (around 1900°C), the large amounts (up to 10 wt%) of sintering additives required due to a high degree of covalency in the Si-N bond, and the large linear shrinkage (15-20%) which makes it essential to perform time-consuming and costly post-sintering machining steps to get the required sample dimensions [19]. In terms of wet processing techniques which are capable of producing homogeneous ceramics, working with Si_3N_4 suspensions is also undesirable due to the rheological problems of the

suspensions including inconsistency in Si_3N_4 slurries required for the industrial production [20, 116] and high shear thickening behavior of these slurries [21].

In this study a new fabrication procedure was designed in order to produce a Si_3N_4 foam with an open-cell structure and a controlled level of porosity but without the issues associated with Si_3N_4 as a starting powder. To the best of the authors' knowledge there is no classified study on reaction bonded silicon nitride (RBSN) foams per se and there are also no reports of the fabricated Si_3N_4 foam with open-cell structures and pore interconnectivity. There are only a few investigations in the area of RBSN foams in which the utilization of the dry-processing techniques such as uniaxial pressing or extrusion has led to inhomogeneous closed-cell structures with low levels of porosity [108 - 110]. The fabrication procedure designed in this study relies on the combination of the sacrificial template technique, gel-casting, and reaction bonding processes which leads to homogeneous RBSN foams with interconnected porosity. The sacrificial template method was selected in this study as the foam fabrication technique since it is capable of tailoring foam properties including pore size, pore morphology, pore size distribution, total porosity, and pore interconnectivity [1]. The fabrication procedure was also based on wet colloidal processing to improve homogeneity of the foam and reduce the microstructural defects which typically form in dry processing techniques due to poor particle packing and distribution. The combination of gel-casting as a near-net shape, in-situ, consolidation technique and the reaction bonding process in this study offers advantages including a short processing time, high wet and dry strengths, possibility of producing high-quality homogeneous bodies with complex shapes, the possibility of using different mold materials, machinability, higher reliability, less flaws and defects in

the final products, the capability of producing large samples and an easy and economical fabrication procedure [11, 40, 70, 71]. Table 3-1 and Table 3-2 compare the advantages and disadvantages of RBSN, sintered silicon nitride (SSN), and gel-casting technique. The tables show that the newly designed foam fabrication procedure eliminates all the fabrication disadvantages of SSN and RBSN ceramics while combining the advantages of RBSN and gel-casting techniques.

Table 3-1. Comparing the advantages and disadvantages of RBSN and SSN

Reaction bonded Si_3N_4		Sintered Si_3N_4	
Advantages	Disadvantages	Advantages	Disadvantages
• Low cost Si powder [117] • Almost no dimensional changes during nitriding; increasing the process reliability and reduces post machining [11] • Low nitriding temperature • Low production cost [117]	• Very long procedure for dense and large bodies [118] • Residual Si in the dense nitrided sample • 10 to 20% residual porosity in the dense body [11]	• High mechanical Strength [119] • Good thermal shock resistance [99] • High toughness	• 15-20% linear shrinkage during sintering [19] • Very high sintering temperature • Large dimensional changes and costly post-sintering machining steps [19] • Large amounts of sintering additives

Table 3-2. Advantages and disadvantages of the gel-casting technique

	Advantages	Disadvantages
Gel-casting	• Near net-shape fabrication technique even for complex shapes [40] • Highly homogeneous and uniform bodies with high green strengths [20] • High machinability • Low levels of organic additives [85]	• Reactive components [40] • Irritating monomers with the capacity to sensitize exposed workers [40]

The main goal of this investigation was to fabricate an RBSN foam with an open-cell structure and a controlled level of porosity. Silicon-PMMA suspensions were made and characterized in terms of stability and rheology to optimize the suspension behavior and consequently the foam properties. The gel-casting step was also optimized in terms of the monomer content, monomer to cross-linker ratio, and polymer pyrolysis. Furthermore, this investigation examines the nitriding conditions and the dominating nitriding mechanisms. Finally, the RBSN foams were also studied in terms of foam properties including the porosity, pore interconnectivity, and microstructure.

3.2. Material and methods

3.2.1. Foam fabrication

Porous RBSN foams have been fabricated from Si powder (ABCR, 99.995%, -8 microns) and PMMA beads (Microbeads, 10-40 μm) as the pore former via the gel-casting technique. Acrylamide (AM, $C_2H_3CONH_2$, Sigma-Aldrich) was used as the monomer and N,N′-methylenbisacrylamide (MBAM, $(C_2H_3CONH_2)_2CH_2$ Sigma-Aldrich) was utilized as the cross-linker. Three different dispersants were used in this study including Darvan® 821A (R.T. Vanderbilt Minerals LLC, poly(acrylic acid) ammonium salt, PAA-NH_4), DS001 (Polymer Innovations Inc.), and Dolapix PC 75 (Zschimmer & Schwarz GmbH & Co KG). Poly(acrylamide) (PAM, Acros Organics, M.W.= 5,000,000-6,000,000) and DF002 (Polymer Innovations Inc.) were the binder and the antifoaming agent, respectively. Ammonium persulfate (APS, $(NH_4)_2S_2O_8$, Sigma-Aldrich) and N,N,N′,N′-tetramethylethylenediamine (TEMED, $C_6H_{16}N_2$, Sigma-Aldrich) were utilized as the free radical initiator and catalyst, respectively. Ammonium hydroxide and nitric acid were also used to adjust pH.

To prepare the premix solution, the monomer and cross-linker were dissolved in water based on different ratios. Silicon powder, PMMA beads and other rheological agents were also added to the premix solution. Ball milling was performed in polyethylene jars using Si_3N_4 balls to break any residual agglomerate and make a homogenous suspension. Suspension pH was adjusted and it was de-aired under vacuum to remove air bubbles introduced during milling. After the addition of TEMED and APS, the suspensions were cast in silicone rubber molds. Drying of the samples was performed for two days at room temperature followed by one day at 50°C, one day at 70°C and 5 h at 120°C. The polymer burn-out step was the next step which was done at 525°C for 2 h with a heating rate of 1 °C/min. After pyrolysis, the nitriding step was performed at different temperatures between 1200°C to 1450°C and under N_2-H_2. Some samples were Ar-sintered for 2 h at 1200°C prior to the nitriding step. Ar sintering was only performed to increase the sample strength; therefore, sample handling and preparation for microstructural analysis would be possible before the nitriding step.

3.2.2. Characterization

Zeta potential measurements were performed on very dilute silicon and PMMA suspensions in an aqueous 10^{-3} M KCl solution. Si suspensions were aged for six days for ionic equilibration and for the suspension pH to stabilize. At least 15 potential measurements were performed at each pH value. Sedimentation tests were performed in long test tubes to find the best dispersant and the optimum quantity required to get the highest suspension stability. Rheological characteristics of the suspensions were also analyzed at different pH values and solid contents via a coquette rheometer (Anton Paar, MCR 500). To measure the viscosity, a pre-shearing step was performed on the

suspensions. They were sheared at 1000 s^{-1} for 1 min to destroy any previous structures in the suspensions and remove any historical influence of the suspension preparation procedure. Then they were left standing for 1 minute before the test initiation. During the tests, the shear rate was kept constant for 30 sec at each value to make sure that the system has stabilized before reading the viscosity. Both ascending and descending shear rate methods were performed to investigate any time dependent behavior in the suspensions. DSC/TGA (TA Instruments, Q10) tests were performed on the PMMA beads and polyacrylamide polymer made by gel-casting to find the burn-out temperatures and to design and control the pyrolysis step to avoid the formation of any flaws or cracks in the foams. Four-point bending tests were carried out on bar-like samples using a uniaxial tensile testing machine (Instron®, Model 3382) to determine the optimum amount and the ratio of the monomer to cross-linker. The lower span was 40 mm and the upper one was 20 mm, moving at a crosshead speed of 0.1 mm/min. The porosity and density of the foams were measured based on the Archimedes technique according to the ASTM C373-88 standard. The BET test was performed to investigate the specific surface area of the foams. X-ray diffraction analysis (XRD, X'PertPro; PANalytical) and scanning electron microscopy (SEM, HITACHI, S-3400N) techniques were also utilized to investigate the phases, microstructure, and interconnectivity of the foams.

3.3. Results and discussion

3.3.1. Suspension characterization

Knowledge of the suspension's properties and rheological behavior is necessary since they significantly affect the foam properties. Although there is broad research on the processing of ceramic suspensions, to our knowledge the rheological behavior of Si-

PMMA suspensions has not been investigated. The suspension stability was investigated in terms of zeta potential measurements, sedimentation tests, and particle size analysis. Figure 3-1 shows the zeta potentials of the silicon and PMMA suspensions versus pH. The Si graph shows three minima within the tested pH range, namely at pH 6, 8.5, and 10. There are some criteria to select the optimum pH value at which the suspension has the highest stability.
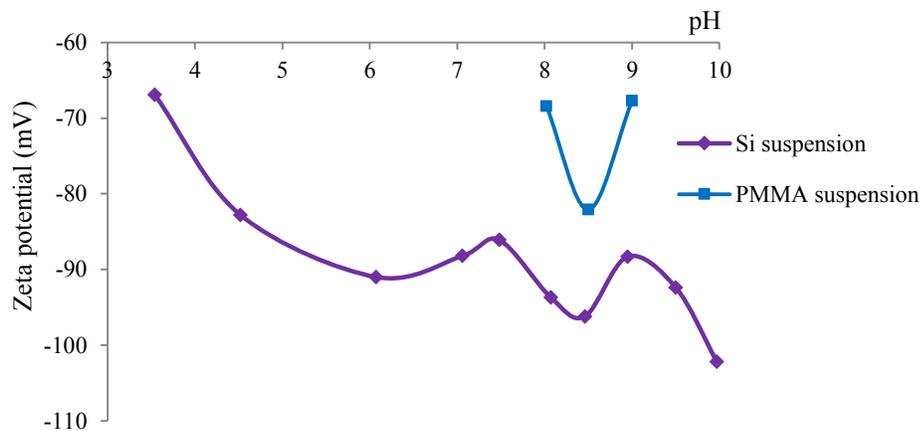
Figure 3-1. Zeta potentials of silicon and PMMA suspensions versus pH.

In gel-cast silicon bodies, Si oxidation is an issue which occurs during suspension preparation. It leads to SiO_2 formation on the particle surfaces and consequently H_2 release (Reaction 3-1). Like other oxides in water, particle surfaces will be hydrolyzed by chemisorbed water molecules resulting in the formation of silanol (SiOH) groups on the surface which enhance the wetting of Si particles in water [120]. These silanol groups will be charged either by giving H^+ or by receiving OH^-. The charging reactions are completely dependent on suspension pH and will make the particle surfaces positively or negatively charged (Reactions 3-2 and 3-3) [119 - 121]. Hydrogen release during suspension preparation causes processing difficulties and results in uncontrolled porosity

formation in the foam; therefore, the reaction intensity must be lowered. The intensity of the hydrolysis reaction is strongly dependent on pH and it was observed that the rate of H_2 release increases significantly above pH 9. Although the SiO_2 layer forms a protective coating around Si particles, the coating is not stable above pH 9 and it dissolves in water to form silicic acid [119]. Therefore, H_2 release is much more severe at high pH values. Another issue of using very basic pH values is the compression of the electrical double layer which causes suspension destabilization. The electrical double layer thickness is dependent on the electrolyte concentration and valence of the counter-ions, and this thickness decreases when increasing the suspension ionic strength. Therefore, although Figure 3-1 shows the highest zeta potential at pH 10, the electrical double layer is compressed and the suspension is partially flocculated at this pH. It is concluded that the optimum pH value for Si suspensions is 8.5. At this pH value the zeta potential of -96 mV shows a strong repulsion between the particles and consequently the maximum stability in the suspension and in addition, the H_2 release issue is negligible. As Figure 3-1 shows, pH 8.5 also gives the highest repulsion between the PMMA beads.

$$Si \text{ (s)} + 2H_2O = SiO_2 \text{ (s)} + 2H_2 \text{ (g)} \quad\quad\quad (3\text{-}1)$$

$$SiOH + H^+ \text{ (aq)} = SiOH_2^+ \quad\quad\quad (3\text{-}2)$$

$$SiOH + OH^- \text{ (aq)} = SiO^- + H_2O \quad\quad\quad (3\text{-}3)$$

Figure 3-2 shows the influence of the three dispersants used in this study on the sedimentation behavior of Si suspensions. All the suspensions had 20 wt% solids and they were stirred for 24 h at pH 8.5 to reach equilibrium between the particle surfaces and the dispersant. It can be seen from Figure 3-2 that Si suspensions with DS001 as the dispersant show the lowest sedimentation height with the optimum amount of 1.5 wt%.

Based on visual observations, the sediment in the suspension containing 1.5 wt% DS001 is also very dense which is a sign of a deflocculated suspension. Figure 3-3 compares the sedimentation heights of Si suspensions based on the optimum amounts of each dispersant after 2 days. It can be seen from the figure that the difference between the influences of these three dispersants becomes larger for longer sedimentation times. It is observed that DS001 reveals the lowest sedimentation height for longer times while Darvan® 821A shows the highest sediment height. From Figure 3-3 it is observed that some dispersants may have an inverse influence on the suspension stability and increase the sedimentation height when the aging time is long. The reasons for the higher sedimentation heights can be less compatibility of the dispersant with SiO_2 or the higher ionic strengths of the suspension which results in double layer compression. It must be mentioned that since Darvan® 821A is a common dispersant, suspensions with dispersant contents higher than 1 wt% were also tested. It was observed that these suspensions were highly flocculated due to high ionic strengths and the sedimentation heights were quite high.
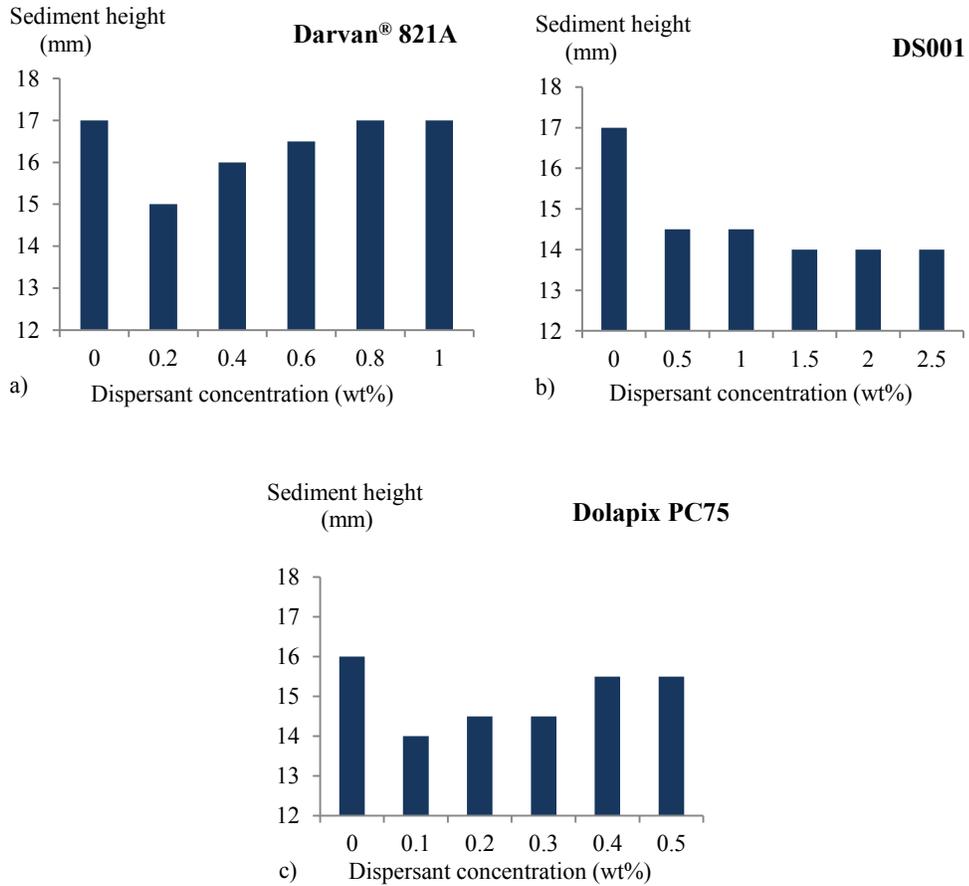
Figure 3-2. Sediment heights of Si suspensions after 1 day for three different dispersants used in this study; a) Darvan® 821A, b) DS001, c) Dolapix PC75.
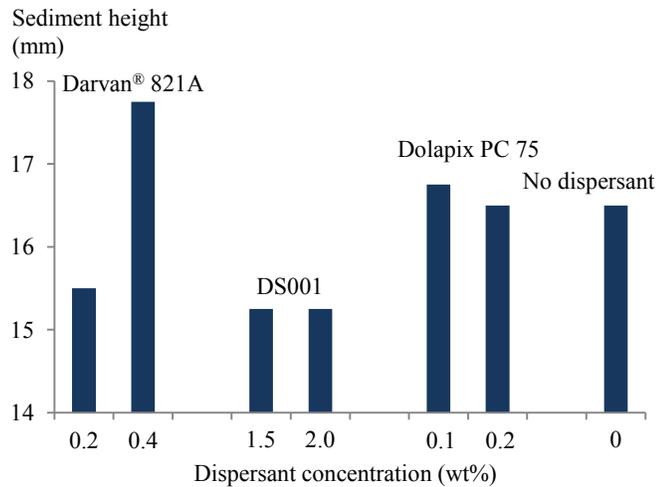
Figure 3-3. A comparison between sediment heights of Si suspensions with three different dispersants used in this study, Darvan® 821A, DS001, and Dolapix PC75 after 2 days.

It can be seen from the sedimentation tests that Darvan® 821A does not significantly improve the Si suspension stability at high pH compared to the other dispersants. It was observed that more H_2 is also released in the presence of Darvan® 821A than other dispersants. Generally, there are issues in stabilizing oxide ceramic particles with anionic polyelectrolytes above the isoelectric point (IEP) where they are negatively charged. The dissociation of the ionizable group in anionic polyelectrolytes is strongly dependent on pH and increases with pH. As the dissociation fraction increases in the basic pH range, the polymer chains become highly negative and they acquire expanded conformations due to repulsion between these negatively charged segments. Although at this point the dissociation fraction is very high, the adsorption of polymers on the particle surfaces is very difficult since both are negatively charged. On the other hand, at lower pH values there is less dissociation of the ionizable groups and consequently less negatively charged chain segments which results in less repulsion between the particles and the dispersant above the IEP. This may help with the polymer adsorption phenomenon on the particle surfaces but since the polymer conformation is fairly compact and small under this condition, the steric interactions which operate at shorter particle separations are poor. Therefore, the dispersant does not stabilize the suspension at its full potential [122].

At this stage the best pH was determined to be 8.5 based on the zeta potential measurements shown in Figure 3-1 and the optimum quantity of each dispersant was also determined based on Figure 3-2 and Figure 3-3. Therefore, the zeta potential measurements were only performed in the presence of the optimum amount of the each dispersant to prove the sedimentation results. Table 3-3 shows the zeta potential of the suspensions in the presence of the dispersants at pH 8.5. It is observed that the highest

zeta potential is obtained in the presence of DS001 which is in accordance with the sedimentation test results.

Table 3-3. The zeta potential of Si suspensions in the presence of different dispersants

Dispersant	Darvan® 821A (0.2 wt%)	DS001 (1.5 wt%)	Dolapix PC75 (0.1 wt%)
Zeta potential (mV)	-91.26	-94.13	-86.4

The particle size distribution of Si suspensions with and without dispersant was measured. Figure 3-4 shows the Si particle size distribution in the presence of DS001. It was observed that all the suspensions show the same particle size distribution with the mean particle size of 3.3 μm. It is concluded that there is no agglomerate present in the suspensions and they are highly homogeneous. It was also observed that the dispersants have no influence on the Si particle size distribution in the suspensions. It can be seen that electrostatic stabilization is mainly responsible for breaking the agglomerates and reducing the particle size and the dispersants only increase the suspension stability based on electrosteric interactions.
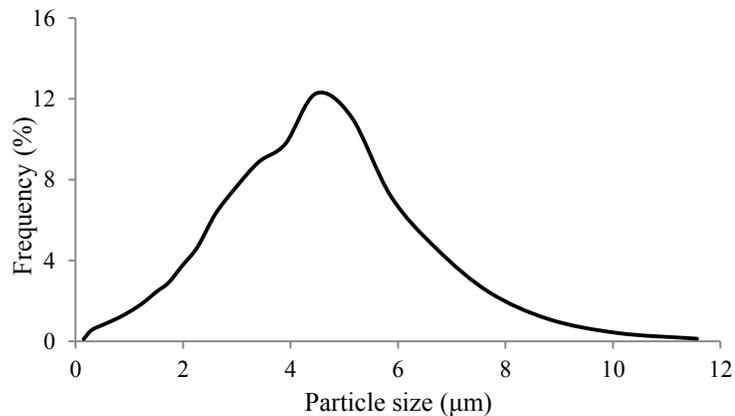
Figure 3-4. Particle size distribution of Si suspensions at pH 8.5 with 1.5 wt% DS001 as the dispersant.

Figure 3-5 and Figure 3-6 reveal the rheological behaviors of silicon and PMMA suspensions at pH 8.5 and for 60 wt% solid content. Both the viscosity and shear stress were measured with ascending and descending shear rates to check the presence of any time dependent behavior in the suspensions. The hysteresis in the PMMA graph in Figure 3-5 clearly shows the time dependent rheological behavior of PMMA suspensions. The PMMA suspensions are thixotropic at low shear rates and slightly rheopectic at higher shear rates. Compared to PMMA, silicon suspensions have a much lower viscosity at the same pH and solid content and for all shear rates. The lower viscosity of Si suspensions is due to higher zeta potential of the Si particles, their finer particle sizes, continuous particle size distribution, and much lower volume fraction of silicon in the suspension for the same weight fraction of solid due to the higher density of Si compared to PMMA. Figure 3-5 and Figure 3-6 also show that Si suspensions are slightly shear thinning at low shear rates with no time dependent behavior and they become highly shear thickening with a time dependent behavior at shear rates higher than 200 s^{-1}. The shear thickening behavior of Si suspensions is due to elongated and anisotropic shape of the particles, their large size (several microns based on Figure 3-4), and high suspension concentration. This behavior is a consequence of shear-induced flocculation or a transition from ordered to disordered structures due to shear [120]. At higher shear rates the dense packing of particles is disrupted which results in a random arrangement of particles. Therefore, more packing space and more liquid are required for free particle motion; therefore, an increase in viscosity is observed [71]. Figure 3-6 reveals that PMMA suspensions show much less shear thickening behavior than Si suspensions, although the PMMA beads are much larger in size than Si particles. It is concluded that the shear thickening behavior of the Si

suspensions is due to anisotropic shape and high zeta potential of the particles. These factors amplify the shear thickening behavior in Si suspensions [120].
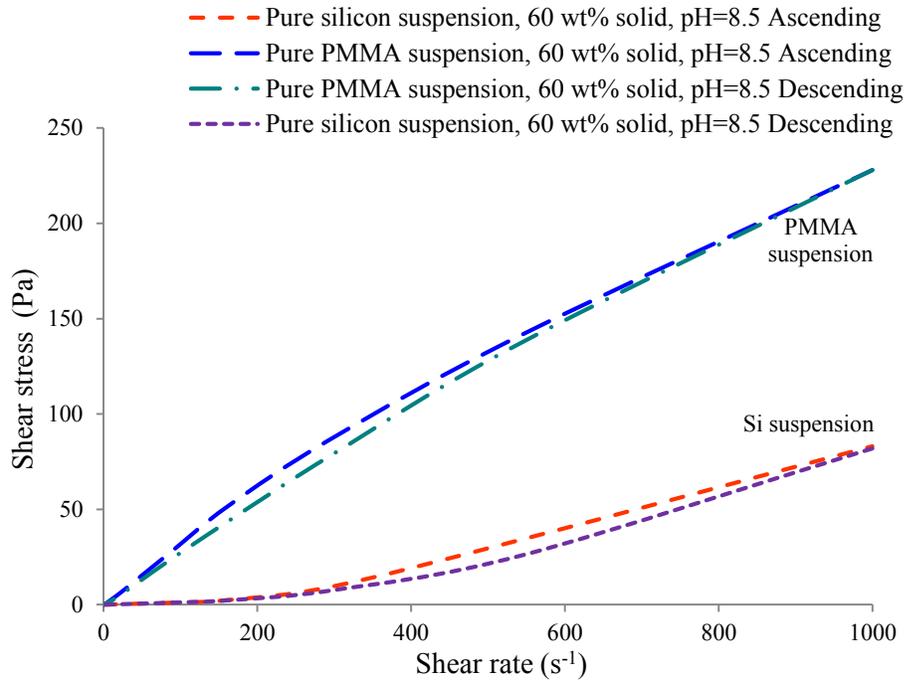
Figure 3-5. Shear stress versus shear rate for silicon and PMMA suspensions at pH 8.5 and 60 wt% solid content.
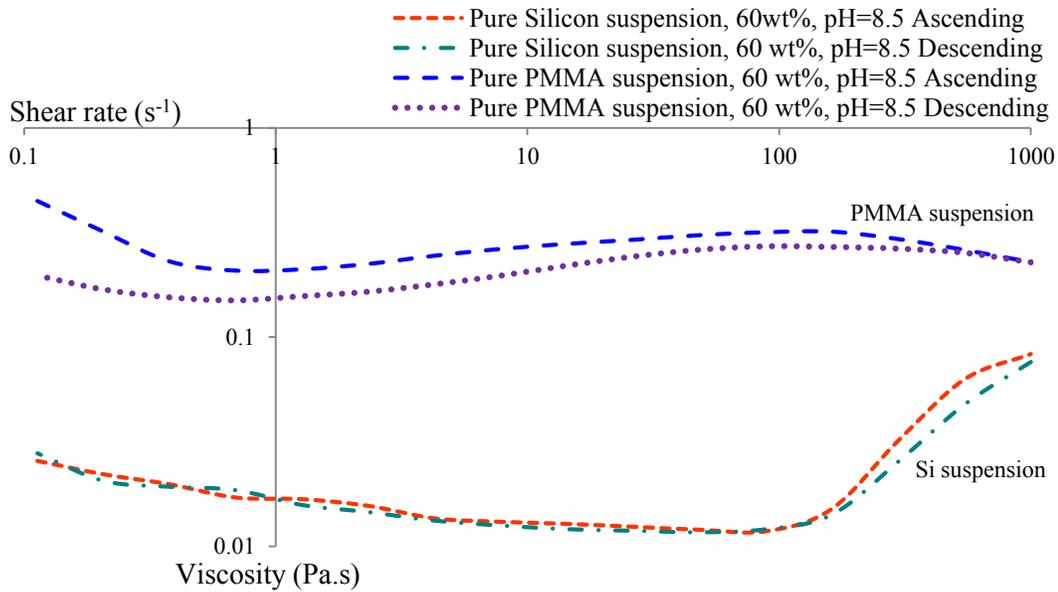
Figure 3-6. Viscosity versus shear rate for silicon and PMMA suspensions at pH 8.5 and 60 wt% solid content.

Figure 3-7 and Figure 3-8 reveal the influences of solid content and pH on the rheological behavior of Si-PMMA suspensions. It is observed that for suspensions with 60 wt% solid, the lowest viscosity can be obtained at pH 8.5 which is in accordance with the zeta potential measurements. Figure 3-8 shows that Si-PMMA suspensions are near Newtonian with a slightly shear thinning behavior at pH 8.5. Based on the figures, Si-PMMA suspensions show much higher viscosities and also a shear thinning behavior at lower pH values (e.g. 7.22) and higher solid contents (e.g. 63.5 wt%). These suspensions also reveal a time-dependent behavior in a form of a small hysteresis (not shown in here). This shear thinning behavior is due to suspension flocculation caused by a weak repulsion between the particles or a very high solid content. These flocculated structures which trap the liquid in the spaces between the particles break down at higher shear rates, therefore, the viscosity decreases as the shear rate increases.

A comparison between Figure 3-6 and Figure 3-8 reveals that Si-PMMA suspensions are not shear thickening at high shear rates compared to Si suspensions. In the Si-PMMA suspensions, due to the isotropic and spherical shape of the PMMA beads and their high volume fraction in the suspension which lowers the net zeta potential, shear thickening behavior is not observed even at 63.5 wt% solid content. It was also observed in this study that due to the shear-thinning behavior of Si-PMMA suspensions, the maximum solid content of these suspensions, especially at high PMMA/Si ratios is about 63 wt%. Above this value, the suspensions have very high viscosities and poor flowability. Suspensions with very high solid contents also contain trapped air bubbles which are not removed during vacuum de-airing due to the suspension's high viscosity. These air bubbles affect the pore homogeneity and mechanical properties of the foam significantly.
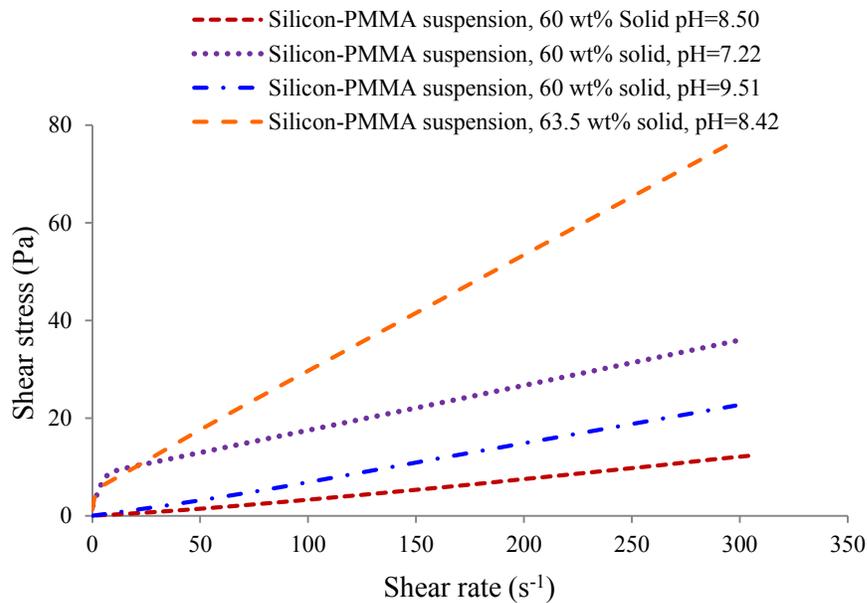
Figure 3-7. Shear stress versus shear rate for silicon-PMMA suspensions at different pH values and solid contents.
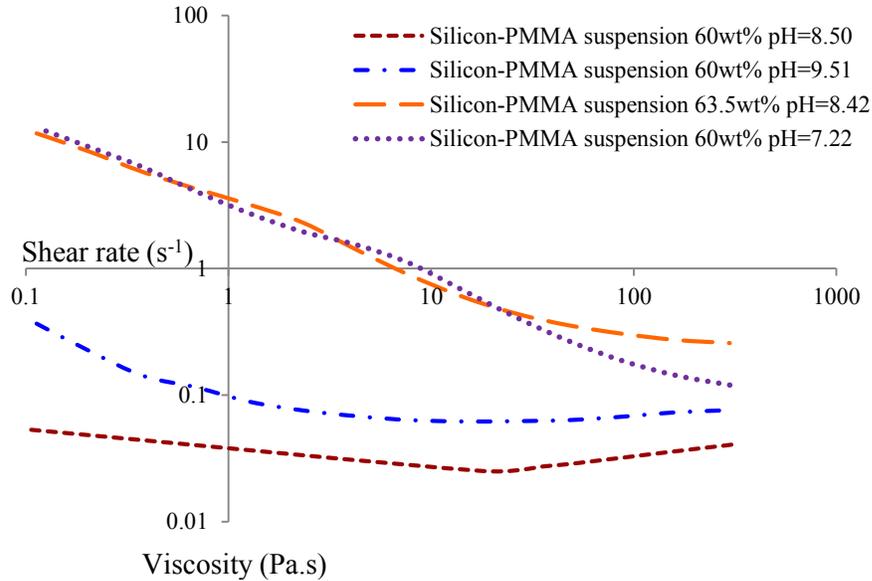
Figure 3-8. Viscosity versus shear rate for silicon-PMMA suspensions at different pH values and solid contents.

Based on the zeta potential analysis, the best pH is 8.5 which leads to the highest electrostatic repulsion between the particles and consequently the highest stability of the suspension while maintaining the ionic strength at its minimum. Sedimentation tests show that at pH 8.5, DS001 provides the lowes sediment height and consequently the highest suspension stability among all the tested dispersants. The rheological measurements also show that under this condition Si-PMMA suspensions have the lowest viscosity and near Newtonian flow behavior with a little shear thinning characteristic. It was observed that at lower pH values, the suspensions are highly flocculated while at higher pH values, beside the suspension flocculation, H_2 release due to Si oxidation will make the fabrication process more difficult.

3.3.2. Gel-casting and polymer pyrolysis

There are some gel-casting parameters which directly influence the properties of the fabricated RBSN foam. Monomer content is one of those important parameters that

influences the properties of the gel-cast body including the sample warpage and strength. Warpage and sample distortion may occur during drying due to stresses caused by non-uniform shrinkage of the sample. In gel-cast bodies, water is not absorbed by the mold like in slip casting and is trapped inside the structure; therefore, drying of gel-cast bodies is of significant importance. It was observed in this study that there are two parameters that significantly affect the sample distortion and warpage during drying. They are the sample geometrical symmetry and the monomer content. The highest amount of warpage is observed when the sample does not have a symmetrical geometry and the premix solution has a low monomer content. Figure 3-9 shows the green strength of a gel-cast sample for different monomer contents. The figure reveals that increasing the monomer content from 6 wt% to 12 wt% in the premix solution enhances the sample strength more than threefold. This implies that the macromolecular network of the gel is finer and more widespread for higher monomer contents which results in a more uniform distribution of Si particles and PMMA beads in the gel-cast body. Therefore higher monomer contents give on one hand, a more uniform particle distribution and consequently higher sample homogeneity and on the other hand, a higher sample strength which results in less distortion during drying. It must be kept in mind that a high monomer content also makes the polymer pyrolysis step more difficult since samples may crack and collapse during polymer burn out.
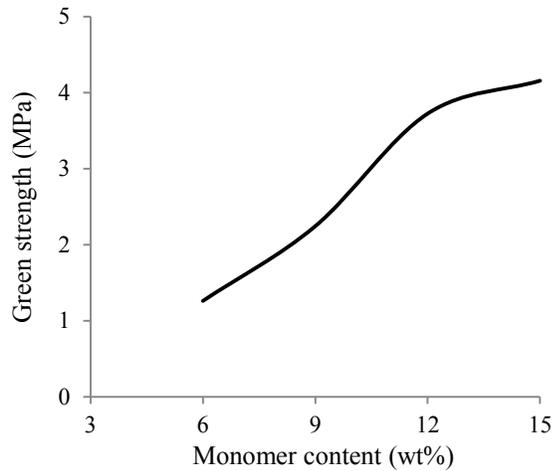
Figure 3-9. Green strength of the gel-cast body versus the monomer content in the premix solution.

The monomer to cross-linker ratio also affects the sample properties such as strength. In order to optimize the monomer to cross-linker weight ratio (AM/MBAM), 4-point bending tests were performed on green samples with different AM/MBAM ratios while keeping the monomer content constant. Figure 3-10 shows that the flexural strength of the green sample increases with increasing AM/MBAM weight ratio and reaches a maximum value and then decreases. When the AM/MBAM ratio is too high (a small amount of cross-linker), the gel network suffers from a low cross-linking density; therefore, it is very weak and loose. This results in a reduction of the sample strength. On the other hand, for very low ratios of AM/MBAM (too much cross-linker) homopolymerization of MBAM increases the length of the linking bridges connecting the polyacrylamide chains. Consequently, it again results in a decrease of the cross-linking density and sample strength. The graph in Figure 3-10 shows that the ratio of 15 to 20 provides us with the highest cross-linking density in the gel network and consequently the greatest strength.

87
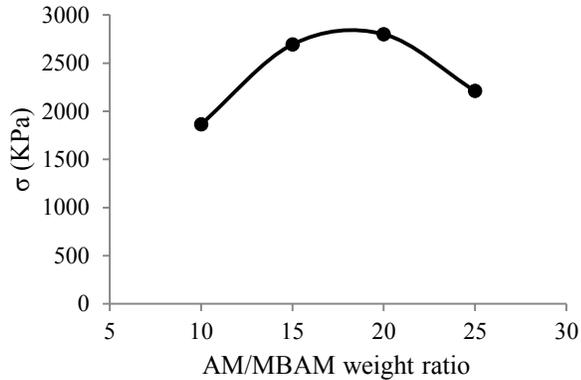
Figure 3-10. Green strengths of samples with different AM/MBAM weight ratios.

Gelation time is another critical parameter in gel-casting of RBSN foams which is dependent on the amounts of APS and TEMED. Figure 3-11 shows the relationship between the initiator content and the setting time for a suspension with 60 wt% solid made from a premix solution with 7 wt% monomer content. It can be seen that doubling the initiator content results in a six-fold decrease of the gelation time. It was observed in this study that the setting time affects the homogeneity of the gel-cast body significantly since both particle sedimentation and particle segregation phenomena occur even for the stabilized suspensions. Particle sedimentation happens as a result of gravity and particle segregation occurs due to the size dependence of the particle precipitation rate; therefore, a higher concentration of larger particles precipitate at the bottom of the gel-cast body. Both particle sedimentation and segregation phenomena result in a density gradient in the foam in a way that green samples have a higher density at the bottom than the top. The resulting inhomogeneity causes non-uniform shrinkage during drying and polymer pyrolysis which consequently causes cracking and sample collapse. It was observed that for long setting times, samples would collapse even for very long polymer pyrolysis steps. Therefore, it is very important that the setting time is long enough for the deairing and casting steps but short enough to avoid or minimize particle sedimentation and

segregation. It was also observed in this study that other suspension parameters such as the chemical composition, solid content, and ratio of Si particles to PMMA beads influence the gelation time. Higher solid contents in the suspension decrease the gelation time for the same monomer content. This is due to an increase in the probability of network formation between poly(acrylamide), Si particles, and PMMA beads which results in a faster gelation. This network will be discussed later in Section 3.3.4. Higher ratios of Si particles to PMMA beads in the suspension also shorten the gelation time. This can be due to the catalyzing effect of Si on the polymerization of acrylamide and N,N′-methylenbisacrylamide. Ultrasonication was also observed to cause premature polymerization especially for high Si to PMMA ratios; therefore, it was omitted from the fabrication procedure.
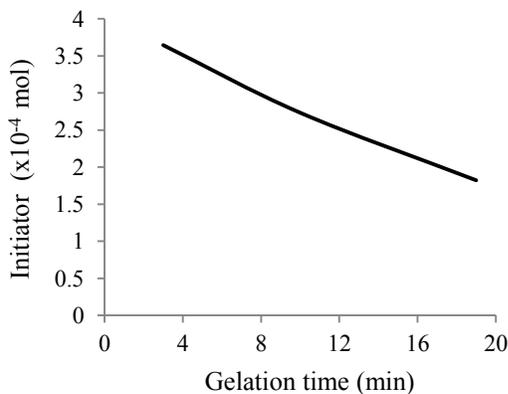
Figure 3-11. Gelation time versus initiator content for a suspension with 60 wt% solid made out of a premix solution with 7 wt% monomer content.

Polymer pyrolysis in foams fabricated by the sacrificial template technique is critical since sample collapse occurs easily during this step. A perfect design of the burn-out process avoids crack or defect formation in the sample. According to the DSC/TGA results, the burn-out temperatures of the PMMA beads and polyacrylamide polymer are

410°C and 480°C, respectively, and they do not leave any residue after burn-out. The burn-out temperature was set at 525°C to make sure that the polymers are completely removed in 2 h with the least amount of Si oxidation. Generally, the burn-out step is one of the most problematic steps in foam fabrication by sacrificial template technique since it may easily cause cracks and defects in the sample and it must be peformed extremely slowly. During polymer burn-out, PMMA beads pyrolyze first and open a large amount of interconnected channels in the sample at the beginning of the burn-out step. When the polyacrylamide network pyrolyzes at a higher temperature, those channels help easily remove the gaseous by-products from the foam. Therefore, due to the open-cell structure and homogenity of the foam, there is less chance of cracking and sample collapse during pyrolysis even at higher polymer contents and the pyrolysis step can be conducted easily and quickly.

3.3.3. Foam Properties

Figure 3-12 shows the porosity and density of the RBSN foams measured based on the Archimedes method. The maximum porosity was 87 vol% which gave the lowest density as 0.41 g/cm^3. In the fabrication of composites with a three dimensional interpenetrating network of the ceramic reinforcement, the porosity level of the foam determines the volume fraction of the ceramic material in the final metal or polymer matrix composite. Therefore, the ability to obtain such a high porosity level is very important. It must also be mentioned that achieving high levels of porosity and pore interconnectivity is very challenging since at high porosity levels, foams collapse due to any inhomogeneity in the structure. Both graphs show that there is a specific PMMA content of 44 wt% at which the maximum porosity and minimum density are obtained. By measuring the sample

linear shrinkage during polymer burn-out, it was observed that at a specific PMMA content the sample shrinkage increases suddenly as shown in Figure 3-13. This sharp increase in shrinkage occurs at high PMMA contents since in these samples there are not enough Si particles to form solid foam struts and as the PMMA beads and polyacrylamide gel network burn out, a large shrinkage occurs inside the sample. It must be mentioned that although a large amount of shrinkage is observed at very high PMMA contents, the foam quality was outstanding and no crack or defect was observed due to the well-designed pyrolysis step.
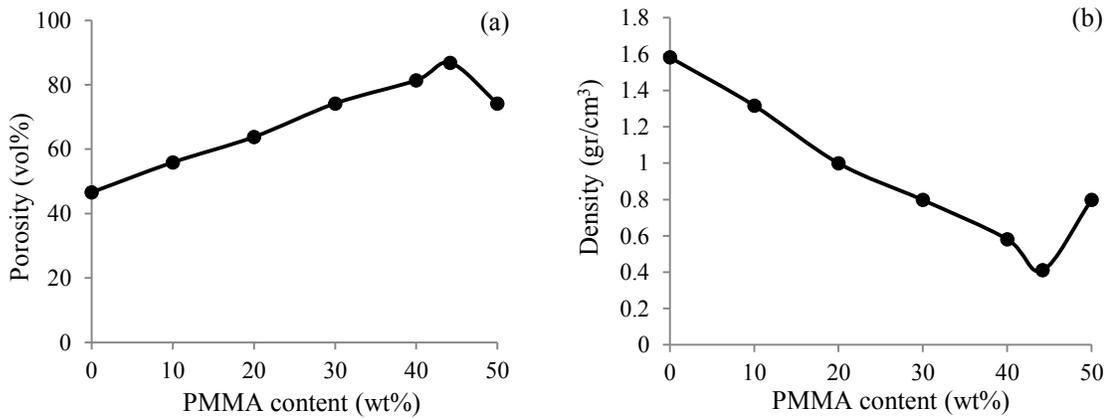
Figure 3-12. a) Foam porosity versus PMMA content, b) foam density versus PMMA content.
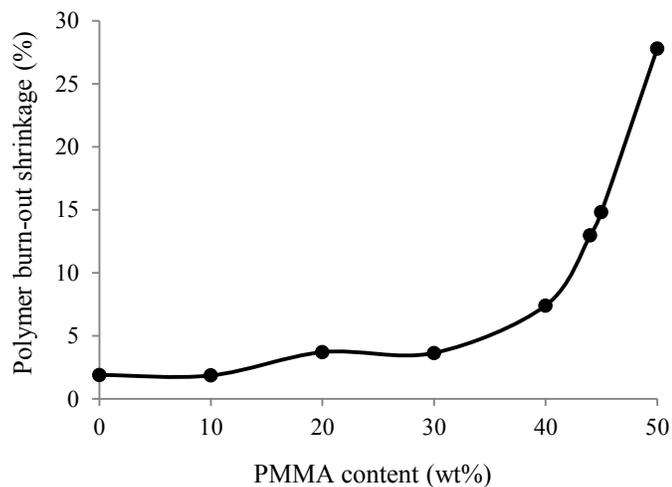
Figure 3-13. Linear shrinkage during polymer burn-out versus PMMA content.

91

BET results of the foam with 87 vol% show that the RBSN foam has a specific surface area of 2.01 m^2/g. This test was also performed on a piece of commercial RBSN. The measured surface area in this case was 0.66 m^2/g which is less than one third of the RBSN foam.

3.3.4. Microstructure and phase analyses

Figure 3-14 shows the fracture surface of the gel-cast body after drying and before polymer pyrolysis. The figure shows continuous struts of silicon particles among which the rounded PMMA beads are distributed. The figure obviously shows that the pore interconnectivity of the foam is strongly dependent on the size range of the PMMA beads. An open-cell foam is only produced if both the Si particles and the PMMA beads form two separate continuous struts. When the continuous PMMA phase is pyrolized, an interconnected network of the porosity is produced in the foam. The polyacrylamide network which holds the Si particles and PMMA beads in the gel-cast sample can also be clearly seen in Figure 3-14. It can be seen from the image how a higher monomer content leads to a more uniform distribution of both Si particles and PMMA beads resulting in a homogeneous foam. As was mentioned before, the rheological properties of the Si-PMMA suspensions significantly affect the foam structure. The uniform distribution of Si particles and PMMA beads in the gel-cast body which results in a defect-free homogenous foam with interconnected porosity is dependent on how the Si-PMMA suspension behaves in terms of rheology and stabilization. Any inhomogeneities, including agglomeration and flocculation, disrupt pore interconnectivity and results in cracks and sample collapse.
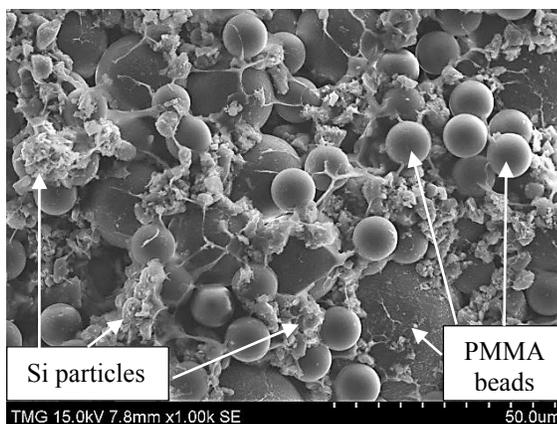
Figure 3-14. Fracture surface of the gel-cast body after drying and before polymer pyrolysis.

The microstructure of the foam before the nitriding step is of significant importance since the foam condition at this stage significantly affects the pore interconnectivity of the nitrided foam. It must be mentioned that after polymer pyrolysis, the foam is quite fragile and has a low strength; therefore, sample preparation for the microstructural analysis is difficult. Ar-sintering was only performed to increase the sample strength and make SEM analysis possible without changing the sample morphology and structure. Figure 3-15 shows the microstructure of the silicon foam after polymer pyrolysis. Figure 3-15-b clearly shows silicon struts which form an open-cell foam in which pores are fully connected. It also shows the importance of the size range of the PMMA beads in forming a continuous network of the sacrificial phase. A continuous network of the Si particles is also required at this point since any discontinuity results in cracks and sample collapse.
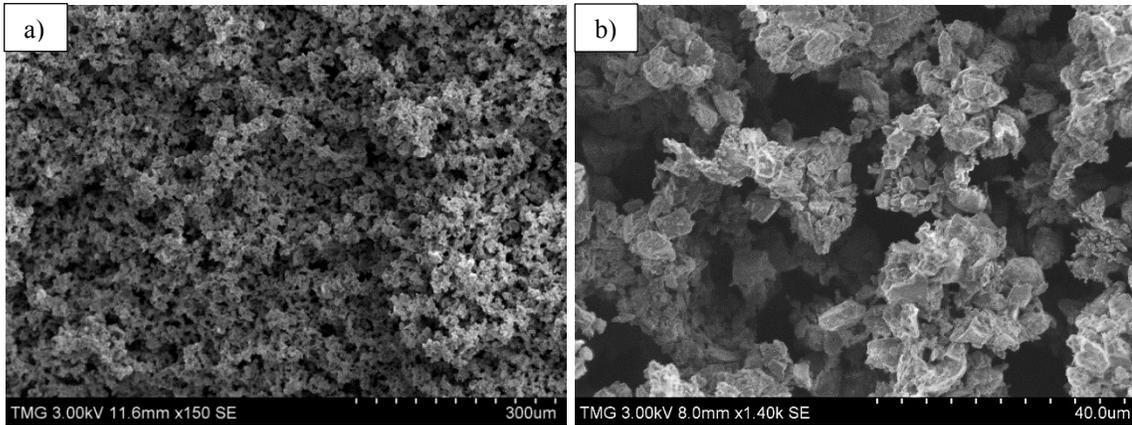
Figure 3-15. Microstructure of the highly porous silicon foam showing its pore interconnectivity.

In order to investigate the pore interconnectivity of the foam before nitridation, the silicon foam was infiltrated with polyester resin. Figure 3-16 shows an SEM micrograph of an infiltrated Si foam. It can be seen that a continuous network of polymer has filled the porosity network of the silicon foam which proves that the foam is completely interconnected.
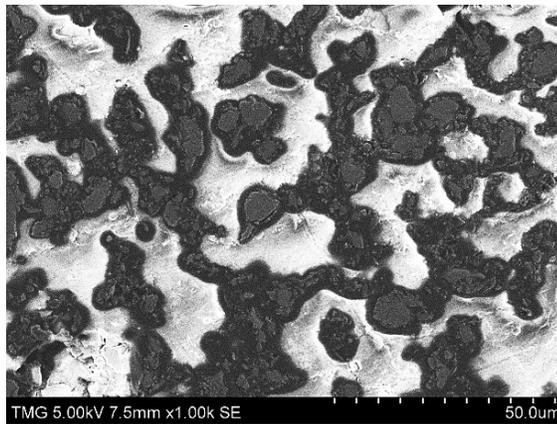
Figure 3-16. A polyester-infiltrated silicon foam; the dark regions are polyester resin and the bright regions are silicon struts of the foam.

Figure 3-17 shows the XRD result of a foam nitrided under N_2-4%H_2 at 1400°C. It can be seen that the Si nitridation reaction was completed in about 4 h and there is no residual silicon in the sample. This short nitriding step has significant advantages especially in the

production of large-sized RBSN foams. As was shown in Table 3-1, one of the major challenges in nitriding dense silicon bodies is a very long nitriding step which may take up to several days. It has been mentioned that in the case of dense RBSN ceramics, even after extremely long reaction times, the wall thickness which can be nitrided completely is about 3 cm [23]. This thickness limits the size of a dense RBSN ceramic which can be produced by nitriding and results in extremely long nitriding steps for large-sized sample [23]. Therefore, another advantage of the fabrication procedure designed in this study is that large Si_3N_4 foams can be produced based on very short nitriding cycles. XRD results also show that α-Si_3N_4 is the dominating phase in the microstructure.
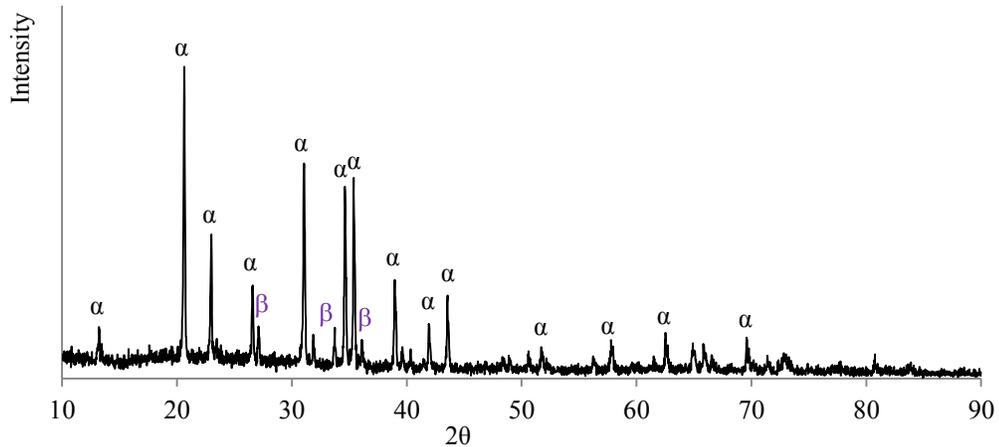
Figure 3-17. XRD pattern of an RBSN foam nitrided under N_2-4%H_2; the foam has been nitrided for 4 h at 1400°C. α is α-Si_3N_4 and β is β-Si_3N_4.

Figure 3-18 shows the microstructure of a nitrided foam with 87 vol% porosity. This is the microstructure of the final RBSN foam. As was shown by the XRD results, the figure shows that α-Si_3N_4 whisker is the dominant phase in the microstructure of the RBSN foam. It also reveals that some α-Si_3N_4 matte is also present in the form of fine grains. The whisker diameters vary from less than a micron (e.g. 0.1 µm) to a few microns. On

one hand, this whiskery structure forms due to the large surface area of the foam originating from its high level of porosity. The large surface area enhances the volatilization rate of Si resulting in more gaseous Si which participates in Reaction 3-4 to form α-Si_3N_4. On the other hand, the SiO_2 layer on Si particles which forms either due to oxidation during suspension preparation or during polymer pyrolysis is reduced to $SiO(g)$ vapor based on Reactions 3-5 and 3-6. SiO vapor then reacts with N_2 to form α-Si_3N_4 whiskers based on Reaction 3-7. It has been also concluded that α-Si_3N_4 whiskers are formed through a vapor-liquid-solid (VLS) mechanism [23, 27]. The presence of H_2 in the nitriding atmosphere has a great influence on the nitriding reactions. Hydrogen enhances the devitrification of the native oxide layer on Si particles formed during the foam fabrication process and it improves the mechanical properties of the specimen by creating a finely textured and defect-free microstructure [19]. In the presence of H_2, the SiO/N_2 reaction proceeds faster than the vapor Si/N_2 and β-Si_3N_4-forming reactions which leads to a high α/β ratio [11]. It must be mentioned that during nitriding of a dense silicon body and under normal nitriding conditions the reaction between SiO and N_2 is not dominating, but in the current investigation and under the N_2-H_2 atmosphere, it is the main nitriding mechanism.

Figure 3-18-a shows that α-Si_3N_4 whiskers grow in the porosity network of the foam where there is enough free space for whiskers to grow. This whisker-reinforced structure significantly increases the surface area of the RBSN foam due to its higher surface area per unit mass. On the other side, there is no individual regularly-shaped pore in the microstructure due to whisker growth. This makes it difficult to determine the pore size of the foam although it has 87 vol% porosity.

XRD results of the foam shows that minor amounts of β-Si_3N_4 are also present in the system. β-Si_3N_4 phase may form during nitriding in the presence of a liquid phase and to a minor extent it may form due to a reaction between solid silicon and N_2 as shown in Reactions 3-8 and 3-9, respectively [11, 23, 29]. It has also been concluded more recently that β-Si_3N_4 formation is primarily by a solid-state diffusion mechanism in the presence of atomic nitrogen, through Reactions 3-4 or 3-9 [18, 19]. Under this condition, the presence of a liquid phase is not necessary for β-Si_3N_4 formation although it enhances the formation of this phase [18, 19]. Since nitrogen can diffuse easily through the large interstitial positions of β-Si_3N_4, the rate-determining step after the formation of a dense Si_3N_4 layer is the reaction at the Si-Si_3N_4 interface [23].

$$3\ Si\ (g) + 2\ N_2 \leftrightarrow Si_3N_4\ (s) \tag{3-4}$$

$$SiO_2 + H_2 \leftrightarrow H_2O\ (g) +\ SiO\ (g) \tag{3-5}$$

$$SiO_2 + Si\ (s) \leftrightarrow 2\ SiO\ (g) \tag{3-6}$$

$$3\ SiO\ (g) + 2\ N_2 \leftrightarrow Si_3N_4\ (s) + 3/2\ O_2 \tag{3-7}$$

$$3\ Si\ (l) + 2\ N_2 \leftrightarrow Si_3N_4\ (s) \tag{3-8}$$

$$3\ Si\ (s) + 2\ N_2 \leftrightarrow Si_3N_4\ (s) \tag{3-9}$$

97
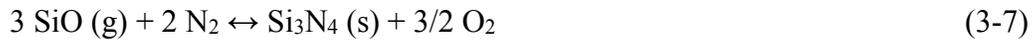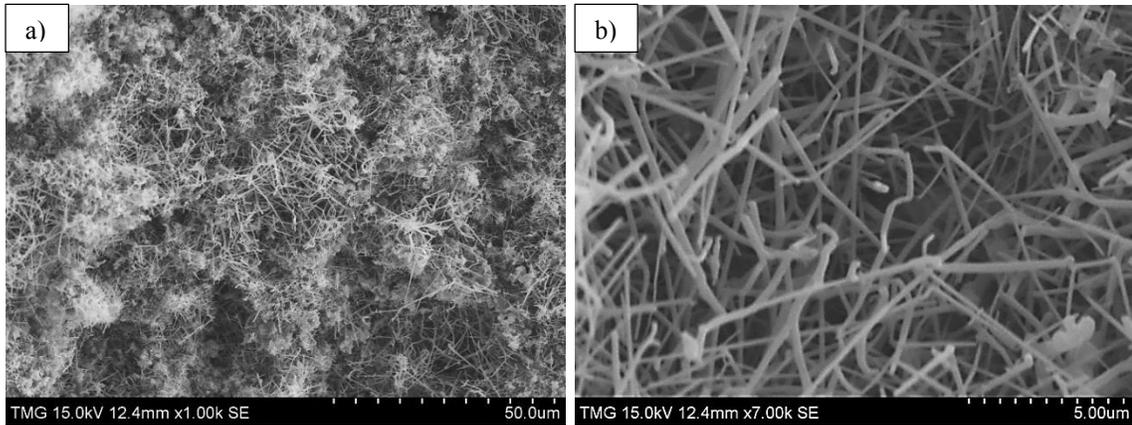
Figure 3-18. Fracture surface of an RBSN foam nitrided under N_2-4%H_2; the foam has been nitrided for 4 h at 1400°C.

The fabricated RBSN foam was infiltrated with polyester resin in order to investigate the pore interconnectivity of the foam. It can be seen from Figure 3-19 that a polymer matrix composite reinforced with a continuous network of the Si_3N_4 whiskers was obtained. It shows that the fabricated RBSN foam has a completely interconnected network of porosity.
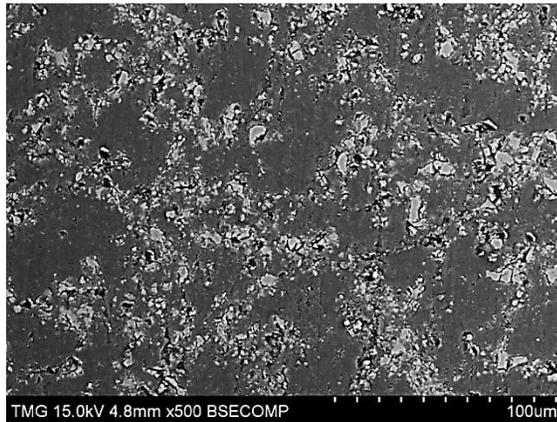
Figure 3-19. A polyester-infiltrated RBSN foam; the dark regions are polyester resin and the bright regions are Si_3N_4 whiskers.

3.4. Conclusions

A Si_3N_4 foam with interconnected porosity has been fabricated in this study via gel-casting and reaction bonding techniques. The fabrication procedure in terms of Si-PMMA suspensions, gel-casting parameters, and polymer pyrolysis were characterized and optimized. The complete infiltration of the fabricated foam both before and after the nitriding step shows that the foam has an open-cell structure with interconnected porosity. The porosity level of the foam can be controlled based on the amount of PMMA beads and the monomer content of the premix solution and it can reach up to 87 vol%. XRD results reveal that the foams can be nitrided completely in a few hours without any residual Si left in the system. Phase and microstructural analysis of the foam show that the gaseous phase reactions are dominating during nitriding which lead to α-Si_3N_4 formation in the form of whiskers. The designed fabrication procedure offers low cost, short production time, high levels of porosity, and pore interconnectivity which introduces novel applications such as fabrication of interpenetrating composites.

Chapter 4

4.1. Preface to chapter 4

One of the most important properties of ceramic foams is the mechanical strength. It determines whether the foam can function in any specific application or not. Therefore, the next step of the investigation was focused on the parameters, which influence the foam's mechanical strength. There are various processing factors, which must be considered. The first parameter that clearly influences the foam strength is its level of porosity. Depending on the application, the desired porosity level can be quite different. Therefore, it is of major importance to determine the relationship between the porosity and the mechanical strength of the fabricated RBSN foam. In this chapter it was also explained how the monomer content may affect the distribution of the Si particles and PMMA beads and consequently how it may influence the foam homogeneity. This is the second parameter that may affect the foam strength and must be investigated. The nitriding condition also plays a major role on the foam strength. Understanding the nitridation phenomenon is a key step in designing RBSN foams with desirable properties including the mechanical strength. Depending on the nitriding atmosphere and temperature, a diverse range of microstructures and consequently different mechanical strengths may be obtained. In order to study and correlate the observed microstructures to the nitriding conditions and then to the foam strength, an extensive investigation on the nitriding reactions and mechanisms is required. Therefore, the nitridation process and its mechanisms will be the third part of the investigation provided in the next chapter.

The influence of the nitriding parameters on the microstructure and strength of the open-cell reaction bonded silicon nitride foams fabricated via wet processing

Ali Alem, Robin A.L. Drew, Martin D. Pugh

Mechanical and Industrial Engineering Department, Concordia University, 1455 De Maisonneuve Blvd. W., Montreal, Quebec, Canada H3G 1M8

Abstract

In this study the parameters which influence strength of the open-cell reaction bonded silicon nitride (RBSN) foams were investigated. These parameters include the monomer content in the suspension, the porosity level of the foam, the nitriding atmosphere including N_2 and N_2-4%H_2, and the nitriding temperature ranging from 1350 to 1425°C. The nitriding mechanisms dominating under different nitriding conditions were also studied based on the phase and microstructural analysis.

It was observed that there is a minimum monomer concentration of 25 wt% required in the premix solution to obtain a defect-free and homogeneous RBSN foam. Increasing the monomer content only from 15 wt% to 20 wt% resulted in a threefold increase in the foam strength. The high porosity level of the foam and consequently its large surface area significantly affect the nitriding mechanisms and microstructures compared to conventional RBSN ceramics. The maximum strength was obtained for foams nitrided under N_2-H_2 atmosphere and the nitriding temperature had a negligible effect on the foam strength when H_2 is present in the atmosphere. α-Si_3N_4 is also the dominant phase in the microstructure in the presence of H_2 regardless of the nitriding temperature. It was observed that β-Si_3N_4 can also be present in high quantities when N_2 atmospheres are used. β-Si_3N_4 is present in the microstructures in two different morphologies, namely

interlocking rods and angular grains. Each morphology forms based on a specific nitriding mechanism.

Keywords: Foam; Silicon nitride; Reaction bonding; mechanical strength; Pore interconnectivity

4.2. Introduction

Cellular ceramics have been recently found to have many remarkable properties which enable them to be utilized in many high-tech applications including diesel particulate filters (DPF), separation membranes, and the fabrication of interpenetrating composites. In all these applications the strength of the ceramic foam is very important and will determine the in-service condition of the final product.

RBSN foams which are fabricated based on direct nitridation of Si compacts have many advantages over other ceramic foams. These advantages can make RBSN foams a good candidate for many industrial and engineering applications. On one hand, they offer the properties of Si_3N_4 ceramics including good mechanical properties, excellent chemical and high temperature stability, and good thermal shock resistance and on the other hand; they benefit from a lower fabrication cost via avoiding the use of costly Si_3N_4 powder as the starting material. It must be mentioned that working with Si_3N_4 starting powder has other major fabrication issues including very high sintering temperatures (>1900°C), large amounts of sintering additives, high linear shrinkage (15-20%), and poor rheological properties [19 - 21, 116]. All these issues mentioned can be avoided through the reaction bonding technique.

Open-cell RBSN foams with pore interconnectivity and a high level of porosity (87 vol%) have been fabricated in our previous investigation [123]. Understanding the nitridation mechanisms and morphologies of the Si_3N_4 phases formed via the reaction bonding phenomenon has always been very challenging. There is still disagreement in the literature regarding the proposed mechanisms for Si_3N_4 formation. In addition, the nitriding situation will be much more complicated when dealing with RBSN foams with their high level of porosity and pore interconnectivity. In this case the dominant reaction bonding mechanisms and consequently the morphology of the Si_3N_4 phases may be quite different compared to "normal" RBSN ceramics. The high porosity level of the silicon foam prior to nitriding and its pore interconnectivity affect the system in several ways including the Si volatilization rate, free space available for Si_3N_4 to form and grow, and the nitridation rate. Therefore, this investigation focuses on the influence of the nitriding parameters including the nitriding atmosphere and the temperature on the foam microstructure and its mechanical strength. This study also investigates the nitriding mechanisms dominating the RBSN foams and the resulting microstructures in terms of the phases present and their morphologies. The relationships between the observed microstructure and the obtained strength are also discussed. Therefore, the investigation helps one understand the nitridation mechanisms of the porous RBSN foams.

4.3. Experimental procedure

4.3.1. Foam fabrication

The RBSN foams with interconnected porosity have been fabricated from Si powder (ABCR, 99.995%, -8 microns) and PMMA beads (Microbeads, 10-40 μm) as the sacrificial pore former via the gel-casting and the reaction bonding techniques [123]. The

monomer (Acrylamide, $C_2H_3CONH_2$, Sigma-Aldrich) and cross-linker (N,N'-methylenbisacrylamide, $(C_2H_3CONH_2)_2CH_2$, Sigma-Aldrich) were dissolved in water to obtain a premix solution containing 25 wt% monomer. Silicon powder, PMMA beads and other rheological agents were also added to the premix solution. Suspension stabilization and homogenization were performed through pH adjustment and ball milling, respectively. After the addition of the catalyst (ammonium persulfate, $(NH_4)_2S_2O_8$, Sigma-Aldrich) and the initiator (N,N,N',N'-tetramethylethylenediamine, $C_6H_{16}N_2$, Sigma-Aldrich), the suspension was cast in to silicone rubber molds. Drying of the samples was followed by the polymer burn-out step. Finally, the nitriding step was performed to produce an open-cell RBSN foam with a controlled level of porosity. More details of the fabrication procedure and the properties of the fabricated foam have been discussed elsewhere [123]. Figure 4-1 shows a flowchart of the fabrication procedure.

This study focuses on the factors that affect the RBSN foam strength especially the nitriding parameters. The nitriding step was performed at different temperatures between 1350°C to 1425°C and under different static atmospheres including N_2 and N_2-4%H_2. The heating rate during nitriding was 5 °C/min up to 1350°C, 1 °C/min up to 1390°C, and 0.3 °C/min up to 1425°C. The dwell time was between 6 to 10 h at the maximum nitriding temperature. In order to study the effect of Ar-sintering on the strength of the foams, some samples were sintered under Ar-4%H_2 for 2 h at 1200°C prior to the nitriding step. Based on the nitriding conditions, specific codes have been used for samples. In the sample codes used in the rest of the study, ArH shows the performance of a sintering step under the Ar-4%H_2 atmosphere, NH shows nitriding under N_2-4%H_2, and N represents nitriding under the N_2 atmosphere. The final nitriding temperature is also

included in the last part of the sample code. As an example, ArH-NH1400 shows a sample that has been sintered under Ar-4%H_2 and then nitrided under N_2-4%H_2 at 1400°C.
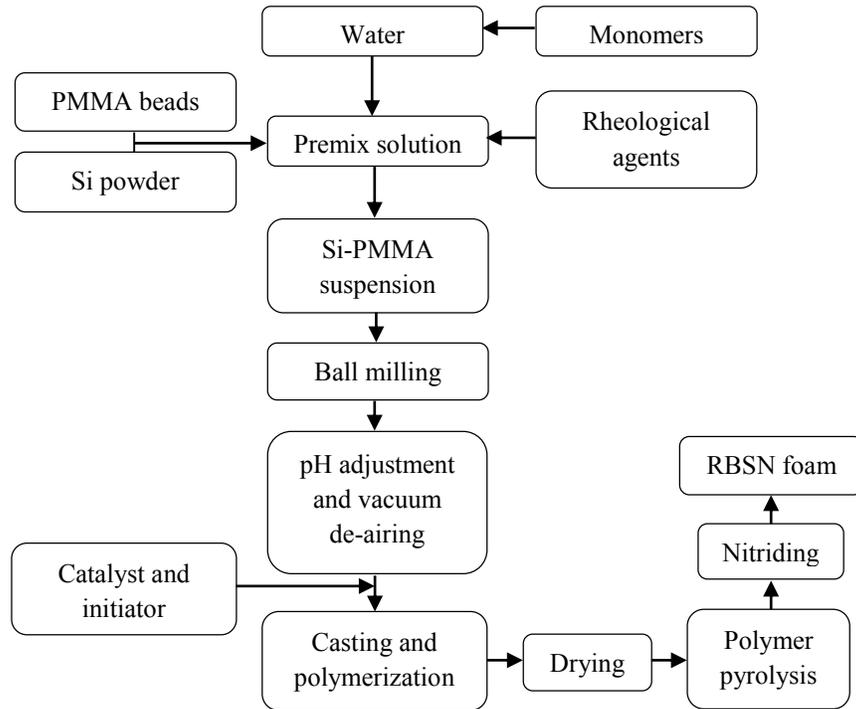
Figure 4-1. Flowchart of the experimental procedure.

4.3.2. Characterization

The porosity and density of the foams were measured based on the Archimedes technique according to the ASTM C373-88 standard. Four-point bending tests were carried out on bar-like samples using a uniaxial tensile testing machine (Instron®, Model 3382) to determine the foam strength. The dimensions of the bending samples were 10 x 10 x 70 mm^3 and they were not polished before the bending test. The lower span was 40 mm and the upper was 20 mm, moving at a crosshead speed of 0.1 mm/min. A minimum of three and a maximum of six samples were tested under each specific condition. X-ray

diffraction analysis (XRD, X'PertPro; PANalytical) and scanning electron microscopy (SEM, HITACHI, S-3400N) equipped with energy-dispersive X-ray spectroscopy (EDS; Oxford Instruments; Wave Model) techniques were also utilized to investigate the phases present and the microstructure of the RBSN foams nitrided under different conditions.

4.4. Results and Discussion

4.4.1. The effect of porosity on the foam strength

Figure 4-2 shows the porosity and density of the foam versus the PMMA content. As the figure shows the PMMA content of the suspension varies from the minimum of 0 to the maximum of 45 wt% resulting in a range of porosity from 41 vol% to 83 vol%, respectively. The sample without any PMMA beads (0 wt%) is a silicon gel-cast body which exhibits 41 vol% porosity. It is known that even conventional RBSN ceramics have about 20 vol% porosity which comes from the nature of the reaction bonding phenomenon [11]. Therefore, the rest of the porosity in this sample, which is 21 vol%, is due to the fabrication technique and the presence of 25 wt% monomer in the premix solution. Obviously, during polymerization, the monomers form a polymer network which holds the particles together in the gel-cast body. This polymer network leaves some porosity in the body after polymer pyrolysis.
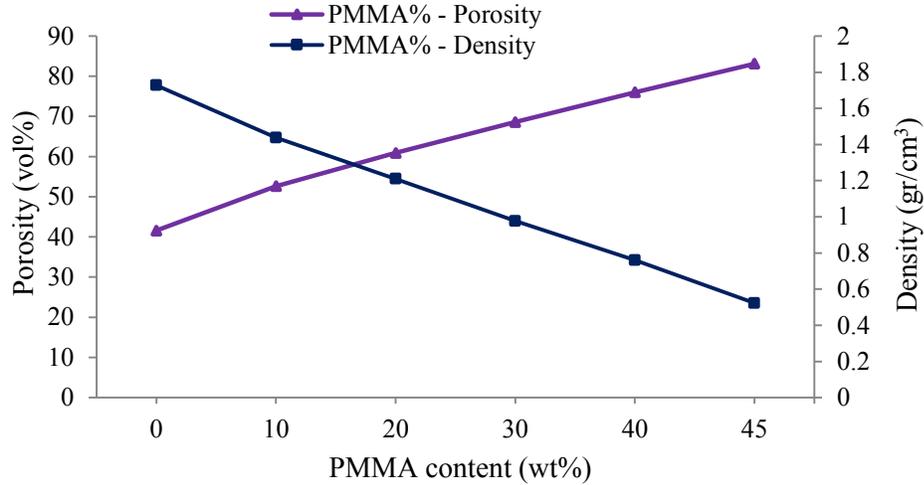
Figure 4-2. Porosity and density of the RBSN foam versus the PMMA content; samples nitrided under N_2-4%H_2 at 1390°C.

Figure 4-3 shows the flexural strength of the foams versus the PMMA content. The sample with the lowest porosity level shows the highest strength of 18 MPa. As mentioned before, this is a gel-cast Si body fabricated from Si suspensions with no PMMA beads. The foam strength decreases to 1 MPa for the sample containing 45 wt% PMMA beads and consequently 83 vol% porosity. It is clear that as the foam porosity increases, the strength decreases as would be expected.
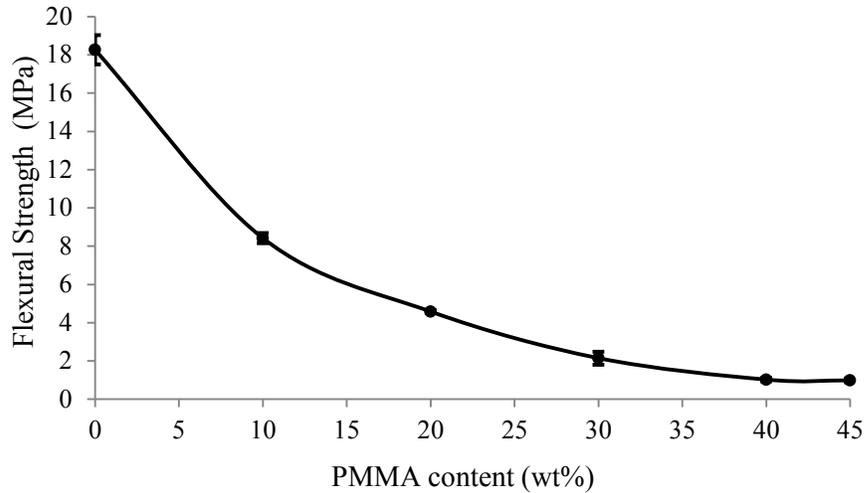
Figure 4-3. Flexural strength of the RBSN foams versus the PMMA content; foams were nitrided under N_2-4%H_2 at 1390°C.

The main goals of this investigation are first, to study the influence of the nitriding parameters on the RBSN foam strength and second, to determine the dominating nitriding mechanisms. It was observed in this study that the foams with very high porosity levels (e.g. 83 vol% porosity in the case of 45 wt% PMMA in the suspension) do not show large differences in terms of strength even if they are nitrided under different nitriding conditions. In this case, the comparison between the foam strengths might be difficult and contain errors due to small differences between the strength values. Therefore, the PMMA content for the rest of this investigation was selected to be 34 wt% in the suspension. This PMMA content provides an RBSN foam with a porosity level of more than 70 vol% which is high enough to affect the nitriding mechanisms. Under this condition, the RBSN foams also reveal considerable differences in terms of strength when they are nitrided under different nitriding conditions.

4.4.2. The effect of monomer content on the foam strength

The first parameter which significantly influences the RBSN foam strength is the monomer content in the premix solution. Figure 4-4 shows how the strength increases via increasing the monomer content of the premix solution. Obviously, increasing the monomer content from 9 wt% in the premix solution to 25 wt% results in an increase in the final foam porosity; therefore, one expects to see a decrease in the foam strength instead of an increase. The graph shows that by increasing the concentration of the premix solution from only 15 wt% to 20 wt%, a threefold increase in the nitrided strength is observed.

The observed increase in the foam strength is due to an improvement in the sample homogeneity which is obtained in the presence of a higher monomer content. It was observed that a combination of a low monomer content and a high Si to PMMA weight ratio in the suspension creates defects and inhomogeneities in the as-cast samples. Those defects are also in the interior parts of the samples and they only show up after grinding the sample surfaces. Figure 4-5 shows these defects in the microstructure of the as-cast sample containing 12 wt% monomer in the premix solution. It was observed that the population of these defects is entirely dependent on the monomer concentration and as the monomer concentration increases, the population of the defects decreases. These defects finally disappear at 25 wt% of monomer. From Figure 4-3 it can be seen that the PMMA content of the suspension varies between 0 and 45 wt% to achieve different porosity levels in the fabricated foam while the suspension solid content is always constant at 68.5 wt%. As the PMMA content in the suspension decreases from 45 wt%, the Si content must be increased in order to keep the suspension solid content constant.

Therefore, lower PMMA contents in the suspension mean higher Si to PMMA weight ratios in the suspension. Since Si particles (< 8 μm) used in this study are much finer than PMMA beads (10-40 μm), a high Si to PMMA weight ratio results in a larger surface area in the suspension. A higher surface area also requires a higher concentration of monomers to obtain a homogeneous gel network during polymerization. When the premix solution has a low monomer content e.g. 15 wt% or less, the poly(acrylamide) network which forms due to polymerization of the monomers is not widespread enough to form a defect-free gel-cast body. Therefore, those defects are present in the cast samples and they cause a significant decrease in the strength of the nitrided foam. It is concluded that for suspensions with high Si to PMMA ratios, 25 wt% monomer in the premix solution is required to avoid the formation of such defects in the foam. It must be mentioned that increasing the monomer content also makes the polymer pyrolysis step more difficult; therefore, monomer concentrations above 25 wt% may cause sample collapse during polymer burn-out.
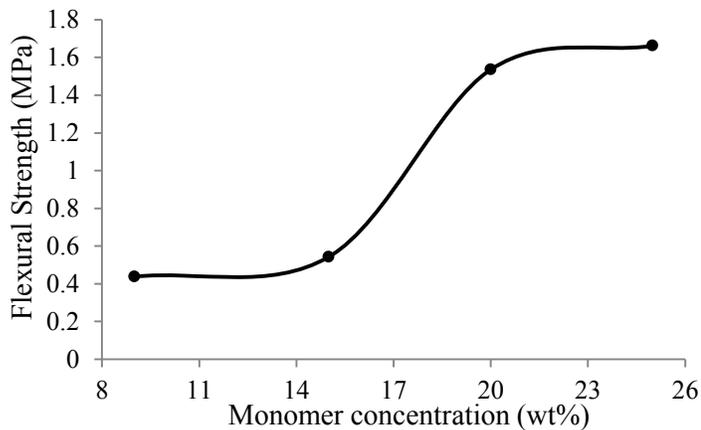
Figure 4-4. The influence of the monomer content on the RBSN foam strength; all foams have been nitrided under N_2-4%H_2 at 1400°C.

110
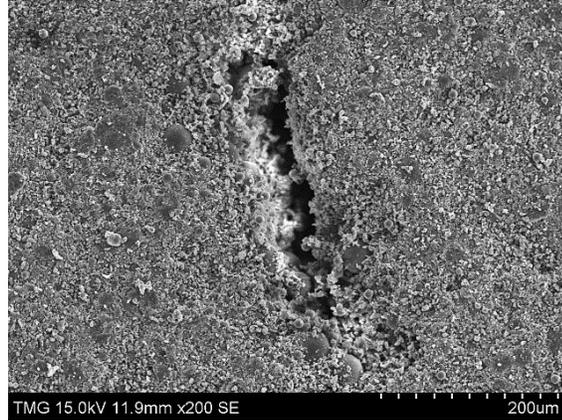
Figure 4-5. Defects and inhomogeneities in the as cast sample with 12 wt% monomer in the premix solution.

4.4.3. The influence of the nitriding conditions on the foam strength

Figure 4-6 shows the effect of different nitriding parameters on the strength of the RBSN foams. The figure reveals that the maximum strength was obtained for foams sintered under Ar-H_2 atmospheres followed by nitriding under N_2-H_2 atmosphere and that the minimum strength was observed for the foams nitrided under N_2 at 1425°C.

It can be seen from the figure that a short Ar sintering step improves the foam strength by 10% and 14% for the foams nitrided under N_2-H_2 and N_2 atmospheres, respectively. It is also observed that increasing the nitriding temperature from 1390°C (below the Si melting point) to 1425°C (above the Si melting point) has a negligible effect on the foam strength when the N_2-H_2 atmosphere is used. This is probably due to the formation of a silicon nitride network in the presence of H_2 during the early stages of nitriding and the resulting microstructure of the RBSN foam. On the other hand, results show a significant difference in terms of strength between the foams nitrided at 1425°C under N_2 and N_2-H_2 atmospheres. It can be seen that at 1425°C, the N_2-H_2 atmosphere enhances the foam strength by 35% compared to the N_2 atmosphere. This can be probably due to the

111

formation of a continuous skeletal network of silicon nitride in the presence of H_2 during early stages of nitriding [124]. This network can play the role of the foam struts; therefore, a higher strength is obtained under N_2-H_2. The relationship between the microstructure and the strength will be discussed in the following section.

It must be mentioned that since the foam has been fabricated based on a wet processing of silicon-PMMA suspensions, isothermal nitridation of the foam under N_2 and below the silicon melting point e.g. 1390°C was very slow compared to other nitriding conditions. This is due to the oxidation of Si particles during suspension preparation which results in the formation of SiO_2 layers around Si particles. Si oxidation in water has been shown in Reaction 4-1. This oxide layer either slows down the nitriding reactions or even stops them if it has a significant thickness. Therefore, if nitridation is performed under N_2, the maximum nitriding temperature must be above the silicon melting point to accelerate the nitridation step and avoid residual silicon in the nitrided foam. Otherwise, the reaction would be quite slow. The presence of H_2 in the nitriding gas removes the SiO_2 layer around the Si particles based on Reaction 4-2; therefore, nitridation can be performed below the Si melting point (e.g. at 1390°C) to get full Si to Si_3N_4 conversion in quite a short time.

$$Si \ (s) + 2H_2O \rightarrow SiO_2 \ (s) + 2H_2 \ (g) \tag{4-1}$$

$$SiO_2 + H_2 \rightarrow H_2O \ (g) + SiO \ (g) \tag{4-2}$$
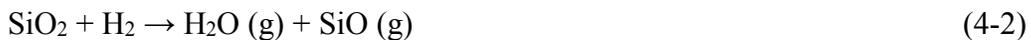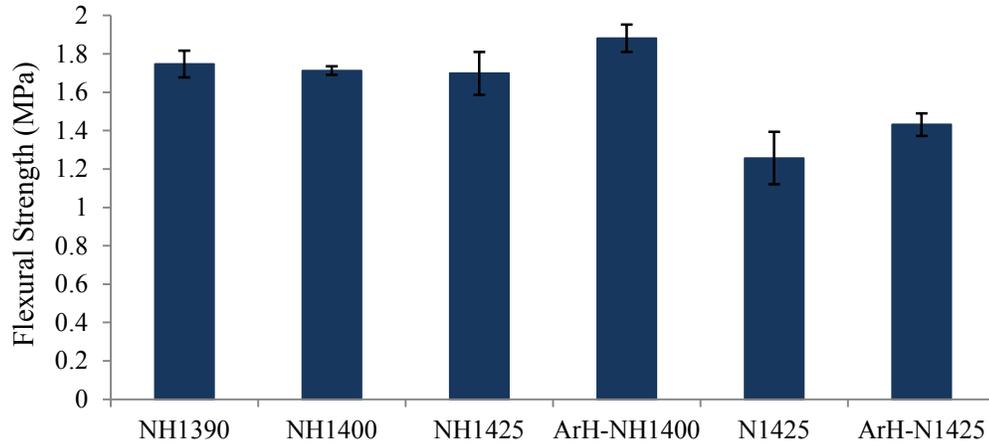
Figure 4-6. The influence of the nitriding atmosphere and the temperature on the strength of the RBSN foam.

It was observed in this study that for some higher nitriding rates and temperatures, Si may melt during nitriding. Due to the poor wettability of Si with Si_3N_4, molten Si is pushed out of the foam porosity and forms spherical droplets on the surface of the RBSN foam. It was also observed that partial melting of Si does not decrease the foam strength. It is known that the strength of RBSN ceramics is controlled by the stress required for the propagation of the largest defect present in the body [125, 126]. Since the size of the PMMA beads (10-40 μm) used as a pore-forming agent in this study is much larger than the size of the Si particles (<8 μm), partial melting of Si does not affect the size of the largest pore or defect present in the fabricated RBSN foam. Therefore, no significant change in the foam strength was observed when Si partially melts during nitriding. Melting of Si was also more probable under N_2 atmospheres than N_2-H_2 atmospheres. The presence of H_2 results in fast Si nitridation and in addition, helps with the formation of a skeletal network of Si_3N_4 during the early stages of the nitridation; therefore, there is less chance to get molten Si squeezed out of the foam.

4.4.4. The effect of nitriding conditions on the nitriding mechanisms

Table 4-1 shows the physical properties of the RBSN foams. The α- and β-Si_3N_4 contents of the foams nitrided under different nitriding conditions are also included in the table. The ratio of the Si_3N_4 phases has been determined from the XRD patterns of the foams based on Gazzara's method [127].

It is known that vapor phase reactions are responsible for α-Si_3N_4 formation when molecular nitrogen is involved in nitriding reactions. Reactions 4-3 and 4-4 show these gaseous phase reactions [11, 22, 23]. The table clearly shows that regardless of the nitriding temperature, the α-Si_3N_4 content is always constant at about 86 wt% when a N_2-H_2 atmosphere is utilized. H_2 significantly reduces the concentration of the atomic nitrogen in the atmosphere; therefore, the formation of α-Si_3N_4 is considerably promoted. In the presence of H_2, the SiO/N_2 reaction (Reaction 4-4) also precedes faster than the vapor Si/N_2 reaction (Reaction 4-3) [11, 19]. It must be mentioned that during nitriding of a dense silicon body and under normal nitriding conditions the reaction between SiO and N_2 is not dominating, but in the current investigation and under the N_2-H_2 atmosphere, it is probably the main nitriding mechanism resulting in more than 85 wt% α-Si_3N_4. More details related to the nitriding mechanisms and reactions are included in the following discussion.

$$3\ Si\ (g) + 2\ N_2 \leftrightarrow Si_3N_4\ (s) \tag{4-3}$$

$$3\ SiO\ (g) + 2\ N_2 \leftrightarrow Si_3N_4\ (s) + 3/2\ O_2 \tag{4-4}$$

Table 4-1. Density, porosity, α- and β-Si$_3$N$_4$ contents of the RBSN foams nitrided under different nitriding conditions.

Sample code	Density (g/cm^3)	Porosity (%)	α-Si$_3$N$_4$ content (wt%)	β- Si$_3$N$_4$ content (wt%)
NH1390	0.91	70.9	86.34	13.66
NH1400	0.90	71.1	86.32	13.68
NH1425	0.93	70.5	85.4	14.6
ArH-NH1400	0.92	69.9	86.29	13.71
N1425	0.90	71.5	58.6	41.4
ArH-N1425	0.92	70.9	54.1	45.9

It is known that β-Si$_3$N$_4$ forms in the presence of atomic nitrogen [22]. β-Si$_3$N$_4$ forms if Si can react either in a liquid form or in a vapor form with atomic nitrogen [18, 19, 25]. Therefore, it has been suggested that both α- and β-Si$_3$N$_4$ can form from gas phase reactions occurring on a solid surface depending on the presence of molecular and atomic nitrogen, respectively [22].

As was mentioned before, Table 4-1 shows that the β-Si$_3$N$_4$ content of the microstructure is minimum under N$_2$-H$_2$ regardless of the nitriding temperature and the α-Si$_3$N$_4$ phase is always dominant. Therefore, in the presence of H$_2$ in the nitriding atmospheres, even higher nitriding temperatures do not promote β-Si$_3$N$_4$ formation. There are two reasons why the β/α ratio is quite low in RBSN foams nitrided under N$_2$-H$_2$. First of all, as was mentioned before, H$_2$ removes atomic nitrogen from the nitriding atmosphere; therefore, α-Si$_3$N$_4$ is encouraged to form in the presence of molecular N$_2$. Since the silicon gel-cast body has a high level of interconnected porosity, a high Si volatilization rate is expected

during nitriding. Therefore, more silicon vapor participates in Reaction 4-3 in the presence of molecular nitrogen resulting in α-Si_3N_4 formation. On the other hand, the SiO_2 layer which forms around Si particles during suspension preparation and casting is reduced either by H_2 or Si; which have been shown in Reactions 4-2 and 4-5, respectively. Therefore, a large amount of SiO vapor also forms which can participate in Reaction 4-4 to form more α-Si_3N_4. In conclusion, gaseous phase reactions are dominant during nitriding of the highly porous RBSN foams under the N_2-H_2 atmospheres, resulting in a high α/β ratio. Another reason for a high α/β ratio is the acceleration of nitridation during early stages of the reaction since the induction time required to reduce the SiO_2 layers on Si particles is greatly shortened in the presence of H_2. Therefore, the Si_3N_4 which forms during early stages of the reactions and at lower temperatures, will be in the form of α-Si_3N_4 since this is the low-temperature polymorph of Si_3N_4. This α-Si_3N_4 can also act as a nucleus and favors the nucleation and growth of more α-Si_3N_4 phase during nitridation.

$$SiO_2 + Si \text{ (s)} \leftrightarrow 2 \text{ SiO (g)} \tag{4-5}$$

Table 4-1 also shows that foams nitrided under N_2 reveal more than 40% β-Si_3N_4 in their microstructures. In the absence of H_2, higher concentrations of atomic nitrogen increase the β-Si_3N_4 content [22]. Also, in the absence of H_2, Reaction 4-4 which results in α-Si_3N_4 formation, is significantly reduced. A comparison between the β contents of N1425 and ArH-N1425 foams in Table 4-1 also shows the effect of Ar sintering on increasing the β content when H_2 is not present in the nitriding atmosphere. For the same nitriding profile, Ar sintering increased the β content by 4.5%. This can be due to the reduction of the SiO_2 layer on Si particles during Ar sintering under the Ar-H_2 atmosphere resulting in

less SiO vapor formation which forms α-Si_3N_4 via Reaction 4-4. On the other hand, since oxygen also removes all the atomic nitrogen [22], reduction of SiO_2 also lowers the oxygen partial pressure in the atmosphere resulting in more β-Si_3N_4.

It can also be seen from the table that although Ar sintering has a considerable influence on the foam strength, it causes a negligible decrease (around 1 vol%) in the foam porosity. Therefore, this short step can be used both to increase the foam strength and to increase the β-Si_3N_4 content.

Figure 4-7 shows the XRD pattern of the NH1400 foam. As can be seen from Table 4-1, there is almost no difference between the α- and the β-Si_3N_4 contents of the RBSN foams nitrided under N_2-H_2 even at different temperatures. Therefore, only the XRD pattern of the NH1400 foam is shown to represent all the other RBSN foams nitrided under N_2-H_2. It can be seen from the pattern that there is no residual silicon in the foam and the nitridation is complete. The pattern clearly shows the high α/β phase ratio obtained in the presence of H_2.
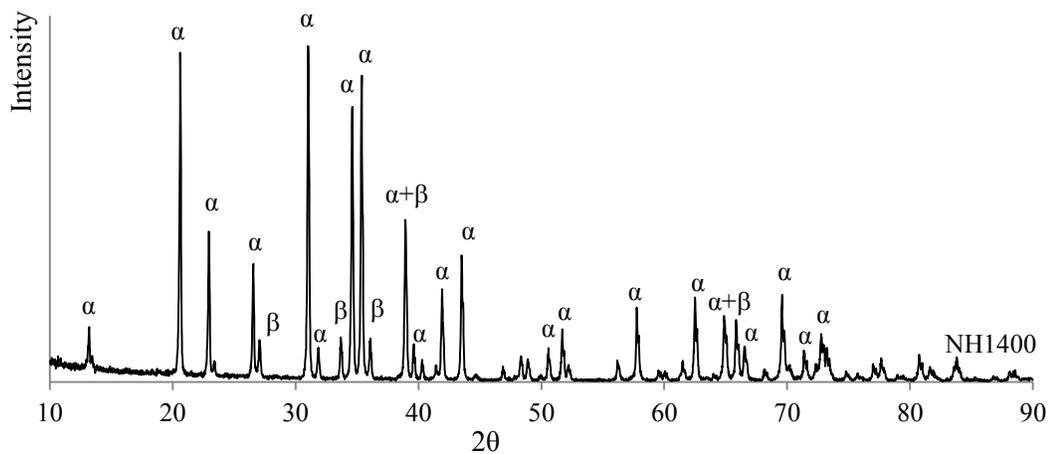
Figure 4-7. XRD pattern of the NH1400 foam; only α- and β-Si_3N_4 phases are present with no residual Si.

117

Figure 4-8 shows the XRD patterns for the N1425 and ArH-N1425 foams. The difference

between the β contents due to the Ar sintering step is clearly observed based on the β

peak intensities. The higher β/α phase ratio in the absence of H_2 is also clearly seen.
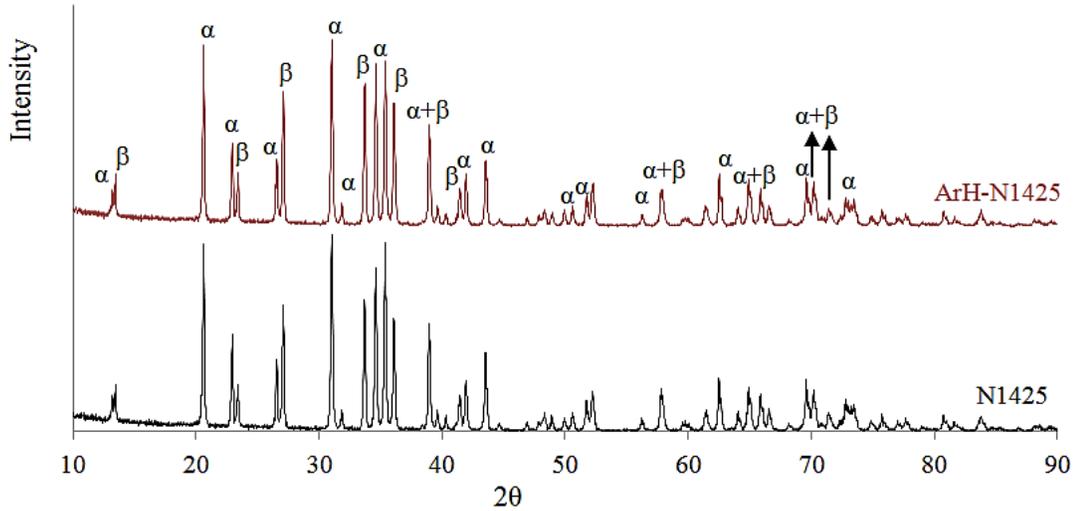
Figure 4-8. XRD patterns of the N1425 and ArH-N1425 foams; only α- and β-Si_3N_4 phases are present

with no residual Si.

4.4.5. Microstructure of the RBSN foams

Figure 4-9 shows the microstructure of the NH1390 foam. The figure shows α-Si_3N_4 both

in the form of whiskers with high aspect ratios and also fine grained α-matte. In the case

of α-Si_3N_4 whiskers, gaseous silicon reacts with nitrogen to form α-Si_3N_4 [10]. In the case

of α-matte which forms as fine grains, nitrogen will be adsorbed chemically on the Si

surface resulting in Si_3N_4 nuclei formation at the beginning of the reaction. Then Si will

be transported to the reaction site by evaporation-condensation and/or surface diffusion

mechanisms to continue the nitriding reactions. When a dense layer of Si_3N_4 forms, new

spaces must be created for the reaction to go forward. The formation of the new spaces

can be either through vacancy condensation to form new pores or via silicon

118

volatilization [22, 26]. The nitrogen which has diffused through the Si_3N_4 layer can then react with either Si or SiO in these pores to form more α-Si_3N_4 [22, 23]. Since the fabricated foam has a high level of interconnected porosity (above 70 vol%) and a large surface area, the dominating pore formation mechanism is not vacancy condensation. In this case, Si volatilization is the most likely source of pore formation. Therefore, the nitriding time is significantly shorter compared to a conventional RBSN ceramic, without leaving any residual Si in the body. The RBSN foam dimensions can also be much larger compared to a conventional RBSN body since the interconnected porosity of the foam avoids premature closure of the porosity which affects the supply of N_2 to the interior parts of the sample.
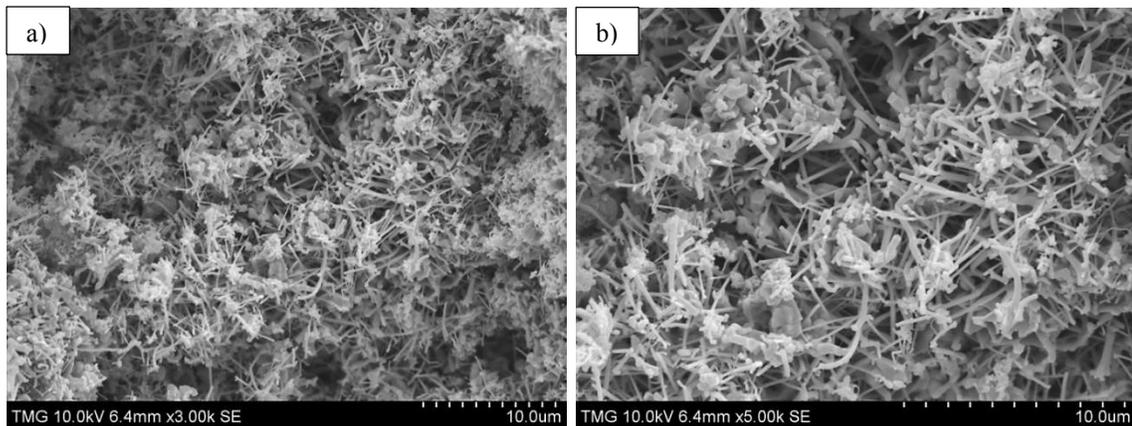
Figure 4-9. a) and b) Microstructures of the NH1390 foam showing α-whiskers with high aspect ratios and α-matte, c) whiskers at a higher magnification.

Figure 4-10 shows the microstructure of the N1425 foam. The microstructure shows α-whiskers and α-matte similar to the NH1390 microstructure. The microstructure also shows more interlocking rod-like β-Si_3N_4. These β-whiskers have a lower aspect ratio compared to α-whiskers and they have larger diameters. They form based on the reaction between Si vapor and atomic nitrogen; therefore, they get the rod-like morphology and grow through the porosity network of the foam. The only reason that these β-whiskers can grow in an empty space is that they form based on gas phase reactions in the presence of atomic nitrogen.
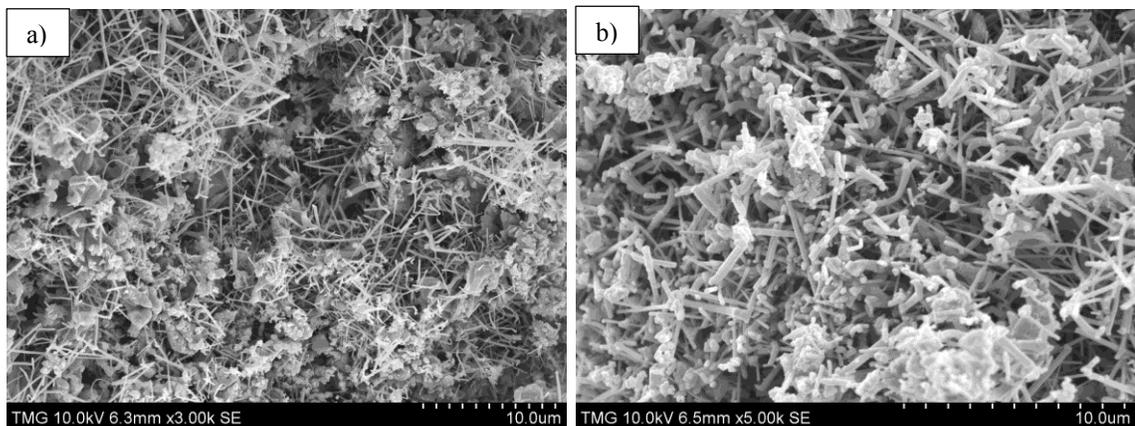
Figure 4-10. Microstructures of the N1425 foam.

The other possibility to get β-Si_3N_4 is when silicon melts [22]. In this case, β-Si_3N_4 forms as hexagonal-shaped grains shown in Figure 4-11. These grains do not form due to gas-phase reactions and they probably grow from molten Si. These angular grains are observed more in the interior part of the foam. This is due to the exothermic nature of the nitriding reactions which causes a temperature rise in the interior. The higher temperatures in those regions promote β-Si_3N_4 formation. As shown in Figure 4-12, it was also observed that a group of these grains grow together and they do not form individually. This is further proof that these grains grow from a puddle of molten Si and not based on gaseous phase reactions. It was also observed that in some cases these angular β-Si_3N_4 grains form in fewer quantities under the N_2 atmosphere. This can be due to the fast rate of gaseous phase reactions due to the high surface area of the foam and the presence of atomic nitrogen. In this case, gaseous Si reacts with atomic nitrogen resulting in rod-like β-Si_3N_4. Therefore, under a nitrogen atmosphere, gas phase reactions might be dominant in the β-Si_3N_4 formation. Since in the presence of H_2, nitrogen is mainly in molecular form, the chance of β-Si_3N_4 formation based on gas phase reactions is very low. Therefore, β-Si_3N_4 might mainly form in the presence of atomic nitrogen dissolved in molten Si resulting in the formation of these angular grains.
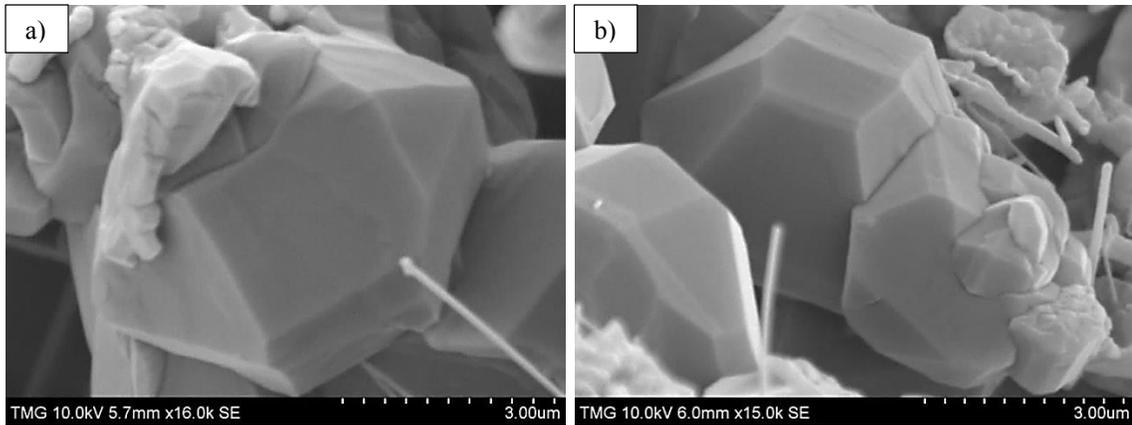
Figure 4-11. β-Si_3N_4 grains form from molten Si.
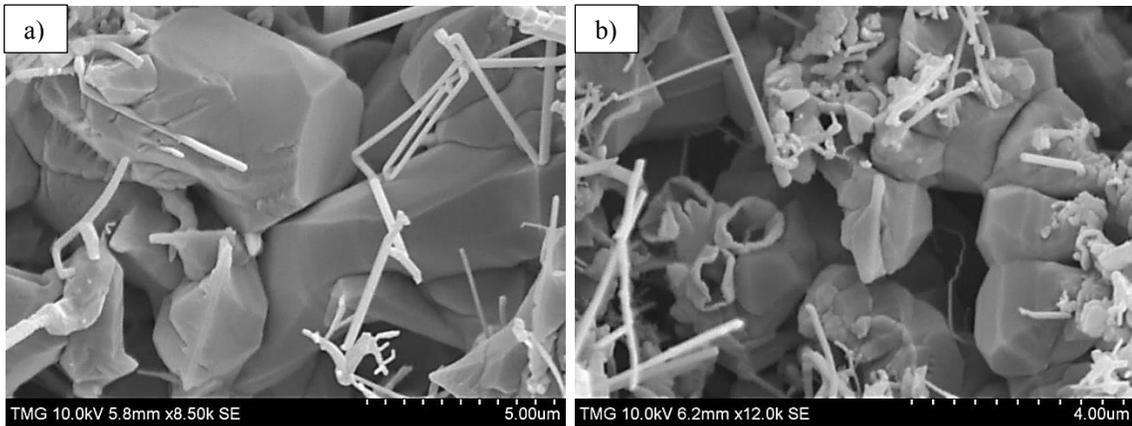
Figure 4-12. A group of angular β-Si_3N_4 grains growing from molten Si.

Figure 4-13 shows the microstructure of the ArH-N1425 sample. The microstructure shows more interlocking rod-like β-Si_3N_4 which is a characteristic of the β-Si_3N_4 phase. As Table 4-1 shows, the β content in this sample is 45.9 wt%. The more interlocking rod-like morphology in this microstructure can form due to the removal of the SiO_2 layer during Ar sintering which results in less SiO formation during nitriding. Therefore, the lower oxygen partial pressure would result in more active nitrogen participating in gas phase reactions, resulting in more rod-like β-Si_3N_4.
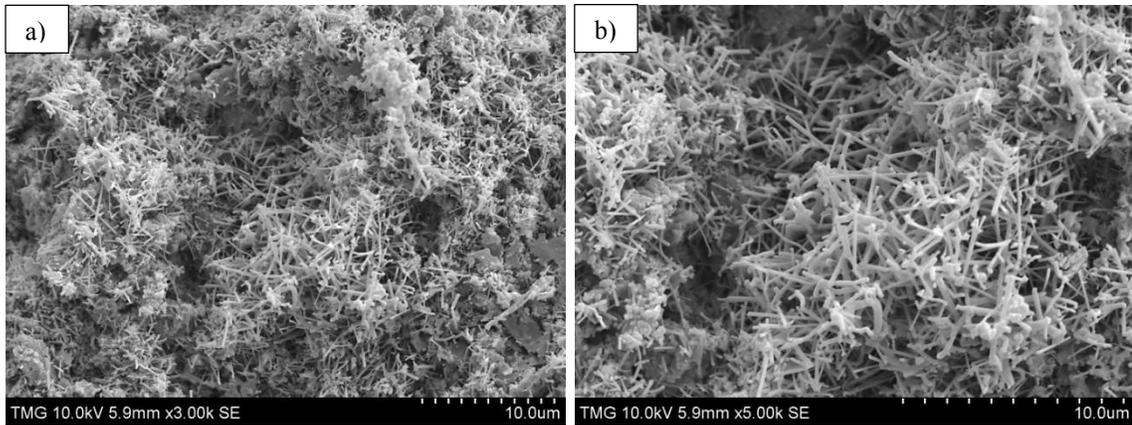
Figure 4-13. Microstructures of the ArH-N1425 foam; more interlocking rod-like β-Si$_3$N$_4$.

Based on Figure 4-6, the RBSN foams nitrided under N$_2$ show lower strengths than those nitrided under N$_2$-H$_2$. Under the N$_2$ atmosphere, the β content of the foam is tripled, as shown in Table 4-1. This results in a more interlocking network of rod-like β-Si$_3$N$_4$ which fills the porosity network of the RBSN foam. Figure 4-14 shows these interlocking rods, which grow in the foam porosity. The arrows in the figure show the initial position of the PMMA beads. This can be another reason why RBSN foams nitrided under N$_2$ show lower strengths than those nitrided under N$_2$-H$_2$.
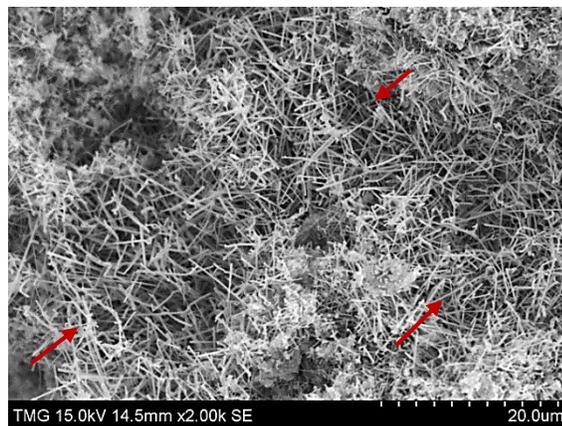
Figure 4-14. Interlocking rod-like β-Si$_3$N$_4$ forms the porosity network of the ArH-N1425 foam; the arrows show the positions where PMMA beads used to exist before polymer pyrolysis.

4.5. Conclusion

In this study the influence of different parameters on the strength of the open-cell RBSN foams have been investigated. The phases present, the dominant nitriding mechanisms and the microstructure of the foams have also been studied in depth. It was found that for higher Si to PMMA weight ratios in the suspension, there is a minimum monomer content of 25 wt% required to produce a homogenous and defect-free RBSN foam. Depending on the porosity level of the RBSN foam, strengths may vary from 18 MPa for 41 vol% porosity to 1 MPa when the foam porosity is 83 vol%.

There are major differences between the nitridation of a conventional RBSN ceramic and the RBSN foam fabricated in this investigation. The high porosity level of the silicon foam and also the SiO_2 layer which forms around Si particles during suspension preparation, all affect the dominating nitriding mechanism in RBSN foams. The high porosity level of the Si foam also prevents premature closure of the porosity network of the body; therefore, N_2 is almost always provided for the reaction. The large pores in the foam also create sufficient space for Si_3N_4 to form and grow. Local atmospheres are also created inside the pores which affect the product phases and their morphologies. It was observed that the presence of H_2 in the nitriding atmosphere can improve the strength of the foam by 35% compared to N_2 atmospheres. This improvement can be due to the formation of a continuous skeletal network of silicon nitride in the presence of H_2 during the early stages of nitriding. In the presence of H_2, increasing the nitriding temperature to values higher than the silicon melting point has a negligible effect on both the foam strength and the β-Si_3N_4 content. On the other hand, under the N_2 atmosphere, the beta content can increase to above 40 wt%. The β-Si_3N_4 phases were observed with both rod-

like and granular morphologies, which may form based on vapor Si and molten Si reactions with atomic nitrogen, respectively.

Acknowledgment

Chapter 5

5.1. Preface to chapter 5

One of the most important elements typically present in RBSN ceramics is iron. Fe and Fe compounds are present in the nitrided bodies since they are considered as the main impurities of the starting Si powder. The presence of Fe is almost inevitable in Si powder especially in industrial grades that may contain large amounts of Fe of up to 1 wt%. Fe may play a significant role during nitridation even at very low concentrations. The influence of Fe compounds on the nitriding process may originate from the low melting point of these compounds resulting in the formation of liquid phases during nitridation. These liquid phases may affect the kinetics of the reactions and preferentially promote specific Si_3N_4 phases or morphologies to form.

Understanding the influence of the Fe compounds on the nitriding processes would first make it possible to use inexpensive Si powder, which certainly contains Fe. This would lower the fabrication cost significantly. Secondly, it can be utilized as a tool to modify and design the RBSN microstructure and properties. Therefore, the next step of the study would be focused on the influence of iron disilicide addition, as a low melting temperature Fe-containing additive, on the RBSN foam properties including microstructure and mechanical strength.

Reaction bonded silicon nitride foams; the influence of iron disilicide on the foam microstructure and mechanical strength

Ali Alem, Martin D. Pugh, Robin A.L. Drew

Mechanical and Industrial Engineering Department, Concordia University, 1455 De Maisonneuve Blvd. W., Montreal, Quebec, Canada H3G 1M8

Abstract

In this study the effect of iron disilicide ($FeSi_2$) additions on the strength and properties of open-cell reaction bonded silicon nitride (RBSN) foams has been investigated. Different nitriding atmospheres including N_2 and N_2-4%H_2 and a range of nitriding temperatures from 1350 to 1450°C were employed.

It was observed that 1 wt% of $FeSi_2$ significantly increased the strength of the RBSN foams regardless of the tested nitriding temperature and atmosphere. The addition of $FeSi_2$ also accelerates nitridation through formation of a molten $FeSi_2$ phase and also reduction of SiO_2 content, which forms extensively during foam fabrication. It was observed that the influence of the nitriding conditions can be quite strong on the RBSN foam strength. A maximum strength of 3.41 MPa was achieved under a N_2 atmosphere at 1390°C, with a foam of 71 vol% porosity. At the same temperature, the combined effect of $FeSi_2$ and a N_2-H_2 atmosphere led to a lower strength compared to N_2 atmospheres.

The high porosity level of the foam significantly affects the nitriding mechanisms and consequently the foam microstructure compared to conventional RBSN ceramics. The presence of $FeSi_2$ up to 1 wt% caused a considerable increase in α-Si_3N_4 content. However, above 1 wt% $FeSi_2$, the β-Si_3N_4 content starts to increase. $FeSi_2$ addition also increases the whisker content of the foam microstructure due to an increase in SiO and Si

vapor formation. The XRD and microstructural analyses showed that α-Si$_3$N$_4$ is present in the form of both matte and whiskers while β-Si$_3$N$_4$ formed as whiskers and large angular grains. The α- and β-whiskers are quite different in terms of dimensional uniformity, degree of interlocking, and aspect ratio.

5.2. Introduction

Ceramic foams have recently been found to be very interesting since they have opened up many new applications including filters, membranes, catalyst supports, interpenetrating composites, and bioimplants [2, 4, 6]. Among the engineering ceramic materials, Si$_3$N$_4$ foams have not received sufficient attention due to the difficulties of working with Si$_3$N$_4$ powder [19, 20, 116] and also the high cost of the material [128]. Therefore, it is of great interest to fabricate Si$_3$N$_4$ foams with tailored properties based on a cost-effective fabrication procedure. The foams must possess a homogeneous open-cell structure with a high level of porosity which can be easily controlled. All the above-mentioned advantages can be achieved through gel-casting of Si suspensions containing sacrificial phases combined with subsequent reaction bonding. The fabricated RBSN foam benefits from high levels of porosity (up to 87 vol%), pore interconnectivity, ease of fabrication, and low production cost. The details of the fabrication procedure and the foam properties have been fully explained in our previous study [123].

Design and optimization of the microstructure and consequently the properties of the RBSN ceramics are not possible unless the reaction bonding phenomenon is completely understood. There are many processing parameters involved in the reaction bonding process, all of which strongly affect the properties of the final RBSN ceramic. In

addition, nitriding of porous foams can also be much more complicated compared to nitridation of conventional RBSN ceramics. There are two foam properties, namely a high porosity level and interconnectivity of the pore network, which markedly influence the nitriding mechanisms and consequently the morphology of the Si_3N_4 polymorphs formed during reaction bonding. These microstructural features affect nitridation in terms of the Si volatilization rate, the free space required for Si_3N_4 formation and growth, and the nitridation rate. The creation of local atmospheres within the porosity network of the foam also influences the dominant nitriding reactions since the vapor pressure of the gaseous phases including Si, SiO, atomic, and molecular nitrogen in the nitriding atmosphere is very influential.

One of the important processing parameters which significantly affects the properties of the final RBSN ceramic is the presence of iron compounds in the system either as an impurity or as an additive. It must be mentioned that commercial Si powder has approximately 0.9 wt% of iron [11, 29]. Even in high purity Si powder, the presence of minor amounts of iron impurity which may have a substantial influence on the nitriding reactions is almost unavoidable [129]. The effect of Fe compounds was always of great concern in conventional RBSN ceramics. Iron may influence both the dominant nitriding mechanism and the ratio of the α- to β-Si_3N_4 phases. It has also been mentioned that Fe significantly affects the mechanical strength of the conventional RBSN ceramics in a deleterious way [29]. Therefore, it has always been recommended to avoid even minor concentrations of Fe in conventional RBSN ceramics. Understanding the influence of Fe on the nitriding reactions makes it possible to utilize commercial grades of Si powder to fabricate RBSN foams. This results in a much more cost-effective foam compared to the

utilization of high-purity grades of Si powder. Therefore, investigating the role of Fe and Fe compounds on the nature of the nitriding reactions and consequently on the RBSN foam properties is significantly important. To the best of the authors' knowledge, there is no investigation on the influence of Fe compounds on the microstructure, mechanical strength, and properties of highly porous RBSN foams. This investigation helps one understand the nitridation mechanisms of the porous RBSN foams in the presence of $FeSi_2$. The mechanical strength of the foams has been tested under different nitriding conditions including different temperatures and atmospheres. The Si_3N_4 phases formed during nitriding, and their morphologies, have also been investigated in depth via XRD and SEM analyses. Finally, the influence of $FeSi_2$ on the foam microstructure is investigated and discussed.

5.3. Experimental procedure

5.3.1. Foam fabrication

RBSN foams with interconnected porosity have been previously fabricated based on a combination of gel-casting, sacrificial templating, and reaction bonding techniques [123]. Suspensions containing Si powder (ABCR, 99.995%, -8 microns), PMMA beads (Microbeads, 10-40 μm), and $FeSi_2$ (Alfa Aesar, 99.9%) were transformed into a two-phase solid body via gel-casting in silicone rubber molds. The gel-casting system was based on acrylamide (AM, $C_2H_3CONH_2$, Sigma-Aldrich) as the monomer and N,N′-methylenbisacrylamide (MBAM, $(C_2H_3CONH_2)_2CH_2$, Sigma-Aldrich) as the cross-linker with the weight ratio of AM to MBAM of 15. After suspension preparation, casting and polymerization occur in the molds. Drying and polymer pyrolysis were performed as the next steps in order to remove water and the sacrificial phases from the cast bodies,

respectively. At this stage, a silicon foam has been produced and the Si to Si_3N_4 conversion was finally performed through the reaction bonding process. The details of the RBSN foam fabrication procedure, the foam characterization, and its properties can be found in our previous study [123]. Figure 4-1 shows a flowchart of the fabrication procedure.

This study focuses on the influence of $FeSi_2$ on the strength and microstructure of the RBSN foams fabricated by this procedure. The RBSN foams have been nitrided under different nitriding conditions including temperatures ranging from 1350°C to 1450°C and static atmospheres of N_2 and N_2 -4%H_2. The heating rate during nitriding was 5 °C/min up to 1350°C, 1 °C/min up to 1390°C, and 0.3 °C/min up to 1450°C. The dwell time was between 6 to 10 h at the maximum nitriding temperature. The temperature range used in this study covers nitriding temperatures both below and above the silicon melting point (1410°C) which can be used to study the influence of Si melting on the foam strength. In order to study the effect of Ar-sintering on the microstructure and strength of the foams, some samples were sintered under Ar-4%H_2 for 2 h at 1200°C prior to the nitriding step. Based on the nitriding conditions, specific codes have been used for sample identification. In the sample codes used in the rest of the study, ArH shows the performance of a short sintering step under the Ar-4%H_2 atmosphere, NH shows nitriding under N_2-4%H_2, and N represents nitriding under the N_2 atmosphere. The final nitriding temperature can also be found in the last part of the sample code. As an example, ArH-NH1400 shows a sample that has been sintered under Ar-4%H_2 and then nitrided under N_2-H_2 at 1400°C.
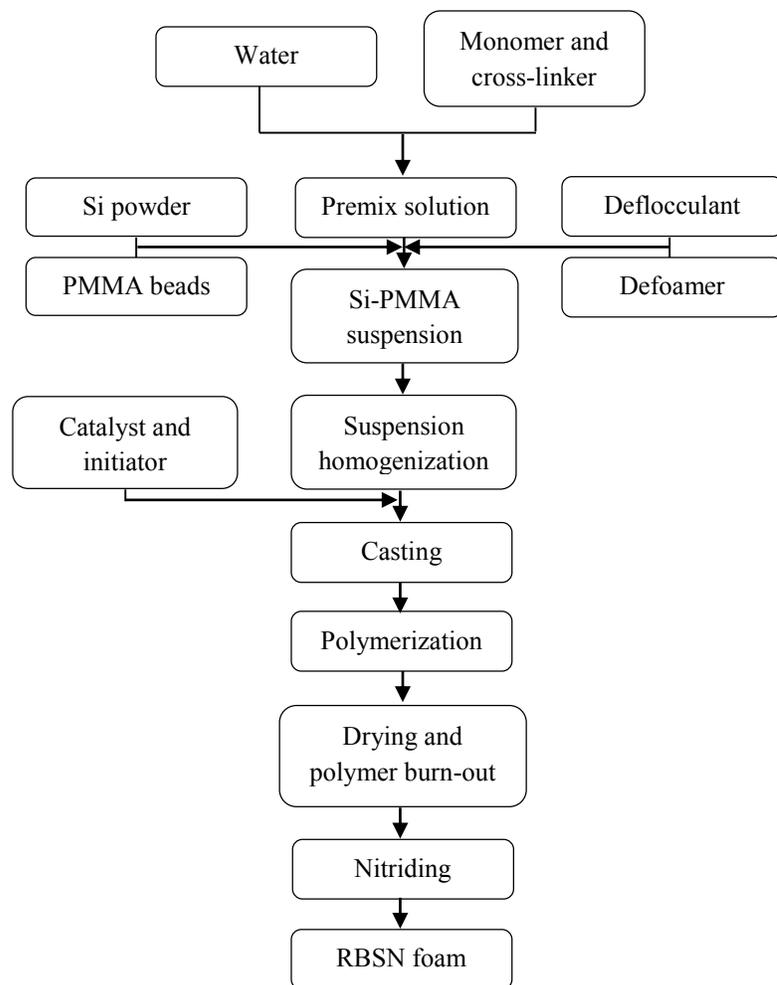
Figure 5-1. The flowchart of the RBSN foam fabrication procedure.

5.3.2. Characterization

The porosity and density of the foams were measured based on the Archimedes technique according to the ASTM C373-88 standard. Flexural strengths of the foams were measured in four-point bending of rectangular bars using a tensile testing machine (Instron®, Model 3382). The bend sample dimensions were 10 x 10 x 70 mm^3 and the samples were in the as-nitrided state before the test. The lower and upper spans were 40 mm and 20 mm, respectively. The upper span was moving at a crosshead speed of 0.1 mm/min. A minimum of three and a maximum of six samples were tested under each

specific condition. X-ray diffraction analysis (XRD, X'PertPro; PANalytical) and scanning electron microscopy (SEM, HITACHI, S-3400N) equipped with energy-dispersive X-ray spectroscopy (EDS; Oxford Instruments; Wave Model) techniques were also utilized to investigate the phases present and the microstructures of the RBSN foams nitrided under different conditions. Quantitative analysis of the α- and β-Si_3N_4 phases was performed based on Gazzara's technique [127].

5.4. Results and discussion

5.4.1. Foam strength versus nitriding conditions

The main goal of this investigation is to study the influence of $FeSi_2$ on nitridation of RBSN foams and consequently its effect on the foam microstructure and mechanical properties. To achieve that, the weight ratio of the suspension's main components; PMMA, Si, and water, was fixed at 34 wt%, 34 wt%, and 32 wt%, respectively. In this case, the RBSN foam has a porosity of higher than 70 vol% which is high enough to affect the nitriding phenomenon in terms of Si volatilization rate, the creation of local atmospheres, the formation of gaseous Si and SiO species, the availability of the free space for Si_3N_4 formation, and the nitridation rate. Higher PMMA contents than 34 wt% in the suspension and consequently higher porosity levels of the foam, led to small differences between the strength of the foams nitrided under different nitriding conditions. In this case, the influence of the foam porosity dominates the effect of nitriding conditions; therefore, the comparison between foam strengths might be difficult and contain errors due to small differences between the strength values. Thus the PMMA content was fixed at 34 wt% for this study. It must be mentioned that the PMMA content

of the suspension can be increased up to 44 wt% resulting in an increase in the RBSN foam porosity to a maximum value of 87 vol% [123].

Figure 5-2 shows the strength of the RBSN foams containing 1 wt% $FeSi_2$ nitrided under different nitriding conditions. It is observed from the figure that the maximum strength of 3.41 MPa is obtained under a N_2 atmosphere when the nitriding temperature is at 1390°C, below the silicon melting point. Increasing the temperature to 1425°C under N_2 causes a 30% decrease in the foam strength where the minimum strength of 2.40 MPa is obtained. This can be due to the partial melting of Si during nitriding. As the temperature increases, the size and population of these Si melt-induced defects and structural inhomogeneities increase resulting in a decrease in the foam strength. As the error bars in Figure 5-2 show, increasing the nitriding temperature from 1390 to 1425°C, also increases the variation in foam strength. This is due to partial melting of Si which affects the mechanical strength of the RBSN foam. On the other hand, RBSN foams nitrided under N_2-H_2 do not show much variation in terms of strength. It is observed that under a N_2-H_2 atmosphere, increasing the nitriding temperature to higher than the Si melting point (e.g. 1425°C) does not cause a significant change in the strength. Therefore, under N_2-H_2 atmospheres, the foam strength is not strongly dependent on temperature. The figure also shows that a short Ar-sintering step also increases the strength by 7% and 6% when N_2 and N_2-H_2 atmospheres are used, respectively.
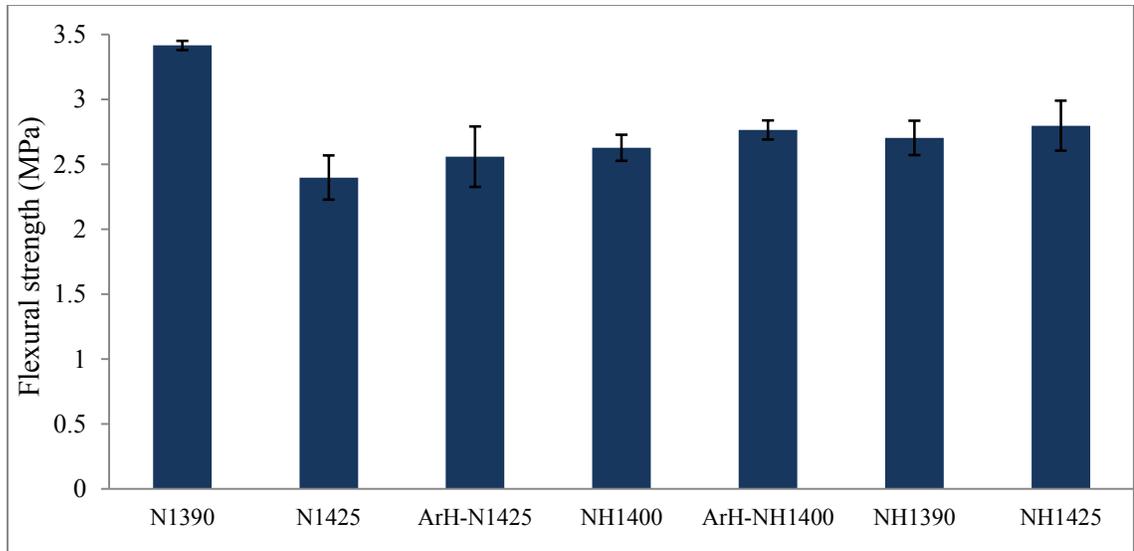
Figure 5-2. The influence of the nitriding parameters on the strength of the RBSN foam with 1 wt% $FeSi_2$.

It has been reported that the presence of H_2 improves the strength of "dense" RBSN ceramics [19]. However, Figure 5-2 shows that below the Si melting point e.g. at 1390°C, the foam strength will be 26% higher if processed under N_2 rather than N_2-H_2. Under the N_2-H_2 atmosphere and in the presence of $FeSi_2$, the Si_3N_4 phases which form during nitriding do not contribute to the continuous network of the foam struts; therefore, lower strength is observed compared to N_2 atmospheres. The presence of H_2 in the nitriding atmosphere leads to a higher SiO vapor pressure due to the reduction of the SiO_2 layer on Si particles. The combined effect of H_2 and $FeSi_2$ makes the system more reducing in a way that SiO vapor may also be reduced to Si vapor. It has been previously concluded that SiO contributes more to form a continuous skeletal network in RBSN ceramics [124]; therefore, the reduction in SiO vapor pressure in the presence of both $FeSi_2$ and H_2 may result in the formation of whiskers which may not contribute that much to the foam struts. This is most likely the reason why the foam strength is lower under N_2-H_2 than N_2 at 1390°C. It must be mentioned that there are many processing parameters which affect

the extent and the contribution of the series of reactions which occur during nitriding and this situation is even more complicated in RBSN foams due to the existence of local atmospheres within the pores. The most important parameters which affect the intensity of the gas phase reactions are the amount of SiO_2 which exists on Si particles and the presence of H_2 in the atmosphere. These parameters significantly influence the ratio of SiO to Si vapor and also the dominant nitriding reaction resulting in different phase morphologies and consequently different foam strengths.

On the other hand, Figure 5-2 also shows that at 1425°C which is above the Si melting point, N_2-H_2 atmospheres led to 17% increase in strength compared to N_2. At temperatures higher than the Si melting point, the partial melting of Si can have a deleterious influence on the foam strength. Si melting is reduced in the presence of H_2 due to a faster Si to Si_3N_4 conversion during the early stages of the nitriding reactions. Therefore, N_2-H_2 atmospheres result in a higher foam strength at 1425°C compared to N_2 atmospheres. In conclusion, depending on the nitriding temperature, the atmosphere which provides the highest mechanical strength of the RBSN foam will change.

5.4.2. Nitriding reactions and RBSN foam properties

Regarding the nitriding mechanisms, Si can react with nitrogen in both vapor and liquid forms. In the case of α-Si_3N_4 which exists either in the form of whisker or matte, gaseous Si reacts with molecular nitrogen [22]. The second path for α-Si_3N_4 formation is the reaction of SiO vapor with nitrogen [19]. These reactions are shown in Reactions 5-1 and 5-2. However, it is known that β-Si_3N_4 forms in the presence of atomic nitrogen [22, 25]. Therefore, the β-Si_3N_4 forming reactions can occur between vapor and liquid silicon with atomic nitrogen [19, 22, 25]. These reactions have been shown in Reactions 5-3 and 5-4.

$$3 \text{ Si (g)} + 2 \text{ N}_{2 \text{ (molecular form)}} \leftrightarrow \alpha\text{-Si}_3\text{N}_4 \text{ (s)} \qquad (5\text{-}1)$$

$$3 \text{ SiO (g)} + 2 \text{ N}_{2 \text{ (molecular form)}} \leftrightarrow \alpha\text{-Si}_3\text{N}_4 \text{ (s)} + 3/2 \text{ O}_2 \qquad (5\text{-}2)$$

$$3 \text{ Si (g)} + 4 \text{ N}_{\text{ (atomic form)}} \leftrightarrow \beta\text{-Si}_3\text{N}_4 \text{ (s)} \qquad (5\text{-}3)$$

$$3 \text{ Si (l)} + 4 \text{ N}_{\text{ (atomic form)}} \leftrightarrow \beta\text{-Si}_3\text{N}_4 \text{ (s)} \qquad (5\text{-}4)$$
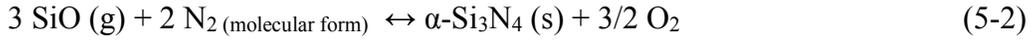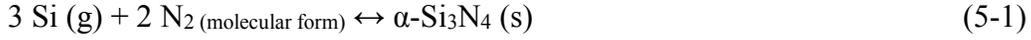
Table 5-1 shows the porosity, density, and the α- and β-Si$_3$N$_4$ contents of the RBSN foams nitrided under different nitriding conditions. The ratio of the Si$_3$N$_4$ phases has been determined from the XRD patterns of the foams based on Gazzara's method [127]. It can be seen from the table that the porosity of the RBSN foam is not dependent on the nitriding conditions but it is entirely dependent on the prior foam processing conditions. The table also shows that in the presence of H$_2$, the α content is always constant at its maximum value (~87 wt%) regardless of the nitriding temperature.

Table 5-1. Porosity, density, and α and β phase contents of the RBSN foams with 1 wt% FeSi$_2$ nitrided under different nitriding conditions.

Sample code	Density (gr/cm^3)	Porosity (vol%)	α-Si$_3$N$_4$ content (wt%)	β- Si$_3$N$_4$ content (wt%)
N1390	0.86	71.3	74.69	25.31
N1390-1425	0.92	70.6	70.18	29.82
N1425	0.89	71.4	67.02	32.98
ArH-N1425	0.90	71.0	65.70	34.30
NH1390	0.90	71.0	88.07	11.93
NH1400	0.89	70.8	87.87	12.13
NH1425	0.90	71.5	86.63	13.37
ArH-NH1400	0.91	70.7	88.16	11.84

XRD patterns of three RBSN foams have been selectively shown in Figure 5-3. ArH-N1425 was shown as the foam with the highest β-Si_3N_4 content of 34 wt%. The foam N1390 has the highest strength and the foam NH1390 is representing all the foams nitrided under N_2-H_2 with the highest α-Si_3N_4 content of 88 wt%. It can be seen from the XRD patterns that there is no residual Si in the RBSN foams and nitridation is complete. In accordance with Table 5-1, the figure shows the increase in β-Si_3N_4 by increasing the nitriding temperature under N_2. The XRD analysis of the RBSN foams nitrided at both 1425°C and 1450°C for longer times did not show any α to β transformation.
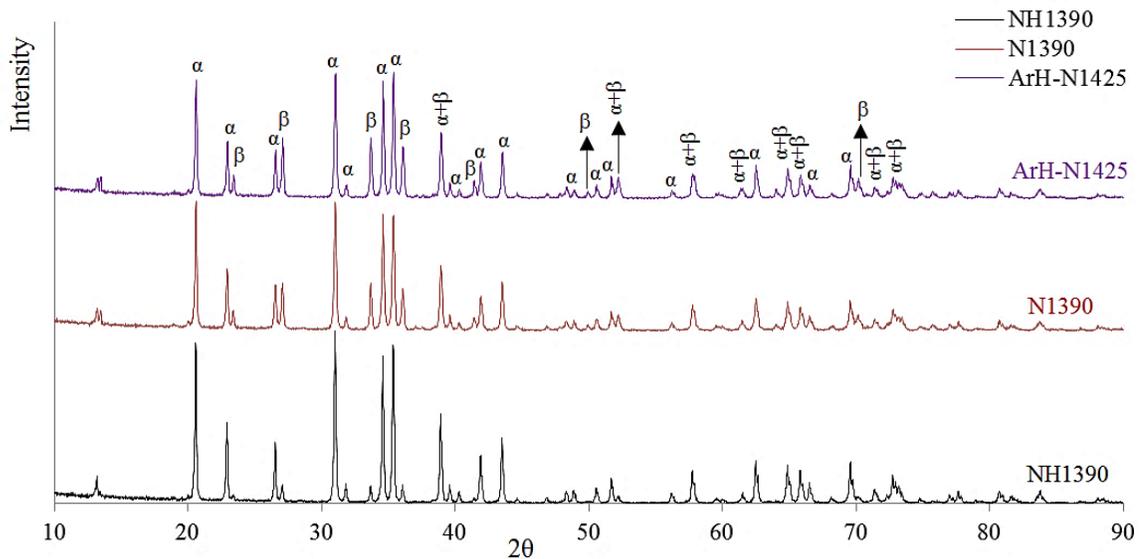
Figure 5-3. XRD patterns of three different foams including ArH-N1425, N1390, and NH1390; α is α-Si_3N_4 and β is β-Si_3N_4.

5.4.3. Microstructural analysis of the RBSN foams

Figure 5-4 shows the microstructure of the RBSN foams nitrided under different conditions. As shown in Table 5-1 the foams have more than 70 vol% porosity. The three phases observed in all these microstructures are α-matte, α-whisker, and β-whisker which all form based on the gas phase reactions shown in Reactions 5-1 to 5-3. Based on Table

5-1, the presence of H_2 keeps the α-Si_3N_4 content at its maximum value and consequently the β-Si_3N_4 will be minimal. Therefore, it is expected that whiskers observed in parts (a) and (b) of the figure are mainly α-Si_3N_4. A comparison between the NH1390 and N1390 foams shows that the whiskers are different in terms of shape and size uniformity which is a consequence of the nitriding atmosphere. As shown in Table 5-1, the β-Si_3N_4 content increases under N_2; therefore, under N_2 a higher quantity of β-whiskers is expected. These whiskers are both α- and β-Si_3N_4. Therefore, a higher population of β-whiskers is expected in parts (c) and (d) of the figure compared to NH1390 foams shown in parts (a) and (b). More explanation in this regard has been provided in Section 5.3.4.

α-matte which forms as small grains can be clearly observed in NH1425 and N1425 foams. Since the presence of H_2 has a significant influence on the formation of α-matte, a higher quantity of α-matte can be clearly seen in NH1425 foams (parts (e) and (f)) compared to N1425 samples (parts (g) and (h)). The last four images also show the influence of the Ar-sintering step on the microstructure of the RBSN foams in terms of whisker content. The differences in whisker quantity, and also whisker shape and size uniformity are also obvious in ArH-NH and ArH-N microstructures. This is the influence of the N_2 atmosphere as discussed earlier.

c) N1390

TMG 10.0kV 12.1mm x3.00k SE   10.0um

d) N1390

TMG 10.0kV 12.0mm x5.00k SE   10.0um

e) NH1425

TMG 10.0kV 10.2mm x3.00k SE   10.0um

f) NH1425

TMG 10.0kV 10.2mm x5.00k SE   10.0um

g) N1425

TMG 10.0kV 9.7mm x3.00k SE   10.0um

h) N1425

TMG 10.0kV 9.1mm x5.00k SE   10.0um
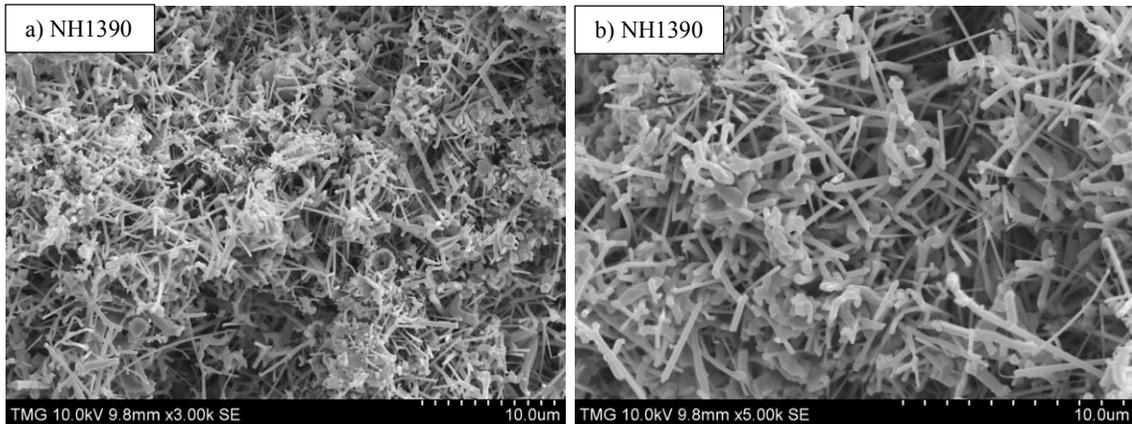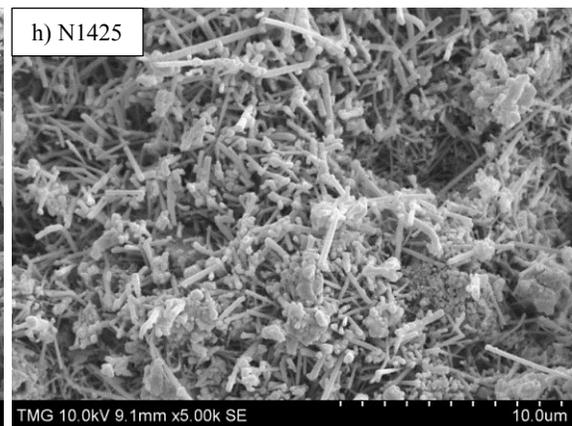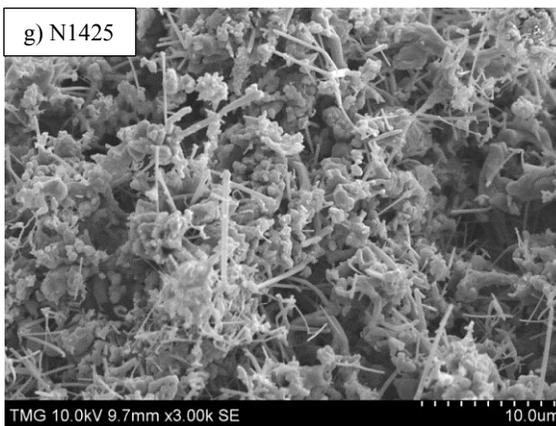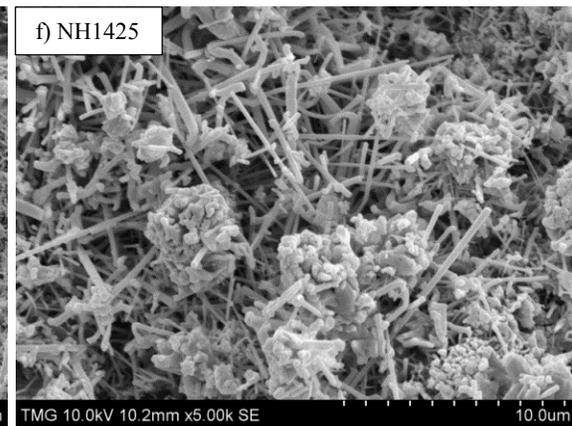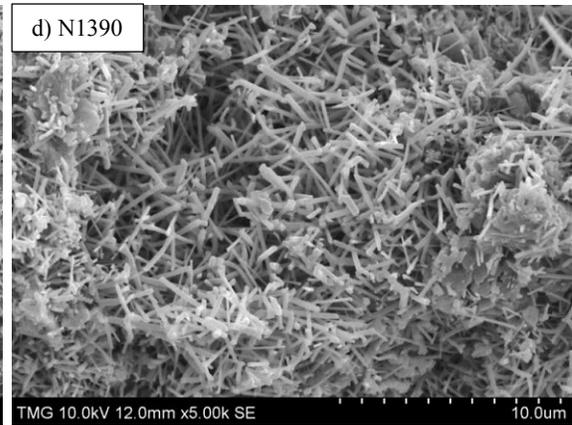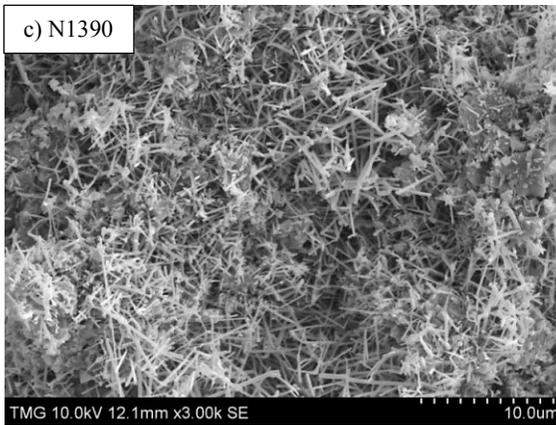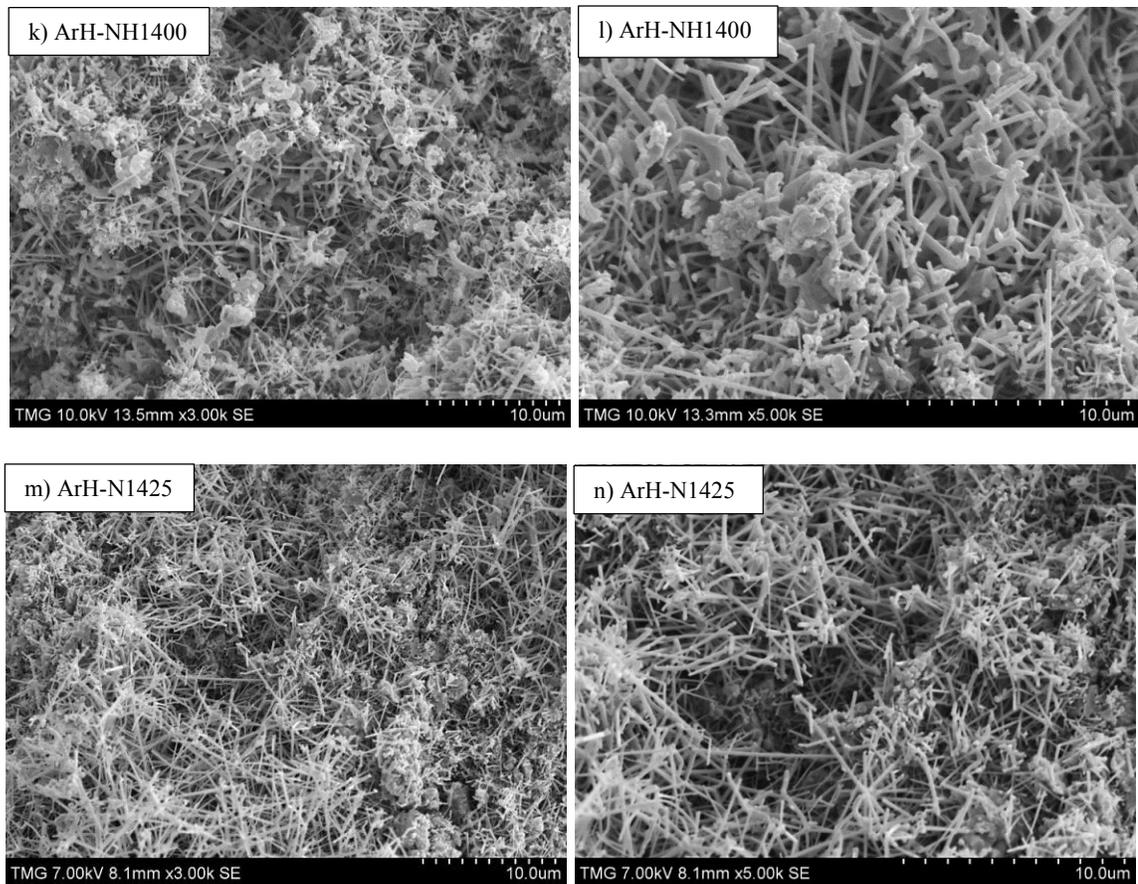
Figure 5-4. The microstructures of the RBSN foams nitrided under different conditions.

Besides the whisker morphology, the β-Si_3N_4 phase also forms as large, facetted grains as shown in Figure 5-5. These grains, which show the hexagonal geometry, are presumed to form based on the reaction between molten Si and atomic nitrogen shown in Reaction 5-4. In contrast to the whiskers that form from the vapor phase reactions and grow individually, Figure 5-5-a shows how these β-Si_3N_4 grains can grow in groups from the liquid phase. This hexagonal morphology shown in Figure 5-5-b is a characteristic of the β-Si_3N_4 phase [27, 28].
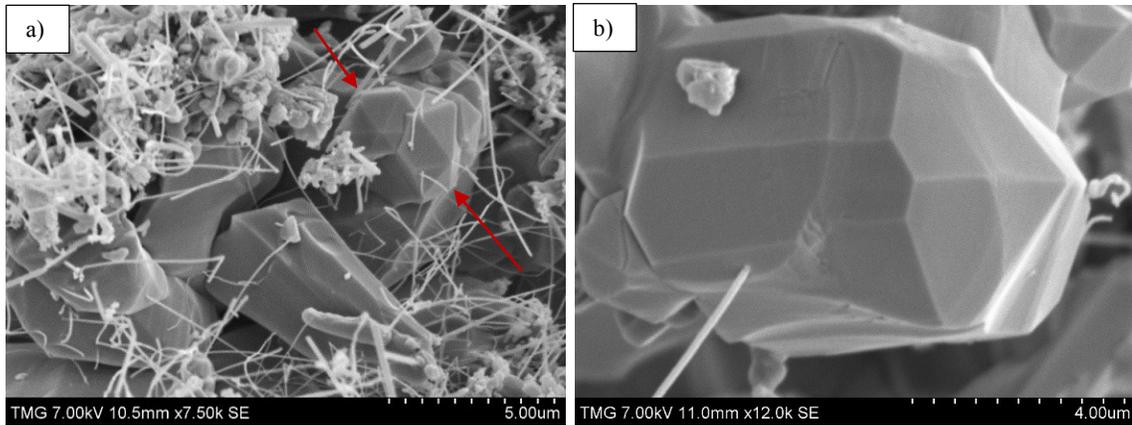
Figure 5-5. β-Si$_3$N$_4$ phase in the form of hexagonal grains formed from the reaction between molten Si and atomic nitrogen. The arrows show the hexagonal-shaped grains.

5.4.4. Comparison between the nature of the whiskers when N$_2$ and N$_2$-H$_2$ atmospheres are used

It was observed that the whiskers which grow inside the porosity of the foams, especially where PMMA beads previously existed, are quite unalike when different nitriding atmospheres were employed. Under N$_2$ atmospheres, a higher quantity of β-whiskers form. These β-whiskers are shorter, straighter, and more uniform in terms of size and shape. The degree of interlocking is also much higher for β-whiskers formed under N$_2$ atmospheres. On the other hand, when H$_2$ is present in the nitriding atmosphere, both the whisker uniformity and the degree of interlocking decrease. These differences can be clearly observed in parts (a) and (b) of Figure 5-6 showing RBSN foams nitrided under N$_2$ and N$_2$-H$_2$ atmospheres, respectively. It is concluded that depending on the type of nitrogen (molecular or atomic) involved in the nitriding reactions both α-Si$_3$N$_4$ and β-Si$_3$N$_4$ whiskers may form. Under the N$_2$ atmosphere, β-Si$_3$N$_4$ whiskers are encouraged to grow since the concentration of atomic nitrogen is higher compared to the case when nitriding is performed under N$_2$-H$_2$ atmospheres. As was mentioned before, H$_2$ is capable

of removing atomic nitrogen from the nitriding atmosphere [22]. A higher degree of interlocking which is a characteristic of the β-Si$_3$N$_4$ phase [19] can be clearly seen in Figure 5-6-a.
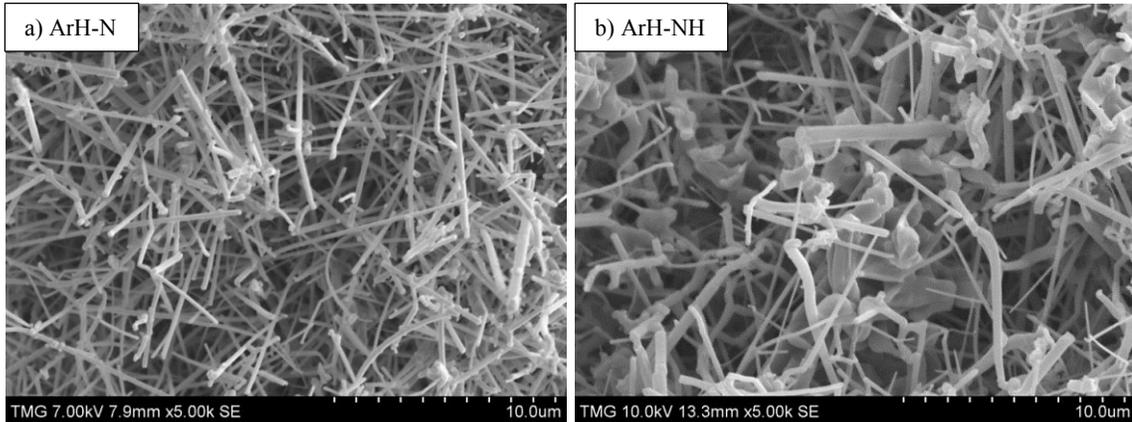
Figure 5-6. α- and β-Si$_3$N$_4$ whiskers growing in the porosity of the RBSN foams under a) N$_2$ and b) N$_2$-H$_2$ atmospheres.

It must be mentioned that some thick whiskers have grown in the large pores of the foam structure where PMMA beads were initially present before polymer pyrolysis. Figure 5-7 shows these oversized whiskers which could be observed in RBSN foams nitrided under both N$_2$ and N$_2$-H$_2$ atmospheres. Since these thick whiskers need more space to grow, they prefer to form in the large pores of the foam (former PMMA beads). These thick whiskers are expected to form based on the Vapor-Liquid-Solid (VLS) mechanism. Based on the VLS mechanism, the whiskers grow from a liquid bead attached to the end of the whisker or from a liquid puddle on the surface of a large grain which must support the weight of the whisker as it grows [27]. In the VLS mechanism, Si or SiO vapor is transported to the liquid-solid interface where it reacts with N$_2$. Therefore, Si$_3$N$_4$ is produced and the whisker grows [27]. As the whisker grows, it may turn and make angles due to the change in the growth direction. It was observed that the population of these

thick whiskers was higher for the foams nitrided under N_2-H_2 than N_2. As was mentioned before, the presence of H_2 increases the vapor phase reactions; therefore, the VLS phenomenon can be accelerated resulting in the formation of these oversized whiskers. Since the population of these thick whiskers is higher under N_2-H_2 atmospheres, they are likely to be α-Si_3N_4 whiskers.
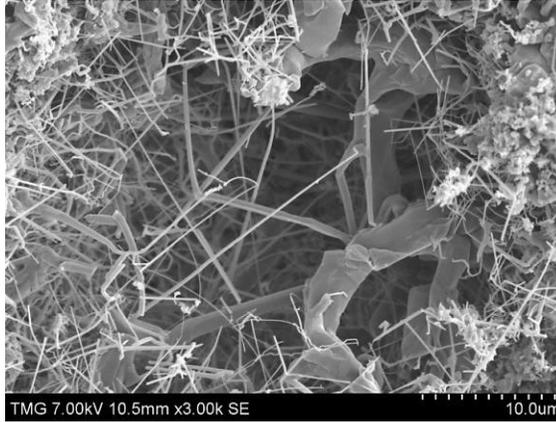
Figure 5-7. Oversized whiskers in the porosity network of the foams where PMMA beads used to exist before polymer pyrolysis.

5.4.5. The effect of FeSi₂ additions on the foam strength and the α/β phase ratio

It was observed in this study that the $FeSi_2$ content can have a strong influence on the foam properties including the mechanical strength and the microstructure. Figure 5-8 shows the effect of $FeSi_2$ additions on the strength of the RBSN foams nitrided under N_2 at two different temperatures: 1425°C and 1390°C. It is observed from Figure 5-8-a that at 1425°C the strength increases significantly up to 1 wt% of $FeSi_2$ and then it shows a very slight decrease as the $FeSi_2$ content increases to 4 wt%. The figure shows that the addition of 1 wt% $FeSi_2$ causes a two fold increase in the foam strength compared to the case when no $FeSi_2$ is added. It is generally expected that the addition of Fe compounds even in minor concentrations have a detrimental influence on the mechanical strength of

144

the conventional RBSN ceramics since melting of Fe compounds can cause large defects in the body [11, 29]. As shown in Figure 5-8-a, the opposite trend was witnessed for RBSN foams fabricated in this study. It was observed in this study that 1 wt% of $FeSi_2$ significantly increases the strength of the RBSN foams for any nitriding atmosphere and temperature. This can be due to the sintering effect of $FeSi_2$ which markedly improved the mechanical strength of the RBSN foam. $FeSi_2$ is completely molten during nitriding since it melts at 1220°C. This low melting point will help with sintering of the RBSN foam.
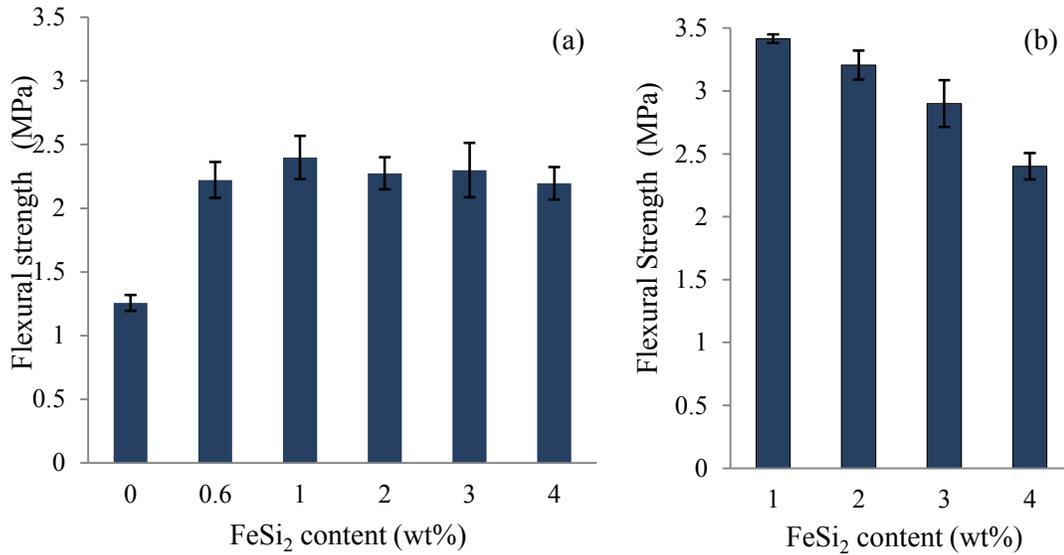
Figure 5-8. The effect of $FeSi_2$ concentration on the strength of the RBSN foams nitrided under N_2; RBSN foams were nitrided at a) 1425° and b) 1390°C.

Generally, there may be three types of defects in RBSN ceramics. The first one is the intrinsic defects, which exist in Si green compacts like all the other ceramic bodies. The second one can be created by partial melting of Si during the exothermic nitriding process. The last type, which only exists in the presence of Fe compounds either as impurities or as additives, can form by melting of these compounds during nitriding. In

145

"dense" RBSN ceramics containing Fe compounds, melting of Fe compounds significantly affects the size of the largest defects in the body in a way that Fe-induced defects will dominate; therefore, the strength decreases even in the presence of minor amounts of Fe [11, 29]. On one hand, the foam fabrication technique used in this study and on the other hand, the high level of porosity of the foam create a more uniform distribution of Fe-Si compounds on the surface of the Si particles during nitriding. Therefore, the size of the defects which form through melting of the Fe-Si compounds does not reach the size of the intrinsic defects of the RBSN foam, which are the pores of the structure. Therefore, the addition of 1 wt% of $FeSi_2$ to RBSN foams does not decrease the strength but it significantly improves the flexural strength of the RBSN foam due to its sintering capability.

Figure 5-8 also reveals that the foam strength decreases slightly above 1 wt% $FeSi_2$. The decrease in strength which is observed for $FeSi_2$ concentrations higher than 1 wt% can be due to the defect-forming behavior of Fe compounds which dominates at higher concentrations of $FeSi_2$. In this case, the size of the Fe-induced defects may increase upon increasing the amount of $FeSi_2$ resulting in a decrease in the RBSN foam strength. A comparison between parts (a) and (b) of Figure 5-8 firstly shows that the RBSN foam strength is always higher at 1390°C compared to 1425°C and secondly the foam strength decreases faster at 1390°C as the $FeSi_2$ content increases. Both phenomena occur due to partial melting of Si. At 1425°C, which is above the Si melting point, partial melting of Si creates defects which are either of the same size or even larger than the Fe-induced defects. Therefore, as Figure 5-8-a shows the increase in $FeSi_2$ concentration does not lead to a significant decrease in the foam strength when the nitriding temperature is

146

higher than the Si melting point. However, as Figure 5-8-b shows, the Fe-induced defects are dominating the defects which form due to Si partial melting at 1390°C; therefore, the strength decreases in a more pronounced way as the $FeSi_2$ concentration increases.

Table 5-2 shows the effect of $FeSi_2$ concentration on the α/β phase ratio determined based on the XRD analysis. The presence of up to 1 wt% $FeSi_2$ significantly increased the α-Si_3N_4 content compared to the RBSN foam which does not contain any $FeSi_2$. It is generally reported that the addition of Fe compounds increases the β-Si_3N_4 content due to liquid formation during conventional nitriding [11, 19] and an increase in the concentration of atomic nitrogen [22]. However, it was observed in the current investigation that the α-Si_3N_4 content increases substantially with up to 1 wt% $FeSi_2$ while above this value, there is an increase in the β-Si_3N_4. The increase in the α-Si_3N_4 content is due to the reducing effect of Fe. Fe accelerates the devitrification and consequently the volatilization rate of surface SiO_2 based on Reaction 5-5 [11, 19]. Reaction 5-6 also shows the reduction of the SiO_2 layer by underlying Si leading to SiO formation. This reaction is also accelerated in the presence of Fe [11]. The underlying Si may also participate in oxidation reactions shown in Reaction 5-7 to form more SiO_2.

$$SiO_2 \leftrightarrow SiO\ (g) + \tfrac{1}{2}\ O_2 \hspace{4cm} (5\text{-}5)$$

$$Si + SiO_2 \leftrightarrow 2\ SiO\ (g) \hspace{4cm} (5\text{-}6)$$

$$Si + O_2 \leftrightarrow SiO_2 \hspace{4.5cm} (5\text{-}7)$$

Table 5-2. The effect of $FeSi_2$ on the α- and β-Si_3N_4 phase contents of the RBSN foams nitrided under N_2 at 1425°C.

$FeSi_2$ content (wt%)	α-Si_3N_4 (wt%)	β-Si_3N_4 (wt%)	α/β ratio
0	58.6	41.4	1.4
0.6	62.44	37.56	1.7
1	67.02	32.98	2.1
2	64.59	35.41	1.8
3	62.55	37.45	1.7
4	63.57	36.43	1.7

In this study, RBSN foams have been fabricated based on wet processing of aqueous Si-PMMA suspensions. Therefore, during suspension preparation and foam fabrication, the oxidation of Si particles results in a considerable amount of SiO_2 which forms around Si particles. The SiO_2 layer is later reduced to SiO vapor in the presence of iron based on Reactions 5-5 and 5-6. Therefore, the addition of Fe may lead to a significant amount of SiO formation during nitriding. SiO vapor may then participate in Reaction 5-2 to form α-Si_3N_4 [19]. This is the reason why α-Si_3N_4 content increases up to 1 wt% of $FeSi_2$. It may be thought that the increase in α-Si_3N_4 content with up to 1 wt% of $FeSi_2$ can also be due to the oxidation of $FeSi_2$ particles during suspension preparation and milling which results in an increase in the oxygen content of the sample. Since oxygen removes atomic nitrogen from the nitriding atmosphere [22], more α-Si_3N_4 is expected to form. However, this cannot be the case since the α-Si_3N_4 content decreases for $FeSi_2$ concentrations higher than 1 wt%. If the oxidation of $FeSi_2$ was the reason for the α-Si_3N_4 increase, the same trend would be expected for higher concentrations of $FeSi_2$.

As Table 5-2 shows, above 1 wt% of $FeSi_2$, the α-Si_3N_4 content starts decreasing and consequently β-Si_3N_4 content will increase. Above 1 wt% of $FeSi_2$, the SiO formation

may not increase while the liquid forming role of $FeSi_2$ dominates. On the other hand, higher concentrations of Fe also increase the concentration of atomic nitrogen in the nitriding atmosphere. More atomic nitrogen and higher amounts of molten Fe-Si phases lead to more β-Si_3N_4 formation as shown in Reactions 5-3 and 5-4.

$FeSi_2$ also affects the RBSN foam microstructure. Figure 5-9 shows the microstructure of the N1425 foams with 1 and 4 wt% $FeSi_2$. It can be observed that higher $FeSi_2$ contents result in a higher and finer whisker content. As was mentioned before, Fe compounds can increase the amount of SiO vapor due to reduction of SiO_2 based on Reactions 5-5 and 5-6. $FeSi_2$ also increases the amount of liquid phase which form during nitriding due to its low melting point. This liquid phase can be considered as a source of Si vapor since Si volatilization can be accelerated from molten Fe-Si phases. Both of these two phenomena increase the amount of Si and SiO vapor leading to more whisker formation in the presence of more $FeSi_2$. This can be another reason why the foam strength decreases as the $FeSi_2$ content increases above 1 wt% since these whiskers may not contribute to form the foam struts.
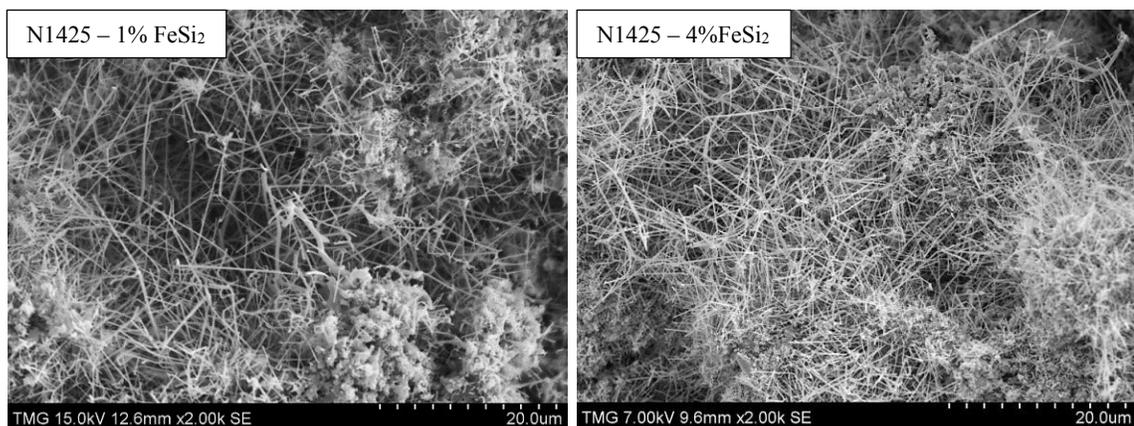
Figure 5-9. The microstructures of the N1425 foams containing a) 1 wt% $FeSi_2$, b) 4 wt% $FeSi_2$.

It must be mentioned that the overall reaction rate increases significantly in the presence of $FeSi_2$. This increase can be explained based on several phenomena including the fast removal of the SiO_2 layer based on Reactions 5-5 and 5-6 and the formation of $FeSi_x$ liquid phases. This liquid phase can be considered as a source of Si vapor and molten silicon both of which accelerate the overall rate of nitridation reactions especially when Si_3N_4 layers seal off the unreacted Si particles from nitrogen. In conclusion, α-Si_3N_4 forms if the dominant role of $FeSi_x$ liquid phases is the formation of either SiO or Si vapor which reacts with molecular nitrogen. However, β-Si_3N_4 formation can be encouraged if $FeSi_2$ promotes the formation of more liquid phases and also atomic nitrogen. These roles are dependent on the $FeSi_2$ concentration.

Finally, it must be mentioned that Si_3N_4 whiskers show superior properties compared to other ceramic whiskers. They display high mechanical properties, good thermal and corrosion resistance, good oxidation resistance and low thermal expansion coefficient [130]. These properties combined with the pore interconnectivity and the high porosity level of the produced open-cell RBSN foam can open up a variety of applications especially fabrication of interpenetrating composites reinforced by a continuous network of the Si_3N_4 whiskers.

5.5. Conclusions

This work highlighted the influence of $FeSi_2$ on the microstructure and mechanical properties of the RBSN foams. RBSN foams fabricated based on wet processing of Si-PMMA suspensions were nitrided under both N_2 and N_2-H_2 atmospheres and also at different temperatures, both below and above the Si melting point. It was observed that 1 wt% of $FeSi_2$ improves the foam strength significantly regardless of the nitriding

conditions. This improvement is thought to be due to the low melting temperature of FeSi$_2$ and consequently its sintering capability. FeSi$_2$ also decreases the induction time of nitridation by accelerating the removal of surface SiO$_2$ on Si particles during foam fabrication and also by formation of molten FeSi$_2$. This also affects the microstructure of the RBSN foam.

The nitriding atmosphere and the temperature can significantly influence the strength of RBSN foams. The maximum foam strength of 3.41 MPa was obtained under a N$_2$ atmosphere when the temperature is below the Si melting point (e.g. 1390°C). On the other hand, the employment of N$_2$-H$_2$ atmospheres at 1390°C, resulted in a 20% decrease in the RBSN foam strength compared to N$_2$ atmospheres. The reduction of strength can be attributed to the combined effect of H$_2$ and FeSi$_2$, which reduces the concentration of vapor phases which contribute more to the formation of a continuous skeletal network and the creation of the foam struts. It was also observed that under N$_2$-H$_2$, the foam strength is almost independent of the nitriding temperature and the variation in the strength is quite small. However, under N$_2$ atmosphere, increasing the nitriding temperature from 1390°C to 1425°C causes a 30% decrease in the foam strength. This decrease is due to partial melting of Si which increases the size of the largest defects present in the microstructure.

Regarding the FeSi$_2$ concentration, it was observed that the maximum strength of the RBSN foam is achieved at 1 wt% of FeSi$_2$ and above this concentration, the foam strength starts to decrease. The α-Si$_3$N$_4$ content also increases up to 1 wt% of FeSi$_2$ and declines thereafter. Depending on the concentration of FeSi$_2$ and the nitriding conditions, different microstructures were observed. It was observed that α-Si$_3$N$_4$ forms based on gas

phase reactions between vapor Si and SiO with molecular nitrogen and it has two different morphologies including α-whiskers and α-matte. The β-Si$_3$N$_4$ phase which forms based on the reaction of molten and gaseous Si with atomic nitrogen can be observed as β-whiskers and angular grains, respectively. The α- and β-Si$_3$N$_4$ whiskers are quite different in terms of uniformity, degree of interlocking and aspect ratio.

Acknowledgment

Chapter 6

6.1. Preface to chapter 6

It was observed in our previous studies that the RBSN foams might have quite different microstructures in terms of the α and β phase contents and their morphologies. These microstructural features can influence the properties of the foams including its mechanical strength. The other parameter, which had a considerable influence on the foam strength, was the partial melting of Si leading to inhomogeneities in the RBSN body. Therefore, it is of great interest to have a more precise control over the nitriding reactions and consequently the foam microstructures in terms of α/β phase ratio and the phase morphologies and also improve the degree of homogeneity of the RBSN foam.

α- and β-Si_3N_4 seeds can be utilized as another tool to design the microstructure of the RBSN foams. They may have a strong influence on the foam's physical and mechanical properties. They may also affect the nitridation process and the nitriding mechanisms. Therefore, the next step of the investigation is devoted to the influence of both α- and β-Si_3N_4 seeds on the properties of the RBSN foams.

The influence of α- and β-Si$_3$N$_4$ seeds on the properties of reaction bonded silicon nitride foams produced via wet processing

Ali Alem, Robin A.L. Drew, Martin D. Pugh

Mechanical and Industrial Engineering Department, Concordia University, 1455 De Maisonneuve Blvd. W., Montreal, Quebec, Canada H3G 1M8

Abstract

This work presents the influence of α- and β-Si$_3$N$_4$ seeds on the properties of reaction bonded silicon nitride (RBSN) foams fabricated via wet processing of Si-PMMA-Si$_3$N$_4$ suspensions. Characterization of the seeded foams was performed in terms of porosity, density, and mechanical strength. Phase and microstructural analyses were also used to investigate the influence of α- and β-seeding on the α/β phase ratio and microstructure of the RBSN foams.

It was observed that both α- and β-seeds can improve the foam strength by 30% and 85%, respectively, due to more uniform nitridation. A foam strength of 2.23 MPa was obtained for RBSN foams seeded with 5 wt% α-Si$_3$N$_4$ with a foam porosity of 72 vol%. Higher contents of α-seeds create a loose structure of the Si$_3$N$_4$ seed particles within the nitrided matrix resulting in a considerable decrease in foam strength. The addition of 10 wt% of β-Si$_3$N$_4$ resulted in the maximum strength of 2.31 MPa at a porosity level of 72 vol%. The addition of β-seeds also resulted in an increase in the vapor phase reactions during nitridation leading to a significant increase in the β-whisker content of the microstructure. It was observed that even 30 wt% of β-seed addition increases the strength of the RBSN foams compared to the unseeded foams.

Keywords: Foam; Reaction bonding; Silicon nitride; Seeding

6.2. Introduction

Si_3N_4 is a promising ceramic material which has always been of great interest. Sintered Si_3N_4 foams have many outstanding properties and can open up many new applications. However, sintered Si_3N_4 foams have not received sufficient attention and there have been quite limited investigations on their fabrication to date. This is due to the difficulties of working with Si_3N_4 powder including very high sintering temperatures, large linear shrinkage, costly post-sintering machining processes [19], and poor rheological properties [20, 131] which all result in high fabrication costs [132, 133]. The alternative to take advantage of outstanding properties of Si_3N_4 foams while making the manufacturing process more straightforward and cost effective is the reaction bonding technique. In reaction bonding, Si compacts are transformed directly to Si_3N_4 under N_2-containing atmospheres. The final product is an RBSN ceramic.

It is of great interest to be able to control and properly design the microstructure of the foams since the microstructure affects the physical and chemical properties of the foam including porosity, pore interconnectivity, surface area, permeability, mechanical strength, etc. The fabrication technique has the most significant influence on the foam microstructure. Different foam fabrication techniques such as replication, direct foaming, and sacrificial template methods result in different foam microstructures [3]. In each fabrication method, there are also other fabrication parameters which influence the foam properties. One of the important parameters with which the microstructure of the Si_3N_4 ceramics can be modified and designed is the addition of α- and/or β-Si_3N_4 seeds. Each Si_3N_4 polymorph promotes the formation of its own structure since they provide preferential nucleation sites for the Si_3N_4 phases which grow during the reactions.

155

Therefore, the phase ratio and the morphology of the resultant Si_3N_4 phases in the microstructure can be controlled and modified in this way. Previously, self-reinforcing has been utilized as a technique to modify the final microstructure and properties of dense sintered Si_3N_4 ceramics [16, 134, 135]. In this case, β-Si_3N_4 seeds are added to a mixture of α-Si_3N_4 and sintering additives. The goal is to obtain a bimodal microstructure in which elongated β-Si_3N_4 grains with high aspect ratios are distributed in a fine matrix. The result would be an increase in toughness due to crack bridging and crack deflection mechanisms while a high mechanical strength is maintained [16, 134]. The seeding technique has also been used to modify the microstructure of both conventional RBSN and also sintered reaction bonded silicon nitride (SRBSN) ceramics [133, 136, 137]. The presence of α- and β-Si_3N_4 seeds are considered as inert phases which do not participate in the nitriding reactions but they promote the preferential nucleation and growth of the α- and β-Si_3N_4 phases, respectively. The addition of these phases also affects the nitridation rate in conventional RBSN ceramics resulting in higher rates of Si to Si_3N_4 conversion [136]. Therefore, seeding can also affect the microstructure and the physical properties of the RBSN ceramics.

Seeding studies have been mainly focused on sintered Si_3N_4 ceramics in which Si_3N_4 seeds were added to the Si_3N_4 powder to increase fracture toughness. To the best of the authors' knowledge, there are only a few investigations on seeded "dense" RBSN ceramics [138] while there is no study on seeded RBSN foams where high levels of porosity in the structure play important roles. Therefore, in this study the influence of both α- and β-Si_3N_4 seeds on the nitriding reactions and consequently the microstructures and properties of the RBSN foams has been studied. Different amounts of α- and β-seeds

have been added to the RBSN foams fabricated based on gel-casting of Si-PMMA suspensions. The influence of the seeds on the microstructural features of the foams, including the ratio and morphology of the Si_3N_4 phases which form during nitriding, has been investigated in depth. The mechanical strength and physical properties of the foams such as porosity and density have also been measured. The influence of seeding on the nitriding mechanisms will be discussed.

6.3. Experimental procedure

6.3.1. Foam fabrication and seeding

Silicon powder (ABCR, 99.995%, -8 microns) and PMMA beads (Microbeads, 10-40 μm) were used to produce RBSN foams based on wet processing of aqueous suspensions. α-Si_3N_4 (H.C. Starck, M11, α-Si_3N_4 >90 %, d_{50}=0.5-0.7μm, 99.95%) and β-Si_3N_4 (Denka, SN-F1, d_{50}=2.4 μm) seeds were also used to modify and design the microstructure of the foams. The details of the RBSN foam fabrication procedure can be found elsewhere [123]. Here, the experimental procedure is explained briefly. First, the premix solution containing water and gel-casting components was prepared. The gel-casting components were acrylamide as the monomer ($C_2H_3CONH_2$, Sigma-Aldrich) and N,N′-methylenbisacrylamide (($C_2H_3CONH_2$)$_2CH_2$, Sigma-Aldrich) as the cross-linker. Si powder, PMMA beads, and other rheological agents were added to make a stable Si-PMMA suspension. The weight ratio of the suspension's main components; Si:PMMA:H_2O, was 34:34:32 in weight percentage. The addition of Si_3N_4 seeds to the suspensions was performed in the next step followed by suspension homogenization via milling. The α-seeding content varied from 0 wt% to 30 wt% while the β-seed content

was from 0 wt% to 50 wt% (based on the Si weight in the suspension). In order to keep the suspension solid content constant, seeds were replacing the same amount of Si in the suspensions. In this case the suspension solid content would not be affected by seeding and was always fixed at 68 wt%. Polymerization was promoted at room temperature via the utilization of ammonium persulfate ($(NH_4)_2S_2O_8$, Sigma-Aldrich) as the catalyst and N,N,N′,N′-tetramethylethylenediamine ($C_6H_{16}N_2$, Sigma-Aldrich) as the initiator. Suspensions were then cast in silicone rubber molds followed by polymerization, drying and polymer pyrolysis. The Si foams produced after polymer burn-out were nitrided under two different atmospheres to produce RBSN foams. The α-seeded foams were nitrided under N_2-4%H_2 atmospheres at 1390°C while the β-seeded foams were nitrided under N_2 at 1425°C. The dwell time was 10 h and 6 h for α- and β-seeded foams, respectively. The heating rate during nitriding was 5 °C/min up to 1350°C, 1 °C/min up to 1390°C, and 0.3 °C/min up to 1425°C.

6.3.2. Foam characterization

The RBSN foams were characterized in terms of density and porosity based on the Archimedes method (ASTM C373-88). The flexural strength of the foams was measured via four point bending of rectangular bar samples, with dimensions of 70 x 10 x 10 mm^3, using a universal testing machine (Instron®, Model 3382). The upper and lower spans were 20 mm and 40 mm, respectively and a crosshead speed of 0.1 mm/min was used. A minimum of six foams, fabricated under the same condition, were tested. Phase analysis of the nitrided foams was performed with X-ray diffraction (XRD, X'PertPro; PANalytical). The quantitative analysis of the α- and β-Si_3N_4 phases was performed

158

based on Gazzara's technique [127]. The microstructures of the RBSN foams were also studied via scanning electron microscopy (SEM, HITACHI, S-3400N).

6.4. Results and Discussion

6.4.1. The effect of seeding on the α/β phase ratio and foam porosity

Regarding the nitridation process and the nitriding mechanisms, α-Si_3N_4 forms based on gas-phase reactions in which gaseous Si and/or SiO vapor react with molecular nitrogen [19, 22]. There are two possible morphologies for the α-Si_3N_4 phases; α-whisker and α-matte. The former has a high aspect ratio while the latter forms as small grains. On the other hand, β-Si_3N_4 forms only when molten or gaseous Si reacts with atomic nitrogen [22, 25]. Therefore, the concentration of atomic nitrogen in the nitriding atmosphere significantly influences the formation of β-Si_3N_4. The atomic nitrogen concentration is markedly affected by several processing parameters including the presence of hydrogen or oxygen in the nitriding atmosphere; both of which reduce the atomic nitrogen concentration and favor α-Si_3N_4 formation [22, 25]. Therefore, all the α-seeded foams were nitrided at 1390°C and under N_2-H_2 atmospheres to get the highest possible α-Si_3N_4 content in the nitrided foams. On the other side, β-seeded foams were all nitrided under N_2 atmospheres and also at higher temperatures (e.g. 1425°C) to obtain the highest possible β-Si_3N_4 content in the final RBSN foam. Increasing the nitriding temperature favors β-Si_3N_4 formation since this phase is a high temperature polymorph of Si_3N_4.

Table 6-1 shows the properties of the α-seeded RBSN foams. The table clearly shows that as the α-seed content increases to 30 wt%, the foam density decreases while its porosity level increases. During nitridation of Si compacts, Si_3N_4 phases which form due to

159

nitriding reactions are associated with a 22% volume expansion. These newly formed phases fill the empty spaces between the Si particles resulting in a porosity decrease and density improvement without changing the sample dimensions. In the case of seeded RBSN ceramics, the spaces between the seed particles would not be filled completely since a portion of the system which is composed of Si_3N_4 seeds does not participate in nitridation. Therefore, the inertness of the Si_3N_4 seeds which prevents them from participating in the nitriding reactions results in an increase in porosity.

Table 6-1. Porosity, density, α- and β-Si_3N_4 phase contents of RBSN foams seeded with α-Si_3N_4

Initial α-Si_3N_4 seed content (wt%)	Density (g/cm^3)	Porosity (vol%)	α-Si_3N_4 content in the RBSN foam (wt%)	β-Si_3N_4 content in the RBSN foam (wt%)
0	0.91	70.9	86.34	13.66
3	0.88	72.2	87.05	12.95
5	0.88	72.1	86.00	14.00
10	0.86	72.4	83.89	16.11
20	0.83	73.4	77.36	22.64
30	0.82	74.2	79.13	20.87

Table 6-1 also shows that as the α-seed content increases, the β-Si_3N_4 content also increases from 13 wt% to a maximum of 22 wt% in the nitrided foams. This is in contrast with what is expected from seeding Si_3N_4 ceramics since α-seeds should promote the formation of α-Si_3N_4 phases during nitriding due to preferential nucleation and growth phenomena. Therefore, β-Si_3N_4 content in the nitrided foam is expected to decrease as the α-seed content increase; something that was not witnessed in this study. As was explained in the experimental procedure, the RBSN foams have been fabricated based on wet processing of Si-PMMA-Si_3N_4 suspensions. Therefore, a significant amount of SiO_2

forms on the Si particles during suspension preparation and foam fabrication. Replacing Si particles with α-Si_3N_4 seeds results in less surface SiO_2 leading to a reduction of the oxygen concentration in the system. A higher surface SiO_2 content on particles and consequently a higher oxygen partial pressure in the nitriding atmosphere increases the α-Si_3N_4 content in two ways. First, higher SiO_2 content results in more SiO vapor production during nitridation. The reaction of SiO and nitrogen is one of the main reactions which leads to α-Si_3N_4 formation [19]. Second, oxygen also reduces the concentration of atomic nitrogen which is required for β-Si_3N_4 formation [22, 25]. In conclusion, when α-seeds replace Si in the suspension, less oxygen is present in the nitriding reactions resulting in more β-Si_3N_4 formation due to a higher atomic nitrogen concentration and less SiO vapor in the nitriding atmosphere. This is the reason why β-Si_3N_4 content in the nitrided foam increases with the α-seed content. As shown in Reactions 6-1 and 6-2, both Si and Si_3N_4 oxidize in water resulting in SiO_2 formation on the surface of the particles. However, the main source of surface silica is considered to be Si particles which oxidize more quickly [136].

$$Si\ (s) + 2\ H_2O \rightarrow SiO_2\ (s) + 2\ H_2 \hspace{4cm} (6\text{-}1)$$

$$Si_3N_4 + 6\ H_2O \rightarrow 3\ SiO_2 + 4\ NH_3 \hspace{3.5cm} (6\text{-}2)$$

Figure 6-1 shows the XRD patterns of the α-seeded foams for 3 wt%, 10 wt%, and 30 wt% α-seed. The increase in the β-Si_3N_4 content explained above, can be observed from the XRD patterns. Since α-seeded foams have been nitrided under a N_2-H_2 atmosphere which strongly favors α-Si_3N_4 formation, there would be only slight changes in the α-Si_3N_4 content of the final nitrided foams. It has been observed previously that the presence of H_2 in the nitriding atmosphere keeps the α-Si_3N_4 content at its maximum

since H_2 strongly promotes α-Si_3N_4 formation by removing atomic nitrogen from the nitriding atmosphere. The figure also shows that there is no residual Si in the nitrided foams and nitridation is complete.
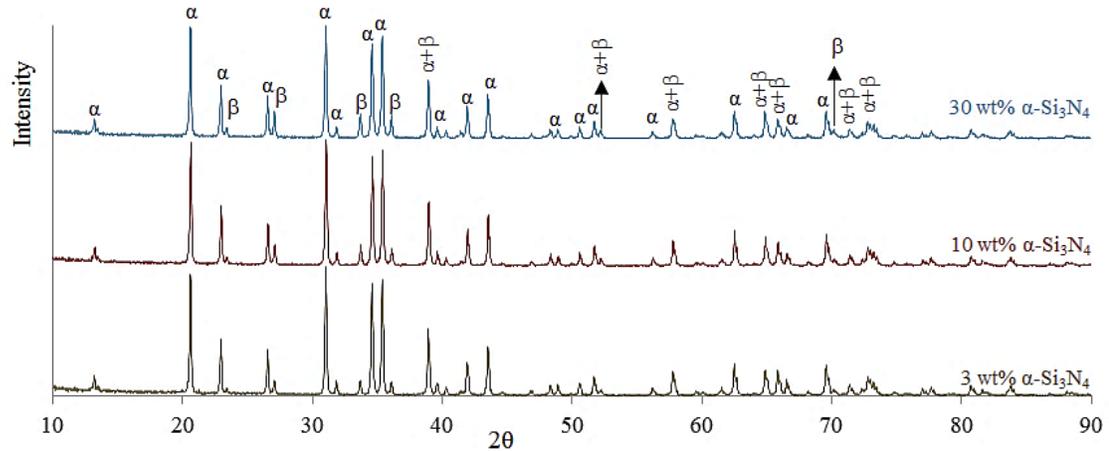
Figure 6-1. The XRD patterns of the α-seeded RBSN foams; the slight increase in β-Si_3N_4 can be observed. α and β show α-Si_3N_4 and β-Si_3N_4 peaks, respectively.

It must be mentioned that the addition of α-Si_3N_4 seed significantly affects the rheological behavior of the suspensions in a deleterious way. It was observed that the viscosity of the Si-PMMA-Si_3N_4 suspensions increases drastically and the suspensions become shear thinning as the α-Si_3N_4 content increases. Therefore, making suspensions with α-Si_3N_4 contents higher than 30 wt% was impractical if the solid content of the suspension is kept constant at 68 wt%.

Table 6-2 shows the properties of the β-seeded RBSN foams as the β-seed content is increased from 0 to 50 wt% of the silicon fraction. It is observed that the foam density decreases and its porosity level increases by 4 vol% as the β-seed content rises to 50 wt%. The increase in porosity of the seeded foams is again due to the inertness of the seeds which prevents them from participating in the nitriding reactions. The table also

162

shows that as the β-seed amount increases, the β-Si$_3$N$_4$ content of the nitrided foam can increase to 67 wt%. The reason would be the preferential nucleation of β-Si$_3$N$_4$ on the β-seeds. It must be mentioned that in contrast to α-seeded foams, the suspension viscosity and its rheological behavior did not change significantly in the presence of even 50 wt% β-Si$_3$N$_4$ seeds. This is probably due to the differences in the surface characteristics of α- and β-Si$_3$N$_4$ phases. Therefore, suspensions containing even 50 wt% β-seeds could be processed with no difficulties.

Table 6-2. Porosity, density, α- and β-Si$_3$N$_4$ phase contents of RBSN foams seeded with β-Si$_3$N$_4$

Initial β-Si$_3$N$_4$ seed content (wt%)	Density (g/cm^3)	Porosity (vol%)	α-Si$_3$N$_4$ content in the RBSN foam (wt%)	β-Si$_3$N$_4$ content in the RBSN foam (wt%)
0	0.93	71.5	58.6	41.40
3	0.87	72.3	66.31	33.69
5	0.87	72.6	56.52	43.48
10	0.86	72.7	53.82	46.18
20	0.83	73.8	46.25	53.75
30	0.81	74.3	41.78	58.22
50	0.77	75.7	32.52	67.48

Figure 6-2 shows XRD patterns of the β-seeded samples. A significant increase in the β-Si$_3$N$_4$ content of the final RBSN foam can be observed as the β-seed content increases. The patterns show that there is no residual Si in the nitrided foams and the Si to Si$_3$N$_4$ conversion was complete after a short nitridation time.
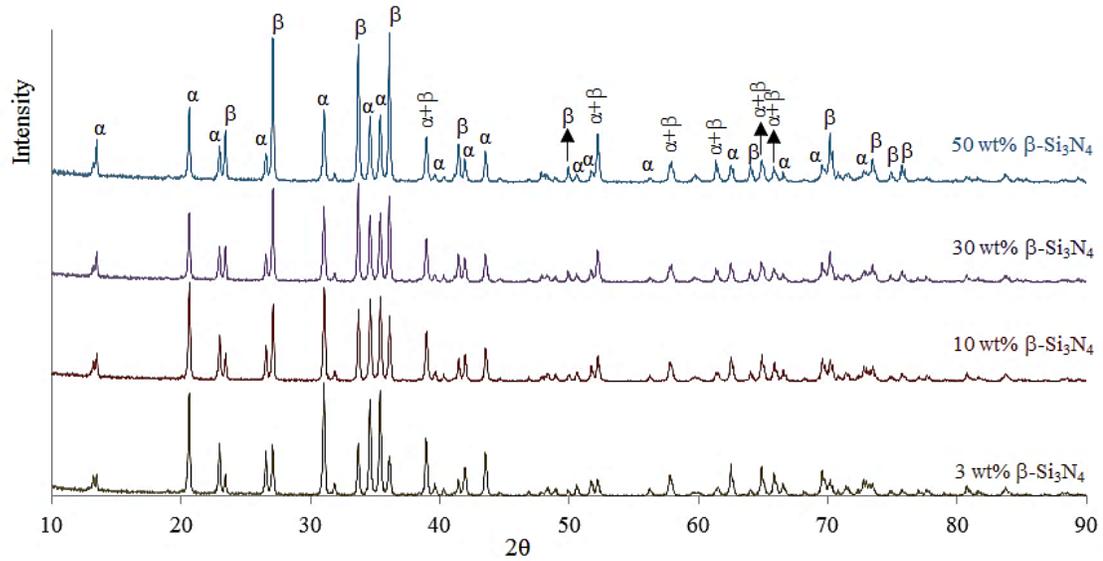
Figure 6-2. The XRD patterns of the β-seeded RBSN foams; the significant increase in β-Si$_3$N$_4$ can be observed. α and β show α-Si$_3$N$_4$ and β-Si$_3$N$_4$ peaks, respectively.

6.4.2. Mechanical strength versus seeding

Figure 6-3 shows the influence of α- and β-seeding on the flexural strength of the RBSN foams. In the case of α-seeded foams, shown in Figure 6-3-a, the foam strength is increased with up to 5 wt% α-seed and decreases thereafter. At 5 wt% α-seed, the strength has been improved by 30% and a maximum strength of 2.23 MPa was obtained while the foam has 72.68 vol% porosity. A significant reduction in the foam strength is observed when the α-seed quantity increases to 30 wt%. At higher α-seed contents, the quantity of the reaction-formed α-Si$_3$N$_4$ decreases which results in weak bonding between the α-Si$_3$N$_4$ seed network and the Si$_3$N$_4$ phases formed during nitridation. Therefore, the strength decreases.

Figure 6-3-b shows the mechanical strength of the β-seeded RBSN foams. It can be seen that the addition of β-Si$_3$N$_4$ seeds enhances the foam strength and a maximum value of 2.31 MPa is obtained at 10 wt% β-seeds. The foam strength decreases thereafter. The

164

figure shows that the strength of the 10 wt% β-seeded foam has increased by 85% compared to the unseeded foam (0 wt%) while the foam porosity has even increased by 3 vol%. In contrast to the α-seeded foams, the β-seeded foam with even with the highest seed content has a higher strength compared to the unseeded foam (0 wt%).
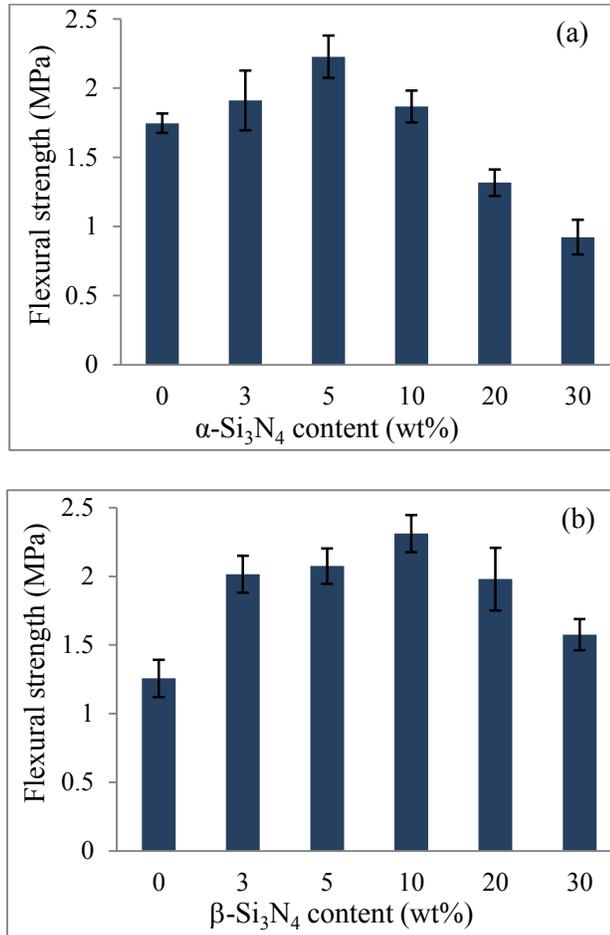
Figure 6-3. Flexural strength of the seeded RBSN foams; (a) α-seeded, (b) β-seeded foams.

The increase in the strength of the α- and β-seeded foams can be due to several reasons. The first reason can be the more uniform nitridation process which occurs in the presence of Si_3N_4 seeds. Neither α- and β-seeds participate chemically in the nitridation reactions; but they do reduce the extent and the influence of the exothermic nitriding reactions on

partial melting of Si. Therefore, there is less chance for Si to partially melt in the sample interior. The defects which form due to partial melting of Si can considerably reduce the foam strength. Therefore, the seeding may increase the strength of the RBSN foams due to an improvement in the uniformity of the silicon nitridation process. Therefore, the heating rate during nitriding can also be increased for the seeded samples resulting in a shorter process without getting molten Si.

It is worth mentioning that the addition of seeds has been reported to both increase and decrease the strength of the "dense" RBSN ceramics depending on the fabrication process and nitriding condition. One of the major fabrication issues of "dense" RBSN ceramics is the residual Si which is usually left even after very long nitriding cycles. The addition of seeds keeps the porosity network of the Si compact open and reduces premature pore blockage. Therefore, N_2 supply is maintained for longer periods during nitridation resulting in less residual Si in the nitrided ceramic [139]. Less residual Si obviously results in a higher strength of the RBSN ceramic. It has also been mentioned that seeding may result in strength reduction in conventional RBSN ceramics. In a study the addition of 0-16 wt% α-Si_3N_4 grog to slip-cast Si bodies resulted in higher Si to Si_3N_4 conversion during nitriding while a reduction in strength was also observed [140]. However, in the RBSN foam fabricated in this study, the nitridation was completed in a very short time even in the unseeded samples and no residual Si was observed. The fast and complete nitridation process is due to high level of interconnected porosity of the fabricated RBSN foams. Therefore, the increase in strength in the seeded RBSN foams is not due to more complete nitridation but it is due to a more uniform nitriding process.

When comparing the strength values of the α- and β-seeded foams, it must be remembered that α- and β-seeded foams have been nitrided under different nitriding conditions. A comparison between the unseeded foams (0 wt% α and 0 wt% β in Figure 6-3 parts (a) and (b)) shows that both the presence of H_2 in the nitriding atmosphere and using lower nitriding temperatures (e.g. 1390°C) result in a 40 % higher foam strength compared to the nitriding conditions used for β-seeded samples (N_2-1425°C). This significant difference observed in the unseeded foams is only due to the differences in the nitriding conditions since both samples have no Si_3N_4 seed. Considering different initial strengths for the unseeded foams nitrided under the two different nitriding conditions, it is clear that β-seeds improved the RBSN strength much more than α-seeds.

6.4.3. Microstructures versus seeding

Figure 6-4 shows the microstructure of the α-seeded foams. Both the α-matte and the α-whiskers are observed in the microstructures. As Table 6-1 shows, these samples contain up to 22 wt% β-Si_3N_4 also. Therefore, β-whiskers also co-exist among the α-whiskers. It must be mentioned that it is very difficult to differentiate between the individual α- and β-whiskers. But a comparison between microstructures in which either α-Si_3N_4 or β-Si_3N_4 is the dominant phase shows the differences in whisker morphologies and also characteristics. More explanation is provided in the following discussion.
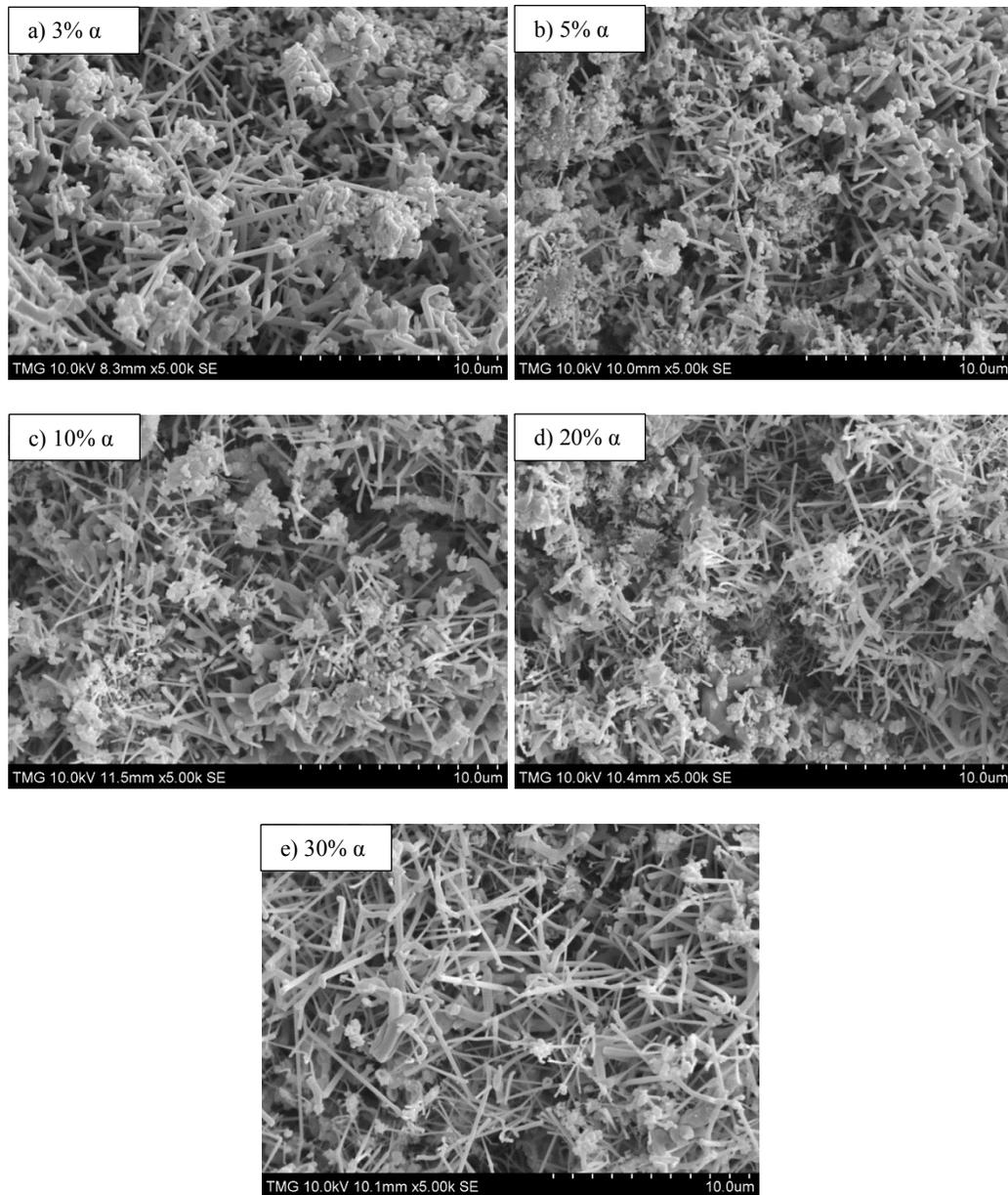
Figure 6-4. Fracture surface of the α-seeded RBSN foams

It can be seen from the Figure 6-4 that the roughness of the fracture surface increases for 10 wt% α-seed and higher. The increase in the roughness can be due to the α-Si_3N_4 seed particles which are loosely bonded to the Si_3N_4 matrix formed through the nitriding reactions. It was also observed from Figure 6-3-a, that above 5 wt% α-seed, the foam strength quickly decreases. It can be concluded that above this optimum content of the α-

seed, the weak bonding between the network of the seeded particles and the Si_3N_4 matrix which forms via nitridation, controls the foam strength resulting in poor foam properties. Figure 6-5 shows the microstructure of the β-seeded foams. These foams also show α-matte, α-whiskers and β-whiskers. As Table 6-2 shows, the $β-Si_3N_4$ content can increase up to 67 wt% depending on the β-seed content. Therefore, the population of β-whiskers would be much higher in β-seeded foams compared to the α-seeded foam shown in Figure 6-4.
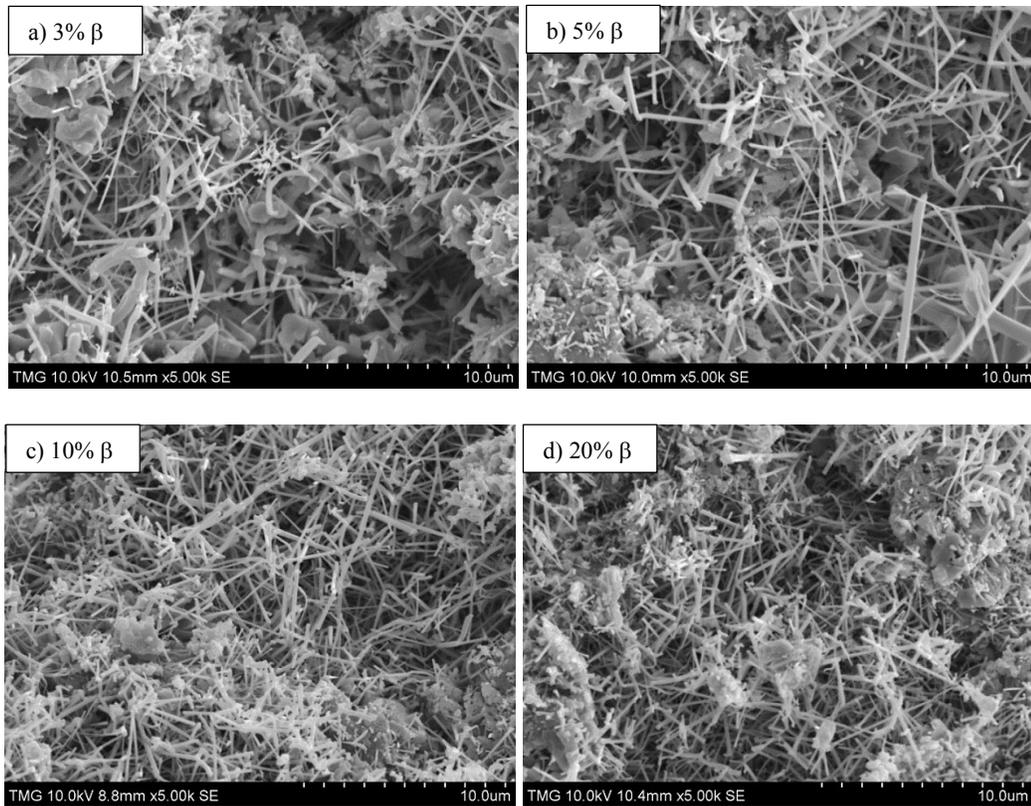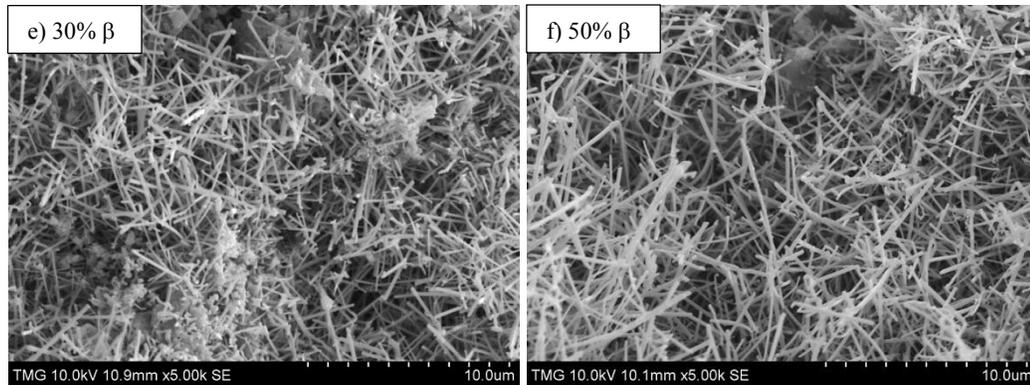
Figure 6-5. Fracture surface of the β-seeded RBSN foams

The increase in the whisker content is clearly seen in the microstructures as the β-seed content increases from 3 wt% to 50 wt%. The increase in whisker content can be due to an increase in vapor phase reactions between gaseous Si and atomic nitrogen. Since β-seeds are inert and do not participate in the nitridation process, they reduce the influence of exothermic nitriding reactions on partial melting of Si. Therefore, the more uniform distribution of heat throughout the sample reduces the chance of Si melting. Consequently, β-Si_3N_4 whiskers have to form based on gas phase reactions between Si vapor and atomic nitrogen. The other alternative for β-Si_3N_4 formation is the reaction between molten Si and atomic nitrogen which results in a facetted and angular grains morphology of β-Si_3N_4.

A comparison between Figure 6-4 and Figure 6-5 shows that β-Si_3N_4 whiskers are more uniform in terms of shape and size compared to α-Si_3N_4 whiskers. The degree of interlocking is also much higher in β-whiskers than α-whiskers.

6.5. Conclusions

This investigation focused on the effect of α- and β-Si_3N_4 seeds on the properties of RBSN foams. It was observed that α- and β-seeds can influence the density and porosity

170

of the RBSN foams. The α/β phase ratio was not significantly affected by the addition of α-seed. However, an increase in the β-Si_3N_4 content of the nitrided foams was observed when the amount of α-seed has increased. This was due to the reduction of oxygen partial pressure in the nitriding atmosphere which results in more atomic nitrogen and less SiO vapor in the nitriding atmosphere, both of which increase the β-Si_3N_4 content in the nitrided foam. An improvement in the foam strength was also observed up to 5 wt% α-seed with a significant decrease occurring thereafter. The loosely bonded α-seed particles within the Si_3N_4 matrix formed via nitriding lead to a decline in the foam strength at higher α-seed contents. An increase in the roughness of the fracture surface at 10 wt% α-seed and higher is another sign of easy detachment of the α-seed particles from the nitrided structure.

In the case of β-seeded foams, the α/β phase ratio changes considerably while adding β-seeds and the β-Si_3N_4 content can reach a maximum of 67 wt%. Similar to the α-seed foams, the foam porosity increases and its density decreases as the β-seed content enhances. The mechanical strength of the RBSN foams can be improved by 85% owing to the addition of 10 wt% β-seeds. Microstructural analysis shows that the addition of β-seeds increases the extent of vapor phase reactions resulting in a higher β-whisker content in the foams. A comparison between the α- and β-seeded foams reveal that β-whiskers have different characteristics in terms of shape, uniformity, and degree of interlocking compared to α-whiskers.

Chapter 7

7.1. Preface to chapter 7

It was observed previously that gas phase reactions resulted in massive whisker growth in the porosity network of the fabricated RBSN foams. These reaction-formed Si_3N_4 phases, especially α- and β-Si_3N_4 whiskers, grow into the porosity network of the foam. This situation would be beneficial in the fabrication of interpenetrating composites in which the matrix is reinforced with a three dimensional network of Si_3N_4 reinforcements, especially whiskers. However, it is also important to keep the porosity network of the RBSN foams clean and without whiskers. A clean porosity network results in a higher foam permeability and is required in applications where fluid transport is crucial. In order to achieve that, the nitriding reactions must be precisely controlled.

Therefore, the next step of this investigation will be focused on the fabrication of Si_3N_4 foams with clean porosity and consequently with the maximum capability of fluid transport. To achieve that, MgO was introduced as a sintering aid. A sintering step will be also performed on the fabricated RBSN foams to fabricate sintered reaction bonded silicon nitride (SRBSN) foams. It is expected that MgO will considerably affect the nitriding reactions and will result in Si_3N_4 foams with noteworthy properties.

Sintered reaction bonded silicon nitride foams with a high level of interconnected porosity

Ali Alem, Robin A.L. Drew, Martin D. Pugh

Mechanical and Industrial Engineering Department, Concordia University, 1455 De Maisonneuve Blvd. W., Montreal, Quebec, Canada H3G 1M8

Abstract

Sintered reaction bonded silicon nitride (SRBSN) foams with very high porosity levels of up to 85 vol% and pore interconnectivity have been fabricated in this study. SRBSN foams were fabricated based on gel-casting of Si-PMMA suspensions followed by nitriding and sintering. The addition of MgO as a sintering additive resulted in significant changes in the foam microstructure. Small amounts of MgO completely prevent the whisker-forming reactions during nitridation resulting in both reaction bonded silicon nitride (RBSN) and SRBSN foams with clean porosity networks. The addition of MgO does not influence the α- and β-Si_3N_4 contents in the RBSN foams. However, SRBSN foams show only β-Si_3N_4 due to the α to β phase transformation, which occurs during the early stages of sintering. The struts of the SRBSN foams are only composed of β-Si_3N_4 rod-like grains embedded in an intergranular amorphous phase.

Keywords: Foam; Silicon nitride; Reaction bonding; Sintering; Interconnectivity

7.2. Introduction

Silicon nitride ceramics have many remarkable properties including outstanding mechanical strength, good thermal shock resistance, good wear and corrosion resistance [128, 141, 142]. However, the high fabrication cost of Si_3N_4 ceramics does not allow the widespread industrial use of this ceramic material. There are two major issues that

considerably increase the production cost of Si_3N_4 ceramics; they include the costly Si_3N_4 powder as the starting material and the necessity of expensive post sintering machining steps. Other major issues in working with Si_3N_4 include the sintering problems [19] and poor rheological characteristics [20] of Si_3N_4 suspensions for wet processing.

Reaction bonding of Si compacts is a great alternative to overcome the fabrication issues of Si_3N_4 ceramics and concurrently reduce the fabrication costs. Reaction bonding is a near-net-shape fabrication technique which relies on the utilization of cheaper Si powder. This technique can be used to fabricate both "dense" and porous RBSN ceramics. Due to negligible dimensional changes during nitridation of RBSN ceramics, the costly machining steps can be minimal or even avoided in this technique.

RBSN foams benefit from an easy and economical fabrication procedure while possessing some of the remarkable properties of Si_3N_4 ceramics. Previously, it was observed that vapor phase reactions are dominant during nitridation of RBSN foams fabricated via wet processing of Si-PMMA suspensions [123]. This would result in massive whisker growth within the foam porosity network during nitridation. The extensive formation of Si_3N_4 whiskers is due to the high surface area of the foam and the availability of large free spaces for whisker growth within the porosity network of the foam. This whisker-reinforced microstructure of the RBSN foam may be beneficial in applications including fabrication of interpenetrating composites or for filtration purposes. In the former, the three dimensional network of the whiskers would efficiently reinforce the matrix of the composite while in the latter the interlocking whiskers improve the filtration efficiency by trapping the particles within the complex-shaped porosity network. However, in some applications where higher fluid transport rates are

required, it is of great interest to have RBSN foams with a clean porosity network where no whiskers exist. The main goal of the current investigation is to stop whisker formation within the pore network of RBSN foams via the addition of a sintering additive. There are only a few studies by Park et al on SRBSN foams fabricated by dry pressing [109, 110]. The foams fabricated in those studies suffer from low porosity levels (50 to 60 vol%) and also lack of pore interconnectivity.

It must be mentioned that sintering additives have been previously used in the production of "dense" SRBSN ceramics to improve density and consequently the mechanical strength of the body [128, 141, 143, 144]. This results in the fabrication of SRBSN ceramics with densities close to the theoretical values and good mechanical properties comparable to those of SSN (sintered silicon nitride) and hot pressed silicon nitride (HPSN) ceramics [145]. In this case the role of sintering additives would be acceleration of nitridation and also densification of the SRBSN ceramic.

However, this study focuses on the fabrication of open-cell SRBSN foams with very high porosity levels and also pore interconnectivity. The main goal of the study is to prevent whisker formation during nitriding, which blocks the foam porosity. To achieve this, different amounts of MgO as a sintering additive were added to the system to change the dominant nitriding reactions and to halt whisker formation. A small amount of MgO influences both the nitriding and sintering processes and significantly affects the foam properties. The fabricated SRBSN foams were characterized in terms of porosity and density. Phase and microstructural analyses were also performed to study the effect of MgO on the foam properties.

7.3. Experimental procedure

7.3.1. Foam fabrication

The SRBSN foams have been fabricated based on gel-casting of Si-PMMA suspensions followed by nitriding and sintering. Gel-casting components including acrylamide ($C_2H_3CONH_2$, Sigma-Aldrich) as the monomer and N,N′-methylenbisacrylamide (($C_2H_3CONH_2$)$_2CH_2$, Sigma-Aldrich) as the cross-linker were dissolved in water. Si (ABCR, 99.995%, -8 microns) and PMMA beads (Microbeads, 10-40 μm) were added to the premix solution. MgO (Sigma-Aldrich, >99%) was incorporated into the suspensions in various amounts between 3 wt% to 12 wt% based on the Si dry weight. Suspensions were stabilized and homogenized via pH adjustment and ball milling, respectively. Polymerization started after the addition of the catalyst (ammonium persulfate, (NH_4)$_2S_2O_8$, Sigma-Aldrich) and the initiator (N,N,N′,N′-tetramethylethylenediamine, $C_6H_{16}N_2$, Sigma-Aldrich). The suspensions were then cast into silicone rubber molds. Drying, polymer burn-out, and nitriding were performed sequentially to make RBSN foams. The nitriding step was performed at 1425°C and under static N_2 atmospheres. The heating rate during nitriding was 10 °C/min up to 1350°C, 0.5 °C/min up to 1425°C. The dwell time was 4 h at the maximum nitriding temperature. More details of the RBSN foam fabrication procedure including suspension preparation, gel-casting, and nitriding can be found in our previous study [123].

The sintering step was performed after nitridation to make SRBSN foams. The RBSN foams containing MgO were sintered at 1700°C for 2 h. The pressureless sintering was done under N_2 atmospheres. The samples were placed in a powder bed comprising Si_3N_4, BN, and MgO to reduce the Si_3N_4 and MgO losses during sintering. The MgO content of

the powder bed was equal to the MgO content of the RBSN foam prior to sintering. It should be noted that in the rest of the study, the term RBSN will be used for the foams which have only been nitrided while SRBSN is applied to foams which contain MgO and have been sintered after nitridation.

7.3.2. Foam characterization

The fabricated SRBSN foams were characterized in terms of density and porosity using Archimedes' method based on the ASTM C373-88 standard. Phase and microstructural analyses of the SRBSN foams were performed with X-ray diffraction analysis (XRD, X'PertPro; PANalytical) and scanning electron microscopy (SEM, HITACHI, S-3400N) equipped with energy-dispersive X-ray spectroscopy (EDS; Oxford Instruments; Wave Model). The quantitative analysis of the α- and β-Si_3N_4 phases in both nitrided and sintered bodies was performed based on Gazzara's technique [127].

7.4. Results and discussion

Figure 7-1 shows the density and porosity of the fabricated RBSN and SRBSN foams. It is observed that for the RBSN foam (0 wt% MgO on the graph) the porosity is 83 vol% while the maximum porosity of 85 vol% is obtained for SRBSN foams with 6 wt% MgO. This level of porosity has never been achieved for SRBSN foams. As the MgO content increases above 6 wt%, the porosity decreases and the density increases. However, at 12 wt% MgO the SRBSN foam still contains 75 vol% porosity.
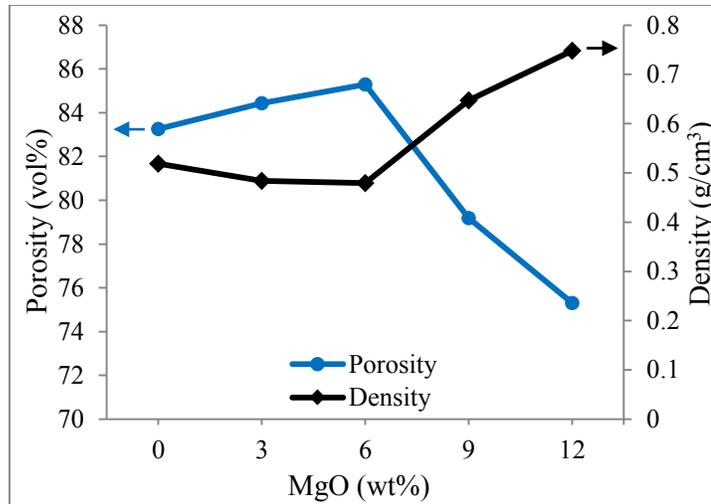
Figure 7-1. Density and porosity of SRBSN foams versus the MgO content. The sample corresponding to 0 wt% MgO is an RBSN foam.

The fabricated SRBSN foams were densified in two steps. The first step of densification occurs during nitridation. Generally, nitridation results in densification of Si compacts since reaction-formed Si_3N_4 phases fill the empty spaces between Si particles due to 22 vol% expansion which occurs during nitriding. Therefore, as nitridation progresses, the density of the RBSN ceramic increases. The second process, during which densification may occur is the sintering step in the presence of a sintering aid. It was expected that the addition of MgO would result in densification and a porosity decrease due to liquid phase sintering. However, it is observed from Figure 7-1 that the addition of up to 6 wt% MgO did not decrease the foam porosity compared to RBSN foams with no MgO addition but in fact an increase of 2 vol% was observed. The slight increase in SRBSN foam porosity containing up to 6 wt% MgO is likely due to MgO loss by evaporation during sintering. Beyond 6 wt% MgO, the sintering phenomenon dominates and the foams start to densify due to liquid phase sintering. Therefore, porosity decreases for SRBSN foams containing 9 and 12 wt% MgO as shown in Figure 7-1.

The microstructures of the two RBSN foams both with and without MgO addition are shown in Figure 7-2. The figure reveals how a small amount of MgO prevents the reaction-formed Si_3N_4 phases from filling the porosity network of the foam during nitriding. The addition of even 3 wt% MgO (based on Si weight) changes the dominant nitriding reactions and hinders whisker-forming reactions. In Figure 7-2-a, the whiskers have filled the porosity network of the RBSN foam while in Figure 7-2-b only a few whiskers are observed and the pore network is completely empty.
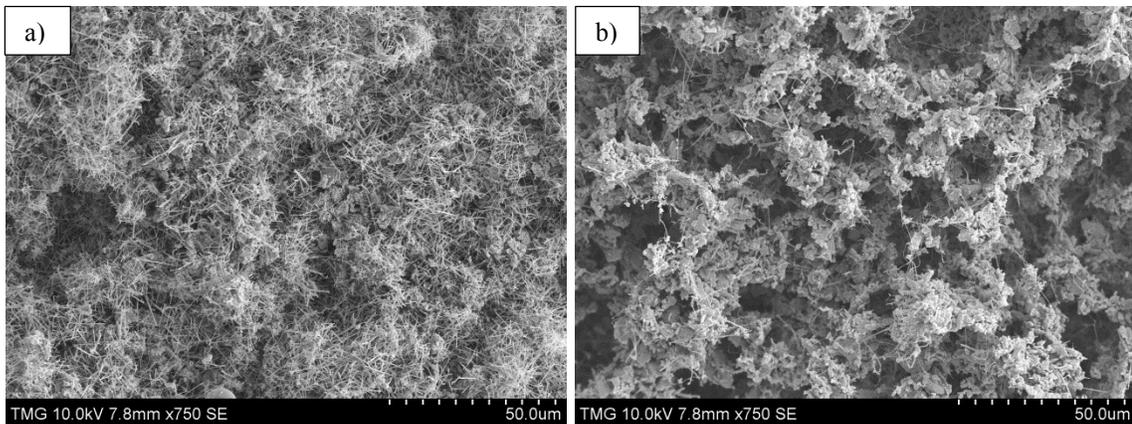
Figure 7-2. RBSN foams nitrided at 1425°C for 4 h with a) 0 wt% MgO and b) 3 wt% MgO.

Table 7-1 shows the α- and β-Si_3N_4 contents of the RBSN foams shown in Figure 7-2. It is observed that although the addition of 3 wt% MgO makes significant changes in the microstructure of the RBSN foam at 1425°C, it does not considerably affect the α- and β-Si_3N_4 phase contents of the microstructure. Therefore, it can be concluded that MgO only changes the morphology of the reaction-formed Si_3N_4 phases and it just prevents whisker-forming reactions. It is worth mentioning that MgO does not form a liquid phase with SiO_2 at the nitriding temperature of 1425°C. Based on the MgO-SiO_2 binary system, the first liquid phases form at 1543°C and 1557°C [146]. Therefore, MgO only influences the gas-phase reactions during nitriding.

179

Table 7-1. The α- and β-Si$_3$N$_4$ contents of the RBSN foams with and without the addition of MgO.

Foam	α-Si$_3$N$_4$ (wt%)	β-Si$_3$N$_4$ (wt%)
RBSN – no MgO	40.47	59.53
RBSN – 3 wt% MgO	38.87	61.13

Nitriding reactions can be divided to α-forming reactions and β-forming reactions. α-forming reactions are those which occur between molecular nitrogen and gaseous Si or SiO [22, 25]. On the other hand, β-Si$_3$N$_4$ forms based on reactions in which molten or gaseous Si reacts with atomic nitrogen [22, 25]. As Figure 7-1 shows, the RBSN foam has 83 vol% porosity prior to sintering; therefore, it has a very large surface area. On the other hand, it is observed from Figure 7-2 that a small amount of MgO can completely stop the whisker forming reactions. The uniform and complete prevention of the whisker-forming reactions can only occur if MgO is involved in the nitriding reactions as a vapor phase and not as a solid or liquid phase. If this were not the case, whisker formation would be stopped in some areas close to MgO particles while in other areas Si$_3$N$_4$ whiskers would form in the porosity network of the foam. Since MgO has a high vapor pressure at this temperature and hence a high volatilization rate, a considerable amount of MgO vapor is present in the nitriding atmosphere and within the pore network. It is clear that whiskers form based on gas phase reactions; therefore, they form within the empty spaces of the foam and fill the porosity network. Therefore, the presence of MgO vapor can considerably affect the gas phase reactions and prevent this whisker formation.

Figure 7-3 compares the microstructures of RBSN foams with SRBSN foams. Part (a) of the figure shows the microstructure of an RBSN foam with no MgO. In Figure 7-3 (b) to (e), the microstructure of SRBSN foams are shown with 3 wt% to 12 wt% MgO. It is

clearly observed that in the absence of MgO, α- and β-Si$_3$N$_4$ phases formed during nitriding fill the porosity network of the RBSN foam. On the other hand, in micrographs (b) to (e), it is observed that the addition of MgO results in SRBSN foams with unique structures. The fabricated SRBSN foams show clean porosity and consequently better pore interconnectivity. A comparison between micrographs (b) to (e) also shows that the foam microstructure becomes coarser due to grain growth as the MgO content increases.

a) RBSN

TMG 10.0kV 7.8mm x1.00k SE   50.0um

b) 3 wt% MgO

TMG 10.0kV 9.1mm x1.00k SE   50.0um

c) 6 wt% MgO

TMG 10.0kV 7.5mm x1.00k SE   50.0um
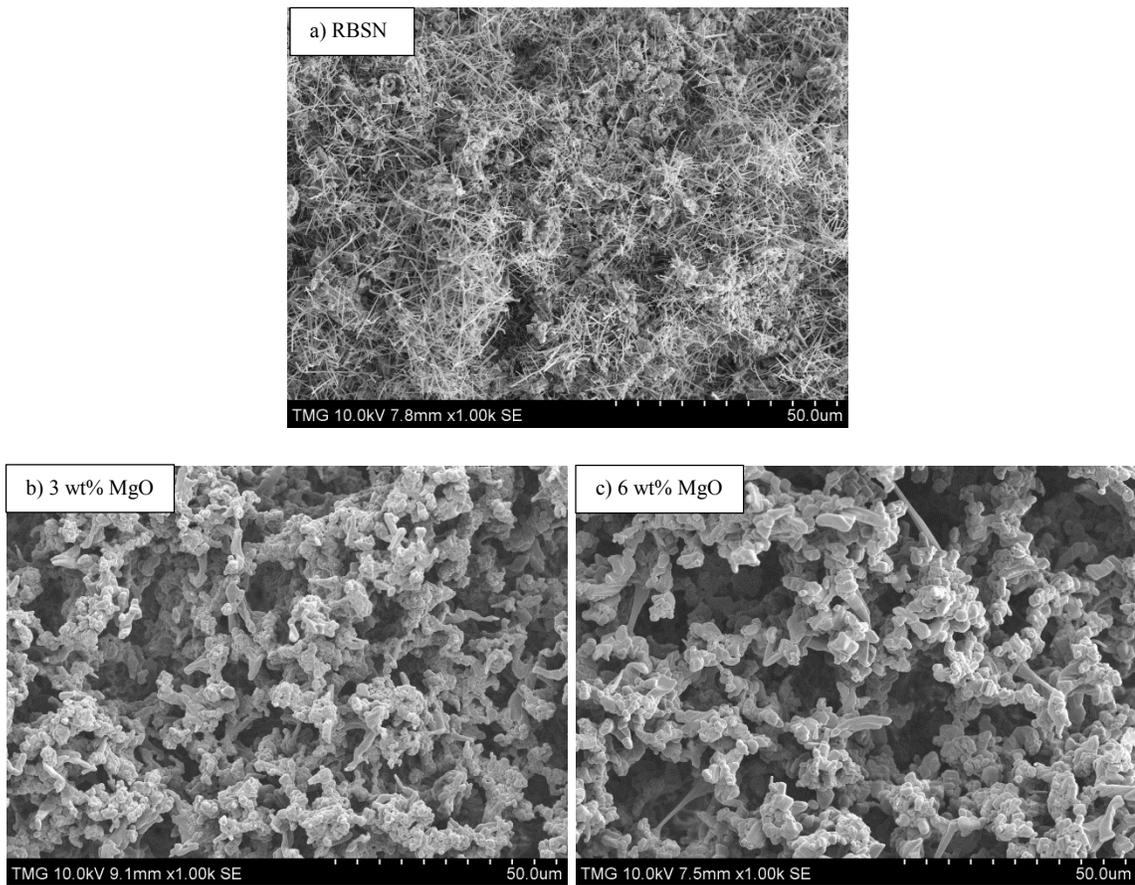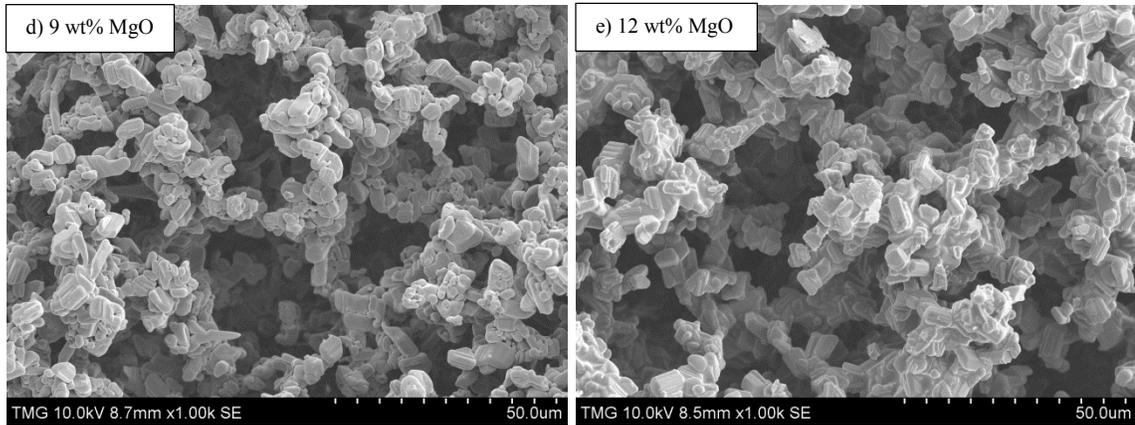
Figure 7-3. Microstructures of (a) RBSN foam with no MgO and (b) to (e) SRBSN foams with 3 wt% to 12 wt% MgO.

Figure 7-4 compares the XRD patterns of the RBSN and SRBSN foams shown in Figure 7-3. It is clearly observed that the SRBSN foam with 3 wt% MgO is composed of 100% β-Si_3N_4 and no α-Si_3N_4 phase was detected. However, the RBSN foam contains both α- and β-Si_3N_4 phases; 40.47 wt% and 59.53 wt%, respectively. It was also observed that at higher MgO contents e.g. 12 wt%, only β-Si_3N_4 was present and the XRD pattern is the same as that of SRBSN with 3 wt% MgO. Therefore, no crystalline phases containing MgO form during sintering and MgO is assumed to form an amorphous phase at the grain boundaries.
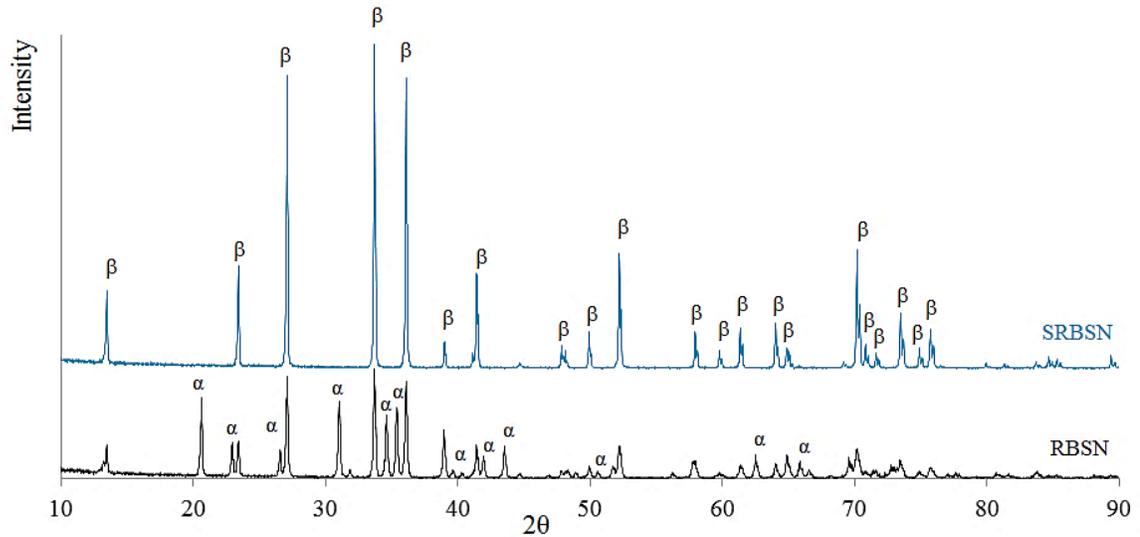
Figure 7-4. XRD patterns of the RBSN foam containing no MgO and the SRBSN foam containing 3 wt% MgO.

Pore interconnectivity is an important property which is necessary in all the applications where fluid transport is required. Achieving a high level of porosity and also pore interconnectivity is very challenging since the combination of these two properties increases the probability of foam collapse during fabrication. Figure 7-5 shows the unique microstructure of the SRBSN foam in which pore interconnectivity is clearly observed. The figure shows the fine and equiaxed β-Si_3N_4 grains which form the foam struts. It was observed that as the MgO content increases, the aspect ratio of the β-Si_3N_4 grains increases. Therefore, they acquire a rod-like morphology rather than equiaxed.

Figure 7-5. Pore interconnectivity in the SRBSN foam containing 3 wt% MgO.

Figure 7-6 shows the rod-like β-Si_3N_4 grains with higher aspect ratios forming the struts of the SRBSN foams containing 12 wt% MgO. The figure clearly shows β-Si_3N_4 grains embedded in an amorphous phase. During sintering, MgO reacts with the surface silica on the nitrided surface resulting in the formation of low melting-point silicate phases. The liquid phase also facilitates the α to β phase transformation and grain growth via solution-precipitation [146]. Upon cooling, the liquid phase forms an intergranular amorphous phase surrounding the β-Si_3N_4 grains. It is observed that the amount of amorphous phase also increases with MgO content. Therefore, grain growth would be facilitated as the MgO content increases and the foam microstructure coarsens (see Figure 7-3 micrographs (b) to (e)).
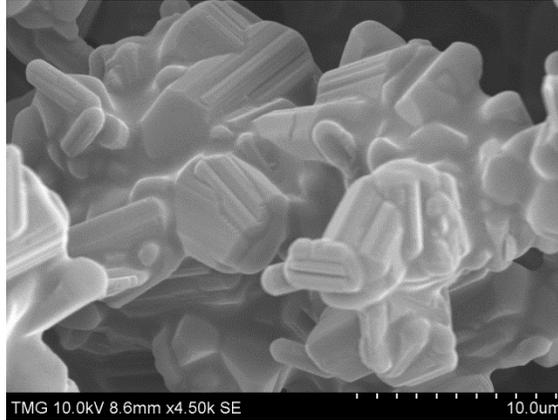
Figure 7-6. Rod-like β-Si$_3$N$_4$ grains with different aspect ratios forming the struts of the SRBSN foam containing 12 wt% MgO.

Figure 7-7 shows the fracture surface of the SRBSN foam with 12 wt% MgO. Both intergranular and transgranular fracture modes can be observed in the image. However, it must be mentioned that the rough fracture surface shows that intergranular fracture is the dominant fracture mode where the cracks propagates along the amorphous grain boundary phase. No pull-out of the rod-like β-Si$_3$N$_4$ grains was observed.
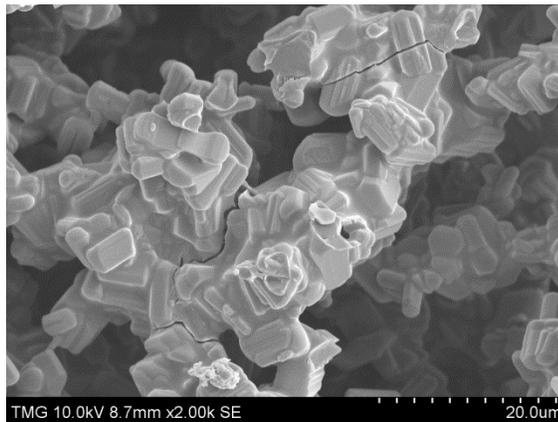
Figure 7-7. Fracture surface of the SRBSN foam with 12 wt% MgO.

7.5. Conclusion

In this study, SRBSN foams with unique microstructures have been fabricated based on gel-casting of Si-PMMA suspensions followed by reaction bonding and sintering. The

foams have very high porosity levels of up to 85 vol% with an interconnected porosity network.

The addition of small amounts of MgO has significant influences on the foam microstructures both before and after sintering. A small amount of MgO completely stops the whisker-forming reactions during nitridation. This is due to the interference of MgO vapor with the whisker-forming reactions resulting in the fabrication of both RBSN and SRBSN foams with clean porosity. The addition of MgO does not affect the α- and β-Si_3N_4 contents in the fabricated RBSN foams and it only changes the morphology of the reaction-formed Si_3N_4 phases. However, MgO addition results in complete α- to β-Si_3N_4 transformation in SRBSN foams. In this case the SRBSN foam struts are composed of only β-Si_3N_4 grains. The β-Si_3N_4 grains can acquire both equiaxed and rod-like morphologies equivalent to low and high aspect ratios, respectively. The grain morphology is dependent on the MgO content and consequently the quantity of the liquid phase present during sintering. As the MgO content increase, the larger β-Si_3N_4 grains with higher aspect ratios will form within the foam struts.

Acknowledgment

Chapter 8

8.1. Summary of conclusions

In this study a new fabrication procedure has been designed to fabricate highly porous and homogeneous silicon nitride foams with open-cell structures. Highly porous RBSN and SRBSN foams with interconnected porosity and a very wide range of controlled porosity were fabricated based on gel-casting of Si-PMMA suspensions followed by nitriding and/or sintering.

It was observed that both Si and PMMA suspensions possess the highest stability at pH 8.5 where the suspensions are completely deflocculated due to the combination of maximum repulsion between the particles and minimum ionic strength. Among the three deflocculants examined in this study including DS001, Darvan® 821, and Dolapix PC 75, 1.5 wt% DS001 provides the optimum condition in terms of stability resulting in the least amount of sedimentation due to higher electrosteric stabilization of the suspensions.

Rheological measurements revealed that Si-PMMA suspensions are near Newtonian with a slightly shear thinning behavior at pH 8.5 and for 60 wt% solid. A considerable increase in viscosity and also shear thinning behavior of Si-PMMA suspensions is observed by increasing the solid content or lowering the pH. In the Si-PMMA suspensions, due to the isotropic and spherical shape of the PMMA beads and their high volume fraction in the suspension, which lowers the net zeta potential, shear thickening behavior is not observed even at higher solid contents.

Investigation of the gel-casting parameters showed that a higher monomer content results in a more uniform distribution of Si particles and PMMA beads in the cast body and consequently a higher homogeneity. On the other hand, the sample strength significantly

increases with monomer content. Both a higher homogeneity and a higher green strength lead to less distortion of the sample during drying. The ratio of monomer to cross-linker significantly affects the cross-linking density of the gel network and consequently the green strength of the cast body. Although the suspensions are completely stable, gelation time must be used as a tool to reduce the effect of particle sedimentation and segregation phenomena both of which lead to cracking and collapse of the foams.

The polyester-infiltrated Si and RBSN foams show complete pore interconnectivity both before and after nitridation. Based on the designed fabrication procedure, the RBSN foam porosity can be accurately controlled over a wide range (46 vol% to 87 vol%) based on the monomer content, solid content, and PMMA to Si ratio in the suspension. The homogeneity of the fabricated foams made it possible to reach such high porosity levels.

Depending on the foam porosity, the flexural strength of the RBSN foams varied between 1 MPa for 83 vol% porosity to 18 MPa for 41 vol% porosity. The monomer content also significantly influences the foam homogeneity and consequently its strength. It was observed that for high Si/PMMA weight ratios, a minimum of 25 wt% monomer is required in the premix solution. Otherwise, defects and inhomogeneities significantly reduce the foam strength. It was also observed that nitriding conditions can markedly influence the foam strength. The highest strength was obtained for the ArH-NH1400 foams while the lowest was observed for the N1425 foams. The variation in nitriding temperature also has negligible effects on the foam strength when nitridation is performed under N_2-H_2 atmospheres while it is significantly influential when N_2 is the nitriding atmosphere.

Investigation of the nitridation reactions and mechanisms revealed that vapor phase reactions including the reactions between gaseous Si and SiO vapor with molecular nitrogen are responsible for α-Si$_3$N$_4$ formation. The reaction between SiO and N$_2$ is likely to be the dominant reaction for the formation of α-Si$_3$N$_4$ in the current investigation and under the N$_2$-H$_2$ atmosphere, resulting in more than 85 wt% α-Si$_3$N$_4$ in the microstructure of the foam. On the other hand, β-Si$_3$N$_4$ forms in the presence of atomic nitrogen. β-Si$_3$N$_4$ forms if liquid or gaseous Si can react with atomic nitrogen. Under N$_2$ atmospheres, the β-Si$_3$N$_4$ content can increase up to 46 wt% which is mainly due to a higher concentration of atomic nitrogen.

Phase and microstructure analyses revealed that α-Si$_3$N$_4$ forms in the form of both whiskers with high aspect ratios and also fine grained α-matte. β-Si$_3$N$_4$ also forms in two different morphologies including β-whiskers and also β-grains with facetted shapes. β-whiskers form based on the reactions between gaseous Si and atomic nitrogen while hexagonal-shaped β-grains form due to the reactions between molten Si and atomic nitrogen. It was observed that β-whiskers grow individually in the porosity network of the foam while β-grains form in groups.

The addition of 1 wt% FeSi$_2$ resulted in a significant improvement of the foam strength regardless of the nitriding condition. In this case, N1390 foams provided the maximum strength of 3.41 MPa. Due to partial melting of Si, N1425 foam shows a 30% reduction in strength when the nitriding temperature increases to 1425°C. On the other hand, RBSN foams containing FeSi$_2$ and nitrided under N$_2$-H$_2$ do not show much variation in terms of strength.

During phase analysis of the $FeSi_2$ containing foams, it was observed that the α-Si_3N_4 content increases with up to 1 wt% $FeSi_2$ and decreases thereafter. The increase in the α-Si_3N_4 content is due to the reducing effect of Fe while the liquid forming role of $FeSi_2$ and also an increase in the concentration of atomic nitrogen lead to more β-Si_3N_4 formation above 1 wt% $FeSi_2$.

It was also observed that α- and β-whiskers are different in terms of shape and morphology. The differences are clearer when different nitriding atmospheres (N_2 vs. N_2-H_2) were employed. The β-whiskers are shorter, straighter, and more uniform in terms of size and shape. The degree of interlocking is also much higher for β-whiskers formed under N_2 atmospheres. On the other hand, when H_2 is present in the nitriding atmosphere, both the whisker uniformity and the degree of interlocking decrease.

It was observed that the addition of either α- and β-seeds decreases the foam density and increases its porosity level. It is interesting that the β-Si_3N_4 content also increases from 13 wt% to a maximum of 22 wt% in the nitrided foams as the α-seed content increases to 30 wt%. The reason is the decrease in the surface SiO_2 and consequently the oxygen content of the system when α-seeds replace for Si in the suspension. Less oxygen results in more β-Si_3N_4 formation due to a higher atomic nitrogen concentration and less SiO vapor in the nitriding atmosphere. It was observed that the addition of α-seed has a detrimental influence on the rheological properties of the suspensions. Due to preferential nucleation and growth phenomena, the β-Si_3N_4 content increases to 67 wt% as the β-seed content increases.

It was observed that both α and β-seeds considerably increase the foam strength. The maximum increase in the foam strength is 30% and 85% for 5 wt% α-seed and 10 wt% β-

seed, respectively. The increase in the strength of the α- and β-seeded foams is due to the more uniform nitridation process which occurs in the presence of Si_3N_4 seeds by reducing the extent and the influence of the exothermic nitriding reactions on partial melting of Si. Beyond the optimum seed contents, the foam strength starts to decrease due to the weak bonding between the network of the seeded particles and the Si_3N_4 matrix which forms via nitridation.

The addition of MgO in the fabrication of SRBSN foams was observed to have strong influences on both the RBSN and SRBSN foam microstructures. MgO prevents whisker-formation during nitriding resulting in foams with clean porosity networks and without any Si_3N_4 whiskers. The fabricated SRBSN foams have complete pore interconnectivity with porosity levels of up to 85 vol%. The struts in SRBSN foams are composed of only β-Si_3N_4 grains, the aspect ratio of which depends on the amount of the amorphous phase present during sintering.

8.2. Contributions

This investigation was focused on a novel fabrication procedure to produce both RBSN and SRBSN foams followed by characterization, optimization, and design of the foam properties. The fabrication part and the idea behind the process are useful to fabricate other ceramic foams based on wet processing techniques. The reaction bonding and the results obtained from foam characterization would definitely help in understanding the nitriding mechanisms of RBSN foams. The fabrication parameters used to modify the foam properties including utilization of additives, seeding effect, and sintering aids and the resulting observations are useful in ceramic processing especially fabrication of Si_3N_4

dense and porous bodies. The details of the contributions of the current investigation have been explained below.

In this study, a novel fabrication procedure was designed based on wet processing of Si-PMMA suspensions to produce open-cell RBSN foams. The designed fabrication procedure avoids all the issues of working with Si_3N_4 powder while taking advantage of the promising properties of this ceramic material. The combination of gel-casting and reaction bonding as near net-shape fabrication techniques is capable of producing complex-shaped products. The designed fabrication procedure reduces or even removes the need of costly post sintering machining steps, which are considered as one of the major disadvantages of sintered silicon nitride ceramics.

Based on the literature, previously produced Si_3N_4 foams, severely lack high porosity levels and also pore interconnectivity. Both the RBSN and SRBSN foams fabricated in this study benefit from a very wide range of controlled porosity which can vary from about 45 vol% to 87 vol% depending on the processing parameters. The combination of this high porosity level and the pore interconnectivity opens up many new applications including the fabrication of interpenetrating composites. The high surface area of the fabricated foams can also be useful in other applications.

The nitriding mechanisms of the porous RBSN foam have been studied in depth for the first time. The high level of porosity and the pore interconnectivity of the fabricated foams influence the nitriding phenomenon in many ways resulting in many differences in the microstructures of the foams compared to conventional RBSN ceramics. The understanding of the nitriding reactions and the mechanisms help in the design of the microstructure and properties of the fabricated RBSN foam.

A widespread investigation was performed on the mechanical strength of the RBSN foams. The effect of various nitriding conditions on the properties and strength of the RBSN foams has been investigated and the reasons were discussed in depth.

The foam strength was significantly improved via small additions of $FeSi_2$. The effect of $FeSi_2$ on nitridation and consequently the foam properties was also studied comprehensively. It was observed for the first time that $FeSi_2$ improves the strength of porous RBSN ceramics while it was previously believed that Fe compounds have detrimental effects on the strength of the conventional RBSN ceramics. The addition of $FeSi_2$ also resulted in interesting outcomes in terms of the foam strength and its microstructures all of which have been thoroughly discussed. This would open up new windows on reaction bonding and its mechanisms.

The seeding effect of both α- and β-Si_3N_4 seeds was used as a tool to redesign the microstructure and properties of RBSN foams. This is the first time that the seeding effect was studied in highly porous RBSN foams. Since Si_3N_4 polymorphs produced based on reaction bonding show different morphologies, the seeding effect can considerably influence the foam properties including strength and permeability. The addition of α- and β-Si_3N_4 seeds improved the RBSN foam strength by 30% and 85%, respectively.

The fabrication of SRBSN foams in the presence of MgO is another major contribution of this study. Both RBSN and SRBSN foams could be fabricated with no whisker formation in the porosity network of the structure. Very high porosity levels and complete pore interconnectivity could be achieved.

8.3. Future works

The following suggestions are proposed as future works to continue the current investigation.

❖ The PMMA bead size range and its size distribution play an important role on the pore interconnectivity of the foam. The porosity network of the foam will be interconnected if the PMMA beads form a continuous network. This network continuity is significantly affected by the size range of the beads and also the size ratio of Si particles to PMMA beads. Designing these parameters can increase the porosity level of the foam and improve its interconnectivity.

❖ Gas pressure infiltration of the fabricated foam with a lightweight metallic alloy e.g. Al-Mg alloys, would result in a three dimensional interpenetrating composite reinforced with a three dimensional network of Si_3N_4. The composite would benefit from improved mechanical properties while being lightweight. Since the fabricated foam can have up to 87 vol% porosity and the pore network is interconnected, metal matrix composites can be fabricated at low infiltration pressures without fracturing the foam network. It must be mentioned that pressureless infiltration was performed in this study (more details can be found in the Appendix 9.4). Severe reactions occurred between Al and Si_3N_4 due to the high infiltration temperature and its slow rate. The aforementioned issue would be fixed by using the pressure infiltration technique.

❖ TEM analysis of the porous foam microstructure is challenging but it would provide useful information about the nitridation process. The TEM results can substantiate the proposed mechanisms for the nitridation of RBSN foams in terms of nitriding

reactions, nucleation and growth of the α and β phases especially the whiskers. However, sample preparation would be extremely challenging due to the high level of foam porosity.

❖ The increase in β-Si_3N_4 content by combining β-seed effect and an appropriate sintering aid system can also be beneficial. It has been observed that β-seeding has significantly improved the foam strength; therefore, the combination of seeding and sintering may result in interesting results in the fabricated foam in terms of strength and microstructural features.

❖ The utilization of other sintering aid systems including Y_2O_3 and Al_2O_3 may result in SRBSN foams with different microstructures and properties compared to those containing MgO as a sintering additive. A recommendation is to investigate whether other sintering aids would affect gas phase reactions during nitridation or not. The mechanical strength of the SRBSN foams may be quite different when the sintering aid system is changed.

Appendix

9.1. Additional details of the experimental procedure

More details of the experimental procedure are explained in this section.

In order to prepare the suspensions, monomer (AM) and then the cross-linker (MBAM) were dissolved in water. The premix solution was stirred for 30 minutes to ensure that both components dissolve completely. In the next step, the proper amount of deflocculant was added followed by Si powder. The polyacrylamide binder and the antifoaming agent were added next followed by the addition of PMMA beads. The suspension was stirred for 5 minutes. In the case of foams containing $FeSi_2$ or Si_3N_4 seeds, these additives were added at this stage. The suspension pH was adjusted by NH_4OH (1 N) addition. Ball milling was performed in polyethylene bottles with Si_3N_4 balls for 30 minutes to obtain a homogeneous suspension. After milling, the suspension pH was checked and readjusted. In the next step, the air bubbles formed during milling were removed under vacuum. The vacuum de-airing step was performed in 3 steps to remove all the trapped air bubbles. The suspension was kept under vacuum for 10 min, followed by slow mixing for 5 min, and finally the last vacuum stage for 5 min removed almost all the trapped air bubbles. A short mixing between the vacuum steps helped the trapped air bubbles to float and be removed in the second vacuum step. In order to start the polymerization reactions, the catalyst (TEMED) was added first followed by slow mixing for 5 min. The addition of initiator would be the last step. The suspension was then mixed for 2 minutes followed by casting in the silicone rubber molds of the desired geometry. After casting, the molds were covered by plastic sheets and kept at 50°C for 3 h to make sure that polymerization of the monomer and the cross-linker is complete. The use of plastic sheets stopped drying

of the cast samples during polymerization. The molds were then kept at room temperature for a couple of hours before sample extraction.

Drying and polymer pyrolysis were the next steps. Depending on the monomer content of the gel-cast body, the heating rate during polymer burn-out varied between 0.5 °C/min for 25 wt% monomer content in the premix solution up to 1°C/min for the monomer concentration of 9 wt%.

Nitridation was performed in an atmosphere controlled furnace. Si foams were placed in the furnace. The furnace chamber was evacuated by both roughing and diffusion pumps up to 10^{-6} torr. The chamber was then backfilled with the nitriding gas and the temperature cycle was started.

The porosity and density of the foams were measured based on the Archimedes technique according to the ASTM C373-88 standard. A minimum of three samples were tested for each specific condition.

The 4-point bending fixture had been fabricated based on the ASTM 1161-02C standard. The load and the support spans are 20 mm and 40 mm, respectively.

In the fabrication of the SRBSN foams, sintering was performed in the same atmosphere controlled furnace. The RBSN foams were placed in an alumina crucible and then covered with the Si_3N_4-BN-MgO powder bed. After evacuating the chamber to 10^{-6} torr, sintering was performed under N_2 atmospheres.

Regarding the zeta potential measurements and the sedimentation height tests, the suspensions were aged for 24 h to reach the most stable situation prior to the measurement.

The sample preparation procedure for SEM analysis was the Au-Pd coating for 200 sec.

9.2. TGA analysis of PMMA beads and polyacrylamide

The figures 9-1 and 9-2 show the TGA analysis of the PMMA beads and the polyacrylamide network of the gel produced based on AM and MBAM polymerization, respectively. It is observed that PMMA beads pyrolyze at lower temperatures than polyacrylamide. The maximum burn-out temperature of the polymeric components was below 500°C. Therefore, the burnout temperature was selected at 525°C to make sure that all the sacrificial phases leave the structure completely.
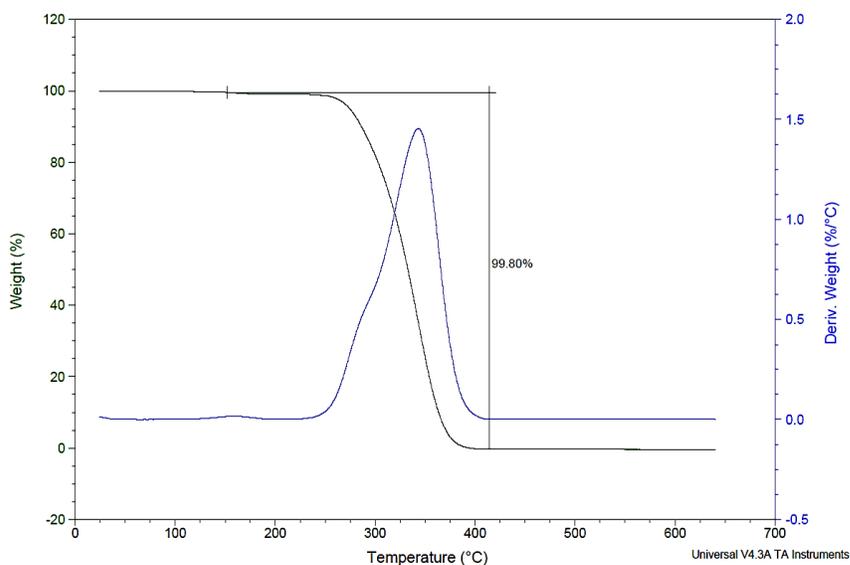
Figure 9-1. TGA analysis of PMMA beads.
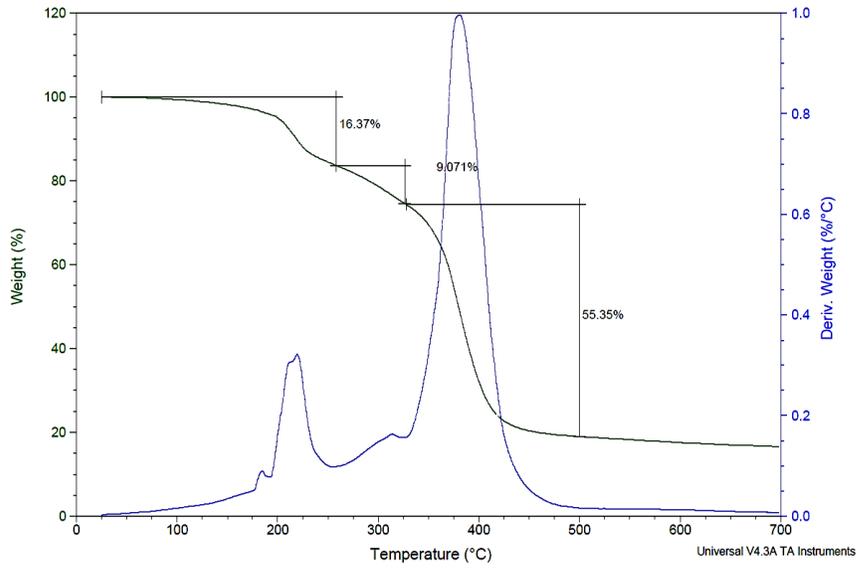
Figure 9-2. TGA analysis of dried polyacrylamide produced via AM and MBAM polymerization.

9.3. The XRD patterns of the foams containing FeSi$_2$

The XRD patterns of three RBSN foams containing 0, 1, and 4 wt% FeSi$_2$ nitrided under N$_2$ at 1425°C is shown in Figure 9-3. The patterns show the increase of the α-Si$_3$N$_4$ content up to 1 wt% FeSi$_2$ and its decrease thereafter.
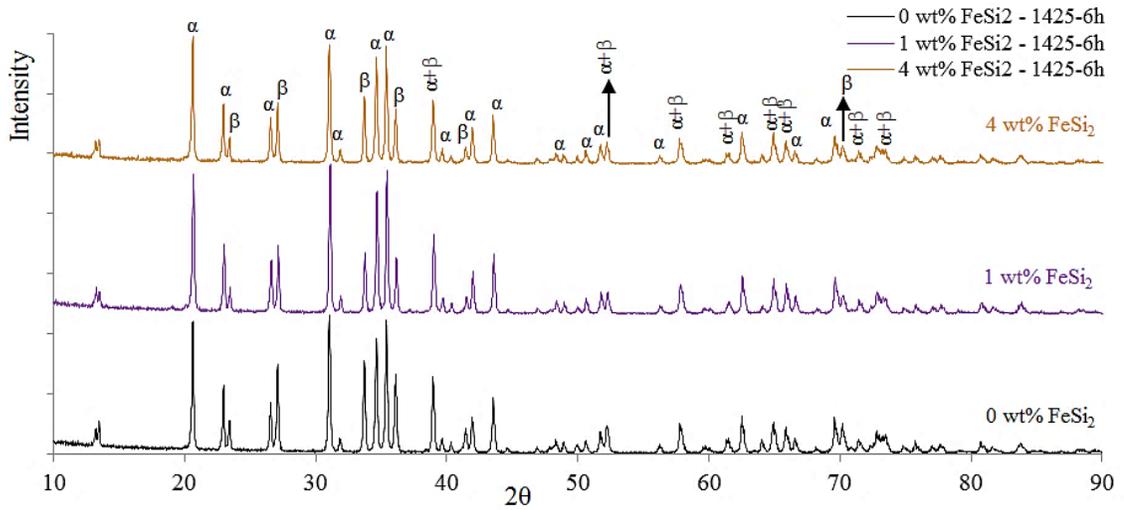
Figure 9-3. XRD patterns of the N1425 foams containing 0, 1, and 4 wt% FeSi$_2$. α and β show α-Si$_3$N$_4$ and β-Si$_3$N$_4$ patterns, respectively.

9.4. Pressureless infiltration of the RBSN foams with Al-Mg alloys

An attempt was made to fabricate an interpenetrating metal matrix composite based on the produced RBSN foam. The foam was infiltrated based on the pressureless infiltration technique.

Regarding the infiltrating alloy, compared to pure Al, Mg addition will decrease the melt viscosity and also reduce the surface tension between Al and Si_3N_4. It may also improve the melt wettability on Si_3N_4. Therefore, Al-15 wt% Mg alloys were prepared based on casting of pure aluminum shots and AZ91 alloy. It was observed that for a short infiltration time of less than 30 min and at temperatures less than 900°C no infiltration occurred. On the other hand, after 1 h and at temperatures above 925°C pressureless infiltration happened. However, severe reactions occurred between the molten alloy and Si_3N_4 resulting in Si_3N_4 decomposition. Figure 9-4 shows the XRD pattern of an RBSN foam infiltrated with an Al-15 wt% Mg alloy. The reaction between Al and Si_3N_4 which leads to AlN and Si formation has been shown in Reaction 9-1. Generally, infiltration of ceramics by molten metals suffers from poor wettability of the system. In pressureless infiltration, some reactions between the metal and ceramic is desirable in order to improve the system wettability but its intensity must be precisely controlled. As can be seen from the foam microstructures provided earlier, the α- and β-whiskers are very fine and the whiskers diameters are of the order of nanometer to submicron sizes. Therefore, as soon as the reaction starts, fine Si_3N_4 whiskers will be decomposed. The only way to improve infiltration is to use gas pressure infiltration or vacuum infiltration techniques. In this case the applied pressure will make it possible to decrease the infiltration time and

temperature in order to control the interfacial reaction intensity. An optimum interfacial

reaction leads to strong bonding between the reinforcement and the matrix.

$$Si_3N_4 + 4\ Al\ (l) = 4\ AlN + 3Si\ (l) \qquad\qquad (9\text{-}1)$$
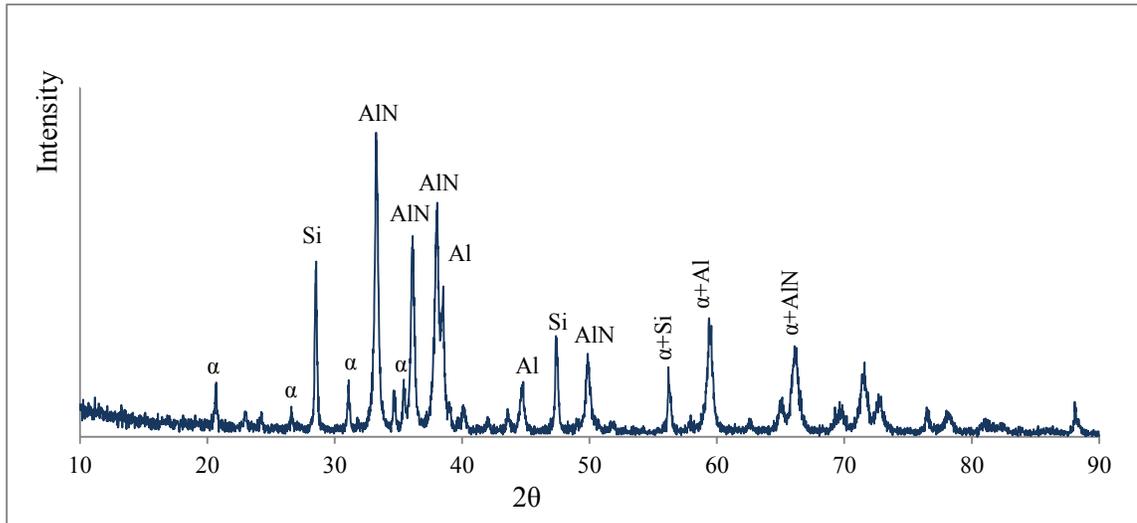
Figure 9-4. XRD pattern of the fabricated RBSN foam infiltrated with the Al-15wt% Mg alloy at 950°C for

1 h.

9.5. The initial study on sintering of Si_3N_4 with Cr_2O_3

9.5.1. The objectives of the initial investigation and its summary

The initial study had been started on densification of silicon nitride ceramics based a novel sintering aid system. The idea was based on the formation of low-melting point phases including Cr_2SiO_4 in CrO-SiO_2 systems. The formation of these phases could result in more than 300°C drop in the sintering temperature of Si_3N_4 ceramics. This improvement could be considered as a significant advancement in sintering of Si_3N_4 ceramics which are typically sintered above 1800°C and under high N_2 pressures. Although in the absence of Si_3N_4, the low melting-point chromium silicate phase could be obtained under the designed experimental procedure, it was observed that the additive system decomposed Si_3N_4 leading to the formation of a series of chromium silicide phases. These phases had very low wettability with Si_3N_4 and could not densify the Si_3N_4 body. Therefore, this study was discontinued and a new investigation on the fabrication and characterization of Si_3N_4 foams was started. A journal article has been published out of the first study. The article has been presented below in the unaltered and original format.

The influence of chromium oxide on the sintering behavior of silicon nitride

Ali Alem, Martin D. Pugh

Department of Mechanical and Industrial Engineering, Concordia University, 1455 de Maisonneuve Blvd.

West, Montreal, Canada H3G 1M8

Abstract

In this study pressureless sintering of silicon nitride via the addition of chromium oxide was investigated. Silicon nitride samples containing additives from the Cr-Cr_2O_3-SiO_2 system were sintered under different conditions. The phase transformation, the degree of densification and the in situ reactions between Si_3N_4 and chromium compounds were investigated and the reactions were validated thermodynamically. It was found that Si_3N_4 reacts with Cr_2O_3 and Cr and these in situ reactions lead to Si_3N_4 decomposition and consequently formation of a series of chromium silicides including Cr_3Si, Cr_5Si, and $CrSi_2$. Due to the presence of chromium silicides as liquid phases during sintering, the α-Si_3N_4 to β-Si_3N_4 phase transformation started around 1400°C and was completed around 1800°C. On the other hand, densification of Si_3N_4 samples with chromium oxide addition was not observed. The participation of Cr_2O_3 in these in situ reactions prevents sufficient formation of chromium silicate and leads to insufficient liquid phase with poor wettability during sintering, resulting in poor densification.

Keywords: Silicon nitride; Sintering; Transition metal oxides; Chromium oxide; Liquid phase sintering

204

9.5.2. Introduction

Silicon nitride is of great interest due to its high strength at elevated temperatures, superior wear resistance, thermal stability, high hardness, low density, and good oxidation resistance [147 - 149]. Although silicon nitride is a candidate material amongst structural ceramics, it still has not reached its full potential due to its sintering difficulties.

Bulk atomic diffusion which leads to solid phase sintering of Si_3N_4 is very difficult and slow since this material is a covalently bonded ceramic [150]. In order to solve the sintering difficulties, one needs to find an additive system which decreases the sintering temperature and yet maintains the high temperature properties of the Si_3N_4. The best compromise is an additive system in which the eutectic occurs at low temperature to get the highest densification rate but which produces highest refractoriness of the glassy phase to avoid degrading the high temperature and creep resistance of Si_3N_4.

Many additive combinations have been added to Si_3N_4 [13- 15, 17, 134, 151 - 173] but no information is available on chromium oxide as an additive for Si_3N_4 systems. Chromium oxide, Cr_2O_3, has interesting properties such as refractoriness, corrosion resistance, and very high hardness. It is widely used in high temperature refractory materials especially in the steel and glass industries. Chromium like many other transition metals can have different oxidation states in silicate melts based on the processing conditions. Its three common oxidation states are Cr^{+6}, Cr^{3+}, and Cr^{2+}. Cr^{3+} forms Cr_2O_3 and Cr^{2+} forms CrO. A comparison between Cr_2O_3-SiO_2 and CrO-SiO_2 phase diagrams reveals that SiO_2 and Cr_2O_3 have very low mutual liquid solubility limits and the first liquid phase forms around 1720°C but on the other hand, CrO and SiO_2 have much higher solubility limits in each other and the eutectic temperature of the system is 1403°C [174, 175]. Therefore, it

is clear that in order to have a lower sintering temperature with a high densification rate, CrO must be stabilized in the system. There are three key parameters which determine the stable oxidation state of chromium: oxygen partial pressure, basicity of the melt, and temperature. Decreasing the oxygen partial pressure, reducing the melt basicity, and increasing the processing temperature may stabilize the lower oxidation state of chromium, which is Cr^{2+}, in CrO [174, 176 - 178]. The reducing conditions required to stabilize Cr^{2+} can be maintained by equilibrating Cr_2O_3 with metallic chromium which creates the most reducing condition or by utilizing reducing gas mixtures such as CO or H_2 [175, 176].

When CrO is stabilized in the system under reducing conditions, the reaction between CrO and SiO_2 may lead to the formation of a blue-colored compound called chromium silicate, Cr_2SiO_4. Based on Figure 9-5-(a) this compound forms at 33 mol% SiO_2-67 mol% CrO [179, 180]. Cr_2SiO_4 liquid is extremely mobile and it may creep up the crucible sides [180, 181]; therefore, it is expected to enhance the rate of particle rearrangement and mass transport and consequently the densification rate of Si_3N_4 significantly. On the other hand, Figure 9-5 reveals the strong dependence of the chromium oxidation valence and consequently the liquidus temperature of the chromium oxide-silica systems on the oxygen partial pressure. It can be seen that the more reducing the condition is, the lower the eutectic point will be. Therefore, by keeping the system in equilibrium with metallic chromium, CrO and Cr_2SiO_4 may be stabilized and consequently a significant drop of more than 300°C can be observed in the melting point of the system [175, 179, 182] which can be advantageous in densifying Si_3N_4 ceramics at lower temperatures.
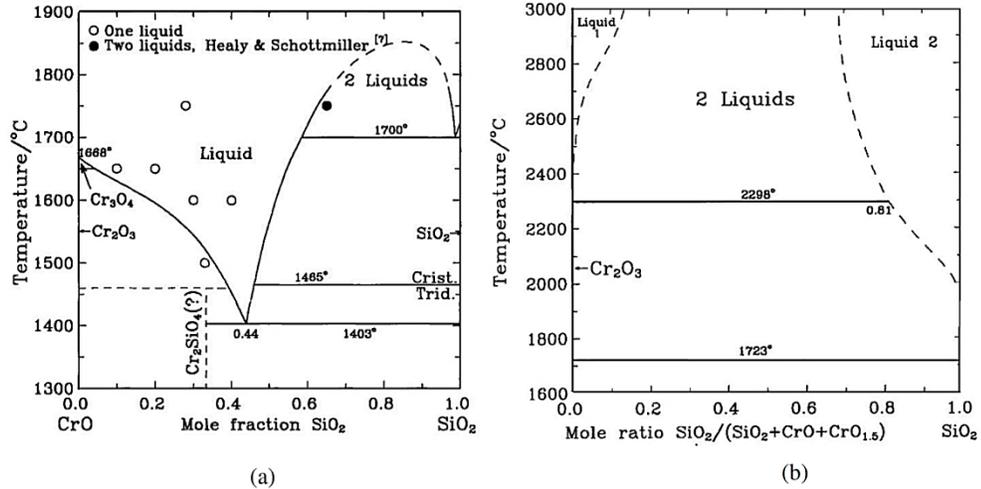
Figure 9-5. The dependence of the eutectic temperature and the eutectic composition of the chromium

oxide-silica system on the oxygen partial pressure; a) in equilibrium with metallic Cr, b) calculated CrO-

Cr_2O_3-SiO_2 phase diagram in air [179].

The stability of Cr_2SiO_4 at room temperature is dependent on the cooling rate of the

process; for low cooling rates it is not stable at room temperature and it decomposes to

Cr, Cr_2O_3, and SiO_2 upon cooling [180]. Decomposition of chromium silicate after

densification and upon cooling of the sample may be advantageous for high temperature

properties of the final product since it decomposes to materials with higher melting points

and consequently higher refractoriness.

In this investigation the influence of Cr_2O_3 on the sintering behavior of Si_3N_4 was

studied. The goal was to form a liquid phase with a low melting temperature based on the

CrO-SiO_2 system by reducing the oxygen partial pressure in the system. The formation of

this liquid is expected to densify silicon nitride at low temperatures (1400-1500°C) and

also it may provide the system with high refractory grain boundary phases which can

improve the high temperature and creep resistance of the final Si_3N_4 ceramic.

9.5.3. Experimental Procedure

The starting powders used in this study were α-rich Si_3N_4 (higher purity silicon nitride, 99.95% grade M11, α-Si_3N_4>90%, H.C. Starck), Cr_2O_3 (chromium (III) oxide, 99.998%, ABCR), metallic Cr (99%, -325 mesh, Alfa Aesar), and SiO_2 (99.8%, -325 mesh, Alfa Aesar).

In order to obtain a liquid phase with a low melting temperature, additive compositions were based on three main groups as given below.

The first composition (I) was based on the Cr_2SiO_4 compound in Figure 9-5-(a) which has a melting point between 1400-1500°C [180]. Reactions 9-2 and 9-3 show the formation of chromium silicate due to the reduction of Cr_2O_3 by metallic Cr and subsequent reaction of CrO with SiO_2. In these samples the molar ratio of SiO_2 to CrO ratio is 33:67.

$$Cr_2O_3 + Cr = 3\ CrO \tag{9-2}$$

$$2\ CrO + SiO_2 = Cr_2SiO_4 \tag{9-3}$$

The second series of compositions (II) were prepared based on the eutectic point in Figure 9-5-(a) in which the molar ratio of SiO_2 to CrO is 44:56. It has the lowest melting point around ~1400°C.

The third series of compositions (III) were prepared based on the reduction of Cr_2O_3 by hydrogen which leads to the formation of CrO based on Reaction 9-4 and consequently forms Cr_2SiO_4 in the presence of SiO_2. It must be mentioned that in these samples hydrogen was playing the role of the reducing agent; therefore, no metallic Cr was utilized.

$$Cr_2O_3 + H_2 = 2\,CrO + H_2O \qquad\qquad\qquad (9\text{-}4)$$

For each composition classification (I, II, and III), different samples with different additive contents were made. The sample composition details are shown in Table 9-1.

Table 9-1. The composition details of the samples with different additive systems

Composition classification	Sample number	SiO_2/CrO molar ratio	Si_3N_4 wt%	Cr_2O_3 wt%	Cr wt%	SiO_2 wt%	Total Additive wt%
III	1	33/67	91.3	8.7	0	0	8.7
I	2	33/67	94	4.5	1.5	0	6
I	3	33/67	89	7	2.4	1.6	11
I	4	33/67	87	6.7	2.3	4	15
III	5	44/56	94.3	5.7	0	0	5.7
II	6	44/56	96.1	2.9	1	0	3.9
II	7	44/56	89	6	2	3	11
II	8	44/56	87	5.7	2	5.3	15

After mixing the components, the powders were wet ball-milled in iso-propyl alcohol for 24 h in a high density polyethylene jar with Si_3N_4 balls. After milling, the slurries were initially stirred and dried on a hot plate and then oven dried at 120°C for 3 h. The powders were sieved and uniaxially die-pressed under 30 MPa. Samples were placed in BN crucibles and sintered with and without powder beds. The powder bed was composed of 50 wt% BN (Saint-Gobain, grade PSHP325) and 50 wt% Si_3N_4 powders. The sintering process was performed in a vacuum furnace at temperatures between 1400 and 1800°C under different atmospheres. The heating rate was 10 °C/min and the sintering time varied between 1 to 4 h.

Three different sintering environments were utilized in this study including N_2 (ultra high purity, grade 5.0, with 0.5 ppm oxygen impurity, Praxair), N_2-4wt% H_2 (Praxair), and Ar (ultra high purity, grade 5.0, Praxair) to investigate the influence of the sintering atmosphere on densification. Before starting the heating cycle, the furnace was evacuated to 1×10^{-5} atm and back-filled with one of the above mentioned gasses.

The final density of the samples was determined based on Archimedes principle. Phase identification was performed by X-Ray Diffraction analysis (XRD, X'Pert Pro, PANalytical) on the different additive systems without Si_3N_4 and also on the final samples containing Si_3N_4. The microstructure of the samples was characterized utilizing scanning electron microscopy (FEGSEM, Philips Xl30) and energy dispersive X-ray (EDS) techniques. The possible reactions between Si_3N_4 and the additives were investigated thermodynamically utilizing Factsage software.

9.5.4. Results and Discussion

9.5.4.1. Density and weight loss measurements

Density measurements revealed that no densification occurred in the sintered samples. In some samples sintered at higher temperatures, the density of the sintered sample was lower than the green density.

By comparing the densities and weight losses of the samples shown in Table 9-1, it was observed that for those with higher Cr content, higher weight losses and lower densities were obtained. It can be concluded that the presence of Cr led to detrimental reactions with Si_3N_4 which increased weight loss and prevented densification.

The second affecting parameter was the SiO_2 content of the sample. It was observed that the higher SiO_2 content results in higher weight loss. Therefore, Reactions 9-5 and 9-6 between Si_3N_4 and SiO_2, which lead to Si_3N_4 decomposition, also contributed to major weight loss in the Si_3N_4 samples. The results are consistent with the literature [183 - 185].

$$Si_3N_4 + 3\ SiO_2\ (l) = 6\ SiO\ (g) + 2\ N_2\ (g) \hspace{3cm} (9\text{-}5)$$

$$Si_3N_4 + SiO_2\ (s,l) = 2\ SiO\ (g) + 2\ Si\ (l) + 2\ N_2\ (g) \hspace{2cm} (9\text{-}6)$$
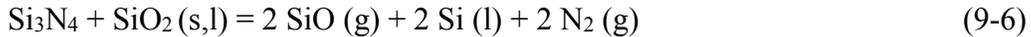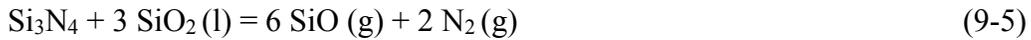
Therefore, in samples with higher additive contents, due to the higher SiO_2 content and also due to the reaction between Cr and Si_3N_4, higher weight losses and lower densities were obtained, especially at elevated temperatures.

9.5.4.2. XRD analysis

9.5.4.2.1. XRD analysis of the additive systems in the absence of Si_3N_4

Since no densification was observed in the samples, the additive systems were studied separately. XRD analyses were performed on the samples containing no Si_3N_4 to investigate all the possible reactions between the additive compounds alone. Figure 9-6 shows the XRD patterns of the additives including SiO_2, Cr, and Cr_2O_3 with the SiO_2-CrO molar ratio of 33:67 at 1500 and 1600°C. It can be observed that Cr_2O_3, Cr_2N, Cr_3Si, Cr, cristobalite, and Cr_2SiO_4 are present in the samples as the reactions products. The formation of blue-colored Cr_2SiO_4 is based on Reactions 9-2 and 9-3.
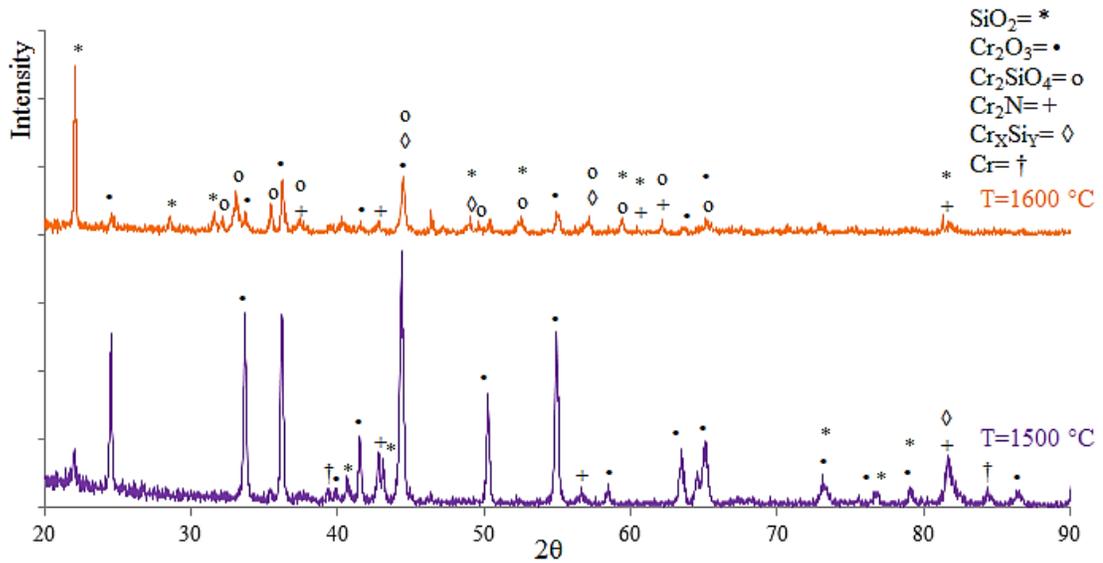
Figure 9-6. XRD patterns of samples containing SiO_2, Cr, and Cr_2O_3 heated under the N_2-4 wt% H_2 gas mixture at 1500 and 1600°C for 1 h; both samples were completely melted. Cr_XSi_Y shows different chromium silicide phases including $CrSi_2$, Cr_5Si and Cr_3Si.

On the other hand, it should be mentioned that CrO was not present in any diffraction pattern. It can be concluded that Reaction 9-3 goes from right to left upon cooling of the system and CrO disproportionates to Cr_2O_3 and Cr which is consistent with the literature [177].

Based on the XRD results of the additive systems, it was observed that SiO_2 is more stable than Cr_2O_3 under the current experimental condition and it cannot be reduced by Cr. This was investigated by preparing different samples containing $SiO_2+Cr_2O_3$, $Si+Cr_2O_3$, and $Cr+SiO_2$ to see which compound can reduce the other. It was observed that Cr_2O_3 does not react significantly with SiO_2 up to 1600°C and no chromium silicides were observed in SiO_2-Cr_2O_3 systems. On the other hand, in samples containing $Si+Cr_2O_3$ and SiO_2+Cr, chromium silicides and cristobalite were formed.

212

Formation of chromium silicides in these samples (without Si_3N_4) may be due to the reactions between SiO_2 and chromium (Reactions 9-7 to 9-9). Reactions between Si and chromium compounds also lead to the formation of chromium silicides. Silicon for these reactions may come from the decomposition of silica under a very low oxygen partial pressure [186] which is shown in Reaction 9-10 or it may also form based on Reaction 9-6.

$$SiO_2 + 3\ Cr = Cr_3Si + O_2 \qquad\qquad (9\text{-}7)$$

$$2SiO_2 + Cr = CrSi_2 + 2\ O_2 \qquad\qquad (9\text{-}8)$$

$$SiO_2 + 5\ Cr = Cr_5Si + O_2 \qquad\qquad (9\text{-}9)$$

$$SiO_2 = Si\ (l) + O_2 \qquad\qquad (9\text{-}10)$$

9.5.4.2.2. XRD analysis of the additive systems in the presence of Si_3N_4

In the previous section the possible reactions between the additives in the absence of Si_3N_4 were studied. XRD analyses were also performed on all the samples containing Si_3N_4 and additives to investigate the possible reactions between Si_3N_4 and chromium compounds.

Figure 9-7 shows the phases present in composition 7 in Table 9-1 sintered under a N_2-4 wt% H_2 gas mixture between 1500 and 1800°C. It can be observed that the phases present are α-Si_3N_4, β-Si_3N_4, Si_2N_2O, and chromium silicides. At 1800°C the α- to β-Si_3N_4 phase transformation is almost complete and mainly β-Si_3N_4 is present. Figure 9-8 and Figure 9-9 also reveal the X-ray diffraction patterns of samples with composition 2 and 1 in Table 9-1 sintered under a N_2-4 wt% H_2 gas mixture, respectively. All the XRD

results reveal the formation of the same phases including α-Si_3N_4, β-Si_3N_4, and chromium silicides ($CrSi_2$, Cr_5Si and Cr_3Si shown as Cr_XSi_Y) between 1400 to 1800°C.
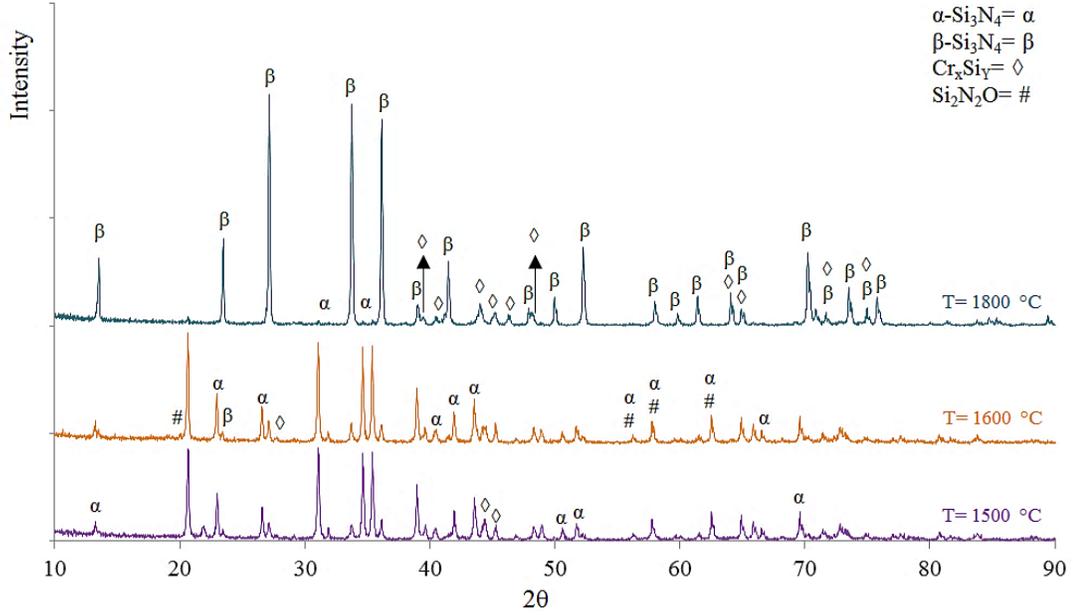
Figure 9-7. XRD patterns of composition 7 in Table 9-1 sintered under the N_2-4 wt% H_2 gas mixture between 1500 and 1800°C; the present phases are α-Si_3N_4, β-Si_3N_4, Si_2N_2O, and chromium silicides (Cr_5Si and Cr_3Si).
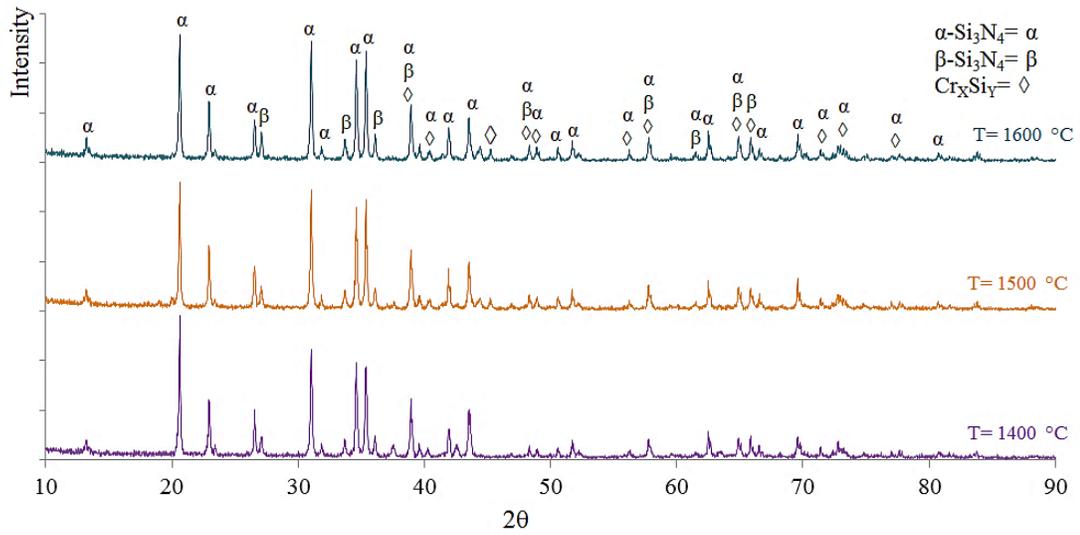
Figure 9-8. XRD patterns of composition 2 in Table 9-1 sintered under the N_2-4 wt% H_2 gas mixture between 1400 to 1600°C; the phases present are α-Si_3N_4, β-Si_3N_4, and chromium silicides ($CrSi_2$ and Cr_5Si).
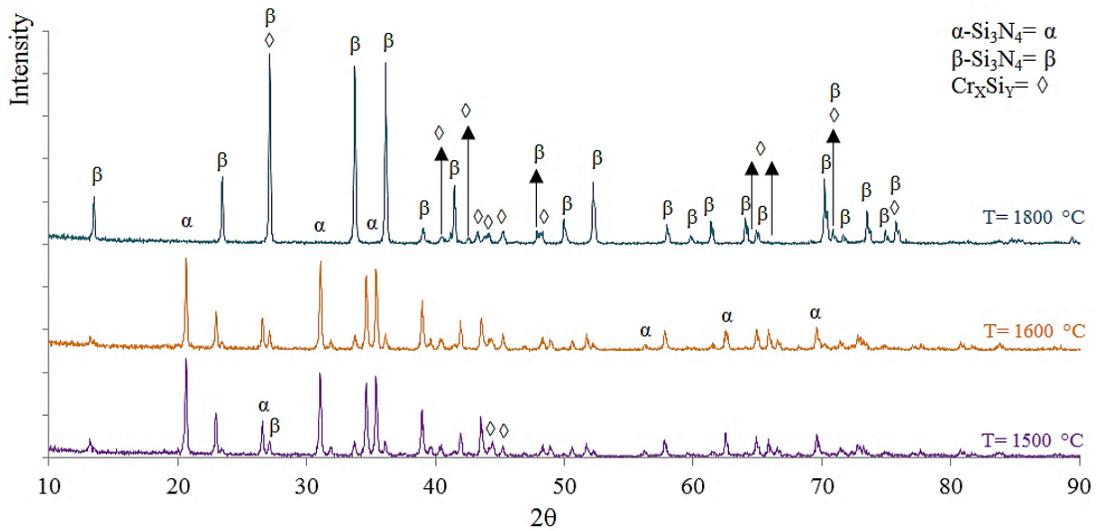
Figure 9-9. XRD patterns of composition 1 in Table 9-1 sintered under N_2-4 wt% H_2 gas mixture between 1500 and 1800°C; the present phases are α-Si_3N_4, β-Si_3N_4, and chromium silicides (Cr_5Si and $CrSi_2$).

Based on a comparison between Figure 9-6 to Figure 9-9, Cr_2SiO_4 which is responsible for liquid phase sintering was formed in samples without Si_3N_4 but not in samples

215

containing Si_3N_4. In conclusion, based on the XRD results, chromium compounds including Cr_2O_3 and Cr react with Si_3N_4 to form chromium silicides instead of Cr_2SiO_4. On the one hand, these in situ reactions consume chromium and decompose silicon nitride and on the other hand, they prevent the formation of chromium silicate and consequently densification of the sample.

9.5.4.3. SEM analysis

As was mentioned before, chromium silicide phases were formed in all samples. Figure 9-10 shows the SEM image of a chromium silicide droplet on Si_3N_4. The spherical shape of the droplets reveals a high surface tension and consequently poor wettability of the silicides on Si_3N_4. Consequently, although liquid chromium silicides are present during sintering, Si_3N_4 densification is not expected to occur due to poor wettability of the silicide phases.

Figure 9-10. The SEM image of a droplet formed on top of the Si_3N_4 sample sintered under the Ar atmosphere at 1650°C for 2 h.

There are two possibilities to get the chromium silicide phases in the Si_3N_4 samples. These silicide phases can form due to the reactions between Si_3N_4 and metallic Cr

(Reactions 9-11 to 9-13) and also due to the reactions between Si_3N_4 and Cr_2O_3 (Reactions 9-14 to 9-19). The reactions between Si_3N_4 and Cr are as follows.

$$Si_3N_4 + 9\ Cr = 3\ Cr_3Si + 2\ N_2 \tag{9-11}$$

$$Si_3N_4 + 15\ Cr = 3\ Cr_5Si + 2\ N_2 \tag{9-12}$$

$$2\ Si_3N_4 + 3\ Cr = 3\ CrSi_2 + 4\ N_2 \tag{9-13}$$

The following reactions occur between Si_3N_4 and Cr_2O_3 which lead to Si_3N_4 decomposition.

$$17\ Si_3N_4 + 15\ Cr_2O_3 = 6\ Cr_5Si + 45\ SiO + 14\ N_2 \tag{9-14}$$

$$7\ Si_3N_4 + 3\ Cr_2O_3 = 6\ CrSi_2 + 9\ SiO + 14\ N_2 \tag{9-15}$$

$$11\ Si_3N_4 + 9\ Cr_2O_3 = 6\ Cr_3Si + 27\ SiO + 22\ N_2 \tag{9-16}$$

$$13\ Si_3N_4 + 18\ Cr_2O_3 = 12\ Cr_3Si + 27\ SiO_2 + 26\ N_2 \tag{9-17}$$

$$11\ Si_3N_4 + 6\ Cr_2O_3 = 12\ CrSi_2 + 9\ SiO_2 + 22\ N_2 \tag{9-18}$$

$$19\ Si_3N_4 + 30\ Cr_2O_3 = 12\ Cr_5Si + 45\ SiO_2 + 38\ N_2 \tag{9-19}$$
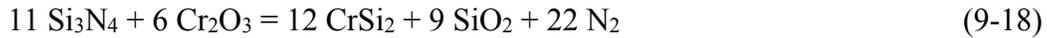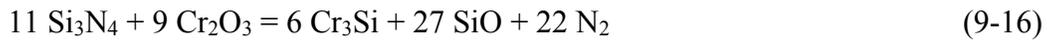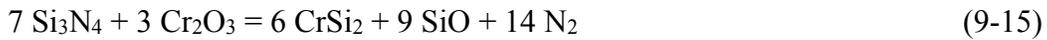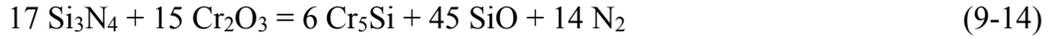
Although the reactions products including the chromium silicide phases have been observed in the XRD and EDS results of the sintered samples, the reactions have been also validated thermodynamically by Factsage. Figure 9-11 reveals the Gibbs free energy (ΔG) versus temperature for the above reactions. The temperatures above which the reactions proceed from left to right ($\Delta G < 0$) are shown in

Table 9-2. It must be mentioned that Cr_5Si could not be found in the Factsage database; therefore, Factsage was not able to predict reactions which gave Cr_5Si as the final product. Thermodynamic analyses in Figure 9-11 reveal that all the mentioned reactions are possible; therefore, Si_3N_4 is expected to be decomposed in the presence of either Cr_2O_3 or Cr. Negita has also studied the effectiveness of a wide range of sintering additives for Si_3N_4 densification based on the standard free energy considerations for oxidation of Si_3N_4 and the additives including metals and metal nitrides at 1727°C [187]. An oxide additive can densify Si_3N_4 if the standard free energies of the metal and metal nitride oxidation reactions are lower than the standard free energies of Si_3N_4 oxidation. Otherwise, decomposition of Si_3N_4 to N_2, SiO, or SiO_2 will occur and the oxide additives tend to form nitrides or be reduced to metals [187]. In the current investigation, the products of the Si_3N_4 decomposition reactions were chromium silicides which were in contrast with Negita's thermodynamic predictions.
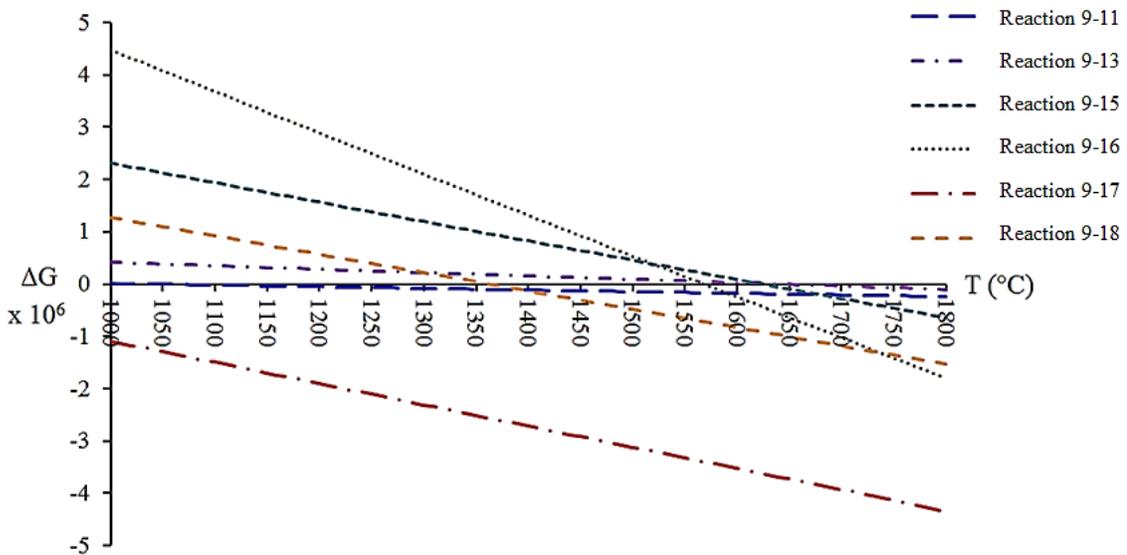
Figure 9-11. Gibbs free energy versus temperature for the reactions between Si_3N_4 and Cr and also between Si_3N_4 and Cr_2O_3 which lead to Si_3N_4 decomposition.

Table 9-2. Thermodynamic validation of the chromium silicide formation by Factsage.

Reaction number	9-11	9-13	9-15	9-16	9-17	9-18
Temperature (°C) above which reaction starts ($\Delta G < 0$)	1040	1650	1630	1570	1000	1370

It can be concluded that chromium either in the form of an oxide or in the form of a metal will react with Si_3N_4 and produce chromium silicide phases. Therefore, chromium oxide will not react with the surface SiO_2 to form chromium silicate and aid the densification process. The situation in the presence of metallic Cr is worse and it will form more chromium silicides.

Therefore, the system is not in equilibrium with Cr and it does not play the role of a reducing agent in the presence of Si_3N_4. Figure 9-12 reveals the microstructures of the sample with composition 2 in Table 9-1 sintered at 1800°C for 2 h. It reveals that even at 1800°C no densification occurred.
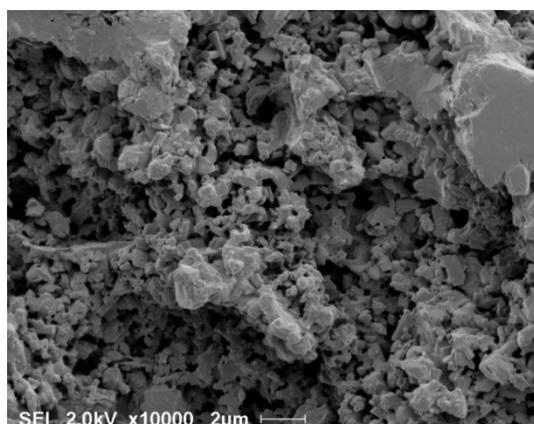
Figure 9-12. Microstructure of the samples with composition 2 sintered at 1800°C for 2 h.

Based on the XRD, EDS, and SEM results, Si_3N_4 phase transformation was observed in the samples but no densification occurred. The phase transformation of Si_3N_4 is based on a solution-diffusion-reprecipitation mechanism [12]; therefore, it occurs only in the presence of a liquid phase. It must be mentioned that densification and phase transformation rates depend on the additive composition and consequently they are dependent on the amount and the viscosity of the liquid phase present during sintering. In Si_3N_4 samples with Cr_2O_3 as an additive, the liquid phase is a series of chromium silicides. On the other hand, as was observed in Figure 9-10 the wettability of chromium silicide with Si_3N_4 is quite low. This liquid phase is adequate to promote phase transformation of Si_3N_4 but densification did not occur due to its poor wettability on Si_3N_4. In this system the densification mechanism is not solution-diffusion-precipitation since phase transformation was completed prior to densification. In order to densify Si_3N_4 with Cr_2O_3, particle rearrangement and porosity filling via liquid distribution were required. However this was not the case due to poor wettability of chromium silicide phases and Si_3N_4 decomposition.

9.5.5. Conclusions

The sintering of Si_3N_4 by chromium compounds was investigated. In the absence of Si_3N_4, chromium silicate could be formed in samples containing mixtures of SiO_2, Cr_2O_3, and Cr at 1500 and 1600°C and the samples were completely melted. In the presence of Si_3N_4, no chromium silicate was observed in the samples. It was found that Si_3N_4 reacts with Cr_2O_3 and Cr and the in situ reactions lead to Si_3N_4 decomposition and consequently formation of a series of chromium silicides including Cr_3Si, Cr_5Si, and $CrSi_2$. These reactions cause pore formation; therefore, they hinder the densification of the samples.

The results show that the higher the amount of additive, the higher the decomposition rate and weight loss in the sample due to more in situ reactions.

Even in the presence of chromium silicides no densification occurred in Si_3N_4 although complete transformation from α- to β-Si_3N_4 was observed. This can be attributed to the high surface tension and low wettability of chromium silicides on Si_3N_4 ceramics. Therefore, the presence of a low melting and a non-wetting liquid does not promote Si_3N_4 densification.

Acknowledgment

References

[1] P. Colombo and H. P. Degischer, "Highly porous metals and ceramics," *Materials Science and Technology,* vol. 26, no. 10, pp. 1145-1158, 2010.

[2] P. Colombo, T. Gambaryan-Roisman, M. Scheffler, P. Buhler and P. Greil, "Conductive ceramic foams from preceramic polymers," *J. Am. Ceram. Soc.,* vol. 84, no. 10, p. 2265–2268, 2001.

[3] A. R. Studart, U. T. Gonzenbach, E. Tervoort and L. J. Gauckler, "Processing routes to macroporous ceramics: a review," *J. Am. Ceram. Soc.,* vol. 89, no. 6, pp. 1771-1789, 2006.

[4] B. V. M. Kumar and Y.-W. Kim, "Processing of polysiloxane-derived porous ceramics: a review," *Sci. Technol. Adv. Mater. ,* vol. 11, pp. 1-16, 2010.

[5] P. Colombo and E. Bernardo, "Macro- and micro-cellular porous ceramics from preceramic polymers," *Composites Science and Technology,* vol. 63, p. 2353–2359, 2003.

[6] P. Colombo and M. Modesti, "Silicon oxycarbide ceramic foams from a preceramic polymer," *J. Am. Ceram. Soc.,* vol. 82, no. 3, pp. 573-578, 1999.

[7] P. Colombo and J. R. Hellmann, "Ceramic foams from preceramic polymers," *Mat. Res. Innovat. ,* vol. 6, pp. 260-272, 2002.

[8] K. Jack, "Review Sialons and related nitrogen ceramics," *Journal of Materials Science,* vol. 11, pp. 1135-1158, 1976.

[9] S. Hampshire, "Silicon nitride ceramics - review of structure, processing and

properties," *Journal of Achievements in Materials and Manufacturing Engineering,* vol. 24, no. 1, pp. 43-50, 2007.

[10] G. Petzow and M. Herrmann, "Silicon nitride ceramics," in *High performance non-oxide ceramics II*, Springer Berlin Heidelberg, 2002, pp. 47-167.

[11] A. Moulson, "Review: Reaction-bonded silicon nitride: its formation and properties," *Material Science,* vol. 14, pp. 1017-1051, 1979.

[12] S. Hampshire, "Silicon nitride ceramics," *Materials Science Forum,* vol. 606, pp. 27-41, 2009.

[13] C. Santos, S. Ribeiro, K. Strecker, P. Suzuki, S. Kycia and C. Silva, "Crystallographic characterization of silicon nitride ceramics sintered with Y2O3–Al2O3 or E2O3–Al2O3 additions," *Ceramics International,* vol. 35, p. 289–293, 2009.

[14] X.-J. Liu, Z.-Y. Huang, Q.-M. Ge, X.-W. Sun and L.-P. Huang, "Microstructure and mechanical properties of silicon nitride ceramics prepared by pressureless sintering with MgO–Al2O3–SiO2 as sintering additive," *Journal of the European Ceramic Society,* vol. 25, p. 3353–3359, 2005.

[15] K. P. Plucknett and H.-T. Lin, "Sintering silicon nitride ceramics in air," *J. Am. Ceram. Soc.,* vol. 88, no. 12, p. 3538–3541, 2005.

[16] H.-D. Kim, B.-D. Han, B.-T. L. Dong-Soo Park and P. F. Becher, "Novel two-step sintering process to obtain a bimodal microstructure in silicon nitride," *J. Am. Ceram. Soc.,* vol. 85, no. 1, p. 245–252, 2002.

[17] P. Becher, N. Shibata, G. Painter, F. Averill, K. v. Benthem, H.-T. Lin and S.

Waters, "Observations on the influence of secondary Me oxide additives (Me= Si, Al, Mg) on the microstructural evolution and mechanical behavior of silicon nitride ceramics containing RE2O3 (RE= La, Gd, Lu)," *J. Am. Ceram. Soc.,* vol. 93, no. 2, p. 570–580, 2010.

[18] S. Danforth, H. Jennings and M. Richman, "The influence of microstructure on the strength of reaction bonded silicon nitride(RBSN)," *Acta Metallurgica,* vol. 27, pp. 123-130, 1979.

[19] R. Pigeon, A. Varma and A. Miller, "Some factors influencing the formation of reaction-bonded silicon nitride," *Material Science,* vol. 28, pp. 1919-1936, 1993.

[20] Y. Huang, L. Zhou, Q. Tang, Z. Xie and J. Yang, "Water-based gelcasting of surface-coated silicon nitride powder," *Am. Ceram. Soc.,* vol. 84, no. 4, pp. 701-707, 2001.

[21] O. Omatete, R. Strehlow and C. Walls, "Gelcasting of submicron alumina, sialon, and silicon nitride powders," in *The 37th Sagamore Army Materials Research Conference*, 1990.

[22] H. Jennings, "Review: On reactions between silicon and nitrogen; Part 1 Mechanisms," *Journal of Materials Science,* vol. 18, pp. 951-967, 1983.

[23] G. Ziegler, J. Heinrich and G. Wotting, "Relationships between processing, microstructure and properties of dense and reaction-bonded silicon nitride," *Materials Science,* vol. 22, pp. 3041-3086, 1987.

[24] P. Longland and A. Moulson, "The growth of a- and b-Si3N4 accompanying the nitriding of silicon powder compacts," *Journal of Materials Science Letters,* vol.

13, pp. 2279-2280, 1978.

[25] H. M. Jennings, B. J. Dalgleish and P. L. Pratt, "Reactions between silicon and nitrogen; Part 2 Microstructure," *Materials Science,* vol. 23, pp. 2573-2583, 1988.

[26] A. Atkinson, P. Leatt, A. Moulson and E. Roberts, "A mechanism for the nitridation of silicon powder compacts," *Materials Science,* vol. 9 , pp. 981-984, 1974.

[27] H. M. Jennings and M. H. Richman, "Structure, formation mechanisms and kinetics of reaction-bonded silicon nitride," *Journal of Materials Science,* vol. 11, pp. 2087-2098, 1976.

[28] H. M. Jennings, S. C. Danforth and M. H. Richman, "Microstructural analysis of reaction-bonded silicon nitride," *Metallography,* vol. 9, pp. 427-446, 1976.

[29] S. Boyer and A. Moulson, "A mechanism for the nitridation of Fe-contaminated silicon," *Materials Science,* vol. 13, pp. 1637-1646, 1978.

[30] P. Colombo, "Conventional and novel processing methods for cellular ceramics," *Phil. Trans. R. Soc. A ,* vol. 364, p. 109–124, 2006.

[31] K. Schwartzwalder and A.V.Somers, "methods of making porous ceramic articles". USA Patent 30990094, 1963.

[32] U. Deisinger, "Generating porous ceramic scaffolds: processing and properties," *Key Engineering Materials,* vol. 441, pp. 155-179, 2010.

[33] M. Nangrejo, X. Bao and M. Edirisinghe, "Silicon carbide–titanium carbide composite foams produced using a polymeric precursor," *International Journal of Inorganic Materials,* vol. 3, p. 37–45, 2001.

[34] D.D. Brown and D.J. Green, "Investigation of strut crack formation in open cell alumina ceramics," *J. Am. Ceram. Soc.,* vol. 77, no. 6, pp. 1467-1472, 1994.

[35] M. Nangrejo, X. Bao and M. J. Edirisinghe, "Preparation of silicon carbide-silicon nitride composite foams from pre-ceramic polymers," *European Ceramic Society,* vol. 20, pp. 1777-1785, 2000.

[36] D. Roy and S. Linnehan, "Hydroxyapatite formed from coral skeletal carbonate by hydrothermal exchange," *Nature,* vol. 247, no. 5438, pp. 220-222, 1974.

[37] J. Klett, R. Hardy, E. Romine, C. Walls and T. Burchell, "High-thermal-conductivity, mesophase-pitch-derived carbon foams: effect of precursor on structure and properties," *Carbon,* vol. 38, p. 953–973, 2000.

[38] X. Bao, M. Nangrejo and M. Edirisinghe, "Synthesis of silicon carbide foams from polymeric precursors and their blends," *Mater. Sci.,* vol. 34, no. 11, pp. 2495-2505, 1999.

[39] Y.-W. Kim, Y.-J. Jin, Y.-S. Chun, I.-H. Song and H.-D. Kim, "A simple pressing route to closed-cell microcellular ceramics," *Scripta Materialia ,* vol. 53, p. 921–925, 2005.

[40] J. Yang, J. Yu and Y. Huang, "Recent developments in gelcasting of ceramics," *European Ceramic Society,* vol. 31, p. 2569–2591, 2011.

[41] E. Williams and J. Evans, "Expanded ceramic foam," *Mater. Sci.,* vol. 31, no. 3, pp. 559-563, 1996.

[42] E. Santos, C. Santilli and S. Pulcinelli, "Formation of zirconia foams using the thermostimulated sol-gel transition," *Non-Crystalline Solids,* vol. 304, no. 1-3, pp.

143-50, 2002.

[43] P. Sepulveda and J. Binner, "Processing of cellular ceramics by foaming and in situ polymerisation of organic monomers," *Journal of the European Ceramic Society,* vol. 19, pp. 2059-2066, 1999.

[44] F. Ortega, P. Sepulveda and V. Pandolfelli, "Monomer systems for the gelcasting of foams," *Journal of the European Ceramic Society,* vol. 22, pp. 1395-1401, 2002.

[45] J. Binner and J. Reichert, "Processing of hydroxyapatite ceramic foams," *Material Science 31,* vol. 31, pp. 5717-5723, 1996.

[46] I. Garrn, C. Reetz, N. Brandes, L. Kroh and H. Schubert, "Clot-forming: the use of proteins as binders for producing ceramic foams," *Journal of the European Ceramic Society,* vol. 24, pp. 579-587, 2004.

[47] C. Tuck and J. Evans, "Porous ceramics prepared from aqueous foams," *Materials Science Letters,* vol. 18, pp. 1003-1005, 1999.

[48] F. R. Rose, L. A. Cyster, D. M. Grant, C. A. Scotchford, S. M. Howdle and K. M. Shakesheff, "In vitro assessment of cell penetration into porous hydroxyapatite scaffolds with a central aligned channel," *Biomaterials,* vol. 25, p. 5507–5514, 2004.

[49] F. Ortega, F. Valenzuela, C. Scuracchio and V. Pandolfelli, "Alternative gelling agents for the gelcasting of ceramic foams," *Journal of the European Ceramic Society,* vol. 23, p. 75–80, 2003.

[50] T. Fujiu, G. L. Messing and W. Huebner, "Processing and properties of cellular silica synthesized by foaming sol gels," *J. Am. Ceram. Soc.,* vol. 73, no. 1, pp. 85-

90, 1990.

[51] T. Tomita, S. Kawasaki and K. Okada, "A novel preparation method for foamed silica ceramics by sol–gel reaction and mechanical foaming," *J. Porous Mater.,* vol. 11, no. 2, p. 107–115, 2004.

[52] P. Sepulveda, J. R. Jones and L. L. Hench, "Bioactive sol–gel foams for tissue repair," *J. Biomedical Mater. Res.,* vol. 59, no. 2, p. 340–348, 2002.

[53] S. Dhara and P. Bhargava, "A simple direct casting route to ceramic foams," *J. Am. Ceram. Soc.,* vol. 86, no. 10, p. 1645–1650, 2003.

[54] P. Colombo and M. Griffoni, "Ceramic Foams from a Preceramic Polymer and Polyurethanes: Preparation and Morphological Investigations," *Sol-Gel Science and Technology,* vol. 13, pp. 195-199, 1998.

[55] T. Takahashi, H. Munstedt, P. Colombo and M. Modesti, "Thermal evolution of a silicone resin/polyurethane blend from preceramic to ceramic foam," *Materials Science,* vol. 36, p. 1627 – 1639, 2001.

[56] P. Colombo and M. Modesti, "Silicon oxycarbide foams from a silicone preceramic polymer and polyurethane," *Sol-Gel Science and Technology,* vol. 14, pp. 103-111, 1999.

[57] Y.-W. Kim, S.-H. Kim, X. Xu, C.-H. Choi, C. B. Park and H.-D. Kim, "Fabrication of porous preceramic polymers using carbon dioxide," *Materials Science Letters,* vol. 21, p. 1667 – 1669, 2002.

[58] T. Fitzgerald, V. Michaud and A. Mortensen, "Processing of microcellular SiC foams; Part II Ceramic foam production," *Journal of Materials Science,* vol. 30, pp.

228

1037-1045, 1995.

[59] E. S. Toberer, J. C. Weaver, K. Ramesha and R. Seshadri, "Macroporous monoliths of functional perovskite materials through assisted metathesis," *Chem. Mater.,* vol. 16, pp. 2194-2200, 2004.

[60] D. Tadica, F. Beckmann, K. Schwarz and M. Epple, "A novel method to produce hydroxyapatite objects with interconnecting porosity that avoids sintering," *Biomaterials,* vol. 25, p. 3335–3340, 2004.

[61] L. B. Linnea Andersson, "Gas-filled microspheres as an expandable sacrificial template for direct casting of complex-shaped macroporous ceramics," *Journal of the European Ceramic Society ,* vol. 28, p. 2815–2821, 2008.

[62] P. Colombo, E. Bernardo and L. Biasetto, "Novel microcellular ceramics from a silicone resin," *J. Am. Ceram. Soc.,* vol. 81, no. 1, pp. 152-154, 2004.

[63] Y.-W. Kim, S.-H. Kim, H.-D. Kim and C. B. Park, "Processing of closed-cell silicon oxycarbide foams from a preceramic polymer," *Journal of Materials Science,* vol. 39, pp. 5647-5652, 2004.

[64] T. Fukasawa, M. Ando, T. Ohji and S. Kanzaki, "Synthesis of porous ceramics with complex pore structure by freeze-dry processing," *Am. Ceram. Soc.,* vol. 84, no. 1, p. 230–232, 2001.

[65] E.-J. Lee, Y.-H. Koh, B.-H. Yoon, H.-E. Kim and H.-W. Kim, "Highly porous hydroxyapatite bioceramics with interconnected pore channels using camphene-based freeze casting," *Materials Letters,* vol. 61, p. 2270–2273, 2007.

[66] F. Ye, J. Zhang, L. Liu and H. Zhan, "Effect of solid content on pore structure and

mechanical properties of porous silicon nitride ceramics produced by freeze casting," *Materials Science and Engineering A,* vol. 528, p. 1421–1424, 2011.

[67] Y.-H. Koh, I.-K. Jun, J.-J. Sun and H.-E. Kim, "In situ fabrication of a dense/porous bi-layered ceramic composite using freeze casting of a ceramic–camphene slurry," *J. Am. Ceram. Soc.,* vol. 89, no. 2, p. 763–766, 2006.

[68] T. Y. Yang, J. M. Lee, S. Y. Yoon and H. C. Park, "Hydroxyapatite scaffolds processed using a TBA-based freeze-gel casting/polymer sponge technique," *J. Mater. Sci.: Mater. Med.,* vol. 21, p. 1495–1502, 2010.

[69] O. O. Omatete, M. A. Janney and S. D. Nunn, "Gelcasting: from laboratory development toward industrial production," *Journal of the European Ceramic Society,* vol. 17, pp. 407-413, 1997.

[70] M. A. Janney, O. O. Omatete, C. A. Walls, S. D. Nunn, R. J. Ogle and G. Westmoreland, "Development of low-toxicity gelcasting systems," *J. Am. Ceram. Soc.,* vol. 81, no. 3, p. 581–591, 1998.

[71] S. Dhara, R. Kamboj, M. Pradhan and P. Bhargava, "Shape forming of ceramics via gelcasting of aqueous particulate slurries," *Bull. Mater. Sci.,* vol. 25, no. 6, p. 565–568, 2002.

[72] O. Omatete, A. Bleier, C. Westmoreland and A. Young, "Gelcast zirconia-alumina composites," *Ceram. Eng. Sci. Proc.,* vol. 12, no. 9-10, pp. 2084-2094, 1991.

[73] Y. Chen, Z. Xie, J. Yang and Y. Huang, "Alumina Casting Based on Gelation of Gelatine," *Journal of the European Ceramic Society,* vol. 19, pp. 271-275, 1999.

[74] K. Prabhakaran, N. Gokhale, S. Sharma and R. Lal, "A novel process for low-

density alumina foams," *Am. Ceram. Soc. ,* vol. 88, no. 9, pp. 2600-2603, 2005.

[75] M. Pradhan and P. Bhargava, "Effect of sucrose on fabrication of ceramic foams from aqueous slurries," *Am. Ceram. Soc.,* vol. 88, no. 1, pp. 216-218, 2005.

[76] R. Mouazer, I. Thijs, S. Mullens and J. Luyten, "SiC foams produced by gel casting: synthesis and characterization," *Adv. Eng. Mater.,* vol. 6, no. 5, pp. 340-343, 2004.

[77] I. Santacruz, M. I. Nieto and R. Moreno, "Alumina bodies with near-to-theoretical density by aqueous gelcasting using concentrated agarose solutions," *Ceramics International,* vol. 31, p. 439–445, 2005.

[78] I. Santacruz, M. I. Nieto and R. Moreno, "Rheological characterization of synergistic mixtures of carrageenan and locust bean gum for aqueous gelcasting of alumina," *J. Am. Ceram. Soc.,* vol. 85, no. 10, p. 2432–2436, 2002.

[79] N. O. Engin and A. C. Tas, "Manufacture of macroporous calcium hydroxyapatite bioceramics," *European Ceramic Society,* vol. 19, pp. 2569-2572, 1999.

[80] H. Katsuki, A. Kawahara and H. Ichinose, "Preparation and some properties of porous alumina ceramics obtained by the gelatination of ammonium alginate," *Journal of Materials Science,* vol. 27, pp. 6067-6070, 1992.

[81] O. Lyckfeldt and J. Ferreira, "Processing of porous ceramics by starch consolidation," *Journal of the European Ceramic Society,* vol. 18, pp. 131-140, 1998.

[82] O. Lyckfeldt, J. Brandt and S. Lesca, "Protein forming- a novel shaping technique for ceramics," *Eropean Ceramic Society,* vol. 20, no. 14-15, pp. 2551-2559, 2000.

[83] X. Guo, Z. Zhou, G. Ma, S. Wang, S. Zhao and Q. Zhang, "Effect of forming process on the integrity of pore-gradient Al2O3 ceramic foams by gelcasting," *Ceramics International,* vol. 38, no. 1, p. 713–719, 2012.

[84] J. Ma, Z. Xie, H. Miao, Y. Huang and Y. Cheng, "Gelcasting of ceramic suspension in acrylamide/polyethylene glycol systems," *Ceramics International,* vol. 28, p. 859–864, 2002.

[85] J.-S. Ha, "Effect of atmosphere type on gelcasting behavior of Al2O3 and evaluation of green strength," *Ceramics International,* Vols. 251-254, p. 26, 2000.

[86] J. Ma, Z. Xie, H. Miao, Y. Huang, Y. Cheng and W. Yang, "Gelcasting of alumina ceramics in the mixed acrylamide and polyacrylamide systems," *the European Ceramic Society ,* vol. 23, p. 2273–2279, 2003.

[87] L. Zhou, Y. Huang and Z. Xie, "Gelcasting of concentrated aqueous silicon carbide suspension," *Journal of the European Ceramic Society,* vol. 20, pp. 85-90, 2000.

[88] Z.-Z. Yi, Z.-P. Xie, Y. Huang, J.-T. Ma and Y.-B. Cheng, "Study on gelcasting and properties of recrystallized silicon carbide," *Ceramics International,* vol. 28, p. 369–376, 2002.

[89] M. Potoczek, "Hydroxyapatite foams produced by gelcasting using agarose," *Materials Letters 62 (2008) ,* vol. 2008, p. 1055–1057, 62.

[90] B. Chen, Z. Zhang, J. Zhang, M. Dong and D. Jiang, "Aqueous gel-casting of hydroxyapatite," *Materials Science and Engineering A,* vol. 435–436, p. 198–203, 2006.

[91] P. Sepulveda, J. Binner, S. Rogero, O. Higa and J. Bressiani, "Production of porous

hydroxyapatite by the gel-casting of foams and cytotoxic evaluation," *Biomed Mater Res.,* vol. 50, no. 1, pp. 27-34, 2000.

[92] J. Yu, H. Wang, H. Zeng and J. Zhang, "Effect of monomer content on physical properties of silicon nitride ceramic green body prepared by gelcasting," *Ceramics International,* vol. 35, p. 1039–1044, 2009.

[93] J. Yu, H. Wang, J. Zhang, D. Zhang and Y. Yan, "Gelcasting preparation of porous silicon nitride ceramics by adjusting the content of monomers," *Sol-Gel Sci. Technol.,* vol. 53, p. 515–523, 2010.

[94] Q. Zhang and M. Gu, "Rheological properties and gelcasting of concentrated aqueous silicon suspension," *Materials Science and Engineering A,* vol. 399, p. 351–357, 2005.

[95] L. Zhou, Y. Huang, Z. Xie and Y.-B. Cheng, "Gas-discharging reactions and their effect on the microstructures of green bodies in gelcasting of non-oxide materials," *Materials Letters,* vol. 45, pp. 51-57, 2000.

[96] P. Xueman, X. Mingxia, L. Hui, L. Xiaolei and J. Huiming, "Rheological properties and thixotropy model of concentrated aqueous silicon slurry for gel casting," *Colloids and Surfaces A: Physicochem. Eng. Aspects,* vol. 317, p. 136–145, 2008.

[97] Z.-P. Xie, Y.-B. Cheng and Y. Huang, "Formation of silicon nitride bonded silicon carbide by aqueous gelcasting," *Materials Science and Engineering A,* vol. 349, pp. 20-28, 2003.

[98] Q. Zhang and M. Gu, "Effect of silicon carbide particles on properties of Al/Sip +

SiCp," *Materials Science and Engineering A,* vol. 419, p. 86–90, 2006.

[99] J.-F. Yang, G.-J. Zhang, N. Kondo, T. Ohji and S. Kanzaki, "Synthesis of porous Si3N4 ceramics with rod-shaped pore structure," *Am. Ceram. Soc.,* vol. 88, no. 4, p. 1030–1032, 2005.

[100] Y. Inagaki, N. Kondo and T. Ohji, "High performance porous silicon nitrides," *European Ceramic Society,* vol. 22, p. 2489–2494, 2002.

[101] X. Pu, X. Liu, F. Qiu and L. Huang, "Novel method to optimize the structure of reticulated porous ceramics," *Am. Ceram. Soc.,* vol. 87, no. 7, p. 1392–1394, 2004.

[102] T. Fukasawa, Z.-Y. Deng, M. Ando, T. Ohji and S. Kanzak, "Synthesis of porous silicon nitride with unidirectionally aligned channels using freeze-drying process," *Am. Ceram. Soc.,* vol. 85, no. 9, p. 2151–2155, 2002.

[103] R. M. Mesquita and A. H. d. A. Bressiani, "Fabrication of porous silicon nitride by sacrificial template method," *Advances in Science and Technology,* vol. 63, pp. 170-174, 2010.

[104] Y. Shao, D. Jia, Y. Zhou and B. Liu, "Novel method for fabrication of silicon nitride/silicon oxynitride composite ceramic foams using fly ash cenosphere as a pore-forming agent," *J. Am. Ceram. Soc.,* vol. 91, no. 11, p. 3781–3785, 2008.

[105] J. Yu, J. Yang, H. Li, X. Xi and Y. Huang, "Study on particle-stabilized Si3N4 ceramic foams," *Materials Letters,* vol. 65, p. 1801–1804, 2011.

[106] J. Yu, H. Wang and J. Zhang, "Neural network modeling and analysis of gel casting preparation of porous Si3N4 ceramics," *Ceramics International ,* vol. 35, p. 2943–2950, 2009.

[107] L. Yuan, J. Yu and S. Zhang, "Effect of pore-forming agent on porous reaction-bonded silicon nitride ceramics," in *IOP Conf. Series: Materials Science and Engineering*, 2011.

[108] J. Xu, D. Zhu, F. Luo, W. Zhou and P. Li, "Dielectric properties of porous reaction-boned Si3N4 ceramics with controlled porosity and pore size," *Mater. Sci. Technol.,* vol. 24, no. 2, pp. 207-210, 2008.

[109] D.-V. Tuyen, Y.-J. Park, H.-D. Kim and B.-T. Lee, "Formation of rod-like Si3N4 grains in porous SRBSN bodies using 6Y2O3–2MgO sintering additives," *Ceramics International,* vol. 35, p. 2305–2310, 2009.

[110] Y.-J. Park, H.-D. Kim and J. W. Halloran, "Permeability enhancement in porous-sintered reaction-bonded silicon nitrides," *Int. J. Appl. Ceram. Technol.,* vol. 8, no. 4, p. 809–814, 2011.

[111] Y.-J. Park, I.-H. Song and H.-D. Kim, "Characterization of pore structures for porous sintered reaction-bonded silicon nitrides with varied pore-former content," *Journal of the Korean Ceramic Society,* vol. 45, no. 11, pp. 675-680, 2008.

[112] Y.-J. Park and I.-H. Song, "Si3N4 with comparable permeability to SiC," *Journal of the European Ceramic Society,* vol. 32, p. 471–475, 2012.

[113] Y.-J. Park, J.-W. Lee, H.-S. Yun and I.-H. Song, "Porous sintered reaction-bonded silicon nitrides with dual-sized pore channel using presintered Si-additive mixture granules," *Int. J. Appl. Ceram. Technol.,* vol. 9, no. 6, pp. 1104-1111, 2012.

[114] Y.-J. Park, B.-W. Park, S.-H. Lee, J.-W. Lee, H.-S. Yun and I.-H. Song, "The characterization of porous sintered reaction-bonded silicon nitride ceramics

fabricated by Si-additive mixture granules," *Int. J. Appl. Ceram. Technol.,* vol. 8, no. 6, pp. 1501-1508, 2011.

[115] J. Xu, F. Luo, D. Zhu, X. Su and W. Zhou, "Effect of presintering on the dielectric and mechanical properties of porous reaction-bonded silicon nitride," *Materials Science and Engineering A,* vol. 488, p. 167–171, 2008.

[116] E. Laarz, B. V. Zhmud and L. Bergstrom, "Dissolution and deagglomeration of silicon nitride in aqueous medium," *Am. Ceram. Soc.,* vol. 83, no. 10, p. 2394–2400, 2000.

[117] B.-T. Lee, J.-H. Yoo and H.-D. Kim, "Size effect of raw Si powder on microstructures and mechanical properties of RBSN and GPSed-RBSN bodies," *Materials Science and Engineering A,* vol. 333, p. 306–313, 2002.

[118] N. Kondo, H. Hyuga, H. Kita and T. Kaba, "Fabrication of thick silicon nitride by reaction bonding and post-sintering," *Journal of the Ceramic Society of Japan,* vol. 115, no. 4, pp. 285-289, 2007.

[119] V. A. Hackley, U. Paik, B.-H. Kim and S. G. Malghan, "Aqueous processing of sintered reaction-bonded silicon nitride: I, dispersion properties of silicon powder," *Am. Ceram. Soc.,* vol. 80, no. 7, pp. 1781-1788, 1997.

[120] R. R. Rao, H. N. Roopa and T. S. Kannan, "The characterisation of aqueous silicon slips," *European Ceramic Society,* vol. 19, pp. 2763-2771, 1999.

[121] R. Stephen and F. Riley, "Oxidation of Si by water," *European Ceramic Society,* vol. 5, pp. 219-222, 1989.

[122] M. N. Rahaman, Ceramic processing and sintering, New York: Marcel Dekker,

2003.

[123] A. Alem, M. D. Pugh and R. A. Drew, "Open-cell reaction bonded silicon nitride foams: Fabrication and characterization," *Journal of the European Ceramic Society,* vol. 34, no. 3, pp. 599-609, 2014.

[124] M. Lindley, D. Elias, B. F. Jones and K. Pitman, "The influence of hydrogen in the nitriding gas on the strength, structure and composition of reaction-sintered silicon nitride," *Materials Science,* vol. 14, pp. 70-85, 1979.

[125] B. Dalgleish and P. Pratt, "The influence of microstructure on the strength of reaction-bonded silicon nitride," *Mechanical Properties of Ceramics,* vol. 2, no. 25, pp. 295-310, 1975.

[126] A. G. Evans and R. W. Davidge, "The strength and oxidation of reaction-sintered silicon nitride," *Materials Science,* vol. 5, pp. 314-325, 1970.

[127] C. P. Gazzara and D. R. Messier, "Determination of phase content of Si3N4 by X-ray diffraction analysis," *American Ceramic Society Bulletin,* vol. 56, no. 9, pp. 777-780, 1977.

[128] X. Zhu, Y. Zhou and K. Hirao, "Processing and thermal conductivity of sintered reaction-bonded silicon nitride. I: Effect of Si powder characteristics," *J. Am. Ceram. Soc.,* vol. 89, no. 11, p. 3331–3339, 2006.

[129] F. Riley, "Silicon nitridation and the development of microstructure in reaction bonded silicon nitride," *Energy and Ceramics Proceedings of the 4th International Meeting on Modern Ceramics,* pp. 550-568, 1980.

[130] H. Hanjun, Z. Wan-cheng, L. Fa, Z. Dong-Mei and X. Jie, "A new synthesis

method for producing Si3N4 whiskers by heat treating porous Si objects," *J. Am. Ceram. Soc.,* vol. 91, no. 11, pp. 3800-3802, 2008.

[131] J.-Q. Dai, Y. Huang and J.-T. Ma, "Surface characteristics and aqueous dispersibility of commercial silicon nitride powders: Effects of acid leaching, surface hydrolysis, and thermal oxidation," *Ceramics International,* vol. 34, p. 1835–1842, 2008.

[132] E. Ewais, M. Attia, A. Abousree-Hegazy and R. Bordia, "Investigation of the effect of ZrO2 and ZrO2/Al2O3 additions on the hot-pressing and properties of equimolecular mixtures of alpha- and beta-Si3N4," *Ceramics International,* vol. 36, p. 1327–1338, 2010.

[133] J.-S. Lee, J.-H. Mun, B.-D. Han and H.-D. Kim, "Effect of b-Si3N4 seed particles on the property of sintered reaction-bonded silicon nitride," *Ceramics International 29 (2003) 897–905,* vol. 29, pp. 897-905, 2003.

[134] B. Wang, J. Yang, R. Guo, J.-Q. Gao and J.-F. Yang, "Microstructure characterization of hot-pressed β-silicon nitride containing β-Si3N4 seeds," *Materials Characterization,* vol. 60, pp. 894-899, 2009.

[135] D. Musca, M. D. Pugh, R. A. L. Drew, H. Pickup and D. Steele, "Microstructure of an extruded B-silicon nitride whisker-reinforced silicon nitride composite," *J. Am. Ceram. Soc.,* vol. 75, no. 10, pp. 2713-2718, 1992.

[136] O. Gregorgy and M. Richman, "The role of Si3N4 additions in the reaction bonding of silicon compacts," *Materials Science,* vol. 3, pp. 112-116, 1984.

[137] S. Y. Lee, K. Amoako-Appiagyei and H. D. Kim, "Effect of b–Si3N4 seed crystal

on the microstructure and mechanical properties of sintered reaction-bonded silicon nitride," *J. Mater. Res.,* vol. 14, no. 1, pp. 178-184, 1999.

[138] R. R. Rao and T. Kannan, "Nitride-bonded silicon nitride from slip-cast Si + Si3N4 compacts," *J. Mater. Res.,* vol. 17, no. 2, pp. 386-395, 2002.

[139] R. Williams and C. Peters, "The effects of additions of a-Si3N4 grog on the a/b ratio of slip cast reaction bonded silicon nitride," *Materials Science Letters,* vol. 1, pp. 257-259, 1982.

[140] R. M. Williams, A. Ezis and J. C. Caverly, "Properties of Si3N4 produced by nitriding slip-cast Si containing Si3N4 grog additions," *Comminications of the American Ceramic Socirty,* pp. C-64 - C-66, 1984.

[141] J.-S. Lee, J.-H. Mun, B.-D. Han, H.-D. Kim, B.-C. Shin and I.-S. Kim, "Effect of raw-Si particle size on the properties of sintered reaction-bonded silicon nitride," *Ceramics International,* vol. 30, p. 965–976, 2004.

[142] H. Hyuga, K. Yoshida, N. Kondo, H. Kita, H. Okano, J. Sugai and J. Tsuchida, "Influence of zirconia addition on reaction bonded silicon nitride produced from various silicon particle sizes," *Journal of the Ceramic Society of Japan,* vol. 116, no. 6, pp. 688-693, 2008.

[143] Y. Zhou, X. Zhu and K. Hirao, "Sintered reaction-bonded silicon nitride with high thermal conductivity and high strength," *International Journal of Applied Ceramic Technology,* vol. 5, no. 2, p. 119–126, 2008.

[144] M. Muller, W. Bauer and R. Knitter, "Processing of micro-components made of sintered reaction-bonded silicon nitride (SRBSN). Part 1: Factors influencing the

reaction-bonding process," *Ceramics International,* vol. 35, p. 2577–2585, 2009.

[145] X. Zhu, Y. Zhou and K. Hirao, "Post-densification behavior of reaction-bonded silicon nitride (RBSN): Effect of various characteristics of RBSN," *Journal of Materials Science,* vol. 39, p. 5785–5797, 2004.

[146] F. L. Riley, "Silicon nitride and related materials," *J. Am. Ceram. Soc.,* vol. 83, no. 2, p. 245–265, 2000.

[147] V. Demir and A. Demir, "Vacuum heat-treatment of MgO-densified silicon nitride ceramics and their compatibility with molten aluminium and copper," *Ceramics International ,* vol. 37, p. 985–988, 2011.

[148] P. Tatarkoa, S. Lojanova, J. Dusza and P. Sajgalik, "Influence of various rare-earth oxide additives on microstructure and mechanical properties of silicon nitride based nanocomposites," *Materials Science and Engineering A,* vol. 527, p. 4771–4778, 2010.

[149] M. Bocanegra-Bernal and B. Matovic, "Mechanical properties of silicon nitride-based ceramics and its use in structural applications at high temperatures," *Materials Science and Engineering A,* vol. 527, p. 1314–1338, 2010.

[150] C. Greskovich, "Preparation of high-density Si3N4 by a gas-pressure sintering process," *J. Am. Ceram. Soc.,* vol. 64, no. 12, pp. 725-730, 1981.

[151] N. Uchida and M. Koizumi, "Fabrication of Si3N4 ceramics with metal nitride additives by isostatic hot-pressing," *J. Am. Ceram. Soc.,* vol. 68, no. 2, pp. C38-C40, 1985.

[152] Z. Tatli and D. Thompson, "Low temperature densification of silicon nitride

materials," *J. of the European Ceramic Society,* vol. 27, p. 791–795, 2007.

[153] V. Demir and D. Thompson, "Vacuum heat treatment of MgO-densified pressureless sintered silicon nitride ceramics," *Materials Science Forum,* vol. 554, pp. 107-112, 2007.

[154] G. Ling and H. Yang, "Pressureless sintering of silicon nitride with Magnesia and Yttria," *Materials Chemistry and Physics,* vol. 90, pp. 31-34, 2005.

[155] Y. Goto and G. Thomas, "Phase transformation and microstructural changes of Si3N4 during sintering," *J. of Materials Science,* vol. 30, pp. 2194-2200, 1995.

[156] W. Lehner, H.-J. Kleebe and G. Ziegler, "Variation of sintering parameters at an early stage of densification affecting β-Si3N4-microstructure," *J. of the European Ceramic Society,* vol. 26, p. 201–208, 2006.

[157] A. Vuckovic, B. Matovic and S. Boskovic, "Influence of additive type on the densification and phase transformation of seeded Si3N4," *Materials Science Forum,* vol. 494, pp. 429-434, 2005.

[158] S. Ordonez, I. Iturriza and F. Castro, "The influence of amount and type of additives on α→ β Si3N4 transformation," *J. of Materials Science,* vol. 34, p. 147–153, 1999.

[159] T. Wasanapiarnpong, S. Wada, M. Imai and T. Yano, "Effect of post-sintering heat-treatment on thermal and mechanical properties of Si3N4 ceramics sintered with different additives," *J. of the European Ceramic Society,* vol. 26, p. 3467–3475, 2006.

[160] W.-H. Lee and H.-E. Kim, "Microstructural evolution of gas-pressure-sintered

Si3N4 with Yb2O3 as a sintering aid," *J. Am. Ceram. Soc.,* vol. 80, no. 10, p. 2737–2740, 1997.

[161] J. Dai, J. Li, Y. Chen and X. Yang, "Effects of rare-earth oxide additions and heat-treatment temperature on the transformation and microstructure of silicon nitride," *Phys. Stat. Sol. (A) ,* vol. 198, no. 1, pp. 91-98, 2003.

[162] M. Cinihulk and G. Thomas, "Fabrication and secondary-phase crystallization of rare-earth disilicate-silicon nitride ceramics," *J. Am. Ceram. Soc.,* vol. 75, no. 8, p. 2037–2043, 1992.

[163] K. Strecker, R. Gonzaga, S. Ribeiro and M. Hoffmann, "Substitution of Y2O3 by a rare earth oxide mixture as sintering additive of Si3N4 ceramics," *Materials Letters,* vol. 45, p. 39–42, 2000.

[164] L. Bai, C. Ge, W. Shen, K. Zhang and X. Mao, "Densification and α/β phase transformation of SHS Si3N4 containing Al2O3 and Y2O3 during sintering," *Materials Science Forum,* Vols. 561-565, pp. 577-580, 2007.

[165] P. Sajgalik and M. Haviar, "Pressureless sntering of Si3N4 with Y2O3 and Al2O3 additives-compatibility of powder beds," *Ceramics International,* vol. 18, pp. 279-283, 1992.

[166] H. Miyazaki, H. Hyuga, Y.-i. Yoshizawa, K. Hirao and T. Ohji, "Crack profiles under a vickers indent in silicon nitride ceramics with various microstructures," *Ceramics International,* vol. 36, pp. 173-179, 2010.

[167] W.-R. Zhang, F. Sun, T.-Y. Tian, X.-H. Teng, M.-C. Ru and Y. Ding, "Effects of sintering additives on the microstructure and mechanical properties of silicon

nitride ceramics by GPS," *Advanced Materials Research,* Vols. 105-106, pp. 27-30, 2010.

[168] T. Wasanapiarnpong, S. Wada, M. Imai and T. Yano, "Thermal conductivity improvement by heat-treatment in Si3N4 ceramics using SiO2-MgO-Y2O3 additive system," *Materials Science Forum,* vol. 352, pp. 233-238, 2007.

[169] B. Matovic, G. Rixecker and F. Aldinger, "Densification of Si3N4 with LiYO2 additive," *J. Am. Ceram. Soc.,* vol. 87, no. 4, p. 546–549, 2004.

[170] S.-H. Lee, "Densification, mass loss, and mechanical properties of low-temperature pressureless-sintered Si3N4 with LiYO2 additive: the effects of additive content and annealing," *J. Appl. Ceram. Technol.,* vol. 7, no. 6, p. 881–888, 2010.

[171] B. Matovic, G. Rixecker and F. Aldinger, "Pressureless sintering of silicon nitride with lithia and yttria," *J. of the European Ceramic Society,* vol. 24, p. 3395–3398, 2004.

[172] Z.-K. Huang, A. Rosenflanz and I.-W. Chen, "Pressureless sintering of Si3N4 ceramic using AlN and rare-earth oxides," *J. Am. Ceram. Soc.,* vol. 80, no. 5, p. 1256–1262, 1997.

[173] P. Becher, G. Painter, N. Shibata, S. Waters and H.-T. Lin, "Effects of Rare-Earth (RE) intergranular adsorption on the phase transformation, microstructure evolution, and mechanical properties in silicon nitride with RE2O3+MgO additives: RE=La, Gd, and Lu," *J. Am. Ceram. Soc.,* vol. 91, no. 7, p. 2328–2336, 2008.

[174] E. Pretorius and A. Muan, "Activity-composition relations of chromium oxide in

silicate melts at 1500°C under strongly reducing conditions," *J. Am. Ceram. Soc.,* vol. 75, no. 6, pp. 1364-1377 , 1992.

[175] J. d. Villiers and A. Muan, "Liquidus-solidus phase relations in the system CaO-CrO-Cr2O3-SiO2," *J Am. Ceram. Soc.,* vol. 75, no. 6, pp. 1333-1341, 1992.

[176] E. Pretorius, R. Snellgrove and A. Muan, "Oxidation state of chromium in CaO-A12O3-CrOX-SiO2 melts under strongly reducing conditions at 1500°C," *J. Am. Ceram. Soc.,* vol. 75, no. 6, pp. 1378-1381, 1992.

[177] Y. Xiao, L. Holappa and M. Reuter, "Oxidation state and activities of chromium oxides in CaO-SiO2-CrOx slag system," *Metallurgical and Materials Transactions B,* vol. 33B, pp. 595-603, 2002.

[178] P. Dong, X. Wang and S. Seetharaman, "Thermodynamic activity of chromium oxide in CaO-SiO2-MgO-Al2O3-CrOx melts," *Steel Research Int.,* vol. 80, no. 3, pp. 202-208, 2009.

[179] S. Degterov and A. Pelton, "Critical evaluation and optimization of the thermodynamic properties and phase diagrams of the CrO-Cr2O3-SiO2 and CrO-Cr2O3-SiO2-Al2O3 systems," *J. of Phase Equilibria,* vol. 17, no. 6, pp. 488-494, 1996.

[180] G. Healy and J. Schottmiller, "The chromium oxide-silica system at low oxygen partial pressures," *Transactions of the metallurgical Society of AIME,* vol. 230, pp. 420-425, 1964.

[181] J. Hauck, "Divalent chromium in alkaline earth silicate systems," *J. of Materials Science,* vol. 12, pp. 1690-1691, 1997.

[182] A. Muan, "Equilibrium relations in the systems containing chromium oxide, with a bearing on refractory corrosion in slagging coal gasifiers," *High Temperatures-High Pressures,* vol. 14, pp. 653-660, 1982.

[183] F. Lange, "Volatilization associated with the sintering of polyphase Si3N4 materials," *J. Am. Ceram. Soc.,* vol. 65, no. 8, p. C120–C121, 1982.

[184] S. Wada, "Control of instability of Si3N4 during pressureless sintering," *J. Ceramic Society of Japan,* vol. 109, no. 10, pp. 803-808, 2001.

[185] K. Yokoyama and S. Wada, "Solid-gas reaction during sintering of silicon nitride ceramics (Part 3)," *J. Ceramic Society of Japan,* vol. 108, no. 3, pp. 230-235, 2000.

[186] D. Messier and E. Deguire, "Thermal decomposition in the system Si-Y-AI-O-N," *J. Am. Ceram. Soc.,* vol. 67, no. 9, pp. 602-605, 1984.

[187] K. Negita, "Effective sintering aids for Si3N4 ceramics," *J. Materials Science Letters,* vol. 4, pp. 755-758, 1985.